DEVELOPMENT AND SIMULATION OF A SINUSOIDAL PULSE WIDTH MODULATION-BASED CONTROL SCHEME FOR IMPROVED EFFICIENCY AND TORQUE PRODUCTION IN SINGLE PHASE INDUCTION MACHINES

BY

Gbenga Abidemi **OLARINOYE**

B.Eng (A.T.B.U) 1999, M.Eng (UNIBEN) 2005

(Ph.D/ENG/00328/08-09)

baolarinoye@abu.edu.ng

A THESIS SUBMITTED TO THE SCHOOL OF POSTGRADUATE STUDIES, AHMADU BELLO UNIVERSITY, ZARIA IN PARTIAL FULFILLMENT OF THE REQUIREMENTS FOR THE AWARD OF DOCTOR OF PHILOSOPHY (Ph.D) DEGREE IN ELECTRIC MACHINES AND INDUSTRIAL DRIVES

DEPARTMENT OF ELECTRICAL AND COMPUTER ENGINEERING

FACULTY OF ENGINEERING

AHMADU BELLO UNIVERSITY,

ZARIA, NIGERIA

FEBRUARY, 2017

DECLARATION

I declare that the work in this thesis entitled“Development and Simulation of a Sinusoidal Pulse Width Modulation-based Control Scheme for Improved Efficiency and Torque Production in Single Phase Induction Machines”has been carried out by me in the Department of Electrical and Computer Engineering. The information derived from the literature has been duly acknowledged in the text and a list of references provided. No part of this thesis was previously presented for another degree or diploma at this or any other Institution.

Gbenga Abidemi**OLARINOYE** _____ _____

(Student) Signature Date

CERTIFICATION

This thesis entitled "DEVELOPMENT AND SIMULATION OF A SINUSOIDAL PULSE WIDTH MODULATION-BASED CONTROL SCHEME FOR IMPROVED EFFICIENCY AND TORQUE PRODUCTION IN SINGLE PHASE INDUCTION MACHINES"by Gbenga Abidemi**OLARINOYE** meets the regulations governing the award of the degree of **Doctor of Philosophy (Ph.D)**of theAhmadu Bello University and is approved for its contributions to knowledge and literary presentation.

Chairman, Supervisory Committee (Prof. U. O. Aliyu)	Signature	Date
Member, Supervisory Committee (Dr. Y. Jibril)	Signature	Date
Member, Supervisory Committee (Prof. B. Jimoh)	Signature	Date
Head of Department (Dr. Y. Jibril)	Signature	Date
Dean, School of Postgraduate Studies (Prof. S. Z. Abubakar)	Signature	Date

DEDICATION

This work is dedicated to the loving memory of my beloved mother, Late Mrs. Rebecca. M. Olarinoye.

ACKNOWLEDGEMENT

I would like to express my gratitude to God Almighty Who helped me to begin this work and Who has been faithful to help me complete this work.

I wish to express my profound gratitude to the chairman of my supervisory committee, Professor U. O Aliyu for his wise counsel throughout the duration of the research. His untiring support and guidance have been the necessary tools that led to the completion of this thesis. I am extremely grateful toDr Yusuf Jibril and Professor Boyi Jimoh who are members of my supervisory committee. Their valuable contributions, guidance and assistance have been timely and crucial to the completion of this thesis. I sincerely wish to thank my Head of Department in the person of Dr. Yusuf Jibril for his generosity and for creating an enabling environment for the progress of postgraduate students in the Department of Electrical and Computer Engineering. I thank Professor B. G. Bajoga for his indispensable guidance and direction in the early stages of the work. His fatherly interventions have ensured the progress of my research. I cannot forget the vital contributions of Dr. Joseph Y. Oricha to the success of my research from the beginning to the end of the work. His untiring counsel and persistent calls have helped me through the difficult times. I am indebted to Professor M. B. Muazuwho facilitated my appointment to the Department of Electrical Engineering and who assisted immensely in my registration for the PhD program. I am grateful for his counsel, encouragements, thoroughness and commitment to reviewing my report at different stages of development. His contributions have helped to improve the quality of this thesis. I am grateful to Dr. S. M. Sani for his encouragements and moral support at times when it mattered the most. I am grateful for his efforts to read and correct mistakes in my progress reports and to give valuable comments that have shaped the character of this thesis. I am also indebted to Dr. Adewale Adedokun whose moral and spiritual interventions

have been a major impetus for the completion of this work. My profound gratitude also goes to Dr. T. H. Sikiru, Dr. A.M.S Tekanyi, Dr. S. Garba,Dr. A. K. Abubilaland Dr. I. J. Umoh for their various contributions and interventions which have helped to propel this work forward.

I would like to also thank all my colleagues and staff of the Department of Electrical and Computer Engineering, A.B.U Zaria for their diverse contributions throughout the course of my PhD research and primary assignment in the Department. I would like to recognize and appreciate the efforts of Alhaji F. O Sadiku and the entire staff of the Electric Machines Laboratory in the Department of Electrical and Computer Engineering, A.B.U Zaria.

I wish to express my immense appreciation to Professor J. O. Ojo for the supervisory role he offered at the early stages of this research work. I acknowledge the United States Department of State's Bureau for Educational and Cultural Affairs and the Institute for International Education (IIE) for awarding me the Fulbright Scholarship which enabled me to acquire the knowledge and skills needed to advance my research and career development goals. My profound gratitude goes to the management of Ahmadu Bello University, Zaria for approving my leave to the United States (US). I am extremely grateful to the management of Tennessee Technological University (TTU) for hosting me during my visit to the US in pursuit of my research objectives. The training I received in the power electronics and machine laboratory with the kind support of the Department of Electrical & Computer Engineering, TTU and the Centre for Energy Systems Research is very much appreciated.

I would also like to recognize and appreciate the uncommon assistance and encouragements that I received from Joseph Aribido, Medhi Ramezani, Medhy Khayami, Eseme Sota, Michael Adenson, Adeniyi Babalola, Waheed Oyekanmi, Tosin, Dare, Dr. K. B. Ranjan and other friends

of mine at the Tennessee Technological University during my stay in the city of Cookeville, Tennessee, U.S.A. The efforts of Dr. P. K. Rajan, Conard Murray, Robert Craven, Tony Greenway and Andrew Murray all of the Centre for Energy Systems Research (CESR), Tennessee Technological University, U.S.A towards the success of my academic program at CESR cannot be forgotten and are hereby deeply appreciated.

Furthermore, I want to express my deepest appreciation to my immediate and extended family for their unquantifiable gift of love, care and support. I am profoundly grateful to my father, Professor R. D. Olarinoye for his continuing care, support and blessings. I thank all my siblings, cousins, uncles and aunts for their moral and spiritual support. I also thank Professor and Dr. (Mrs) M. D. Alegbejo and the rest of my in-laws for their moral and spiritual support. The love and kindness that my immediate family has benefitted from them is immeasurable. I am grateful to the family of Pastor and Mrs Akin Okinbaloye for their moral and spiritual support. Finally, I would like to thank my beloved wife and children; Moji, Somi and Simi for sticking with me through thick and thin over the years of work and research struggles. God bless you all.

G. A. Olarinoye

February 2017

ABSTRACT

This study developedmethods to improve the efficiency and torque production of the single phase induction machine using a sinusoidal pulse width modulation (SPWM) control scheme. This research targets the capacitor-run single phase induction motor(CRSPIM) which is a large consumer of domestic and industrial power supply with the goal of improving its operation at light load conditions.This motor suffers fromlow efficiency when operating under non-rated conditions,leading to wastage of significant amount of electric power since rated voltage is applied fully across its terminals and the flux in the machine operates approximately at rated value regardless of the applied load on the machine. Moreover, during starting time and at steady state, the motor exhibits significant torque pulsations which gives rise to noise and vibration in the machine. In efforts to address these problems, a performance improvement scheme using a pulse width modulated single phase inverter and a PID controller was first developed and implemented in MATLAB/Simulink environment to eliminate steady state torque pulsations in the motor. Although system simulation shows reduction in torque pulsations in the motor under the scheme compared to the performance of the same motor under nominal power supply, this scheme could not eliminate torque pulsations in steady state. Consequently, a pragmatic design modification to the parameters of the auxiliary winding of the existing CRSPIM was proposed. In addition to the design modification, a vector-controlled drive with an efficiency-optimizing function for the modified single phase induction machine was also proposed. This second approachuses a two-phase, two-leg inverter structure. Theproposed scheme was also implemented in the MATLAB/Simulink environment. Simulation results have demonstrated that the proposed strategy eliminates torque pulsations at steady state in comparison to the existing line-operated CRSPIM. It is also shown that the proposed drive control strategy increased machine efficiency over that of the existing CRSPIM significantly at light loads. Specifically, the proposed scheme yielded machine efficiency of 80.8% on all loads whereas the existing CRSPIM gives an efficiency of 79.3%, 47% and 28% for a rated load of 5.1Nm and light loads of 2Nm and 1Nm respectively. Consequently, the proposed drive scheme gives improvements of 1.5%, 33.8% and 52.8% respectively for the 5.1Nm, 2Nm and 1Nm loads over that of the conventionally-driven CRSPIM. The corresponding improvement in power consumption is a decrease of 1.6%, 45.1% and 67.6% for loads of 5.1Nm, 2Nm and 1Nm respectively.These results unveil the capability of the proposed scheme toachieve significant energy saving at light loads. The scheme is potentially able to cancel undesirable noise, reduce energy cost of running the motor, and offer possibility of cumulative savings in electric power resources of electric utilities.

TABLE OF CONTENTS

TITLE PAGE **Error! Bookmark not defined.**

DECLARATION ii

CERTIFICATION iii

DEDICATION iv

ACKNOWLEDGEMENT v

ABSTRACT viii

TABLE OF CONTENTS ix

LIST OF FIGURES xvii

LIST OF TABLES xxiiiiii

LIST OF ABBREVIATIONS xxiiiiv

CHAPTER ONE: INTRODUCTION 1

1.1 BACKGROUND 1

1.2 MOTIVATION 2

1.3 SIGNIFICANCE OF RESEARCH 2

1.4 PROBLEM STATEMENT 3

1.5 AIM AND OBJECTIVES 3

1.6 METHODOLOGY 4

1.7 THESIS OUTLINE 5

CHAPTER TWO: LITERATURE REVIEW 6

2.1 INTRODUCTION 6

2.2 OVERVIEW OF FUNDAMENTAL CONCEPTS 6

2.2.1 Single Phase Induction Machine 6

2.2.2 The Single Phase Induction Motor Theory 8

2.2.2.1 Main winding of the single phase induction machine 9

2.2.2.2 Main and auxiliary windings of the single phase induction machine 11

2.2.2.3 Torque – slip characteristics of the single phase induction machine 14

2.2.2.4 Modeling of the single phase induction machine 17

2.2.2.5 Voltage and torque equations in machine variables 19

2.2.2.6 Voltage and torque equations in the arbitrary reference frame 22

2.2.2.7 Torque produced by the capacitor-run single phase induction machine 26

2.2.2.8 Condition for zero pulsating torque 28

2.2.2.9 Analysis of auxiliary winding voltage control of the single phase Induction machine 28

2.2.2.10 Generalized condition for balanced stator currents 31

2.2.3 Inverters 34

2.2.3.1 Voltage source inverters 34

2.2.3.2 Single phase inverters 35

2.2.3.3 Pulse width modulation in inverters 38

2.2.3.4 Sinusoidal pulse width modulation (SPWM) technique 39

2.2.3.5 Pulse width modulated single phase inverter under the unipolar voltage switching 39
2.2.3.6 Inverter topologies for two phase applications 46

2.2.4 Dynamic Modeling of the Single and Two Phase Inverter 52

2.2.5 LC Filter Design 54

2.2.6 Pulse Width Modulated Induction Motor Drive 55

2.2.7 Controller Design 56

2.2.7.1 Frequency response overview 58

2.2.8 Induction Machine Speed and Torque Control 59

2.2.8.1 Control principles of the induction machine 59

2.2.9 Reference Frame Transformation 62

2.2.10 Vector Control Strategy 65

2.2.11 Efficiency Optimization 70

2.2.12 Harmonic Balance Technique (HBT) 69

2.2.13 Fundamental Concepts of AC Machine Windings 73

2.2.13.1 Machine winding terminologies 73

2.2.13.2 Classification of AC windings 75

2.2.13.3 Single phase induction machine winding design 77

2.2.13.4 Poly-phase double-layer winding 81

2.2.13.5 Two phase winding layout 83

2.3 REVIEW OF SIMILAR WORKS 85

CHAPTER THREE: MATERIALS AND METHOD 93

3.1 INTRODUCTION 93

3.2 GENERALIZED MODEL DEVELOPMENT FOR THE CRSPIM 94

3.2.1 Derivation of Winding Inductances 96

3.2.1.1 Stator magnetizing inductances 97

3.2.1.2 Rotor magnetizing inductances 98

3.2.1.3 Stator mutual inductances 98

3.2.1.4 Rotor Mutual Inductances 98

3.2.1.5 Stator - rotor mutual inductances 99

3.2.2 Turn's Transformation 101

3.2.3 Stationary Reference frame Transformation of Stator Variables 104

3.2.4 Stationary Reference frame Transformation of Rotor Variables 106

3.2.5 Transformation of Flux Linkages 107

3.2.6 Equivalent Circuit of the SPIM with Non-Quadrature Winding 108

3.2.7 Torque Equation 109

3.2.8 Generalized Steady State Model of the CRSPIM Using HBT. 110

3.3 MODEL VALIDATION 114

3.4 INFLUENCE OF SPATIAL ANGLE ∂ ON THE TORQUE PRODUCTION 120

3.4.1 Application of Balanced Condition to the 60^0 and 90^0 Configurations for Best Torque Performance 121

3.4.1.1 Steps taken to study the effects of imposing balanced currents in the stator windings of the single phase induction machine. 121

3.5 DEVELOPMENT OF A PWM INVERTER DRIVE FOR STANDARD SPIM TORQUE PERFORMANCE IMPROVEMENTS 123

3.5.1 Model Equations of the Rectifier and its Filter 124

3.5.2 Model Equations of the Inverter and its Filter 124

3.5.3 Model of the Conventional Single Phase Induction Machine 126

3.6 DEVELOPMENT OF A PID CONTROLLER FOR THE INVERTER DRIVE 126

3.6.1 Modeling of the Single Phase PWM Inverter Drive 128

3.6.2 Controller Structure for a Single Phase Inverter Drive 129

3.6.3 Controller Parameters 131

3.6.4 Computation of Reference Voltage 133

3.6.5 Flow Chart 133

3.7 PROBLEM WITH THE METHOD OF USING A PULSE WIDTH MODULATED INVERTER AND A PID CONTROLLER 138

3.8 MODEL OF THE MODIFIED SINGLE PHASE INDUCTION MACHINE 139

3.9 DEVELOPMENT OF A SINUSOIDAL PWM OPEN LOOP INVERTER DRIVE STRATEGY FOR THE MODIFIED SPIM 140

3.9.1 Model Equations of the Inverter and its Filters 142

3.10 DEVELOPMENT OF CLOSED LOOP CONTROL STRATEGY FOR THE MODIFED SPIM 145

3.10.1 Transformation of the Modified SPIM Model Equations from Stationary to Synchronous Reference Frame 146

3.10.1.1 Transformation of stator voltage equation 146

3.10.1.2 Transformation of rotor voltage equations 147

3.10.1.3 Transformation of flux linkages 147

*3.10.1.4Transformation of torque equatio*n 148

3.10.2 Development of the Vector Control Scheme 148

3.10.2.1 Formulation of the rotor flux oriented vector control scheme 149

3.10.2.2 Controller design 152

3.11 DEVELOPMENT OF THE PROPOSED EFFICIENCY OPTIMIZING SCHEME 157

3.11.1 Voltage Equations in Steady State 158

3.11.2 Electrical Power Loss 159

3.12 MODIFIED SPIM WINDING LAYOUT 165

3.12.1 Development of Modified SPIM Winding Layout Design 165

3.12.1.1 Design of modified SPIM winding layout 166

3.12.1.2 Assignment of coils to phases A and B 166

CHAPTER FOUR: RESULTS AND DISCUSSION 168

4.1 DYNAMIC AND STEADY STATE SIMULATION OF THE CRSPIM 168

4.1.1 Simulation Results of the Dynamic Behavior of the CRSPIM 168

4.1.2 Simulation Results of the Steady State Behavior of the CRSPIM 176

4.2 INFLUENCE OF DISPLACEMENT ANGLE ∂ ON THE TORQUE PRODUCTION AND EFFICIENCY PROFILE OF THE CRSPIM 179

4.3 EFFECTS OF APPLYING BALANCED CONDITION TO THE 60^0 AND 90^0 CONFIGURATIONS FOR BEST TORQUE PERFORMANCE 184

4.4 SIMULATION RESULTS OF PULSE WIDTH MODULATED INVERTER DRIVE USING A PID CONTROLLER 188

4.5 SIMULATION RESULTS FOR OPEN LOOP CONTROL STRATEGY 197

4.5.1 Dynamic Torque Performances of the Modified Single Phase Induction Machine 197

4.6 VARIATION OF ROTOR FLUX WITH ELECTRICAL LOSS AND EFFICIENCY IN THE MODIFIED SPIM 2 202

4.7 SIMULATION RESULTS OFTHE EFFICIENCY OPTIMIZING VECTOR-CONTROLLEDSTRATEGY 212

4.8 MODIFIED SPIM WINDING LAYOUT DESIGN RESULTS 229

4.8.1 Coil Connections 233

4.8.2 Establishing the Direction of Current in Coil Sides 234

CHAPTER FIVE: CONCLUSION AND SUGGESTIONS FOR FURTHER WORK 236

5.1 SUMMARY 236

5.2 CONCLUSION 237

5.3 LIMITATIONS 241

5.4 SIGNIFICANT CONTRIBUTIONS 241

5.5 SUGGESTIONS FOR FURTHER WORK 242

REFERENCES 244

APPENDICES

Appendix A: Parameters of CRSPIM 1 and CRSPIM 2 240

Appendix B: Derivation of Expressions for Winding Currents 241

Appendix C: Program Listings 243

LIST OF FIGURES

Figure 2.1: Squirrel Cage Induction Motor Rotor 9

Figure 2.2: Capacitor-Run Single Phase Induction Machine 9

Figure 2.3: Equivalent Circuit for the Single Phase Induction Motor 10

Figure 2.4: Equivalent Circuits of the Capacitor-Run Single Phase Induction Machine 12

Figure 2.5: Simplified Equivalent Circuits of the Capacitor-Run Single Phase Induction Machine 13

Figure 2.6: Schematic Diagram of the Capacitor-Run Single Phase Induction Machine 14

Figure 2.7: Torque versus Slip Characteristics of the Single Phase Induction Machine 16

Figure 2.8: Cross-section of the Single Phase Induction Machine 18

Figure 2.9: Spatial Arrangement of the Stator and Rotor Circuits 18

Figure 2.10: q – d Equivalent Circuit of the Single Phase Induction Machine 25

Figure 2.11: Schematic Representation of the Stator Windings and Terminal Connections ofthe CRSPIM 32

Figure 2.12 One Phase Leg of an Inverter 35

Figure 2.13: Single Phase Half Bridge Inverter 36

Figure 2.14: Output Waveform of the Half-Bridge Inverter 37

Figure 2.15: Single Phase Full Bridge Inverter 39

Figure 2.16: Comparators used to Control the ON and OFF States of the Power Switches 39

Figure 2.17: Output of the SPWM Circuit with a Sinusoidal Control Voltage Applied to its Input 42

Figure 2.18: Single Phase Full Bridge Topology 46

Figure 2.19: Two-Phase Two Leg Inverter Topology 47

Figure 2.20: Two-Phase Inverter with Six-Transistor Bridge Supplying a Capacitor-lessMotor 48

Figure 2.21: Two Phase Inverter with Six Transistor Bridge 49

Figure 2.22: Two Phase Full Bridge Inverter 49

Figure 2.23: Two Phase Half Bridge Inverter 50

Figure 2.24: Single Phase Half Bridge Inverter with Power Factor Correction 49

Figure 2.25: Single Phase Inverter with Auxiliary Winding Control 49

Figure 2.26: Single Phase AC-DC-AC Converter 54

Figure 2.27: Block Diagram of an Induction Motor Drive System 55

Figure 2.28: Per-Phase Equivalent Circuit of a Three Phase Induction Machine 60

Figure 2.29: α-β and q-d Rotating Frame Vector Representation. 64

Figure 2.30: Phasor Diagram of the Vector Control Strategy 68

Figure 2.31: Block Diagram of the Indirect Rotor Flux Oriented Control Scheme 69

Figure 2.32: One Turn Coil 73

Figure 2.33: Winding Diagram of the Stator of a 4-Pole, 32 slots CRSPIM 81

Figure 2.34: One Line Diagram of a Two Phase Four Pole Winding Layout. 83

Figure 3.1: Schematic Cross-Section of a SPIM with Arbitrary Angle ∂ between the axis of the Stator Windings 94

Figure 3.2: Spatial Arrangement of the Stator and Rotor circuits 95

Figure 3.3: Winding Terminal Arrangement of a Two-Coil Single Phase Induction Machine 97

Figure 3.4: Schematic Representation of Configuration of the Stator Windings of the CRSPIM 106

Figure 3.5: Equivalent Circuit of a SPIM with Non-Quadrature Windings 109

Figure 3.6: Flow Chart for the Solution of the Dynamic Model 116

Figure 3.7: Simulink Model 114

Figure 3.8: Flow Chart for the Solution of the Equations of the Steady State Model 116

Figure 3.9: Pulse Width Modulated Inverter-Drive 124

Figure 3.10: Single Phase PWM Inverter Drive Model 128

Figure 3.11: A Simplified Model of the PWM Single Phase Inverter Drive 129

Figure 3.12: Closed Loop Control of the Single Phase Inverter Drive 130

Figure 3.13: Closed Loop Frequency Response for System 1 132

Figure 3.14: Closed Loop Frequency Response for System 2 133

Figure 3.15: Flow Chart of the Control Algorithm 134

Figure 3.16: Simulink Realization of the PWM Inverter-Driven SPIM 135

Figure 3.17: Rectifier Block 136

Figure 3.18: PWM Block 136

Figure 3.19: Inverter Block 136

Figure 3.20: Single Phase Induction Machine Block 137

Figure 3.21: Reference Voltage Computation Block 138

Figure 3.22: Two Phase Two Leg Inverter Topology Connected to the Modified SPIM 141

Figure 3.23: Simulink Implementation of the Open Loop Control of Inverter-Driven Modified SPIM 145

Figure 3.24: Modified Single Phase Induction Motor q-d axes Equivalent Circuits 150

Figure 3.25: Control Block Diagram for Stator Current Control 153

Figure 3.26: Control Block Diagram for Rotor Flux Control 154

Figure 3.27: Control Block Diagram for Speed Control 155

Figure 3.28: Modified Single Phase Induction Motor q-d Axes Equivalent Circuits with Core Loss Resistance 157

Figure 3.29: Block Diagram of Vector Control Strategy with Efficiency-Optimizing Function 162

Figure 3.30: Flow Chart for the Indirect Vector-Controlled Induction Motor 163

Figure 3.31: Simulink Implementation of the Efficiency-Optimizing Vector- Controlled Modified SPIM 164

Figure 4.1: Machine Variables of the CRSPIM under No-Load 169

Figure 4.2: Starting Characteristics and Load Response of the CRSPIM showing Vqs,Vds, TLoad and Te 171

Figure 4.3: Starting Characteristics and Load Response of the CRSPIM showing ωr, Vc, Iqs and Ids 172

Figure 4.4: Waveform of Voltages across the Main and Auxiliary Windings in about 2 Periods 173

Figure 4.5: Waveform of Currents in the Main and Auxiliary Windings of the Stator in about 2 Periods 174

Figure 4.6: Rotor Speed Super-Imposed on Current Flowing in the Auxiliary Winding 174

Figure 4.7: Dynamic Torque - Speed Characteristics of the CRSPIM 176

Figure 4.8: Torque – Speed Characteristics 177

Figure 4.9: Efficiency versus Speed 178

Figure 4.10: Phase Angle of Currents in Main and Auxiliary Winding versus Speed 179

Figure 4.11: Average Torque versus Motor speed for ∂ between 0^0 and 180^0 180

Figure 4.12: Pulsating Torque Magnitude versus Motor speed for ∂ between 0^0 and 180^0 181

Figure 4.13: Efficiency versus Motor speed for ∂ between 0^0 and 180^0 181

Figure 4.14: Average Torque versus Motor speed for ∂ Equal to 60^0 and 90^0 182

Figure 4.15: Pulsating Torque Magnitude versus Motor Speed for ∂ Equal to 60^0 and 90^0 183

Figure 4.16: Efficiency versus Motor Speed for ∂ Equal to 60^0 and 90^0 183

Figure 4.17: Average Torque versus Motor Speed 185

Figure 4.18: Magnitude of Torque Pulsations versus Motor Speed 186

Figure 4.19: Estimated Auxiliary Winding Voltage versus Speed 186

Figure 4.20: Estimated Auxiliary Winding Phase Angle 188

Figure 4.21: Dynamic Torque Production in the Inverter-driven Machine 1 189

Figure 4.22: Dynamic Torque Production in the Capacitor-Run Machine1 190

Figure 4.23: Speed versus Time Characteristics of the Inverter-Driven Machine 1 190

Figure 4.24: Speed versus Time Characteristics of the Capacitor-Run Machine 1 191

Figure 4.25: Dynamic Torque Production in Inverter-Driven Machine 2 192

Figure 4.26: Dynamic Torque Production in the Capacitor-Run Machine 2 193

Figure 4.27Speed versus Time Characteristics of the Capacitor-Run Machine 2 194

Figure 4.28: Speed versus Time Characteristics of the Inverter-Driven Machine 2 194

Figure 4.29: Sine–Triangular Wave Comparison of the Inverter Drive of Machine 1 195

Figure 4.30: Switching Functions of the Inverter Drive of Machine 1 196

Figure 4.31: Actual Inverter Output Voltage and Reference Voltage versus Time 197

Figure 4.32: Reference and Actual Auxiliary Winding Voltage between 0 and 0.1s for Machine 1 198

Figure 4.33: Main Winding Voltage and Auxiliary Winding Voltage for Machine 1 198

Figure 4.34: Main Winding Voltage and Auxiliary Winding Voltage in 2 Periods for Machine1 198

Figure 4.35: Main Winding Current and Auxiliary Winding Current for Machine1 200

Figure 4.36: Main Winding Current and Auxiliary Winding Current for Machine 1 between 1.1s and 1.13s. 200

Figure 4.37: Sine–Triangular Wave Comparison of the Inverter Drive of Machine 2 200

Figure 4.38: Switching Functions of the Inverter Drive for Machine 2 202

Figure 4.39: Reference and Actual Auxiliary Winding Voltage for Inverter Drive of Machine 2 202

Figure 4.40: Reference and Actual Auxiliary Winding Voltage between 0 and 0.1s for Machine 2 203

Figure 4.41: Main Winding Voltage and Auxiliary Winding Voltage for Machine 2 203

Figure 4.42: Main Winding Voltage and Auxiliary Winding Voltage in 2 Periods for Machine 2 203

Figure 4.43: Main Winding Current and Auxiliary Winding Current for Machine 2 204

Figure 4.44: Main Winding Current versus Auxiliary Winding Current in 2 Periods for Machine 2 204

Figure 4.45: Dynamic Torque of the Inverter-Driven Modified SPIM 1 with Open Loop Control 198

Figure 4.46: Dynamic Torque of the Inverter-Driven Modified SPIM 2 with Open Loop Control 198

Figure 4.47: Sine–Triangular Wave Comparison of the Inverter Drive of the Modified SPIM2208

Figure 4.48Switching Functions of the Inverter Drive of Modified SPIM 2 209

Figure 4.49: Stator Winding Voltages of Modified SPIM 2 over 2 Periods 209

Figure 4.50: Stator Winding Currents in the Modified SPIM 2 for 2 Periods. 210

Figure 4.51: Electrical Power Loss Versus Flux at Rated Speed for Rated, 2Nm and 1Nm Load Torques 211

Figure 4.52: Efficiency versus Flux for Rated, 2Nm and 1Nm load torques 212

Figure 4.53: Load Torque Applied to the CRSPIM 2 and the Modified SPIM 2 214

Figure 4.54: Sine–Triangular Wave Comparison of the Vector-Controlled Drive of the Modified SPIM 2 215

Figure 4.55: Stator Winding Voltages in the Modified SPIM 2 for 2 Periods 217

Figure 4.56: Stator Winding Currents in the Modified SPIM 2 for 2 Periods 217

Figure 4.57: Electromagnetic Torque Produced in the CRSPIM 2 and the Modified SPIM 2 218

Figure 4.58: Speed with Time in the CRSPIM 2 and the Modified SPIM 2 219

Figure 4.59: Flux in the CRSPIM 2 and the Vector-Controlled Modified SPIM 2 with Time 219

Figure 4.60: Reference and Actual d-axis Current in the Vector-Controlled Modified SPIM 2 220

Figure 4.61: Reference and Actual q-axis Current in the Vector-Controlled Modified SPIM 2 221

Figure 4.62: Electrical Power Loss in the CRSPIM and the Vector-Controlled Modified SPIM 2 with Time 222

Figure 4.63: Efficiency in the CRSPIM 2 and the Vector-Controlled Modified SPIM 2 with Time 224

Figure 4.64: Input Power in the CRSPIM 2 and the Vector-Controlled Modified SPIM 2 with Time 225

Figure 4.65: Stator Voltages of the vector-controlled Modified SPIM with the Efficiency-Optimizing Function 226

Figure 4.66: Stator Voltages with Time for the CRSPIM 2 227

Figure 4.67: Stator Currents of the Vector-Controlled Modified SPIM 2 with the Efficiency-Optimizing Function 228

Figure 4.68: Stator Currents of the CRSPIM 2 with Time 228

Figure 4.69: Winding Clock Diagram 232

Figure 4.70: Two Phase, Double layer, Fractional Pitch Integral Slot Winding Layout 233

LIST OF TABLES

Table 2.1: Switching State of the Unipolar SPWM and the Corresponding Voltage Levels 45

Table 2.2: Classification of Induction Motor Control Strategies 59

Table 2.3: Arrangement of the Main Winding in Slots for a 4-Pole, 32 Slots CRSPIM 80

Table 3.1: Drive Circuit Pameters of Machine 1 125

Table 3.2: Drive Circuit Pameters of Machine 2 125

Table 3.3: Parameters of the Modified SPIM 1 143

Table 3.4: Parameters of the Modified SPIM 2 143

Table 3.5: DC Voltage and Filter Component Values for the Drive of Modified SPIM 1 144

Table 3.6: DC Voltage and Filter Component Values for the Drive of Modified SPIM 2 144

Table 4.1: Winding Layout Design Parameters 229

Table 4.2: Winding Layout Table for the Modified SPIM 2 230

Table 4.3: Differences between the Modified SPIM 2 Winding Layout and the Layout of the Existing SPIM 2 234

Table A.1: Parameters of the CRSPIM 1 252

Table A.2: Parameters of the CRSPIM 2 252

LIST OF ABBREVIATIONS

AC	Alternating Current
CRSPIM	Capacitor-Run Single Phase Induction Machine
CSI	Current Source Inverter
d	Direct
DC	Direct Current
E.M.F	Electromotive Force
GTOs	Gate Turn-on Thyristors
HBT	Harmonic Balance Technique
HVACs	Heating, Ventilating and Air Conditioning Systems
Ids	d-axis stator current
IGBTs	Insulated Gate Bipolar Transistors
Iqs	q-axis stator current
k_D	Derivative Gain
k_I	Integral Gain
k_p	Proportional Gain
LC	Inductance Capacitance
MMF	Magneto-Motive Force
PI	Proportional plus Integral
PID	Proportional Derivative Integral
PWM	Pulse Width Modulation
q	Quadrature
S_m	Slip at the point of maximum torque
SPIM	Single Phase Induction Machine
SPWM	Sinusoidal Pulse Width Modulation

T_{avg}	Average or useful torque
Te	Electromagnetic Torque
TLoad	Load torque
T_m	Maximum torque
T_{puls}	Pulsating torque
T_{st}	Starting torque
Vc	Capacitor voltage
Vds	d-axis stator voltage
VFDs	Variable Frequency Drives
Vqs	q-axis stator voltage
VSDs	Variable Speed Drives
VSI	Voltage Source Inverter
ω_n	Natural frequency
ωr	Rotor speed
α	Alpha
β	Beta
∂	Del
ζ	Damping ratio

CHAPTER ONE

INTRODUCTION

1.1 BACKGROUND

Capacitor-run single phase induction motors (CRSPIMs) are designed to operate at a fixed speed and to drive rated loads in a variety of applications such as heating, ventilating and air conditioning systems (HVACs), pumps, compressors, fans, washing machines, hand driers, machine tools, grinding machines, vacuum cleaners, elevators etc. While driving rated loads, the currents in the main and auxiliary windings of the motors are approximately balanced at the rated load and speed (Pei *et al*,2016). Balanced currents refer to currents whose phase angle difference is equal to 90^0 and whosemagnitude ratio is equal to the effective winding turns' ratio. At any other load and speed, the winding voltages and currents are unbalanced (Muljadi *et al.*, 1993; Krause *et al.*2002; Chomat and Lipo, 2003; Krischan *et al.*, 2008) and this situation causes low efficiency and increased torque pulsations with associated high noise levels (Blaabjerg *et al.*, 2004; Mademlis *et al.* 2005; Asghari and Fallah, 2012; Hosseini, 2016). In reality, some industrial, commercial and residential loads driven by SPIMs reduce with time and this load reduction is accompanied by increase in speed (Spirov, 2016). As a result, motor efficiency reduces and torque pulsation levels in the machine increase, leading to undesirable noise and vibrations in the machine (Park, 2001; Zahedi and Vaez-Zadeh, 2009). Furthermore, a lot of energy is wasted at light load operations because conventional SPIMs typically utilize between 60% and 80% of rated input power even when operating at less than half load (Saidur *et al.*, 2012). It is known that electrical losses in alternating current (ac) induction machines can be reduced by reducing the magnitude of currents in the machine windings and by reducing the air-gap flux (Benbouzid *et al.*, 1996; Dong, 2005). Studies have shown that there is an air-gap flux density in

an ac induction motor that produces minimum losses for any given load applied to the machine(Naxin *et al.,* 2004; Dong, 2005). By adjusting motor flux to meet load requirements, significant improvements in motor efficiency can be achieved. In addition, significant energy savings can be achieved as well because power losses are reduced with reductions in flux levels in the machine. In this research,the supply of balanced voltages and currents to the windings of the single phase induction machine has been examined and a drive system that regulates the flux and the output torque, while maintaining a constant speed, in a single phase induction machinehas been developedto eliminate torque pulsations at steady state and to increase motor efficiency at light loads.

1.2 MOTIVATION

The problem of high torque pulsations and low efficiency in existing single phase induction machines has been examined by several researchers for more than fifteen years now. Most of these research have been dedicated to improving motor efficiency and reducing torque pulsations at or near rated load operating point. Only very few publications treat performance improvement of these machines at light load (or non-rated) operations and even then these publicationssuch as (Mademlis *et al*., 2005;Zahedi and Vaez-Zadeh, 2009;Caruso *et al*, 2012; Jang, 2013)have focused on speed regulation and not optimal flux regulation in single phase induction motors. The motivation for this research, therefore, arises from a desire to fill this gap in the research to improve the performances of single phase induction machines.

1.3 SIGNIFICANCE OF RESEARCH

In Nigeria today, people still experience severe shortage of electric power to meet domestic and industrial needs. To alleviate this shortage situation, there is need for installation of new generating plants and the effective utilization of existing power resources. Unfortunately, very

little attention has been focused on efficiency improvement and effective utilization of existing resources. This research starts to look at the single phase induction machine which is a large consumer of domestic power supply with the goal of improving its operation. Efficiency improvement will potentially enable this machine to consume less power and hence reduce running cost thereby making it possible for the limited electric power resources of electric utilities to meet the needs of more customers. With reduced heat loss and noise as consequences of the elimination of torque pulsations, the environment will be safer. It is within this context that this research finds significant national importance and relevance at this time.

1.4 PROBLEM STATEMENT

The Capacitor-run single phase induction motorsuffers from low efficiency when operating under non-rated conditions. This situation leads to wastage of significant amount of electric power since rated voltage is applied fully across its terminals and the flux in the machine operates approximately at rated value regardless of the applied load on the machine. Moreover, during starting and at steady state, the motor exhibits a significant level of torque pulsations which gives rise to noise and vibration in the machine. These conditions of low efficiency at light loads and vibrations lead to electrical, thermal and mechanical stresses on the machine which invariably threatens its useful life. Furthermore, the use of centrifugal switch and capacitors make this motor susceptible to failure should there be a malfunction of any or both of these devices.

1.5AIM AND OBJECTIVES

The aim of this study is to developa scheme to improve the efficiency and torque production in the single phase induction machine using a sinusoidal pulse width modulation (SPWM) control scheme. The objectives of the research are as follows;

a) To evaluate the performances of the existing CRSPIM and to change the spatial angular displacement of stator windings in the existing CRSPIM with a view to exploring any gains in terms of torque production and efficiency.
b) To formulate a method to supply balanced currents to existing CRSPIMs with a view to eliminating torque pulsations during steady state operation.
c) Toformulate a method to increase the efficiency and to reduce the level of power consumption in the existing SPIMsignificantly at light loads.
d) To simulate and compare performances of the SPIM under the proposed drive scheme with performances of the line operatedCRSPIM.
e) To develop an improved stator winding layout for torque and efficiency improvement in existing single phase induction machines.

1.6METHODOLOGY

A brief summary of the methodology followed in this research work is outlined as follows;

a) Application of reference frame transformation and harmonic balance techniques to develop a generalized model for the simulation of the dynamic and steady state performances of the existing CRSPIM.
b) Adoption of an appropriate inverter topology for the scheme. Identification and development ofcontrol strategies utilizing sinusoidal pulse width modulation that will enable elimination of torque pulsations at steady state.
c) Engagement of an efficiency-optimizing formulation to be used for investigatingthe performance of the inverter-drive schemeand assessing its contribution to efficiency improvement.

d) Application of MATLAB/Simulink software to simulate and compare the performances of the proposed motor drive scheme to those of an existing line-operated capacitor-run single phase induction machine.

e) Application of standard winding layout design techniques to develop an improved stator winding layout for the existing machine.

1.7THESIS OUTLINE

Chapter one of this thesis provides the research background information. It also provides information on the aim and objectives of the research. The research motivation, problem, methodology and the significance of research are discussed as well.

Chapter two reviews existing literature and fundamental concepts relevant to the research.

Chapter three details the materials and methods applied to tackle the research problem while chapter four discusses the results obtained in this work.

Chapter five summarizes the research findings. It gives the limitations observed in the work and suggestions for further work. It also outlines the significant contributions made to the body of knowledge and finally concludes the thesis.

CHAPTER TWO

LITERATURE REVIEW

2.1 INTRODUCTION

This section contains an overview of concepts fundamental to the research. It also contains a review of research works that are similar to this study.

2.2 OVERVIEW OF FUNDAMENTAL CONCEPTS

The concepts discussed in this section include the general introduction of the single phase induction motors, the theory of single phase induction motor, inverters and associated pulse width modulation (PWM) techniques. The principles of inductance capacitance (LC) filter design, the induction motor control and associated controller design are described as well. Finally, the concepts of efficiency optimization and ac machine winding with focus on single and two phase winding are also discussed in this section.

2.2.1 Single Phase Induction Machine

The traditional single phase induction machine has only one winding and a push of its shaft makes its rotor rotate either clockwise or anti-clockwise depending on the direction of push. If the machine is, however, run at a low speed, it tends to generate a high temperature rise due to excessive power loss and consequently operates at very low efficiency. Theories such as the cross field and the double revolving field theory (Veinott, 1970) have been used to explain this behavior. The quest for improved starting of the motors, higher efficiency and reliability prompted the introduction of a second winding on the stator called the auxiliary winding. The auxiliary winding is designed to have parameters that are different from those of the main

winding(Campos *et al.*2007; Feraga and Bouldjedri, 2012). A phase shift between the voltages or currents applied to the two windings makes the motor start all by itself(Baek *et al.,* 1996).

The connection of the auxiliary winding defines the type of single phase induction motor. In the split phase and capacitor-start type, the auxiliary winding is cut off from the supply by a centrifugal switch after the motor attains about 75% of rated speed(Mera and Câmpeanu, 2012; Sobhani *et al.,* 2013b).In the capacitor-run type, the auxiliary winding is left in the circuit when the motor operates. This type of single phase induction machines is the most common(Blaabjerg *et al.* 2004; Hosseini, 2016).The split phase type has a lower average torque than the capacitor-run type and cannot be used in applications where a high starting torque is required. The capacitor-run types have a higher average torque because they use capacitors in the auxiliary winding in order to produce a phase shift between the currents in the two asymmetric stator windings so that the motor may operate as a balanced two phase machine (Mademlis*et al*, 2005). Unfortunately, the magnitude of the current in the auxiliary winding is not the same as that of the current in the main winding throughout the motor speed range. Usually, two capacitors are used with the auxiliary winding to obtain a large starting torque and the best performance at rated conditions(Liu, 1995). Although these motors exhibit better performance than the traditional single phase induction machines, they are not able to give a balanced operation at speeds below or above the rated motor speed (Pei *et al*,2016).

Conventional single phase induction machines are supplied from a single phase fixed frequency ac power source and are used for residential, commercial and industrial applications (AsghariandFallah, 2012; Caruso *et al*, 2012). These applications include washing machines, hand driers, fans, pumps, compressors, refrigerators, dish washers, hand tools, etc. The machines are designed to operate at a single or fixed speed and are not controlled(Lee *et al.,* 2001;

Blaabjerg *et al.*, 2004; Vaez-Zadeh and Reicy 2005). In some applications like fans, single phase induction machines are made to run at two or more different values of speed but these values of speed are provided by means of winding tap changing brought about by manual intervention(Lee *et al.* 2001). Because of their large volume already in use worldwide, single phase induction machines consume a significant amount of the total electric power supplied to electric motors (Fating *et al,.* 2008; Latt and Win, 2009; Asghari and Fallah 2012). Unfortunately they operate at very low efficiencies when used in non-rated conditions (Zahedi and Vaez-Zadeh, 2009; Mera and Câmpeanu 2012; Ling *et al.* 2014). The single phase induction motor theory is discussed briefly in the next sub-section.

2.2.2 The Single Phase Induction Motor Theory

The single phase induction motor derives its name from the fact that the machine receives power from a single phase source and rotor currents are induced by the action of the magnetic fields set up by the stator windings. Most single phase induction motors use a squirrel cage rotor. This type of rotor has copper or aluminum bars placed inside slots cut in the inner surface of the rotor core. The bars are mutually short-circuited together at each end by means of a shorting ring. The squirrel cage rotors are generally cheap, reliable and easy to maintain. The squirrel cage rotor with iron laminations removed is illustrated in Figure 2.1 while the stator winding circuit diagram and machine frame are shown in Figure 2.2.



Figure 2.1: Squirrel Cage Induction Motor Rotor(Boldea and Nasar, 2002)

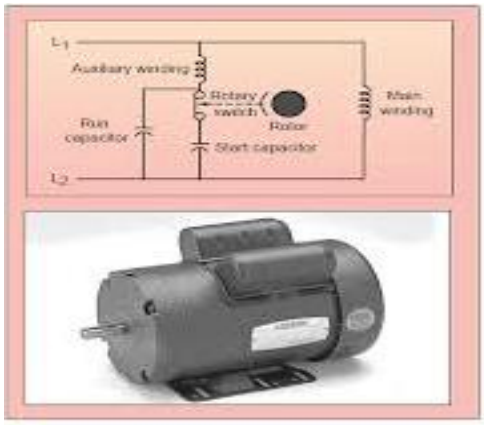


Figure 2.2: Capacitor-Run Single Phase Induction Machine
(http://www.studyelectrical.com/2015)

2.2.2.1 Main winding of the single phase induction machine

The traditional single phase induction motor has only one winding in the stator which has a resistance, leakage reactance and a given number of turns. It produces a magnetic field that is stationary in space and pulsates with time when the winding is excited by a single phase ac source. The field does not rotate and hence there is no tendency for the machine to start by itself. Two theories are used, traditionally, to analyze the operation and performance of single phase induction motors. These are the cross field and the revolving field theory. Although both theories have been used to develop quantitative methods of analysis which give similar results, the cross field theory is weak in the sense that it does not show the presence of currents of two frequencies

in the rotor bars as captured by the revolving field theory and as demonstrated by experimental investigations (Veinott, 1970).

As a result, the revolving field theory is more popular for use in analyzing the steady state behavior of the single phase induction motor than the cross field theory. From the point of view of the revolving field theory, the pulsating field set up by the main winding acting alone on the stator is considered to be the resultant of two synchronously rotating fields which have constant magnitude equal to one-half of the magnitude of the pulsating field but rotating in opposite directions. The two rotating magnetic fields are popularly called the forward and the backward rotating magnetic fields. These two fields theoretically impact on the rotor independently and have different effects on the rotor because of the difference in their speeds in relation to the rotor. The effect of each of the rotating fields on the rotor is represented by a parallel circuit consisting of two branches as shown in Figure 2.3. The figure gives the equivalent circuit of the single phase induction machine with only one winding present on the stator.

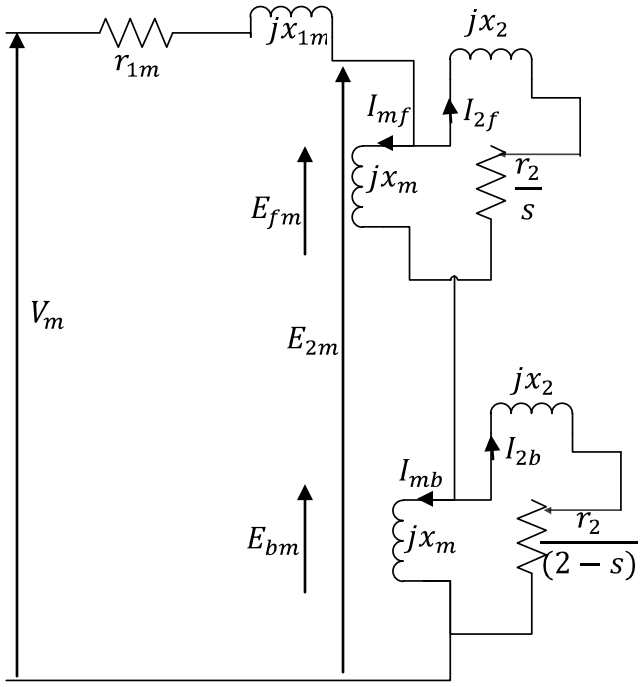


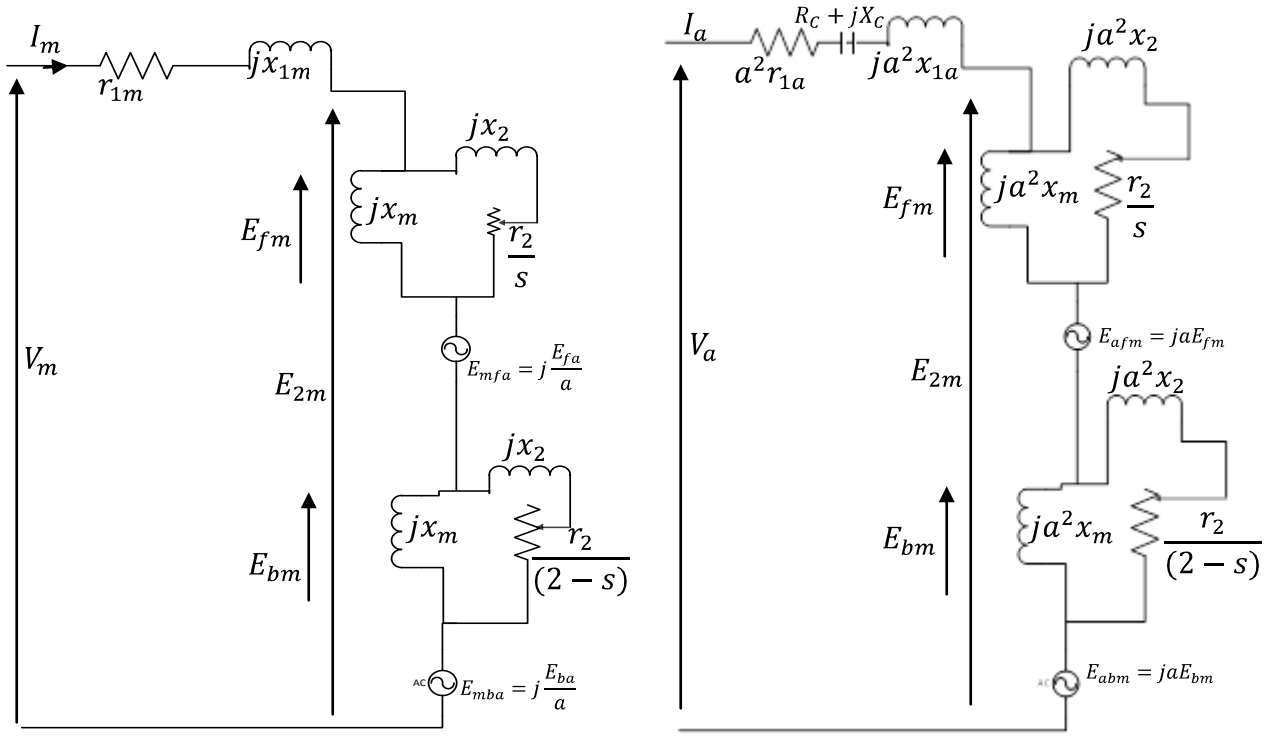
Figure 2.3: Equivalent Circuit for the Single Phase Induction Motor(Veinott, 1970)

$r_{1m}$is the resistance of the main winding; x_{1m} is the leakage reactance of the stator main winding. $x_m$is the magnetizing reactance due to mutual flux linking the stator and the rotor windings; V_m is the voltage applied to the main winding; E_{2m} is the total voltage induced in the stator; E_{fm} and E_{bm} are the voltages induced across the magnetizing branches of the main winding. *s* is the slip of the motor; I_{2f} and I_{2b} are the currents induced by the forward and backward fields in the rotor bars at frequencies *sf* and *(2-s)f* respectively; *f* is the frequency of the supply voltage. I_{mf}andI_{mb} are the magnetizing currents in the forward and backward field circuits of the rotor; r_2 and x_2 are respectively the resistance and leakage reactance of the rotor. As seen from Figure 2.3, the total voltage induced in the stator by the air-gap flux at any speed is the vector sum of $E_{fm}$and E_{bm}. (Veinott, 1970).

2.2.2.2 Main and auxiliary windings of the single phase induction machine

With an auxiliary winding in place on the stator having *a*-times as many turns as main winding (where *a* is positive real number) and displaced 90^0 in space away from the main winding, machine starting operation is improved over that of the machine with only the main winding on the stator (Ling *et al*, 2014). According to the revolving field theory, if both the auxiliary and main windings are supplied with power simultaneously, each winding sets up its own separate forward and backward fields. These fields superimpose withoutdistortion. The effect of these fields is represented in the equivalent circuits of Figure 2.4. Compared to Figure 2.3, there are two additional voltages E_{mfa} and E_{mba} in series with the forward and backward branches respectively for the main winding. These are the voltages induced in the main winding by the forward and backward rotating fields produced in the auxiliary winding. E_{afm} and E_{abm} apply to the auxiliary winding circuit and they are respectively the voltages induced in the auxiliary winding by the forward and backward rotating fields produced in the main winding. The

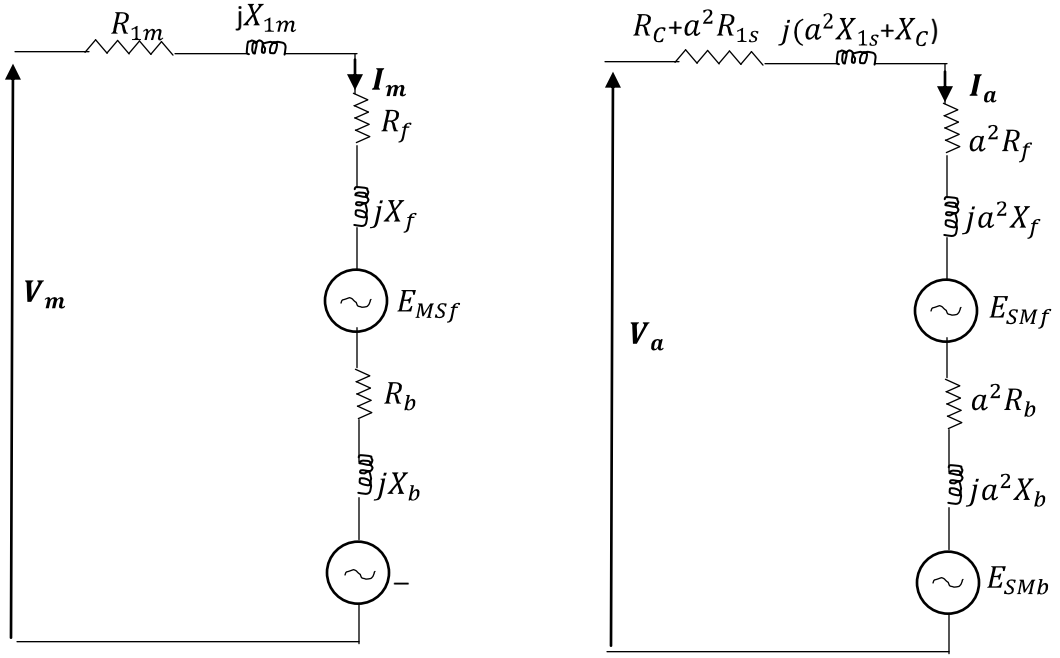
auxiliary winding, in the case of the capacitor-run motor, has a series capacitor connected to it as shown in Figure 2.4 (b) (Zahedi and Vaez-Zadeh, 2009).



(a) Stator Main Winding (b) Stator Auxiliary Winding

Figure 2.4: Equivalent Circuits of the Capacitor-Run Single Phase Induction Machine (Veinott, 1970)

$X_c$is the capacitive impedance of the series capacitor; $R_c$is the resistance of the capacitor; V_m is the voltage impressed on the main winding while V_a is the voltage applied to the auxiliary winding;$I_m$and $I_a$are the currents flowing in the main and auxiliary windings respectively. Figure 2.4 is often simplified to the equivalent circuit given in Figure 2.5 (Collins *et al*., 1988; Asghari and Fallah, 2012).



(a) Stator main winding (b) Stator auxiliary winding

Figure 2.5: Simplified Equivalent Circuits of the Capacitor-Run Single Phase Induction Machine(Collins *et al*. 1988)

R_f and X_f are the equivalent forward field resistance and reactance respectively while R_b and X_b are the equivalent backward field resistance and reactance respectively. They are defined as follows (Morrill 1929; Collins *et al.* 1988; Jang 2013):

$$R_f = \frac{\left[\frac{X_m^2 r_2}{2s}\right]}{\left[\left(\frac{r_2}{s}\right)^2 + (X_2 + X_m)^2\right]} \tag{2.1}$$

$$R_b = \frac{\left[\frac{X_m^2 r_2}{2(2-s)}\right]}{\left[\left(\frac{r_2}{(2-s)}\right)^2 + (X_2 + X_m)^2\right]} \tag{2.2}$$

$$X_f = \frac{\frac{X_m}{2}\left[\left(\frac{r_2}{s}\right)^2 + X_2(X_2 + X_m)\right]}{\left[\left(\frac{r_2}{s}\right)^2 + (X_2 + X_m)^2\right]} \tag{2.3}$$

$$X_b = \frac{\frac{X_m}{2}\left[\left(\frac{r_2}{(2-s)}\right)^2 + X_2(X_2 + X_m)\right]}{\left[\left(\frac{r_2}{(2-s)}\right)^2 + (X_2 + X_m)^2\right]} \tag{2.4}$$

The auxiliary winding is introduced for the purpose of starting the machine. When a capacitor is connected in series with the auxiliary winding, the capacitor ensures that a current whose phase lead is approximately $90^0$with respect to the main winding current, flows in the auxiliary winding and in addition tries to keep the ratio of the main winding current to the auxiliary winding current as close as possible to the turns ratio of the two windings at rated conditions. By so doing, the run capacitor reduces the torque pulsations significantly at rated conditions while also maintaining maximum efficiency at that operating point. This arrangement, however, has the disadvantage that motor performance is sacrificed at speeds other than the rated speed (Collins *et al.* 1988; Chomat and Lipo 2003; Asghari and Fallah 2012; Sobhani *et al.,* 2013a).The schematic diagram of the capacitor-run single phase induction machine is given in Figure 2.6

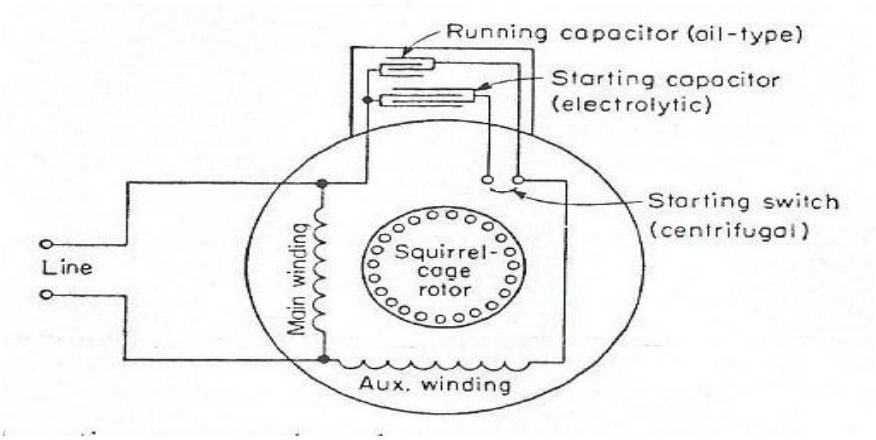


Figure 2.6: Schematic Diagram of the Capacitor-Run Single Phase Induction Machine (Veinott, 1970)

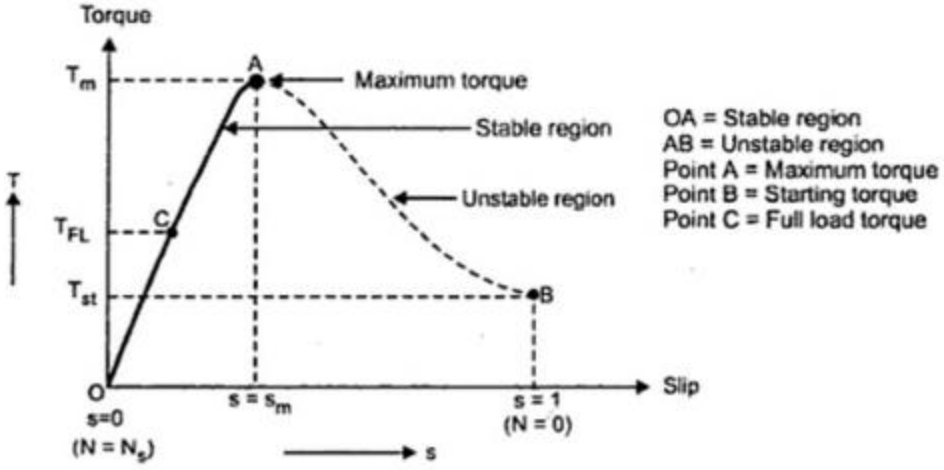
2.2.2.3 Torque – slip characteristics of the single phase induction machine

The behavior of the capacitor-run single phase induction motor can be understood from the torque – slip characteristics. A typical induction motor torque slip characteristics is shown in Figure 2.7. The plot is usually obtained by plotting the torque produced in the machine against the slip, *s* from standstill (i.e. *s = 1*) to synchronous speed (i.e. *s = 0*). The torque slip curve can

be divided into two regions, namely the low slip region and the high slip region. The two regions are discussed as follows;

a) Low Slip Region

In the low slip region, motor speed is high. The slip increases linearly with the torque produced in the machine. This is because as the load on the machine increases, the speed reduces thereby increasing slip. When slip increases, torque increases as well in order to satisfy the increasing load demand. However, if the load on the machine decreases, slip reduces since speed will increase while torque will reduce. When $s = 0$ at synchronous speed, torque becomes zero as well. The low slip region is often described as the stable region of operation because of this linearity in the relationship between torque and slip. Motor always operates at a point in this



region.(Chapman, 2012):

Figure 2.7: Torque versus Slip Characteristics of the Single Phase Induction Machine (http://yourelectrichome.blogspot.com.ng/2011)

b) High Slip Region

In the high slip region, slip approaches a value of 1 and motor speed is low. Torque is inversely proportional to the slip. When the load increases in this region, speed reduces as in the low slip region. However, as speed reduces due to increasing load, slip increases and torque decreases. As torque decreases, the slip further increases only to decrease the torque further since torque is inversely proportional to slip. Eventually, motor reaches a standstill condition (i.e. motor comes to rest) and it cannot continue to operate at any point in the high slip region. The high slip region is therefore often called the unstable region of motor operation(Chapman, 2012).

The low slip region ranges from $s = 0$ *to* $s = S_m$. S_m in Figure 2.7 is the slip at the point of maximum torque, (T_m). The maximum torque is the limiting torque. It is also called the breakdown torque. If a motor is loaded beyond its breakdown torque, slip pushes the motor into the high slip region and the motor breaks down at such a load. Motor operation is therefore restricted to the low slip region. The high slip region ranges from $s = s_m$ *to* $s = 1$. The starting torque (T_{st}) is the torque produced at the point when the motor starts (i.e. when the motor is turned on). The rated condition is described as the condition in which the motor is carrying its full or rated load (T_{fl}) while operating continuously at rated speed such that the current drawn from the supply is within safe limits due to such load. Any other condition apart from this is referred to as non-rated conditions(Blaabjerg *et al.* 2004; Zahedi and Vaez-Zadeh, 2009). The modeling of the single phase induction machine is presented next.

2.2.2.4 Modeling of the single phase induction machine

The dynamic modeling of the single phase induction machine is often accomplished using the reference frame theory. The theory establishes the voltage and torque equations in the stationary reference frame(Krause *et al.,* 2002). The dynamic operation of the single phase induction motors istypically predicted from these voltage and torque equations. The phasor equations used for predicting steady state operation of these machines are obtained from the dynamic voltage equations using either the symmetrical components theory or the harmonic balance technique. The basic steps typically followed in the modeling of the single phase induction machine are outlined as follows; (Krause *et al.*, 2002)

a) Making necessary assumptions.
b) Establishingthe voltage equations of the stator and the rotor windings by the application of Kirchoff's voltage law to the stator and rotor circuits.
c) Deriving winding inductances using the principle of winding functions.
d) Transforming real machine variables to an arbritrary (*d-q*) reference frame using the Park's transformation.
e) Applying the turn's transformation with a view to obtaining an equivalent circuit from the voltage equations of the machine.

A schematic cross-section of the single phase induction machine is shown in Figure 2.8

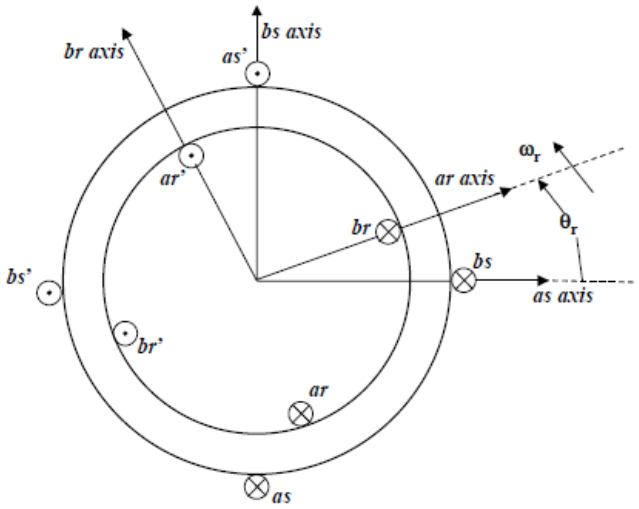


Figure 2.8: Schematic cross-section of the Single Phase Induction Machine (Omozusi, 1998)

Figure 2.9 shows the spatial arrangement of the stator and rotor circuits of the single phase induction motor.

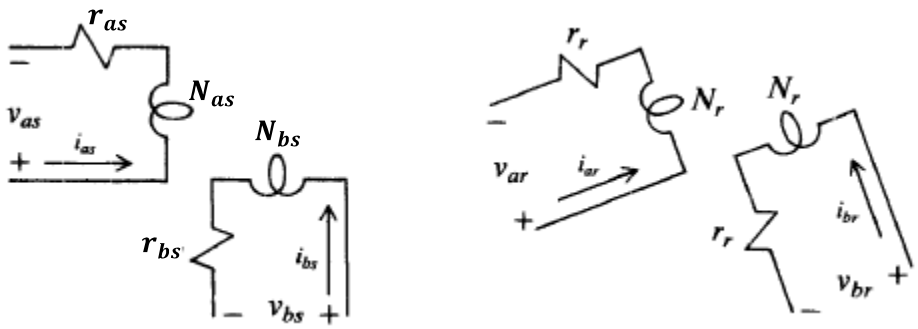


Figure 2.9: Spatial Arrangement of the Stator and Rotor Circuits(Krause *et al*, 2002)

As seen in Figures 2.8 and 2.9, the stator windings are non-identical. The windings are typically sinusoidally distributed and are arranged in space quadrature. The main or 'as' winding has N_{as} equivalent turns with resistance r_{as} while the auxiliary winding or 'bs' winding has N_{bs} equivalent turns with resistance r_{bs}. The rotor windings are considered as two identical sinusoidally distributed windings also arranged in space quadrature. The rotor windings are assumed to have N_r equivalent turns with resistance r_r;$V_{as}$is the voltage applied across the main

winding;$V_{bs}$is the voltage supplied to the auxiliary winding;$i_{as}$is the current flowing in the main winding;$i_{bs}$is the current flowing in the auxiliary winding;$V_{ar}$is the voltage applied across the a-axis winding of the rotor;$V_{br}$is the voltage applied across the b-axis winding of the rotor;$i_{ar}$is the current flowing in the a-axis winding of the rotor;$i_{br}$is the current flowing in the b-axis winding of the rotor.

All variables and parameters with subscript '*as'* are quantities of the main winding while the variables and parameters with subscript '*bs'* are quantities of the auxiliary winding. Similarly, all variables and parameters with subscript '*ar'* are quantities of the a-axis winding of the rotor while the variables and parameters with subscript '*br'* are quantities of the b-axis winding of the rotor. The parameters with subscript '*r*' represent the identical parameters of the two windings of the rotor. The assumptions typically made in the modeling of induction machines are given as follows; (Krause *et al*., 2002; Omozusi, 1998; Nied *et al*, 2013).

a) Stator windings are sinusoidally distributed
b) Saturation effects are ignored
c) Rotor circuit is represented by sinusoidal windings
d) Air gap distance is constant
e) Core has infinite permeability

A brief description of the development ofthe *d-q*voltage and torque equations of the single phase induction machine in the stationary reference frame isprovided in the following sections.

2.2.2.5 Voltage and torque equations in machine variables

The voltage equations expressed in machine variables may be written as follows (Omozusi 1998; Krause *et al.* 2002):

$$\boldsymbol{V}_{abs} = \boldsymbol{r}_{abs}\boldsymbol{i}_{abs} + p\boldsymbol{\lambda}_{abs} \qquad (2.5(a))$$

$$\boldsymbol{V}_{abr} = \boldsymbol{r_r i}_{abr} + p\boldsymbol{\lambda}_{abr} \quad (2.5(b))$$

Where:

$$(\boldsymbol{F}_{abs})^T = [f_{as} f_{bs}] \quad (2.6)$$

$$(\boldsymbol{F}_{abr})^T = [f_{ar} f_{br}] \quad (2.7)$$

$$\boldsymbol{r}_{abs} = diag[r_{as} r_{bs}] \quad (2.8)$$

$$\boldsymbol{r}_r = diag[r_r r_r] \quad (2.9)$$

f represents voltage V, current i or flux linkages λ;p is the differential operator. The stator and rotor flux linkages are given as (Omozusi 1998; Krause *et al.* 2002):

$$\begin{bmatrix}\boldsymbol{\lambda}_{abs}\\ \boldsymbol{\lambda}_{abr}\end{bmatrix} = \begin{bmatrix}\mathbf{L}_{\mathrm{s}} & \mathbf{L}_{\mathrm{sr}}\\ (\mathbf{L}_{\mathrm{sr}})^{\mathbf{T}} & \mathbf{L}_{\mathrm{r}}\end{bmatrix}\begin{bmatrix}\boldsymbol{i}_{abs}\\ \boldsymbol{i}_{abr}\end{bmatrix} \quad (2.10)$$

Where:

$$\boldsymbol{L_s} = \begin{bmatrix}L_{asas} & L_{asbs}\\ L_{bsas} & L_{bsbs}\end{bmatrix} + \begin{bmatrix}L_{las} & 0\\ 0 & L_{lbs}\end{bmatrix} \quad (2.11(a))$$

$$\boldsymbol{L_{sr}} = \begin{bmatrix}L_{asar} & L_{asbr}\\ L_{bsar} & L_{bsbr}\end{bmatrix} \quad (2.11(b))$$

$$(\mathbf{L_{sr}})^{\mathbf{T}} = \begin{bmatrix}L_{asar} & L_{bsar}\\ L_{asbr} & L_{bsbr}\end{bmatrix} \quad (2.11(c))$$

$$\boldsymbol{L_r} = \begin{bmatrix}L_{arar} & L_{arbr}\\ L_{brar} & L_{brbr}\end{bmatrix} + \begin{bmatrix}L_{lr} & 0\\ 0 & L_{lr}\end{bmatrix} \quad (2.11(d))$$

L_{asas} and L_{bsbs} are the magnetizing inductances of the stator windings. L_{arar} and L_{brbr} are the magnetizing inductances of the rotor windings. L_{las}, L_{lbs},*and* $L_{lr}$are the leakage inductances in the stator and rotor respectively. L_{asbs} *and* L_{bsas} are the stator mutual inductances. L_{arbr} *and* L_{brar} are the rotor mutual inductances. L_{asar}, L_{asbr}, L_{bsar}, L_{bsbr}, L_{aras}, L_{arbs}, L_{bras} *and* $L_{brbs}$are the rotor – stator mutual inductances. Each of the inductances are often determined by using winding function principles. This principle states that the inductance between any two windings '*j*' and '*k*' in any machine is expressed as (Omozusi, 1998):

$$L_{jk} = \frac{\mu_0 rl}{g} \int_0^{2\pi} N_j(\theta)\, N_k(\theta) d\theta \quad (2.12)$$

Where:

r is the average air-gap radius

l is the effective motor stack length

g is the length of air gap

θ is the angular position along the stator inner diameter

$N_j(\theta)$ is the winding function of winding '*j*'

$N_k(\theta)$ is the winding function of winding '*k*'

Closed form inductance equations are obtained by representing the winding functions by their respective fundamental components. The fundamental component of the winding functions of the stator and rotor windings are given as; (Omozusi, 1998)

$$N_{as}(\theta) = N_{as} cos\theta \quad (2.13)$$

$$N_{bs}(\theta) = N_{bs} sin\theta \quad (2.14)$$

$$N_{ar}(\theta) = N_r cos(\theta - \theta_r) \quad (2.15)$$

$$N_{br}(\theta) = N_r sin(\theta - \theta_r) \quad (2.16)$$

Where θ_r is the rotor angular position with respect to the stator. For a single phase machine with P number of poles, electromagnetic torque may be evaluated from the following expression (Krause *et al*., 2002):

$$T_e = \frac{P}{2} \frac{\partial W_m(i_j, \theta_r)}{\partial \theta_r} \quad (2.17)$$

Where subscript '*j*' represents the winding of stator and rotor. W_m is the stored mechanical energy assuming a magnetically linear system and is given by (Krause *et al*., 2002):

$$W_m = \frac{1}{2}(\boldsymbol{i}_{abs})^T(\boldsymbol{L}_s - L_{ls}\mathbf{I})\boldsymbol{i}_{abs} + (\boldsymbol{i}_{abs})^T \boldsymbol{L'_{sr}} \boldsymbol{i'}_{abr} + \frac{1}{2}(\boldsymbol{i'}_{abr})^T(\boldsymbol{L'}_r - L'_{lr}\mathbf{I})\boldsymbol{i'}_{abr} \quad (2.18)$$

Where **I** is an identity matrix. Equation (2.18) can be reduced to give the expression of the instantaneous electromagnetic torque, T_e in the machine. This expression is given as follows (Krause *et al.*, 2002):

$$T_e = \frac{P}{2}(\boldsymbol{i}_{abs})^T \frac{\partial}{\partial \theta_r}[(\boldsymbol{L}_{sr})^T]\boldsymbol{i}_{abr} \text{ (Nm)} \tag{2.19}$$

The torque and rotor speed are related as follows (Bhimbra 1980; Krause *et al.* 2002):

$$T_e = \frac{2J}{P} p\omega_r + T_L \tag{2.20}$$

Where J is the inertia of the rotor and the connected load. ω_r is the electrical rotor speed in rad/s and T_L is the load torque.

2.2.2.6 Voltage and torque equations in the arbitrary reference frame

The transformation of stator and rotor variables from the machine variables to an arbitrary reference frame, typically referred to as the Park's transformation, is often necessary in modeling the single phase induction machine in order to simplify the voltage and torque equations. A change of variables which formulates a transformation to the arbitrary reference frame is given as(Krause *et al.* 2002; Krause *et al.* 2013):

$$\mathbf{F}_{\mathrm{qds}}^{\mathbf{x}} = \mathbf{K}_{\mathrm{s}}^{\mathbf{x}}\mathbf{F}_{\mathrm{abs}} \tag{2.21}$$

$$\left(\boldsymbol{F}_{qds}^{\boldsymbol{x}}\right)^T = [f_{qs}^x f_{ds}^x] \tag{2.22}$$

Where superscript '*x*' indicates the reference frame of interest.In the stationary reference framedenoted by 's',the transformation matrix is given as (Krause *et al.* 2002; Krause *et al.* 2013):

$$\boldsymbol{K}_{\boldsymbol{s}}^{\boldsymbol{s}} = \begin{bmatrix} \cos\theta_s & \sin\theta_s \\ \sin\theta_s & -\cos\theta_s \end{bmatrix} \tag{2.23}$$

Where θ_s is the angular position of the stationary reference frame. The angular position θ of any reference frame is related to the speed, ω of the reference frame by the expression given as (Krause *et al.* 2002; Krause *et al.* 2013):

$$\theta = \int \omega \, dt \tag{2.24}$$

The inverse transformation equation is given as follows (Krause *et al.* 2002; Krause *et al.* 2013):

$$\mathbf{F}_{\text{abs}} = (\mathbf{K}_{\text{s}}^{\text{x}})^{-1}\mathbf{F}_{\text{qds}}^{\text{x}} \tag{2.25}$$

For the rotor variables, the following transformation equations apply (Krause *et al.* 2002; Krause *et al.* 2013):

$$\mathbf{F}_{\text{qdr}}^{\text{x}} = \mathbf{K}_{\text{r}}^{\text{x}}\mathbf{F}_{\text{abr}} \tag{2.26}$$

The inverse transformation equation is given as follows (Krause *et al.*, 2002; Krause *et al.*, 2013):

$$\mathbf{F}_{\text{abr}} = (\mathbf{K}_{\text{r}}^{\text{x}})^{-1}\mathbf{F}_{\text{qdr}}^{\text{x}} \tag{2.27}$$

$\mathbf{K}_{\text{r}}$is the rotor transformation matrix and in the stationary reference frame, it is given as (Krause *et al.* 2002; Krause *et al.* 2013):

$$\boldsymbol{K}_r^s = \begin{bmatrix} \cos\sigma & \sin\sigma \\ \sin\sigma & -\cos\sigma \end{bmatrix} \tag{2.28}$$

$$\sigma = (\theta - \theta_r) \tag{2.29}$$

The relationship between the angular displacement of the rotor from the stator θ_r and the rotor speed, ω_r is given as (Krause *et al.*, 2002; Krause *et al.*, 2013):

$$\theta_r = \int \omega_r \, dt \tag{2.30}$$

The variables of the rotor winding are often referred to the stator winding as with the case of the transformer in order to represent the machine as one piece of electromagnetic energy device with a magnetic coupling between the stator and the rotor. This concept is called the turn's transformation. Here, all *q*-axis variables of the rotor are referred to the stator main winding with

N_{as} equivalent turns and all *d*-axis variables of the rotor are referred to the auxiliary winding of the stator with N_{bs} equivalent turns. The model equations of the single phase induction machine expressed in the stationary reference frame is given as (Omozusi, 1998; Krause *et al.,* 2002; Caruso *et al.*, 2012; Jannati *et al.*, 2014):

$$V_{qs} = r_{qs}i_{qs} + p\lambda_{qs} \quad (2.31\ (a))$$

$$V_{ds} = r_{ds}i_{ds} + p\lambda_{ds} \quad (2.31\ (b))$$

$$V'_{qr} = r'_r i'_{qr} - \frac{N_q}{N_d}\omega_r \lambda'_{dr} + p\lambda'_{qr} \quad (2.31\ (c))$$

$$V'_{dr} = r'_r i'_{dr} + \frac{N_d}{N_q}\omega_r \lambda'_{dr} + p\lambda'_{dr} \quad (2.31\ (d))$$

$$\lambda_{qs} = L_{lqs}i_{qs} + L_{mq}\left(i_{qs} + i'_{qr}\right) \quad (2.31\ (e))$$

$$\lambda'_{qr} = L'_{lr}i'_{qr} + L_{mq}(i_{qs} + i'_{qr}) \quad (2.31\ (f))$$

$$\lambda_{ds} = L_{lds}i_{ds} + L_{md}(i_{ds} + i'_{dr}) \quad (2.31\ (g))$$

$$\lambda'_{dr} = L'_{lr}i'_{dr} + L_{md}(i_{ds} + i'_{dr}) \quad (2.31\ (h))$$

$$T_e = \frac{P}{2}\left(L_{mq}i'_{dr}i_{qs} - L_{md}i_{ds}i'_{qr}\right) \quad (2.31\ (i))$$

The equivalent circuit of the single phase induction machine is given as in Figure 2.10; (Omozusi, 1998; Krause *et al.,* 2002):

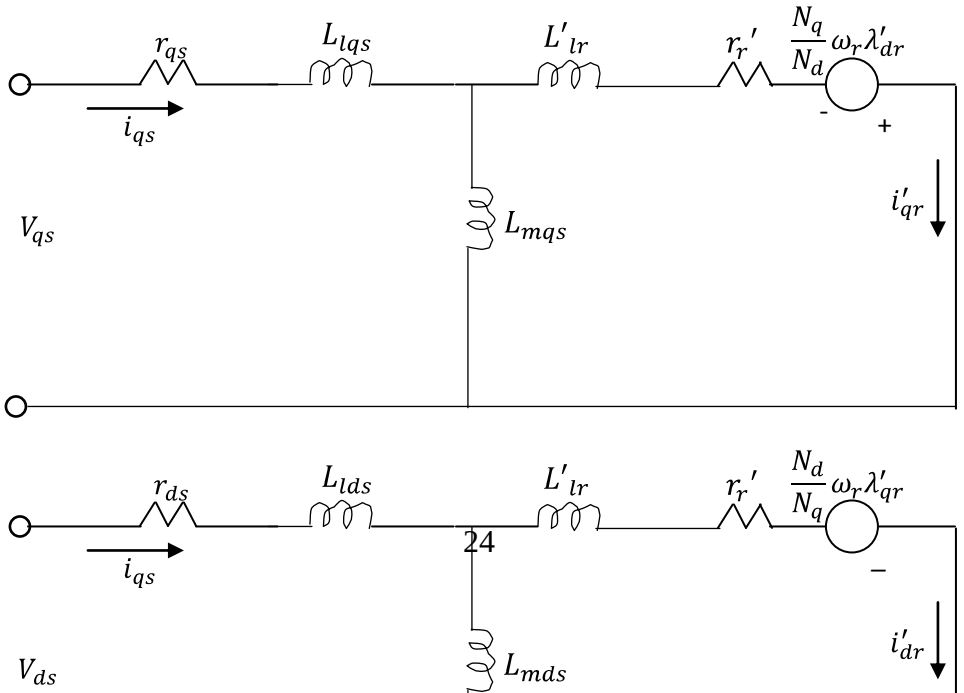


Figure 2.10: q – d Equivalent Circuit of the Single Phase Induction Machine(Omozusi, 1998; Krause *et al.,* 2002):

The single phase induction machines vary widely in size and application. Two examples of the CRSPIM data obtainable in literature are providedin Appendix A. Table A.1 gives a CRSPIM having a voltage and frequency rating of 110V and 60Hz while Table A.2 gives a CRSPIM having a voltage and frequency rating of 220V and 50Hz.

2.2.2.7 Torque produced by the capacitor-run single phase induction machine

The torque produced in the single phase induction motor is the result of interaction between the forward and backward magnetic fields produced in each stator winding and the currents flowing in the windings(Kim *et al.,* 2003). As a result, the torque per pole T, produced in capacitor –run single phase induction machine is given by(Morrill, 1929):

$$T = 2\lambda f 10^{-8} \int_0^{\lambda} [(\Delta\Phi_{fm} + \Delta\Phi_{bm} + \Delta\Phi_{fa} + \Delta\Phi_{ba})(\Delta i_m + \Delta i_a)]\ dx \tag{2.32}$$

$$\Delta i_m = -I_m C_m \frac{\pi}{2\lambda}\left\{\frac{1}{2}\sin\left[\frac{\pi}{\lambda}x - \omega t\right] + \frac{1}{2}\sin\left[\frac{\pi}{\lambda}x + \omega t\right]\right\} \tag{2.33}$$

$$\Delta i_a = -I_a a C_m \frac{\pi}{2\lambda}\left\{\frac{1}{2}\sin\left[\frac{\pi}{\lambda}x + \frac{\pi}{2} - \emptyset - \omega t\right] + \frac{1}{2}\sin\left[\frac{\pi}{\lambda}x + \frac{\pi}{2} + \emptyset + \omega t\right]\right\} \tag{2.34}$$

$$\Delta\Phi_{fm} = \frac{\frac{1}{4}I_m}{\frac{2\pi f\lambda 10^{-8}}{16}C_m}\left[X_f \cos\left(\frac{\pi}{\lambda}x - \omega t\right) - R_f sin\left(\frac{\pi}{\lambda}x - \omega t\right)\right] \tag{2.35}$$

$$\Delta\Phi_{bm} = \frac{\frac{1}{4}I_m}{\frac{2\pi f\lambda 10^{-8}}{16}C_m}\left[X_b \cos\left(\frac{\pi}{\lambda}x + \omega t\right) + R_b sin\left(\frac{\pi}{\lambda}x + \omega t\right)\right] \tag{2.36}$$

$$\Delta\Phi_{fa} = \frac{\frac{1}{4}aI_a}{\frac{2\pi f\lambda 10^{-8}}{16}C_m}\left[X_f \cos\left(\frac{\pi}{\lambda}x + \frac{\pi}{2} - \emptyset - \omega t\right) - R_f sin\left(\frac{\pi}{\lambda}x + \frac{\pi}{2} - \emptyset - \omega t\right)\right] \tag{2.37}$$

$$\Delta\Phi_{ba} = \frac{\frac{1}{4}aI_a}{\frac{2\pi f\lambda 10^{-8}}{16}C_m}\left[X_f \cos\left(\frac{\pi}{\lambda}x + \frac{\pi}{2} + \emptyset + \omega t\right) - R_f sin\left(\frac{\pi}{\lambda}x + \frac{\pi}{2} + \emptyset + \omega t\right)\right] \tag{2.38}$$

where:

$\Delta\Phi_{fm}$ = Total forward flux per inch of periphery produced by main winding.

$\Delta\Phi_{bm}$ = Total backward flux per inch of periphery produced by main winding.

$\Delta\Phi_{fa}$ = Total forward flux per inch of periphery produced by auxiliary winding.

$\Delta\Phi_{ba}$ = Total backward flux per inch of periphery produced by auxiliary winding.

Δi_m= Current per inch of periphery due to main winding.

Δi_a= Current per inch of periphery due to auxiliary winding.

C_m = Number of conductors per pole.

x = Distance around the periphery of the air-gap measured from a reference point.

λ = Pole pitch.

I_m = Peak value of the main winding current.

I_a = Peak value of the auxiliary winding current.

ω is the angular frequency of the supply voltage to the motor; $\emptyset$ is the phase difference between the stator winding currents. R_f, R_b, X_f and $X_b$are as defined in section 2.2.2.2. A simplified form of equation (2.32) is given as (Morrill, 1929):

$$T = I_m^2\left[\left(R_f - R_b\right) + \left(R_f - R_b\right)cos2\omega t - \left(X_f - X_b\right)sin2\omega t\right] + I_a^2 a^2\left[\left(R_f - R_b\right) + \left(R_f - R_b\right)cos2(\emptyset + \omega t) - \left(X_f - X_b\right)sin2(\emptyset + \omega t)\right] + 2I_m I_a a\left(R_f + R_b\right)sin\emptyset \quad (2.39)$$

The average or useful torque is given as; (Morrill, 1929; Collins *et al*, 1988; Kim *et al*, 2003)

$$T_{avg} = [I_m^2 + I_a^2 a^2]\left(R_f - R_b\right) + 2I_m I_a a\left(R_f + R_b\right)sin\emptyset \quad (2.40)$$

The alternating torque or the pulsating component of the torque produced is given as (Morrill, 1929; Collins*et al.*, 1988):

$$T_{puls} = [I_m^2\left(R_f - R_b\right) + I_s^2 a^2\left(R_f - R_b\right)cos\ 2\emptyset - I_s^2 a^2\left(X_f - X_b\right)\ sin\ 2\emptyset]\ \cos\ 2\omega t + [-I_m^2\left(X_f - X_b\right) - I_s^2 a^2\left(R_f - R_b\right)\sin\ 2\emptyset - I_s^2 a^2\left(X_f - X_b\right)\cos\ 2\emptyset]\ \sin\ 2\omega t \quad (2.41)$$

Equation (2.41) indicates that the pulsating torque alternates at twice the supply frequency. In literature, the magnitude of the pulsating torque component is typically used to characterize the strength of the torque pulsations(Vaez-Zadeh and Langari, 2000). This magnitude is obtained from equation (2.41) and is expressed as (Collins *et al.*, 1988; Morrill, 1929):

$$|T_{puls}| = \sqrt{[I_m^4 + I_a^4 a^4 + 2I_m^2 I_a^2 a^2\cos 2\emptyset][\left(R_f - R_b\right)^2 + \left(X_f - X_b\right)^2]} \quad (2.42)$$

2.2.2.8 Condition for zero pulsating torque

Torque pulsations are eliminated if the following relationships can be maintained simultaneously (Morrill, 1929; Veinott, 1970; Miller, 1985; Collins *et al.*, 1988; Jang, 2013):

$$a = \frac{I_m}{I_a} \tag{2.43}$$

$$\emptyset = 90^0 \tag{2.44}$$

The run capacitor connected in series with the auxiliary winding is designed to achieve this objective at one operating point only (i.e. rated condition) but even then it is very difficult to achieve in practice (Jang, 2013). The difficulty of eliminating torque pulsations at all operating points has persisted so much so that in recent times, a lot of researchers have developed different single phase induction machine control schemes aimed at reducing torque pulsations at all operating points for the purpose of improving torque production and drive efficiency (Asghari and Fallah, 2012; Azzolin *et al.*, 2012; Jang, 2013; Hekmati *et al.*, 2014).

2.2.2.9 Analysis of auxiliary winding voltage supplyof the single phase Induction machine

The stator voltage equations of the main and auxiliary windings in terms of the currents and impedances of the equivalent circuit of Figure 2.5are given as (Collins *et al*, 1988):

$$V_m = I_m\left[\left(R_{1m} + R_f + R_b\right) + j\left(X_{1m} + X_f + X_b\right)\right] + I_a\left[a\left(X_f - X_b\right) + j\left(-a\left(R_f - R_b\right)\right)\right] \tag{2.45}$$

$$V_a = I_m\left[-a\left(X_f - X_b\right) + a\left(R_f - R_b\right)\right] + I_a\left[\left(R_{1s} + a^2\left(R_f + R_b\right)\right) + j\left(X_{1s} + a^2\left(X_f + X_b\right)\right)\right] \tag{2.46}$$

The expressions of the main and auxiliary winding currents are given as(Collins *et al.*, 1988):

$$I_a = \frac{V_a Z_1 - V_m Z_4}{Z_1 Z_3 - Z_2 Z_4} = |I_a|\angle\theta_a \tag{2.47}$$

$$I_m = \frac{V_m Z_3 - V_a Z_2}{Z_1 Z_3 - Z_2 Z_4} = |I_m| \angle \theta_m \quad (2.48)$$

where $\theta_a$and $\theta_m$are the phase angles of the auxiliary and main windings currents respectively.

$$Z_1 = a_1 + jb_1 \quad (2.49)$$

$$Z_2 = a_2 + jb_2 \quad (2.50)$$

$$Z_3 = a_3 + jb_3 \quad (2.51)$$

$$Z_4 = a_4 + jb_4 \quad (2.52)$$

$$a_1 = r_{1m} + R_f + R_b \quad (2.53)$$

$$b_1 = X_{1m} + X_f + X_b \quad (2.54)$$

$$a_2 = a(X_f - X_b) \quad (2.55)$$

$$b_2 = -a(R_f - R_b) \quad (2.56)$$

$$a_3 = r_{1a} + a^2(R_f + R_b) \quad (2.57)$$

$$b_3 = X_{1a} + a^2(X_f + X_b) \quad (2.58)$$

$$a_4 = -a(X_f - X_b) \quad (2.59)$$

$$b_4 = a(R_f - R_b) \quad (2.60)$$

The variables $V_m, V_a, I_m, I_a$and parameters $a,\ r_{1m},\ X_{1m},\ r_{1a}, X_{1a} R_f,\ R_b,\ X_f$ and $X_b$have been defined previously in section 2.2.2.2.

Considering the main winding voltage V_m as reference, the auxiliary winding voltage V_a has the form given as(Collins *et al.*, 1988):

$$V_a = V_{aR} + jV_{aI} \quad (2.61)$$

Where V_{aR} and V_{aI} represents the real and imaginary parts of the auxiliary winding voltage.

For a phase difference of 90^0 between the main and auxiliary winding currents, the ratio of equations (2.47) and (2.48) yields an expression relating the real and imaginary parts of the

auxiliary winding voltage to the main winding voltage, machine parameters and the speed of the machine. The expression is given as (Collins *et al.*, 1988):

$$V_{aR}^2 + V_{aI}^2 + XV_{aR} + YV_{aI} + Z = 0 \tag{2.62}$$

Where:

$$X = \frac{V_m[a_1a_3+a_2a_4+b_1b_3+b_2b_4]}{[-a_1a_2-b_1b_2]} \tag{2.63}$$

$$Y = \frac{V_m[a_1b_3+a_2b_4-b_1a_3-b_2a_4]}{[-a_1a_2-b_1b_2]} \tag{2.64}$$

$$Z = \frac{V_m^2[-a_4a_3-b_3b_4]}{[-a_1a_2-b_1b_2]} \tag{2.65}$$

The solution of the quadratic equation of (2.62) for V_{aI} yields (Collins *et al.*, 1988):

$$V_{aI} = -\frac{Y(|V_a|^2+Z)}{X^2+Y^2} \pm \frac{\sqrt{Y^2(|V_a|^2+Z)^2-(X^2+Y^2)(|V_a|^4+|V_a|^2(2Z-X^2)+Z^2)}}{X^2+Y^2} \tag{2.66}$$

The real part of the auxiliary winding voltage is given by:

$$V_{aR} = \pm\sqrt{|V_a|^2 - V_{aI}^2} \tag{2.67}$$

The phase angle of the auxiliary winding voltage, $\emptyset_a$ is expressed as(Collins *et al.*, 1988):

$$\emptyset_a = \arctan\left(\frac{V_{aI}}{V_{aR}}\right) \tag{2.68}$$

This analysis carried out by Collins *et al.,* (1988) determines the relationship between the auxiliary winding voltage phase angle and the phase angle difference between the main and auxiliary winding currents. By fixing the phase angle difference between the main and auxiliary winding currents at 90^0 and applying the following equation (Collins *et al.*, 1988):

$$I_m = aI_a \tag{2.69}$$

to equations (2.47) and (2.48), then the magnitude of the auxiliary winding voltage can be expressed in terms of the main winding voltage and circuit parameters as follows (Collins *et al.*, 1988):

$$|V_a| = V_m \sqrt{\frac{(a_3+aa_4)^2+(b_3+aab_4)^2}{(a_2+aa_1)^2+(b_2+ab_1)^2}} \tag{2.70}$$

2.2.2.10 Generalized condition for balanced stator currents

Miller (1985) established a generalized condition for eliminating the backward rotating magnetic field and therefore the torque pulsations in the unsymmetrical or unbalanced two phase machine. The capacitor-run single phase induction machine is one of the many types of single phase machines classified as an unsymmetrical or unbalanced two phase machine (Miller, 1985; Jang, 2013; Rubio *et al.*, 2013). Miller's analysis established the relationship between the phase difference of stator currents in the unbalanced two phase machines and the spatial angular displacement of stator windings for the elimination of the backward rotating magnetic. This troublesome backward rotating magnetic field is largely responsible for the production of the pulsating component of the electromagnetic torque in the machine. The theory is presented in the following section and it is used to establish a condition to eliminate torque pulsations for the case of the non-quadrature angular displacement of the stator windings. A schematic diagram of the capacitor-run single phase induction machine is given in Figure 2.11.

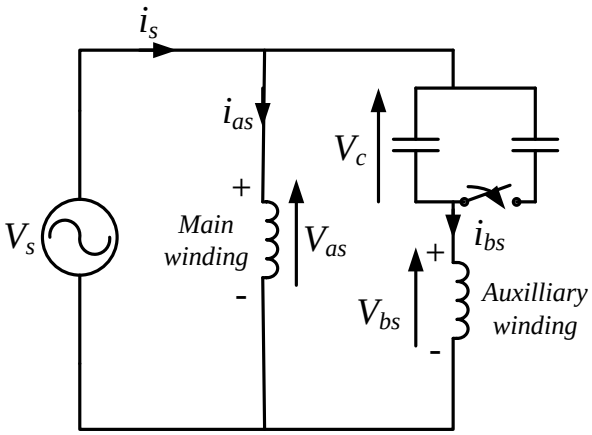


Figure 2.11: Schematic Representation of the Stator Windings and Terminal Connections of the CRSPIM

The equations of the fundamental magneto-motive force (MMF) in the stator main and auxiliary windings are given as follows (Miller, 1985):

$$F_a = I_a N_a Cos(\theta - \partial) Cos\omega t \tag{2.70}$$

$$F_m = I_m N_m Cos\theta Cos(\omega t - \emptyset) \tag{2.71}$$

where ∂ is the spatial angular displacement between the windings and $\emptyset$ is the phase difference between the winding currents. N_m and $N_a$are the equivalent number of sinusoidally distributed turns in the main and auxiliary windings. F_a is the MMF in the auxiliary winding while F_m is the MMF in the main winding. The resultant air-gap MMF of the stator windings is the sum of the individual MMFs of the two windings. This sum is given as(Miller, 1985):

$$F = \frac{1}{2} I_m N_m [Cos(\theta - \omega t) + Cos(\theta + \omega t)] + \frac{1}{2} I_a N_a [Cos(\theta - \omega t - \partial + \emptyset) + Cos(\theta + \omega t - \partial - \emptyset)] \tag{2.72}$$

Equation (2.72) contains two backward rotating MMF waves. According to Miller (1985), for zero pulsating torque, the sum of the backward rotating fields must be zero. The equation is given asMiller (1985):

$$\frac{1}{2}I_m N_m Cos(\theta + \omega t) + \frac{1}{2}I_a N_a Cos(\theta + \omega t - \partial - \emptyset) = 0 \quad (2.73)$$

The requirement of zero pulsating torque is met when the following equations hold true (Miller, 1985):

$$\frac{N_m}{N_a} = \frac{I_a}{I_m} \quad (2.74)$$

$$\partial + \emptyset = \pi \quad (2.75)$$

Equation (2.74) indicates that the ratio of effective turns of the windings must be in inverse proportion to the ratio of the current magnitudes in the two windings. Equation (2.75), on the other hand, indicates that the phase difference between the main and auxiliary winding currents must be $(\pi - \partial)$ radians. This theory is consistent with the condition for eliminating the pulsating torque component given in section 2.2.2.8 for the case of 90^0 spatial angular displacement. These conditions have been commonly referred to as the balanced conditions in unsymmetrical two phase induction machines. (Trickey 1932; Collins *et al.*, 1988; Huang *et al.*, 1988; Krischan *et al.*, 2008; Krause *et al.*, 2013).

In recent times, a lot of researchers have attempted using inverters to supply balanced currents to the single phase induction motor stator windings but have faced challenges of varying degrees depending on the type of inverter topology and the control strategy employed (Blaabjerg*et al.*, 2004; Jang, 2007; Caruso *et al.*, 2012; Asghari and Fallah, 2012). In this work, as with many other related research works, it is of interest to supply power from a power converter otherwise known as an inverter to the conventional single phase induction motor in an effort to improve the machine performance. It therefore becomes pertinent to discuss the relevant theory of inverters and associated control strategies. The theory of the inverter is presented first in the following section.

2.2.3 Inverters

The purpose of the inverter, as far as power conversion process is concerned, is to produce an alternating current (ac) output waveform from a dc voltage input. The ac output waveform so produced can be variable in magnitude, frequency and phase when a pulse width modulation technique is applied on the power converter. Typical applications of the pulse width modulated power converters include but not limited to adjustable speed drives, flexible ac transmission systems, active filters, standby power supplies and uninterrupted power supplies(Holmes and Lipo 2003). There are three different configurations of the inverter. These are the voltage source inverter (VSI), the current source inverter (CSI) and the variable dc linked inverter. The VSI is fed with a fixed dc voltage source. The CSI has a constant current source as input while the variable dc linked inverter is fed with a controllable dc voltage. The inverters applied in ac machine applications, regardless of the configuration are constructed from power switches such as the insulated gate bipolar transistors (IGBTs) and the gate turn-on thyristors (GTOs). Continuous improvements in semiconductor technology have made these power switches available in a wide range of power ratings. The voltage source inverters are by far the most popular of the three different configurations mentioned. This is because most applications require a voltage input for their operations. New application areas for the VSIs continue to emerge as the need for controllable voltage sources continues to grow especially in the industrial centers around the globe. The section that follows looks closely at the voltage source inverters.

2.2.3.1 Voltage source inverters

Voltage source inverters are broadly classified into the single phase inverters and three phase inverters(Rashid 2004). The single phase inverters are typically used for single and two phase applications while the three phase inverters are used mostly for two phase and three phase

applications. Other classes of the voltage source inverters exists and these include the four-leg, five-leg voltage source inverters and multi-level inverters which can either be a single phase or a three phase inverter type. The four-leg and five-leg voltage source inverters are typically used for multiphase applications. Although they may be used for two phase and three phase applications, their popularity for these applications is limited because of cost implications and complexity of controllers associated with these classes of VSIs. The following section examines the single phase inverters which is of interest in this research.

2.2.3.2 Single phase inverters

Single phase inverters are voltage source inverters that have one or two legs in their construction. A leg, in this case, comprises two power semiconductor switches connected in series as given in Figure 2.12. The switches are preferably high performance IGBTs or GTOs for motor applications. These types of switches consist, primarily, of a power transistor and an anti-parallel diode as shown in Figure 2.12.

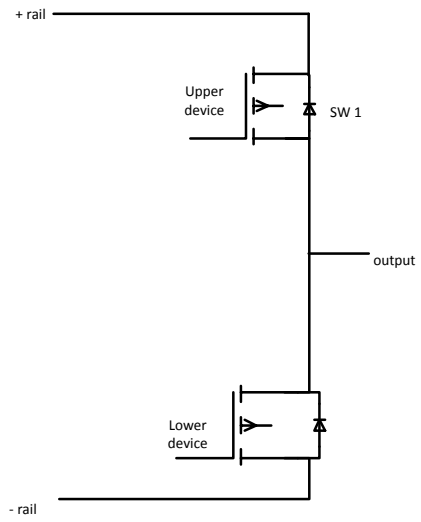


Figure 2.12 One Phase Leg of an Inverter(Rashid, 2004)

Single phase inverters are used for single and two phase applications such as power supplies, variable speed drives (VSDs) or variable frequency drives (VFDs), active filters, etcetera in the low to medium power range(Chapman, 1999). The simplest topology of the single phase inverter is the single phase half-bridge inverter given in Figure 2.13.

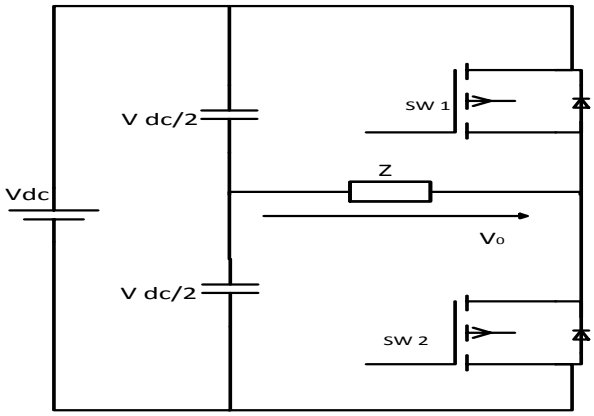


Figure 2.13: Single Phase Half Bridge Inverter(Rashid, 2004)

The single phase half-bridge inverter will be used to describe the basic operation of the inverter. The half bridge inverter typically has an input dc voltage that is normally tapped at the center with the help of two capacitors so that equal dc voltages, precisely half of the input voltage, results as shown in Figure 2.13. The purpose of this arrangement is to produce a symmetrical ac voltage waveform of a given period T across the output of the inverter as shown in Figure 2.14.

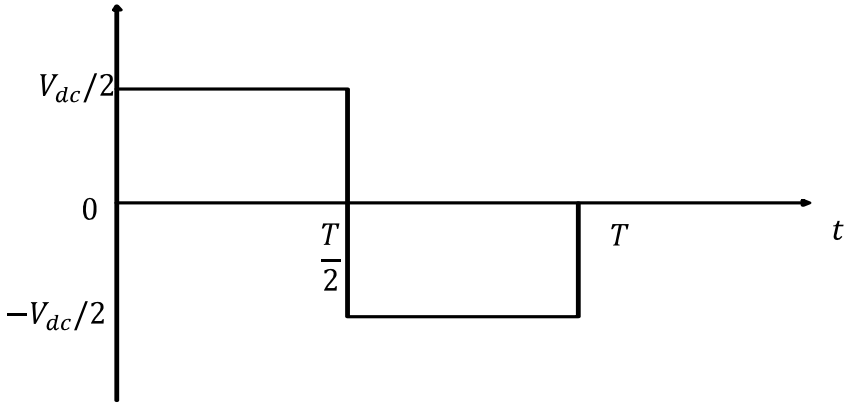


Figure 2.14: Output Waveform of the Half-Bridge Inverter(Rashid, 2004)

The output is a two level square waveform. One level has a value of $V_{dc}/2$ while the other level has a value of $-V_{dc}/2$. In the half-bridge inverter circuit, there is only one inverter leg consisting of two power semiconductor switches. The output voltage V_0 alternates between a positive dc voltage and a negative dc voltage as shown in Figure 2.14. This output is brought about by the action of the switches. As with any other converter, both switches on a leg must not be turned on simultaneously because if both switches are turned on at the same time, a short circuit will be produced across the supply input. Consequently, the switches are turned on one at a time and for a specified period of time. In particular, the top switch SW_1 is turned on for the first half of the period of the desired waveform while the bottom switch SW_2, is turned on for the second half of the period. (Kaźmierkowski and Krishnan, 2002; Holmes and Lipo, 2003; Jain, 2004; Rashid, 2004).In practice, the switches are turned on and off by pulses from the output of digital electronic circuits often controlled by programs embedded in micro-controllers(Patel and Raval, 2015). The duty cycle of the signals and hence that of the output waveform may vary according to the preferred algorithm. This switching action produces an alternating voltage across the load Z. The instantaneous output voltage of the half bridge inverter may be expressed in Fourier series by the following mathematical expression (Rashid, 2004):

$$V_0 = \begin{Bmatrix} \sum_{n=1,3,5}^{\infty} \frac{2V_{dc}}{n\pi} sinn\omega t \\ 0\ for\ n = 2, 4, 6, \ldots . \end{Bmatrix} \tag{2.76}$$

where ω is theangular frequency of the output voltage in rad/s.The output waveform consists of a fundamental component and harmonics. Output harmonics are not desirable in inverter circuits and are therefore usually minimized significantly by the use of filters and a wide range of modulating techniques(Pawar and Kulkarni, 2015; Rokrok and Golshan, 2009; Crowley *et al.*,

2011). For the pulse width modulated inverter, the desired output voltage is produced by the help of a modulating technique which controls the amount of time and sequence used to turn switches on and off.

2.2.3.3 Pulse width modulation in inverters

Broadly speaking, pulse width modulation (PWM) is a process of varying the width of the pulses in a pulse train in direct proportion to a control signal. By extension, the technique by which the width of pulses used to turn on and off, the switches of the inverter are varied in proportion to certain small control signal in order to control the inverter output voltage is referred to as pulse width modulation in inverters. Pulse width modulation techniques are characterized by constant amplitude pulses (Holmes and Lipo, 2003). By varying the width of this pulses in accordance with certain criteria or algorithm, it is possible to adjust the amplitude, phase and frequency of the output voltage regardless of the type of inverter. Several PWM techniques have been developed to control the output voltage of inverters. The basic techniques are listed as follows (Rashid, 2004):

a) Single pulse width modulation
b) Multiple pulse width modulation
c) Sinusoidal pulse width modulation otherwise known as the carrier-based pulse width modulation
d) Modified sinusoidal pulse width modulation

All of these techniques along with several variations, seek to vary the duty cycle of the switches of the power converter to achieve a high average, low frequency output voltage or current. In addition to the remarkable ability to control the ac output voltage of inverters, the PWM technique has the advantage that it is able to minimize and in some cases, eliminate lower order

harmonics from the output voltage. The low order harmonics are shifted to multiples of the switching frequency and as a result, filtering requirements in inverter circuits are significantly minimized since simple L-C filters can now be used to eliminate higher order harmonics(Hingorani and Gyugyi, 2000). Of all the listed PWM techniques, the sinusoidal pulse width modulation (SPWM) technique is especially suited for applications in which it is desired that the ac output voltage follow a given sinusoidal reference otherwise referred to as a control signal, on a continuous basis. This research presents such an application and therefore will focus on the technique of sinusoidal or the carrier-based pulse width modulation as applied in single phase inverter circuits. The SPWM technique is very efficient, simple and easy to implement. (Pawarand Kulkarni, 2015)

2.2.3.4 Sinusoidal pulse width modulation (SPWM) technique

The sinusoidal PWM strategy defines the on and off states of the switches of one leg of the inverter by comparing a sinusoidal modulating signal and a triangular waveform. The former is the control signal having amplitude, phase and frequency relationship with the desired fundamental output voltage while the latter is the carrier signal. There are three different switching schemes under the sinusoidal pulse width modulation. These are the unipolar, bipolar and the modified bipolar SPWM switching schemes.The unipolar sinusoidal pulse width modulation switching scheme will be described in the next section with respect to its application on the single phase full bridge inverter. The scheme has the advantage that it effectively doubles the switching frequency of the inverter thereby making the inverter output filter smaller and cost-effective (Sharma *et al.,* 2014).

2.2.3.5 Pulse width modulated single phase inverter under the unipolar voltage switching Scheme

The single phase full bridge inverter essentially consists of two half bridge inverters. With respect to the single phase inverter topology of Figure 2.15, the states of switches SW_1 - SW_4 are controlled by two comparators as shown in Figure 2.16.

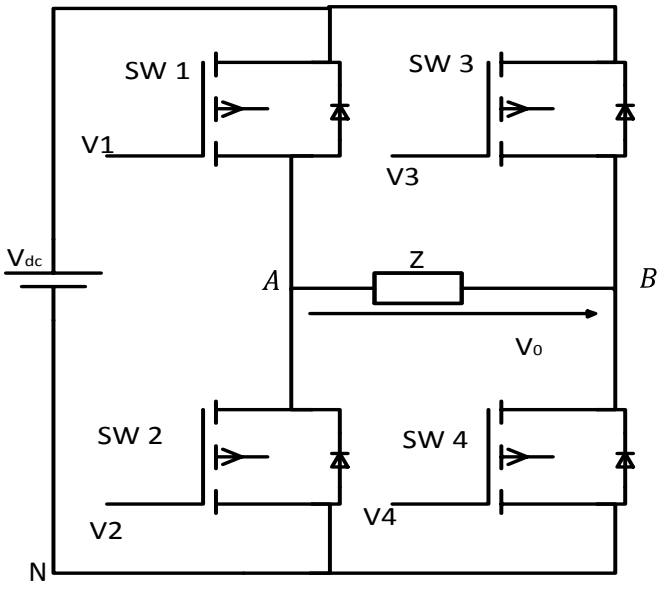


Figure 2.15: Single Phase Full Bridge Inverter(Chapman, 1999)

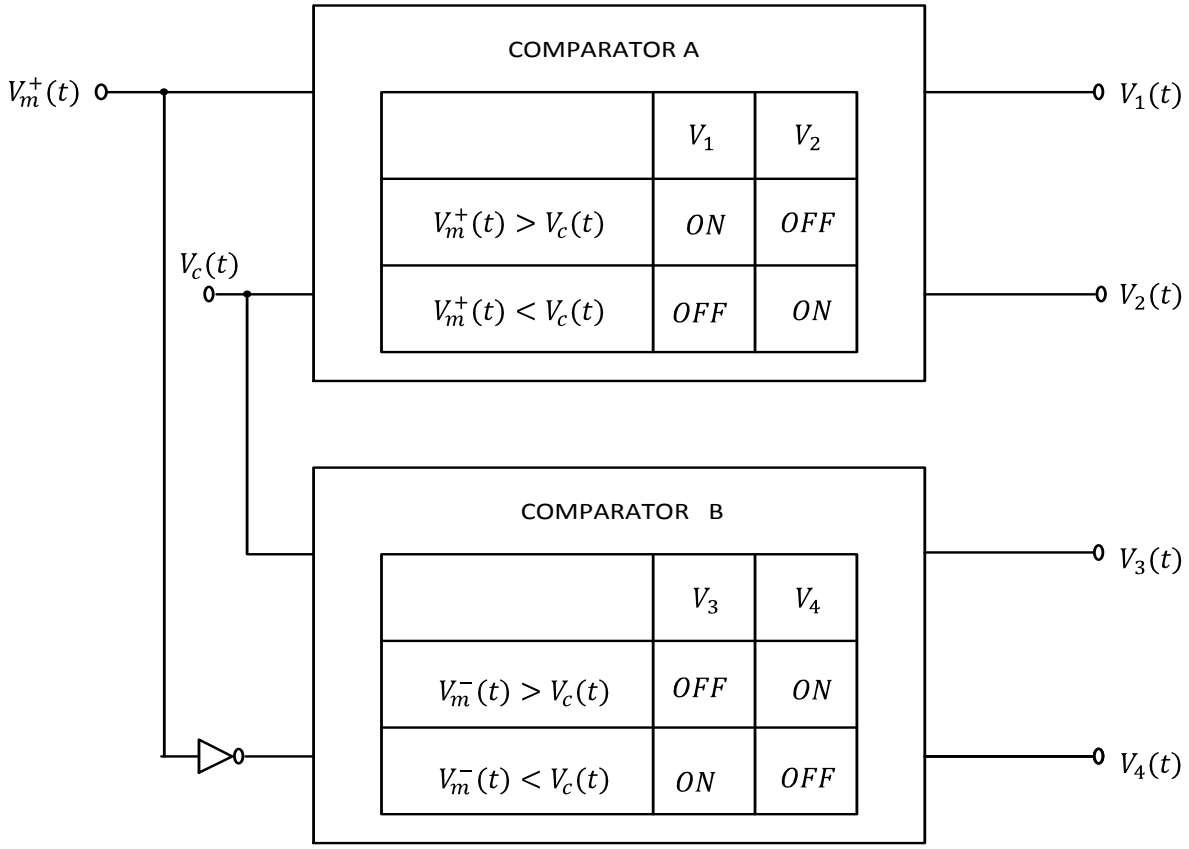


Figure 2.16: Comparators used to Control the ON and OFF States of the Power Switches (Chapman, 1999)

The comparator A compares the reference or control signal $v_m^+(t)$ for phase leg A with a triangular carrier signal $v_c(t)$ and turns the switches on that leg on or off depending on the result of the comparison. Similarly, comparator B compares the inverse of reference or control signal here referred to as $v_m^-(t)$ for phase leg B with the same triangular carrier signal $v_c(t)$ and turns the switches on leg B on or off depending on the result of the comparison. Specifically, comparator A compares $v_m^+(t)$ to the triangular waveform $v_c(t)$ and controls switches SW_1 and SW_2 based on the result of the comparison. Comparator B compares $v_m^-(t)$ to $v_c(t)$ and controls SW_3 and SW_4 based on the result of the test. If $v_m^+(t)$ is greater than $v_c(t)$ at any given time t, then comparator A will turn on SW_1 and turn off SW_2. Otherwise, it will turn off SW_1 and turn on SW_2 as illustrated in Figure 2.16. V_1 and V_2 are the high and low voltage signals (or

pulses) at the base of the top and bottom switches of leg A. Similarly, if $v_m^-(t)$ is greater than $v_c(t)$ at any given time t, then comparator B will turn off SW_3 and turn on SW_4. Otherwise, it will turn on SW_3 and turn off SW_4. Figure 2.17 (a) illustrates the action of the comparators and shows signals $v_m^+(t)$, $v_m^-(t)$ and $v_c(t)$ together. The resulting pulse trains arising from the typical PWM process on a single phase inverter are shown in Figure 2.17 (b)-(e). $V_1(t)$ and $V_2(t)$ are alsoknown as the switching functions of the top and bottom switches of leg A. $V_3(t)$ and $V_4(t)$ are the switching functions of the top and bottom switches of leg BThe waveforms exhibit the varying duty cycle of the power switches. The output voltage synthesized across the load Z is shown in Figure 2.17 (f). It is usually a high power waveform whose average voltage over any small region is directly proportional to the average voltage of the control signal in that region (Jain, 2008).

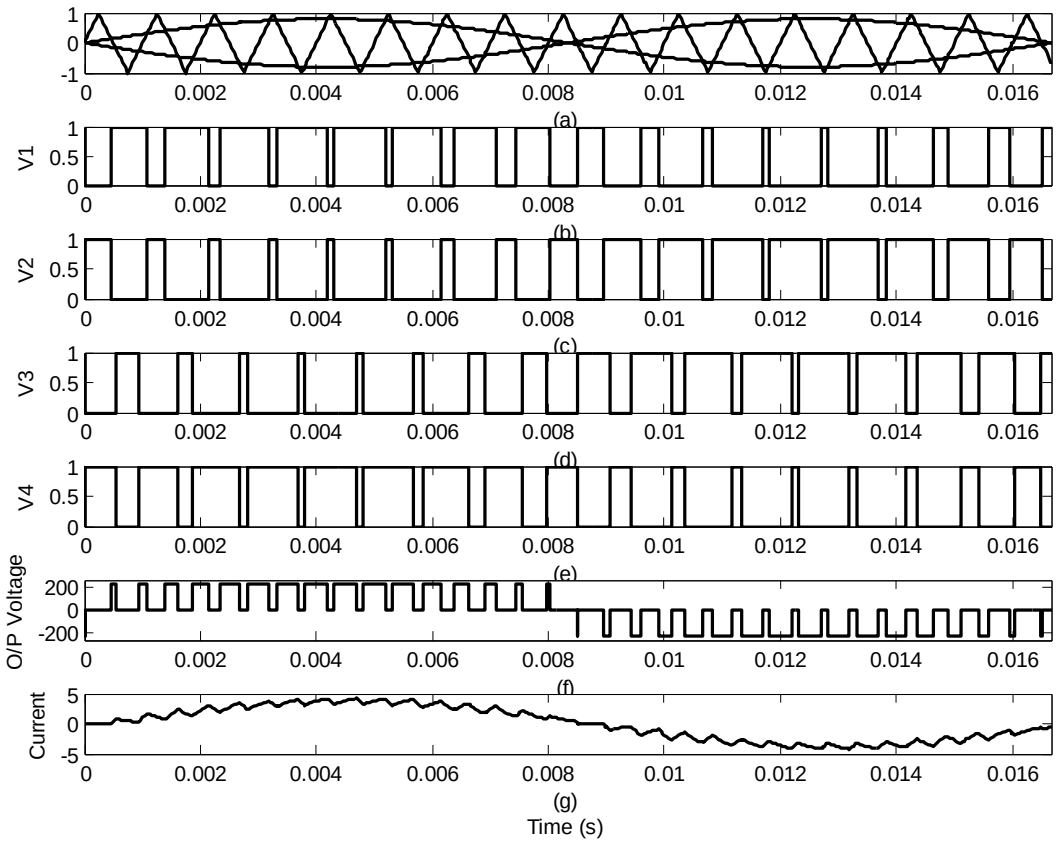


Figure 2.17: Output of the SPWM Circuit with a Sinusoidal Control Voltage Applied to its Input

The width of the pulse train varies sinusoidally as the control voltage. The resulting current wave shown in Figure 2.17 (g) illustrates the fundamental content of the output voltage more clearly. The load across the output of the inverter can range from a linear resistive load to a non-linear inductive load such as an ac motor. The sprectral characteristics of the switching functions of legs A and B can be obtained by Fourier analysis as follows(Holmes and Lipo, 2003; Mihret *et al.,* 2011):

$$V_1(t) = \frac{m_a}{2}\sin(\omega_m t + \emptyset_m) + \frac{4}{\pi}\sum_{m=1}^{\infty}\frac{1}{m}\sum_{n=1}^{\infty}J_n(mm_a\pi)\sin[n(\omega_m t + \emptyset)]\cos[m(\omega_c t + \emptyset_c] \quad 2.77(a)$$

$$V_3(t) = -\frac{m_a}{2}\sin(\omega_m t + \emptyset_m) - \frac{4}{\pi}\sum_{m=1}^{\infty}\frac{1}{m}\sum_{n=1}^{\infty}J_n(mm_a\pi)\sin[n(\omega_m t + \emptyset)]\cos[m(\omega_c t + \emptyset_c] \quad 2.77(b)$$

Where n is the base band index variable. m is the carrier index variable and m_a is the modulation index. $\omega_c$is the angular frequencyof the carrier signal. $\omega_m$is the angular frequency of the modulating signal.The phase angles of the carrier and modulating signals are denoted by θ_c and θ_m respectively. The fundamental component of the switching functions is the same as the modulating signal. The output voltage may be expressed by a complex double Fourier series as (Holmes and Lipo, 2003; Mihret *et al,*. 2011):

$$V_{ab}(t) = \left(\frac{m_a}{2} + \frac{2}{\pi}\right)V_{dc}\sin(\omega_m t + \emptyset_m) + \frac{4}{\pi}\sum_{m=1}^{\infty}\frac{1}{m}\sum_{n=1}^{\infty}J_n(mm_a\pi)\sin[n(\omega_m t + \emptyset)]\cos[m(\omega_c t + \emptyset_c] + \frac{2V_{dc}}{\pi}\sum_{n=3,5,\ldots}\frac{1}{n}\sin[n(\omega_m t + \emptyset)] \quad (2.78)$$

The fundamental component of the output voltageof equation (2.78) is in-phase with the modulating signal. The output voltage contains other components which in general are referred to as harmonics and sideband harmonics of the carrier signal(Sun, 2012). $V_{dc}$is the value of the

dc voltage source. $J_k$is the kth order Bessel function of the first kind. The modulating index,$m_a$is defined as follows (Jang, 2007; Yazdani and Iravani, 2010; Aganah *et al.*, 2012):

$$m_a = \frac{2V_m}{V_{dc}} \tag{2.79}$$

Where V_m is the peak value of the output voltage.

Table 2.1 shows the switching states of the unipolar SPWM scheme and the corresponding voltage levels.

Table 2.1: Switching State of the Unipolar SPWM and the Corresponding Voltage Levels (Omozusi, 1998)

SW1	**SW2**	**SW3**	**SW4**	$\mathbf{V_{AN}}$	$\mathbf{V_{BN}}$	$\mathbf{V_0}$
ON	OFF	OFF	ON	V_{dc}	0	V_{dc}
OFF	ON	ON	OFF	0	V_{dc}	$-V_{dc}$
ON	OFF	ON	OFF	V_{dc}	V_{dc}	0
OFF	ON	OFF	ON	0	0	0

For the unipolar switching scheme, the output voltage changes between 0 and $+V_{dc}$ or between 0 and $-V_{dc}$ voltage levels when switching occurs. V_{AN} and V_{BN} are the potentials between the output of each leg of the inverter and the negative dc rail.The harmonics present in the output voltage are not usually a concern in motor-control applications. They may, however, be significantly minimized by the use of filters at the inverter output(Chapman, 1999). A PWM inverter switches states many times during a single cycle of the resulting output voltage. Switching at very high frequencies require the use of fast switching semi-conductor devices. Depending on the application, such switches may have high power ratings as well. The algorithm used to generate the switching functions is usually implemented digitally by means of micro-controllers and other electronic devices. It is important to make it clear that several variations of the PWM process have been proposed over the years with different carriers and reference waveforms. The particular form of the carrier and reference waveforms depends on the PWM strategy that is implemented. Some PWM schemes have advantages in certain applications and for certain inverter topologies (Holmes and Lipo, 2003). Some topologies for which the SPWM scheme is suitable and that are applicable to single/two phase motor applications have been identified and are presented in the following section.

2.2.3.6 Inverter topologies for two phase applications

Several topologies have been developed for two phase applications. Some of the topologies as applied in adjustable speed drives for the single phase induction machine are given in Figures 2.18– 2.25. The characteristics of each topology, judged on the basis of application of similar motor typeare also given.

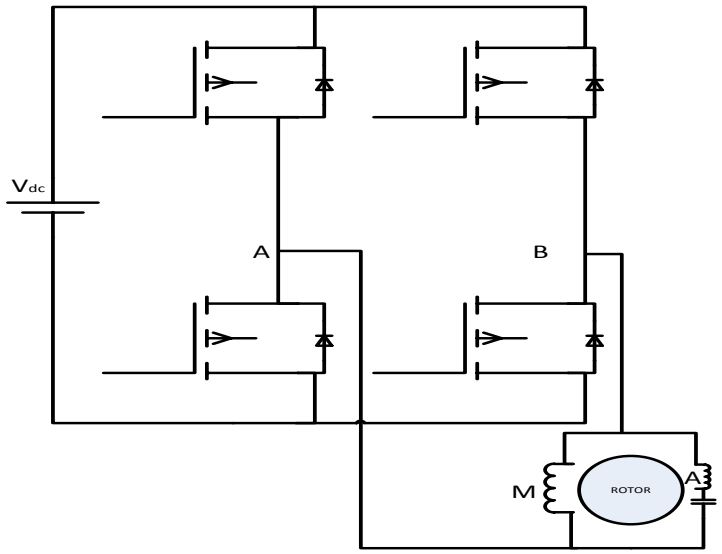


Figure 2.18: Single Phase Full Bridge Topology(Ba-thunya *et al.*, 2001; Blaabjerg *et al.*, 2004)

The topology shown in Figure 2.18 is simple, low cost, robust and easy to control. Both the main and auxiliary windings are supplied by the inverter output voltage. The running capacitor is placed in series with the auxiliary winding. The amplitude and frequency of the supply voltage can be varied. The problem with this topology is the increased capacitive reactance at low supply frequency. This condition leads to diminishing torque in the machine and hence the inability of the motor to carry rated load at low frequencies. Frequency reductions often lead to increasing torque pulsations in the machine. Moreover the efficiency of the machine at low speeds is extremely poor (Ba-thunya *et al*, 2001; Blaabjerg *et al*, 2004).

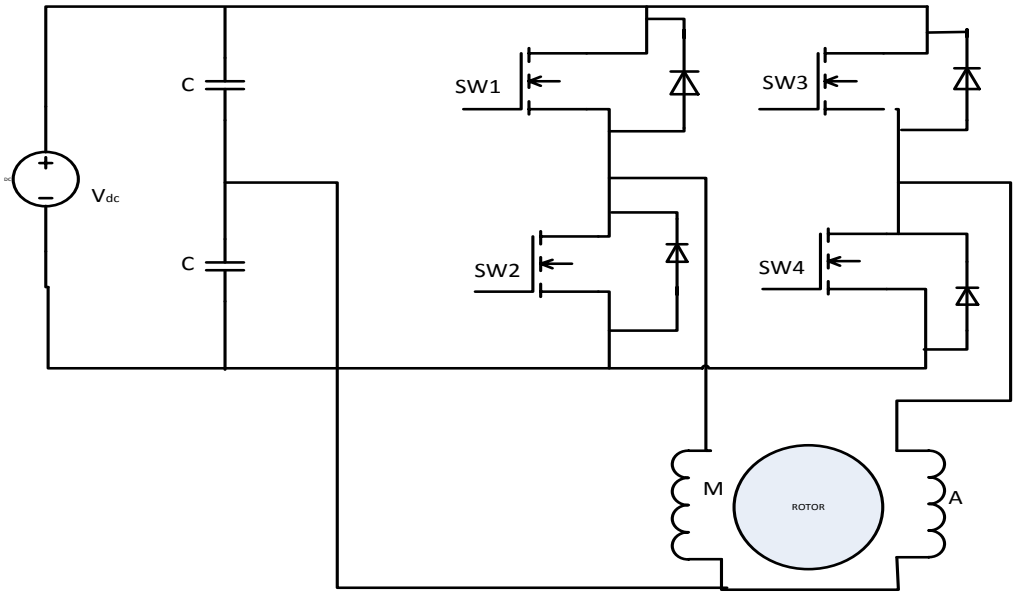


Figure 2.19: Two-Phase Two Leg Inverter Topology(Blaabjerg *et al.*, 2004; Jang, 2007)

The topology of Figure 2.19 enables independent supply of voltage to each of the main and auxiliary windings of the motor. The amplitude and frequency of the voltages applied to each winding may be controlled independently. In addition, the phase angle of the voltage applied to the auxiliary winding may be adjusted with respect to that of the main winding. This topology, especially when used in a way that ensures 90^0 phase difference between the supply currents and the right proportion of supply voltage amplitude, gives an excellent performance. (Blaabjerg *et al.*, 2004). With the application of field oriented motor control technique, this topology can be used to significantly improve motor performance.

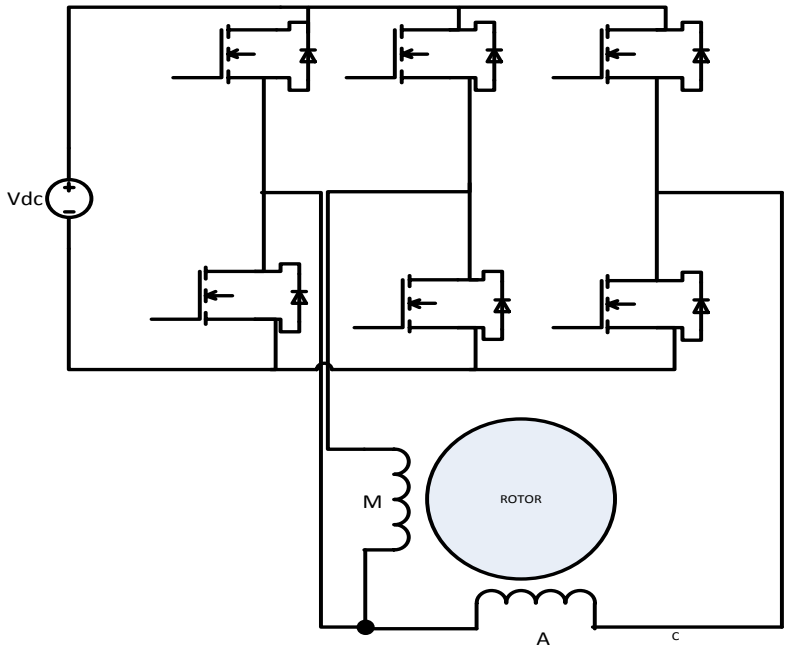


Figure 2.20: Two-Phase Inverter with Six-Transistor Bridge Supplying a Capacitor-less Motor(Blaabjerg *et al.*, 2004)

The two-phase inverter with six-transistor-bridge illustrated in Figure 2.20 is capable of limited phase angle control. Quadrature supply currents cannot be maintained for amplitudes higher than 70% of the value of the dc voltage. The topology requires a voltage booster for the auxiliary winding which increases cost of implementation(Holmes and Kotsopoulos 1993; Blaabjerg *et al.* 2004). It is relatively more expensive than the previous two topologies because of the cost of additional two transistors.

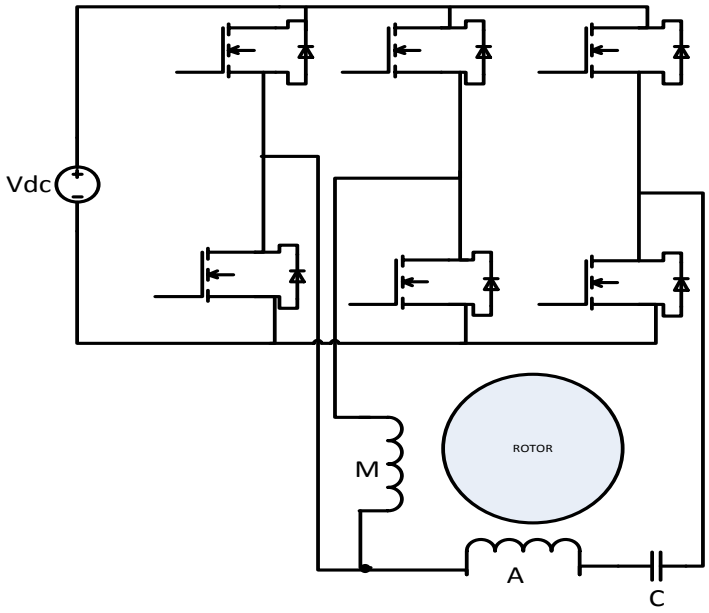


Figure 2.21: Two Phase Inverter with Six Transistor Bridge(Blaabjerg *et al.*, 2004)

The difference between the topology in Figure 2.21 and the topology in Figure 2.20 is that the running capacitor is placed in series with the auxiliary winding. Motor performance is impacted in the topology of Figure 2.21because of the capacitor (Blaabjerg *et al*, 2004).

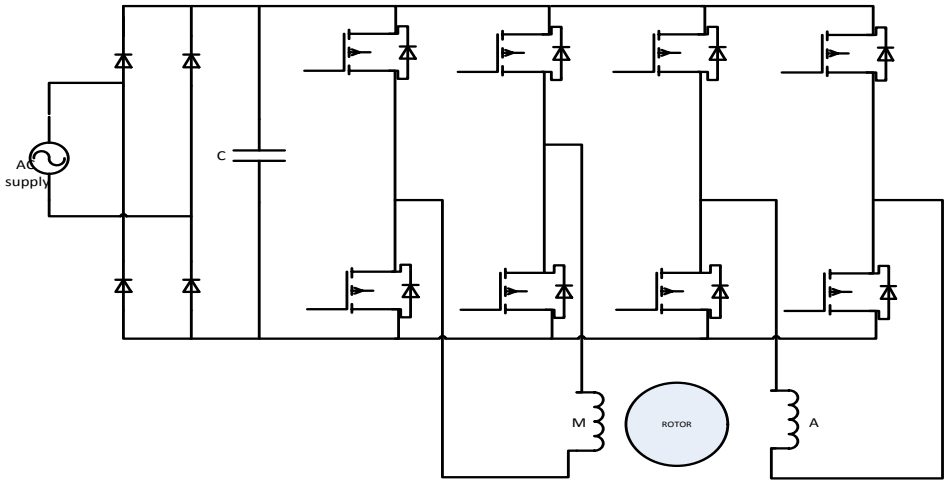


Figure 2.22: Two Phase Full Bridge Inverter (Kumsuwan *et al.*, 2010)

The topology in Figure 2.22 is also referred to as the four-leg inverter for two phase application. In this topology, winding voltages and currents may be controlled independently of each other. The set-up is, however, expensive because it uses eight switches. Any control circuitry associated with this type of topology will be far more complex than in the case of the four switch inverter (Kumsuwan*et al.*, 2010).

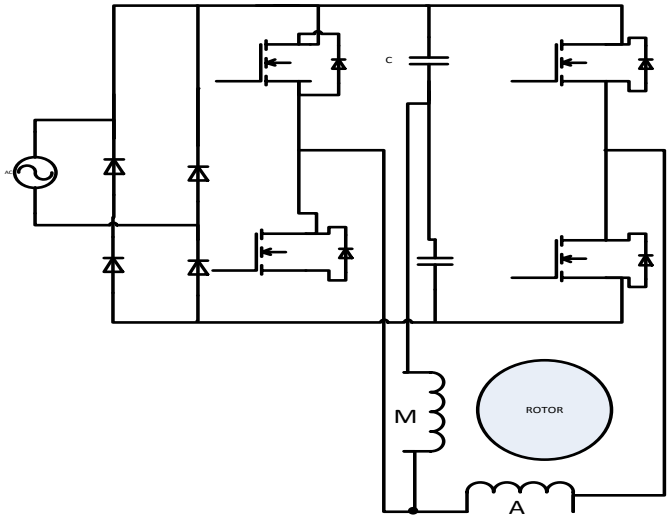


Figure 2.23: Two Phase Half Bridge Inverter(Ba-thunya *et al.*, 2001)

The topology of Figure 2.23 is the half-bridge version of that of Figure 2.22. It uses four switches but only half of the dc voltage is available to each winding leading to an under-utilization of the bus voltage.(Ba-thunya *et al*, 2001)

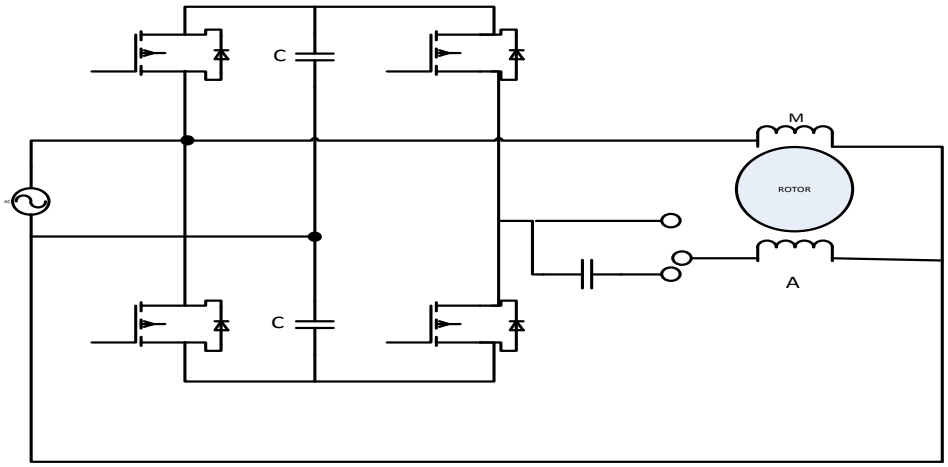


Figure 2.24: Single Phase Half Bridge Inverter with Power Factor Correction(Chomat and Lipo, 2003)

Figure 2.24 presents a topology in which the main winding is connected directly to the mains while the auxiliary winding voltage is supplied from one inverter leg. An ac capacitor is connected to make for a second operating speed. One drawback of the topology is that of insufficient dc voltage. The ac capacitor is tuned for only one frequency thereby limiting the speed of the motor to a fixed value. (Chomat and Lipo, 2003)

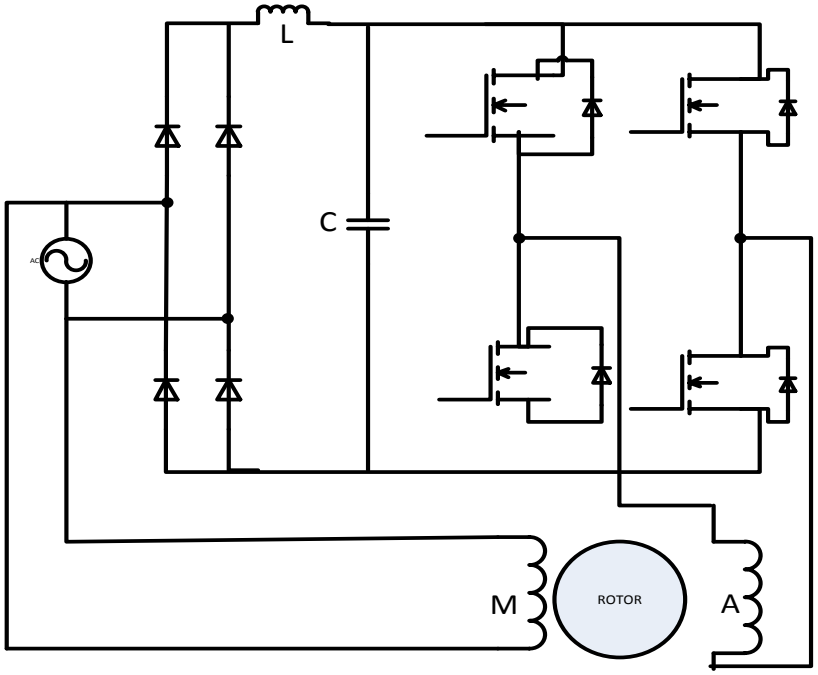


Figure 2.25: Single Phase Inverter with Auxiliary Winding Control (Collins *et al.*, 1988)

Figure 2.25 also presents a topology in which the main winding is connected directly to the mains while the auxiliary winding voltage is supplied from a two leg inverter. This topology does not include a series capacitor in the auxiliary winding circuit. (Collins *et al*, 1988)

2.2.4 Dynamic Modeling of the Single and Two Phase Inverter

For the single phase inverter given in Figure 2.18, the phase voltages with respect to a fictitious neutral point '*o*' are determined as follows (Mihret *et al*., 2011; Yazdani and Iravani, 2010):

$$V_{ao} = \frac{V_{dc}}{2}\left(S_{ap} - S_{an}\right) \tag{2.80}$$

$$V_{bo} = \frac{V_{dc}}{2}\left(S_{bp} - S_{bn}\right) \tag{2.81}$$

The restrictions imposed by Kirchoff's voltage and current laws on the circuit of Figure 2.18 is expressed mathematically as follows; (Séguier and Labrique, 1993; Gholami and Seifi, 2012)

$$S_{ap} + S_{an} = 1 \tag{2.82}$$

$$S_{bp} + S_{bn} = 1 \tag{2.83}$$

The switched phase voltages can be expressed in terms of S_{ap} and S_{bp} by substituting S_{an} and S_{bn} in equations (2.80) and (2.81) respectively using equations (2.82) and (2.83). The switched phase voltages therefore become:

$$V_{ao} = \frac{V_{dc}}{2}\left(2S_{ap} - 1\right) \tag{2.84}$$

$$V_{bo} = \frac{V_{dc}}{2}\left(2S_{bp} - 1\right) \tag{2.85}$$

The inverter output voltage V_{ab} is the difference between the phase voltages and may be given as:

$$V_{ab} = V_{dC}s(t) \tag{2.86}$$

where:

$$s(t) = \left(S_{ap} - S_{bp}\right) \tag{2.87}$$

$V_{ao}$and V_{bo} are the high frequency output voltages of the inverter phases. V_{ab} is the high frequency output voltage at the inverter output.V_{dc} is the DC input to the inverter. S_{ap} and S_{an} are the switching functions of the top and bottom switches of phase A while S_{bp} and S_{bn} are the

If the switch is open, the voltage at

switching functions of the top and bottom switches of phase B of the inverter. The switching function $s(t)$is defined as follows (Yazdani & Iravani, 2010):

$$s(t) = \begin{cases} 1 \\ 0 \end{cases} \tag{2.88}$$

It, however, has the general form given in the following equation(Holmes and Lipo, 2003):

$$s(t) = \frac{m_a}{2}\sin(\omega_m t + \emptyset_m) + \frac{4}{\pi}\sum_{m=1}^{\infty}\frac{1}{m}\sum_{n=1}^{\infty}J_n(mm_a\pi)\sin[n(\omega_m t + \emptyset)]\cos[m(\omega_c t + \emptyset_c] \tag{2.89}$$

Where $J_n(\xi)$ denotes the Bessel function of the first kind with order n and argument ξ. $\emptyset_m$ and $\emptyset_c$ are phase angles of the modulating and carrier signals respectively. The modulating signal, for sinusoidal PWM technique, is expressed as follows (Jang and Yoon, 1999; Kaźmierkowski and Krishnan, 2002; Holmes and Lipo, 2003; Marouchos, 2006):

$$m_s = M\cos(\omega_m t + \emptyset_m) \tag{2.90}$$

where M is the modulating index. When loads are applied at the output of each inverter leg, as indicated in Figure 2.19, then such a topology is referred to as a two phase inverter topology. For this topology, the output voltage is the same as the phase voltages and are given as follows (Yazdani and Iravani, 2010):

$$V_{ao} = \frac{V_{dc}}{2}S_1(t) \tag{2.91}$$

$$V_{bo} = \frac{V_{dc}}{2}S_2(t) \tag{2.92}$$

where:

$$S_1(t) = \left(2S_{ap} - 1\right) \tag{2.93}$$

$$S_2(t) = \left(2S_{bp} - 1\right) \tag{2.94}$$

The output voltage of each phase has the general form given in equation (2.78).

2.2.5 LC Filter Design

Figure 2.26 shows the block diagram of an AC-DC-AC converter. The purpose of such a converter is to convert ac voltage at a fixed magnitude, phase and frequency to one of variable magnitude, phase and frequency. Two low pass LC filters are typically used in these types of converters. One LC filter is used in the rectifier to provide a smooth dc voltage that is applied to the inverter and another LC filter is used at the output stage of the inverter in order to filter out undesirable harmonics from the inverter output thereby providing a smooth sinusoidal ac voltage that is then applied to the load. (Seguier &Labrique, 1993)

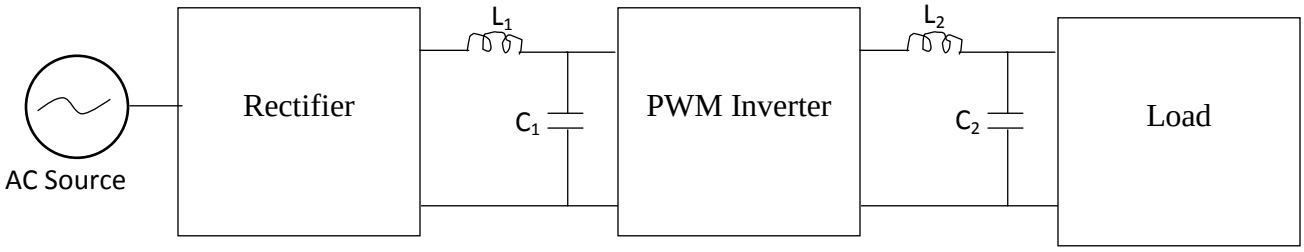


Figure 2.26: Single Phase AC-DC-AC Converter

The design of the filter inductor and capacitor is often guided by the amount of ripples or harmonics that can be tolerated (Rashid, 2004; Pawarand Kulkarni, 2015). In the case of the input filter, the values of filter components L_1 and C_1may be obtained from the following relationships (Seguier &Labrique, 1993):

$$C_1 = \frac{I_m}{U_s \omega k_f k_i} \tag{2.95}$$

$$L_1 = \frac{ki}{k_f} \frac{U_s}{I_m \omega} \tag{2.96}$$

where:

U_s =dc voltage supply to inverter

I_m = peak value of dc current

ω = angular frequency of supply voltage

k_i = current ripple factor

k_f = voltage ripple factor

In the case of the output filter, the values of filter components may be obtained from the relationship given as (Pawarand Kulkarni, 2015; RokrokandGolshan, 2009):

$$f_c = \frac{1}{2\pi\sqrt{L_2 C_2}} \tag{2.97}$$

Where f_c is the cut-off frequency of the filter.

2.2.6 Pulse Width Modulated Induction Motor Drive

An induction motor drive comprises a variable frequency converter also known as an inverter, a controller and an induction machine. Figure 2.27 illustrates the interrelationship between these three components of the machine drive.

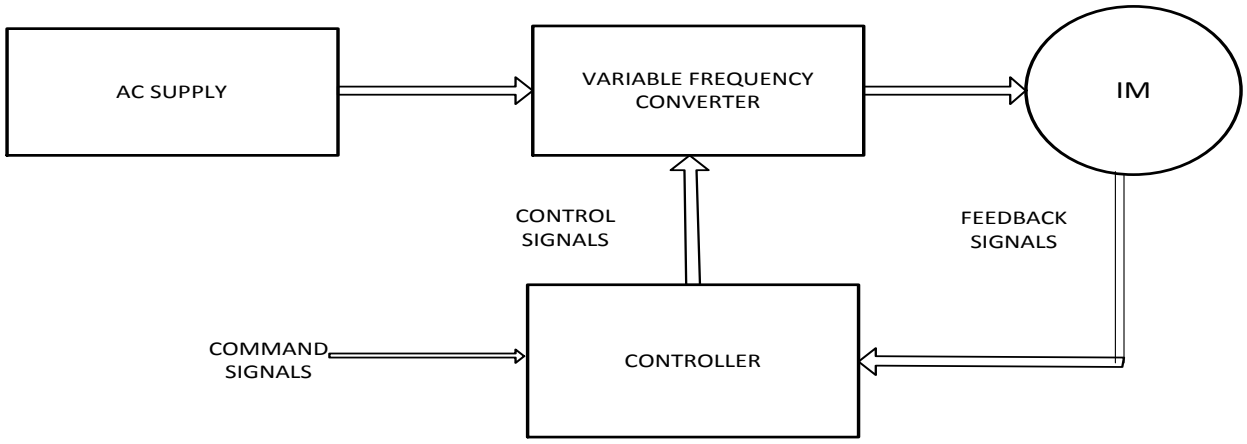


Figure 2.27: Block Diagram of an Induction Motor Drive System (Ong, 1998)

For the continuously variable speed control, the source frequency has to vary and the air gap flux kept constant by controlling the magnitude of the applied voltage in a linear proportion to the frequency. The application of this type of variable voltage variable frequency supply is made

possible by the inverter. Figures 2.18 – 2.25 illustrate different drive systems for the single/two phase induction motor. What is not shown in the figures is the associated controller. The primary function of the controller is to translate the reference signals and feedback signals into control signals for operating the inverter. Therefore, the frequency, phase and the magnitude of the inverter output voltage can easily be controlled by the action of the controller. The control signals for operating the inverter are typically generated by the PWM process similar to that described in section 2.2.3.5. As mentioned previously, the control signal determines the amplitude, frequency and the phase of the voltage supplied to the motor by the inverter. The objective of the motor drive system is to control the speed and torque of the machine with a view to improving machine performance.

2.2.7 Controller Design

For any power converter, a controller corrects any variations in system behavior or compensates for disturbances in the system. Usually, the controller output defines the switching patterns of the converter and derives its decisions as to any corrections or compensations from feedback and/or feed forward paths. Sometimes however, the controller output may be the reference to a process (Mohan, 2014). The feedback or feed forward paths or loops provide information about the current state of the plant or converter. A simple controller subsystem comprises a single loop as indicated in Figure 2.27. Controller subsystems composed of multiple loops also exists but such subsystems are more advanced than the single loop subsystems. There are different types of controllers in existence. The most popular types are the proportional (P), proportional plus integral (PI) and the proportional plus integral plus derivative (PID) controllers. The choice of any controller depends on the type of reference and the objectives for which the given control system sets out to achieve (Yazdani &Iravani, 2010). The PID controller uses the error signal to

generate the proportional, integral and derivative actions according to the following(Ang *et al.*, 2005; Salem and Rashed, 2013):

$$u(t) = k_p e(t) + k_i \int_0^t e(t)dt + k_d \frac{d}{dt}\ e(t) \quad (2.98)$$

Where$u(t)$ is the control signal,$e(t)$ is the error signal. k_p, k_i and k_d are the proportional, integral and derivative gains respectively. The PID controller is able to achieve a steady state error of zero for a step input and at the same time control both the rise time and maximum overshoot.A PI controller is often sufficient in DC command tracking problems and zero steady state tracking error is more easily achieved(Yazdani &Iravani, 2010). PI control is a combination of proportional and integral control. This type of controller outputs a control signal with a component that is proportional to the tracking error of the system and a component proportional to the accumulation of this error over time in accordance to the following equation(Franklin *et al.* 2006);

$$u(t) = k_p e(t) + k_i \int_0^t e(t)dt \quad (2.99)$$

With respect to reference tracking, a sinusoidal reference or command can be tracked with negligible attenuation or phase delay if the closed loop bandwidth is adequately larger than the frequency of the reference signal (Wang *et al.*, 2015). Control in the *d-q* frame essentially transforms a sinusoidal command tracking problem into an equivalent DC command tracking problem. This permits the use of controllers with simple structures(Miranda *et al.*, 2005; Roshan, 2007). A controller can be designed based on the root-locus method or the frequency response approach. Quite often, a trial and error approach is used to fine tune the gains in order to achieve desired specifications.Each method involves the use of an algorithm that accomplishes the controller design. Usually in controller design, certain specifications are given which accomplish desired controller design objectives. Such design specifications border around properties of the

system response which include properties like the percentage overshoot, damping ratio, settling time, rise time, steady state error (SSE), phase margin and bandwidth. (Franklin*et al, 2006)*. The following equations give the relationships between important design specifications (Franklin *et al*, 2006):

$$\% \text{ overshoot} = e^{\frac{-\zeta\pi}{\sqrt{1-\zeta^2}}} \tag{2.100}$$

$$\text{bandwidth} = \omega_n\sqrt{(1-2\zeta^2)+\sqrt{\zeta^4+4\zeta^2+2}} \tag{2.101}$$

where ζ is the damping ratio and ω_n is the natural frequency.

2.2.7.1 Frequency response overview

The frequency response is a representation of the system's response to sinusoidal inputs at varying frequencies. The output of a linear time invariant system to a sinusoidal input is a sinusoid of the same frequency but with a different magnitude and phase. The magnitude and phase differences between the input and output sinusoids at the preferred frequency is referred to as the frequency response of the system. Typically, a sinusoidal input with frequency less than the bandwidth frequency is tracked reasonably well by the system while a sinusoidal input whose frequency is higher than the bandwidth frequency is attenuated in magnitude and is shifted in phase. The bandwidth frequency is about 1.5 times the crossover frequency. The latter is imposed if a certain value is required for the bandwidth (Yazdani &Iravani, 2010). In the case of PWM signals, the switching frequency is usually higher and preferably one or two ordersof magnitude higher than the bandwidth because of the need to avoid interference in the control loop from the switching frequency noise(Mohan, 2009; Mohan, 2014)

2.2.8 Induction Machine Speed and Torque Control

The availability of fast, efficient and low-cost micro-controllers and power semiconductor switches make induction machine drives highly competitive in the motor drive industry. Induction machine drives continue to replace dc motor drives in various applications because of cost, performance and control flexibility requirements. The integration of power converters to ac machines has increased the range of application of these motors in residential, commercial and industrial centers around the globe.Over the years, the success of the integration of power converters to the three phase induction machine has encouraged researchers to apply same to single phase motors but taking into cognizance, the peculiarities of the single phase motors. A lot of motor control techniques applicable to the three phase induction machine is now being applied to the single phase induction machines (Rubio *et al.*, 2013; Jang, 2013). Before highlighting these techniques, it is important to show the relationships that exist between the voltage applied to the induction machine and the torque and speed outputs of the machine. It is within this context that the various motor control strategies used in adjustable speed drives or variable frequency drives find their practical value. These relationships will be highlighted in the following section.

2.2.8.1 Control principles of the induction machine

The induction machine is an electromechanical device in which the mechanical power supplied to the rotor is obtained by electromagnetic induction of voltage and current in the rotor windings due to the cutting action of the stator rotating magnetic field. The rotor of the induction machine therefore runs at a speed near the speed of rotation of the stator magnetic field also called the synchronous speed. The rotor speed never equals the synchronous speed (Krause *et al.*, 2013). The difference between the rotor speed and the synchronous speed is the slip speed which is an

extremely important variable in the control of the induction motor speed. The slip speed divided by the excitation frequency is commonly referred to as the motor slip and this slip is a measure of the motor speed. More elaborate description of the operating principle of the induction machine is available in (Krause *et al.*, 2013; Chapman, 2012).

For a small value of slip, the rotor speed of an induction machine is approximately proportional to the excitation frequency. The air-gap flux rotates at synchronous speed and establishes an electromotive force (E.M.F) which is commonly referred to as the air-gap flux or the magnetizing voltage. This point is illustrated in Figure 2.28 which gives the per-phase equivalent circuit for the three phase induction machine.

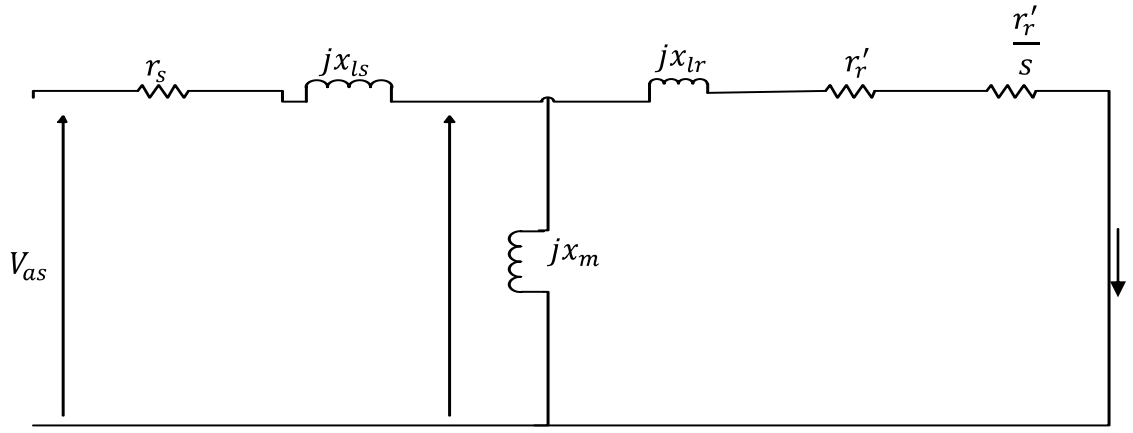


Figure 2.28: Per-Phase Equivalent Circuit of a Three Phase Induction Machine(Ong, 1998)

From magnetic circuit analysis, the air-gap flux, magnetizing voltage and the excitation frequency are related by (Ong, 1998):

$$\lambda_m = \frac{E_m}{\omega_e} \tag{2.102}$$

λ_m, E_m and ω_e represent the air-gap flux, magnetizing voltage and the excitation frequency respectively. Equation (2.102) points to the fact that maintaining a constant air-gap flux requires that the ratio of the magnetizing voltage to the excitation frequency be constant.

The square of the referred rotor current, i_{ar}^2 may be expressed as (Ong, 1998):

$$i_{ar}^2 = \frac{\lambda_m^2}{\left(\frac{r_r'}{\omega_e - \omega_r}\right)^2 + \left(\frac{X_{lr}'}{\omega_b}\right)^2} \tag{2.103}$$

While the electromagnetic torque, T_e induced in the machine may be expressed as (Ong, 1998):

$$T_e = \frac{3P}{2(\omega_e - \omega_r)} \left[\frac{\lambda_m^2}{\left(\frac{r_r'}{\omega_e - \omega_r}\right)^2 + \left(\frac{X_{lr}'}{\omega_b}\right)^2} \right] r_r' \tag{2.104}$$

P is the number of magnetic poles in the machine. $\omega_r$is the rotor speed in rad/s, ω_b is the base frequency of the system, r_r' is the rotor resistance and X_{lr}' is the leakage reactance of the rotor circuit. Equation (2.104) suggests that when the air-gap flux is held constant, the electromagnetic torque becomes a function of only the slip speed. Therefore if the slip speed is maintained constant at a given value then the torque will also remain constant as the excitation frequency changes. Similarly, the rotor current remains constant as excitation frequency varies if the slip speed is maintained at a constant value. This principle is crucial to the development of different control strategies needed for induction machine performance improvement. (Vas, 1992; Ong, 1998; Mohan, 2014). The various control strategies applied to the induction machine can be classified into two categories. These categories are the scalar control strategies and the vector or field-oriented control strategies. These broad strategies can be sub-divided into different types of control techniques given in Table 2.2.

Table 2.2 Classification of Induction Motor Control Strategies (Krishnan, 2001)

Scalar control strategies	**Vector control strategies**
Volts per hertz control	Stator flux oriented control
Slip energy-recovery control	Rotor flux oriented control
Frequency control	Air-gap flux oriented control
Stator voltage control	

The scalar control strategies provide good steady-state motor performance. They however, exhibit poor dynamic performance (Ong, 1998). This is because the air-gap flux linkages in the motor under scalar control, deviate from their set values in magnitude and phase. This limitation may be explained from the point of view of the utilization of the stator phase current magnitudes and their frequencies excluding their phases(Krishnan, 2001). A better and high performance control strategy is the vector control strategy. This is because the vector control strategy provides a coordinated control of stator current magnitudes, frequencies and their phases thereby exhibiting an extremely good dynamic motor performance. Vector control is achieved in field coordinates hence the name field-oriented control strategy. The vector or field-oriented control strategy is described after the section on the reference frame transformation.

2.2.9 Reference Frame Transformation

The reference frame transformation is a mathematical concept in which a change of variables is performed in order to transform real machine variables to a reference frame that rotates at a frequency whose value simplifies the solution of the system of equations relating these real variables. The reference frame is often referred to as the $q - d$ reference frame in which the q (i.e. quadrature) and the d (i.e. direct) axes components are perpendicular to each other. Reference frame transformation is a popular technique used in simplifying the analysis of electric machines. The transformation, in effect, replaces the variables (voltages, currents and flux linkages) associated with either the stator or the rotor windings of electric machines with the variables associated with fictitious windings whose axes are directed along paths perpendicular to each other but may be fixed either in the stator (stationary reference frame), rotor or the rotating magnetic field (synchronous reference frame). The axes of these fictitious machine windings are commonly referred to as 'q' and 'd' axes.

Krause *et al*., (2002) noted that a change of variables which simplifies the analysis of the single phase induction machines is one in which the stator and rotor variables of these machines are transformed to variables associated with fictitious stationary windings. In other words, stator and rotor variables are transformed to a frame of reference that is fixed in the stator. Because the stator of electric machines does not rotate, the speed of such a frame of reference is zero. The stator reference frame is therefore referred to as the stationary reference frame. The benefits of such a transformation includes reducing, if not completely eliminating the time varying inductances from the voltage and torque equations of single phase induction machines.

Furthermore, *q*-*d* transformation is widely used in the analysis and control of three phase systems with sinusoidal quantities. The variables of the three phase systems are typically transformed into α-β reference frame which is a two phase stationary reference frame. The transformation of the α-β variables from the stationary reference frame to a *d*-*q*rotating reference frame with same angular frequency as the fundamental frequency of the supply voltage is referred to as the synchronous reference frame transformation. Such a transformation results in a DC model of the sinusoidal quantities of the three phase system. Synchronous reference frame transformation is performed in machine analysis and control because all time-varying variables (i.e. voltages, currents and flux linkages) are transformed to DC quantities which do not vary with time thereby simplifying system analysis and control design.Figure 2.29 illustrates vector representations of stationary and rotating coordinates.

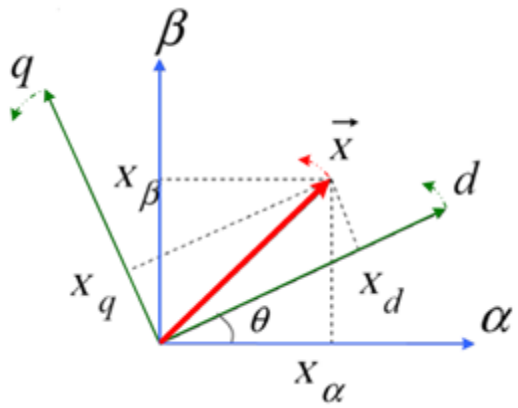


Figure 2.29: α-β and q-d Rotating Frame Vector Representation.(Roshan, 2007)

In Figure 2.29, Vector X is an arbitrary phase variable that is projected onto α-β stationary reference frame. X_α and X_β are the horizontal and vertical components of vector X. As vector X rotates anti-clockwise, its components X_α and X_β change with any change in the magnitude and position θ of X. Assuming, however, that there exists a *q-d* reference frame that rotates with the same angular frequency ω and direction as *X*, then the position of X with respect to components X_q and $X_d$is the same regardless of time. A rotating vector in the α-β stationary reference frame therefore becomes a constant vector in the *q-d* rotating reference frame because of the rotation of the reference frame. In other words, X_q and $X_d$are simply constant over the entire period of rotation of vector X. Their values depend only on the magnitude of *X* and not its position in the stationary reference frame. It is clear from Figure 2.29 that *q-d* components are related to α-β components by the following equations(Roshan, 2007; Krishnan, 2001, Krause*et al*, 2013):

$$\begin{bmatrix} X_q \\ X_d \end{bmatrix} = \begin{bmatrix} \cos\theta & \sin\theta \\ -\sin\theta & \cos\theta \end{bmatrix} \begin{bmatrix} X_\alpha \\ X_\beta \end{bmatrix} \tag{2.105}$$

$$\begin{bmatrix} X_\alpha \\ X_\beta \end{bmatrix} = \begin{bmatrix} \cos\theta & -\sin\theta \\ \sin\theta & \cos\theta \end{bmatrix} \begin{bmatrix} X_q \\ X_d \end{bmatrix} \tag{2.106}$$

Where the transformation matrix T is defined as (Roshan, 2007):

$$T = \begin{bmatrix} \cos\theta & \sin\theta \\ -\sin\theta & \cos\theta \end{bmatrix} \tag{2.107}$$

The reference frame transformation is also applied in the analysis of power system components such as transmission lines, loads, transformers, capacitor banks, etc. and to control systems associated with electric drives.

2.2.10 Vector Control Strategy

Vector control strategy allows precise and rapid control of the electromagnetic torque produced in the three phase induction machine. The torque control is accomplished by varying the stator current in such a way as to produce the amount of torque commanded while at the same time keeping the rotor field constant. Vector control strategy requires the transformation of machine variables such as voltages, currents and flux linkages to the synchronously rotating reference frame in order to achieve a precise control of electromagnetic torque in the machine. The equations that accomplish this transformation for the three phase and the two phase induction machines respectively are given as (Krause, 2013; Jang, 2013; Krishnan, 2001):

$$\begin{bmatrix} i_{qs}^{e} \\ i_{ds}^{e} \end{bmatrix} = \frac{2}{3}\begin{bmatrix} \sin\theta_e & \sin(\theta_e - \frac{2\pi}{3}) & \sin(\theta_e + \frac{2\pi}{3}) \\ \cos\theta_e & \cos(\theta_e - \frac{2\pi}{3}) & \cos(\theta_e + \frac{2\pi}{3}) \end{bmatrix}\begin{bmatrix} i_{as} \\ i_{bs} \\ i_{cs} \end{bmatrix} \tag{2.108}$$

$$\begin{bmatrix} i_{qs}^{e} \\ i_{ds}^{e} \end{bmatrix} = \begin{bmatrix} \cos\theta_e & \sin\theta_e \\ -\sin\theta_e & \cos\theta_e \end{bmatrix}\begin{bmatrix} i_{as} \\ i_{bs} \end{bmatrix} \tag{2.109}$$

i_{qs}^{e}andi_{ds}^{e} are the q and d- axes currents of the stator windings in the synchronously rotating reference frame. i_{as}, i_{bs} and i_{cs} are the real stator current variables. $\theta_e$is the angular distance between the synchronous reference frame and the machine variables reference frame.

The reason for this transformation is because the stator flux or the rotor flux control is made more difficult by the interaction of the rotating stator and rotor magnetic fields and either of these quantities is not easily controlled in the *a-b-c* reference frame in which the quantities exist in real-time(Krishnan, 2001; Vas, 1992). The *d*-axis of the synchronously rotating *q-d* reference frame is usuallyaligned with either the stator flux or the rotor flux. With this alignment, the q-component of the stator flux or rotor flux is set to zero thereby producing what is referred to as either the stator flux or the rotor flux oriented control. In the rotor flux oriented control scheme for example, when a proper alignment of the reference frame is done, the torque equation simplifies to the following equation (Krishnan, 2001; Ong, 1998; Vas, 1992):

$$T_e = \frac{3P}{4}\left(\frac{L_m}{L_m + L'_{lr}}\right)\lambda'^{e}_{dr} I^{e}_{qs} \tag{2.110}$$

$\lambda'^{e}_{dr}$is the d-axis rotor flux representing the rotor flux vector, I^{e}_{qs} is the q-axis component of the stator current and L_m is the mutual inductance. Equation (2.110) suggests that the electromagnetic torque, T_e may be controlled by adjusting either the rotor flux or the stator current since L_m, L'_{lr} and P are machine constants.$L'_{lr}$is the rotor leakage inductance. If the rotor flux is maintained constant then the torque may be precisely controlled by adjusting the stator current. Two methods are usually employed in the field oriented control scheme. The first method is the direct field oriented control scheme in which a direct measurement of the air-gap flux is done. The measured air-gap flux along with measured stator current is then used to determine the magnitude of the rotor flux and its proper orientation in the synchronously rotating *q-d* reference frame. The second method is the indirect field oriented control scheme. This scheme does not rely on direct measurement of the air-gap flux but instead uses the q and d axis components of the stator current to control the rotor field and maintain its proper orientation in

the q-d reference frame. Proper orientation here means the correct instantaneous angle between the synchronously rotating *q-d* and *a-b-c* reference frames (i.e.θ_e). In the case of the rotor flux oriented control scheme, it can be shown that the regulated values of the *q*and *d*-axis components of the stator current are given as (Krishnan, 2001; Ong, 1998; Vas, 1992):

$$i_{qs}^{e*} = \frac{4}{3P}\left(\frac{L_m + L'_{lr}}{L_m}\right)\left(\frac{T_{em}^*}{\lambda_{dr}'^*}\right) \tag{2.111}$$

$$i_{ds}^{e*} = \left(\frac{r'_r + p\left(L_m + L'_{lr}\right)}{r'_r L_m}\right)\lambda_{dr}'^* \tag{2.112}$$

Equations (2.111) and (2.112) describe the interaction between the regulated values of the stator currents and the commanded values of torque and rotor flux in the machine. The regulated values of the stator currents are used to calculate the slip speed required to maintain the proper alignment of the synchronously rotating q-d reference frame with the rotor flux in a manner described by the following equation (Krishnan, 2001; Ong, 1998; Vas, 1992):

$$\omega_e - \omega_r = \left(\frac{L_m}{L_m + L'_{lr}}\right)\frac{I_{qs}^e}{i_{ds}^{e*}} \tag{2.113}$$

Figure 2.30 illustrates the relationship between the properly oriented synchronously rotating *q-d* reference frame along with the *q-d* components of the stator current and the *a-b-c* reference frame (in which thereal machine currents are represented) when the rotor flux vector is properly aligned. The field orientation is the instantaneous angle between the synchronously rotating *q-d* and *a-b-c* reference frames and it is the sum of the rotor angle and the angle derived from the integration of the slip speed. (Krishnan, 2001; Ong, 1998; Vas, 1992)

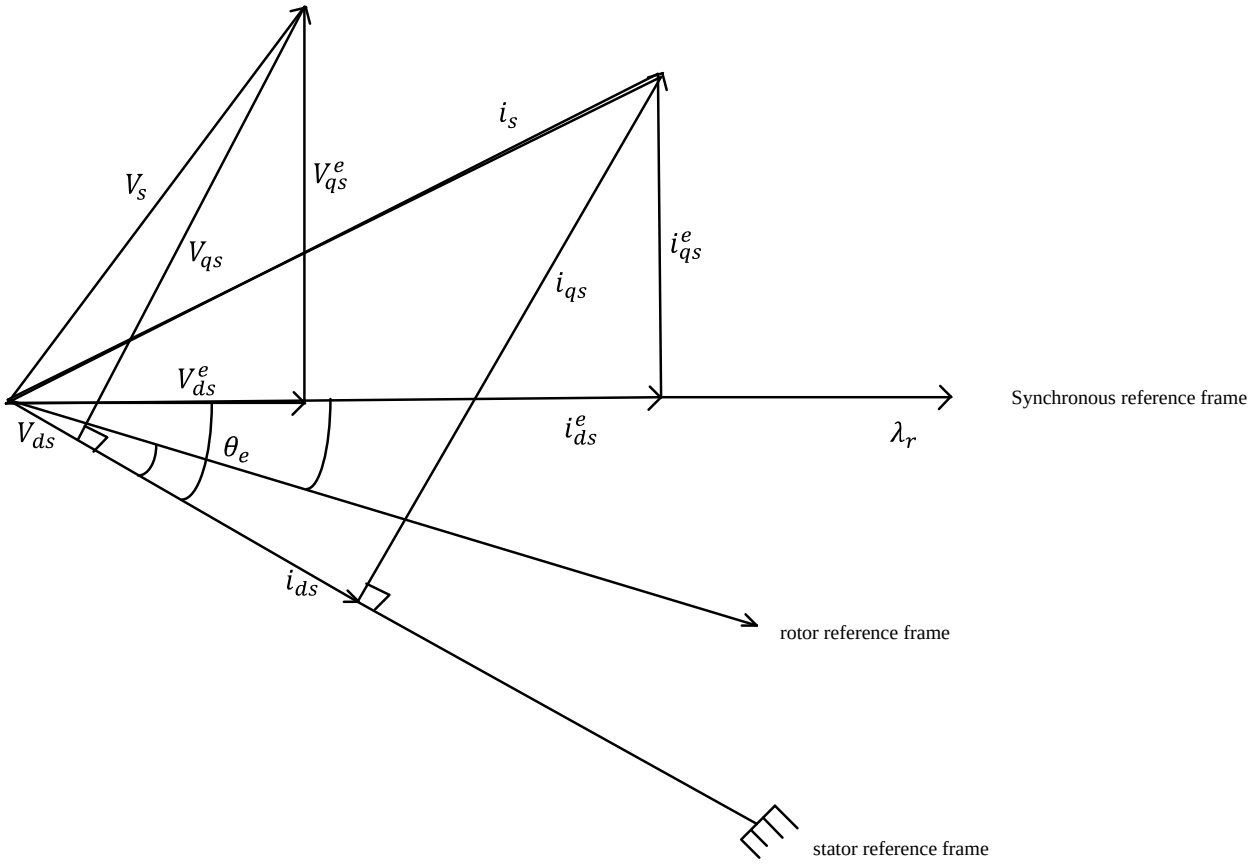


Figure 2.30: Phasor Diagram of the Vector Control Strategy(Krishnan, 2001)

In Figure 2.30, the stator current phasor magnitude remains the same regardless of the reference frame chosen to view it. The d-axis component of this current is seen to be in phase with the rotor flux. The q-axis component of the stator current is seen to be perpendicular to the d-axis component also referred to as the flux-producing component and is thus, the component responsible for producing the torque in the machine. The orientation of the rotor flux or the flux angle is the sum of the rotor angle and the slip speed angle. The rotor flux angle is extremely crucial to the realization of the vector control scheme as its value at every instant of time is

required in order to track the position of the rotor flux and hence maintain the integrity of the vector control scheme. Figure 2.30 shows that;

$$\theta_e = \theta_r + \theta_{sl} \tag{2.114}$$

Where θ_e is the rotor flux angle, θ_r is the rotor position and θ_{sl} is the slip angle. The rotor position is often obtained by measurements while the slip speed may be obtained as follows; (Krishnan, 2001; Ong, 1998; Vas, 1992)

$$\theta_{sl} = \int(\omega_e - \omega_r)dt \tag{2.115}$$

Figure (2.31) gives the block diagram of the indirect rotor flux oriented control scheme and it illustrates the process described in this section.

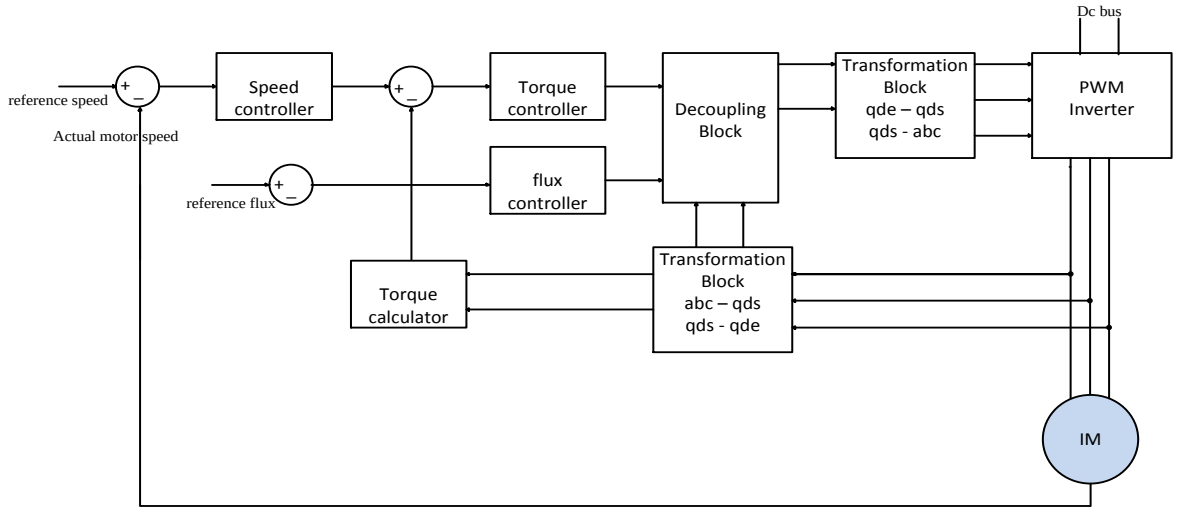


Figure 2.31: Block Diagram of the Indirect Rotor Flux Oriented Control Scheme.(Ong, 1998)

Equations (2.108) and (2.109)are computed inside the *a-b-c* to *q-d* transformation block shown in Figure 2.31. The calculated value of $|\lambda_r|$ is fed back to the input of the flux controller regulating the rotor flux. Inside the torque calculation block, the calculated values of $|\lambda_r|$ and $|i_{qs}|$ are used in equation (2.110) to estimate the value of torque developed by the machine and

the estimated torque is fed back to the input of the torque controller. The respective outputs of the torque and flux controllers are the command values of i_{qs}^{e} and i_{ds}^{e} in the field oriented rotor reference frame. Inside the *q-d* to *a-b-c* transformation block are the following transformations from *q-d-e* to *q-d-s* and then to balanced *a-b-c* reference frames. This operation is simply the inverse of equations(2.108) and (2.109). The vector control scheme is well established for the three phase induction machines. It is, however, still the subject of intense research for the single phase induction machines (Jang, 2013; Nied *et al*, 2013).

2.2.11 Efficiency Optimization

In an age where energy efficiency cannot be over-emphasized, it is imperative to seek methods to better utilize electric power and free up spare capacity for the ever-increasing electric power demand. It is well known that induction machines, particularly the single phase induction machines are major consumers of electricity worldwide. As a matter of fact, there are far more single phase induction machines in use than all other electric machines combined(Liu and Wang, 1994; Liu, 1995; Fating *et al*., 2008; Latt and Win, 2009). Consequently, a lot of efforts is being made to increase the energy-efficiency of machines in this category.

One of such efforts is the use of loss minimization schemes that effectively optimizes energy consumption of the machine during operation. The losses of interest are the copper losses and the core losses which constitute the major losses in a machine. Copper losses can be reduced by reducing the magnitude of currents in the machine windings while the core losses can be reduced by reducing the air-gap flux density of operation(Dong, 2005). Conventional machines operate at rated flux density regardless of the load on the machine (Dong, 2005; Naxin*et al.*, 2004). This essentially means that light loads (i.e., loads smaller than the rated load) generate unnecessary and avoidable losses in the core of the machine owing to excessive flux density in the air-gap; a

situation that leads to sub-optimal levels of efficiency in the machine. Studies have shown that there is an air-gap flux density in a machine that produces minimum losses for any given load applied to the machine (Dong, 2005). In other words, the flux in the air-gap may be adapted to suit any given operating load condition, thereby reducing losses at that level of operation and hence maximizing the efficiency of the machine at that operating point. Methods used to implement loss minimization schemes include the following; (Dong, 2005; Naxin*et al.*, 2004)

a) Model-based loss minimization scheme

b) On-line power search optimization-based loss minimization scheme

The on-line power search optimization technique is slow reaching the optimum and torque pulsations exist in steady state. Model-based optimization technique is fast and does not produce torque pulsations (Naxin*et al.*, 2004). The model-based technique can be integrated with the vector control scheme to bring about an efficient drive system for the induction machine.

2.2.12 Harmonic Balance Technique (HBT)

Harmonic balance technique is a mathematical tool that is used to simplify the analysis of electrical circuits that operate in the sinusoidal steady state. The variables of the voltage and torque equations of the single phase induction machine in the stationary reference frame are not constants in steady state. Instead, they are sinusoids with constant peak values under steady state conditions. Consequently, the variables may be represented by their peak or rms values for the purpose of analyzing the behavior of the machine under steady state conditions. The HBT helps in extracting the peak or r.m.s values of these variables from the voltage, flux linkage and torque equations, thereby simplifying the solution of the steady state equations of the single phase induction machine. Two basic theorems of the HBT are of importance in this work. These theorems are highlighted as follows; (Omozusi, 1998)

a) **Theorem 1 (Linearity rule):** A linear combination of sinusoids with real coefficients is equal to a linear combination of phasors representing the individual sinusoids. Symbolically, the sinusoids are given as (Omozusi, 1998):

$$f_1(t) = F_{m1}\cos(\omega t + \varphi_1) = Re\left[\bar{F}_1 e^{j\omega t}\right] \tag{2.116}$$

$$f_2(t) = F_{m2}\cos(\omega t + \varphi_2) = Re\left[\bar{F}_2 e^{j\omega t}\right]. \tag{2.117}$$

Where F_{m1} and F_{m2} are respectively the peak values of the sinusoids. ω is the angular frequency while φ_1 and φ_2 are the phase angles of the sinusoids. $\bar{F}_1$ and $\bar{F}_2$ are phasors expressed as (Omozusi, 1998):

$$\bar{F}_1 = F_{m1}e^{j\varphi_1} \tag{2.118}$$

$$\bar{F}_2 = F_{m2}e^{j\varphi_2} \tag{2.119}$$

They are complex numbers otherwise known as phasors representing the sinusoids. Then theorem 1 suggests that the linear combination:

$$a_1 f_1(t) + a_2 f_2(t) \tag{2.120}$$

is adequately represented by the linear combination given as:

$$a_1\bar{F}_1 + a_2\bar{F}_2 \tag{2.121}$$

where $a_1$and a_2 are any two real numbers.

b) **Theorem 2 (Differentiation rule):** This theorem states that $\bar{F} = F_m e^{j\varphi}$ is the phasor of a given sinusoid $F_m\cos(\omega t + \varphi)$ if and only if $j\omega\bar{F}$ is the phasor of its derivative given as $\frac{d}{dt}[F_m\cos(\omega t + \varphi)]$. Symbolically (Omozusi, 1998):

$$Re\left[j\omega\bar{F}e^{j\omega t}\right] = \frac{d}{dt}\left(Re\left[\bar{F}e^{j\omega t}\right]\right). \tag{2.122}$$

Equation (2.122) indicates that the linear operators Re and $\frac{d}{dt}$ commute. That is,

$$\frac{d}{dt}\left(Re\left[\bar{F}e^{j\omega t}\right]\right) = Re\left(\frac{d}{dt}\left[\bar{F}e^{j\omega t}\right]\right). \tag{2.123}$$

2.2.13 Fundamental Concepts of AC Machine Windings

Ac machine windings conduct alternating current and are embedded in slots. Slots are equally spaced grooves cut in the inner surface of the stator to accommodate the coils of the windings. The terminologies usually applied in ac machine windings are defined in the following section.

2.2.13.1 Machine winding terminologies

These terminologies are outlined and definedas follows;(Bimbhra, 2004)

a) Conductor:This refers to a length of wire that takes an active part in the energy conversion process. A conductor may be made up of one or more parallel strands.

b) Turn:A turn consists of two or more conductors connected in series.

c) Coil:A coil consists of one or more turns connected in series. Figure 2.32 shows a coil having one turn.

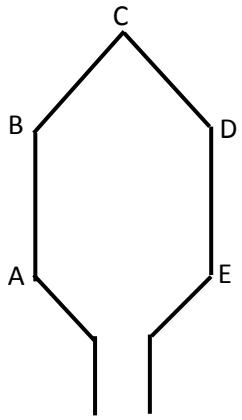


Figure 2.32: One Turn Coil(Bimbhra, 2004)

d) Coil side:This refers to any of the two sides of a coil. Lines AB and DE in Figure 2.32 are the coil sides of coil ABCDE.

e) Coil group: A winding consists of a number of coils that are arranged in groups. A coil group may contain one or more coils. The number of groups per phase is computed using the following equation(Bimbhra, 2004):

$$\text{Number of groups per phase} = \frac{\text{Number of coils/phase}}{\text{Number of coils/group}} \quad (2.124)$$

f) Number of poles: The number of poles, P is determined according to the following equation; (Bimbhra, 2004)

$$P = \frac{120 \times \text{frequency(Hz)}}{\text{Speed(rpm)}} \quad (2.125)$$

g) Slots per pole per phase: The number of slots per pole per phase is equal to the number of slots divided by the number of poles and by the number of phases. This parameter is a very important quantity in the layout of ac windings and is mathematically expressed as (Bimbhra, 2004):

$$\text{Slots/pole/phase} = \frac{\text{Number of slots}}{\text{Number of phases} \times \text{Number of phases}} \quad (2.126)$$

h) Pole phase group: This refers to the coils which belong to one phase and which are under one pole. The number of coils per phase is computed using the following equation (Bimbhra, 2004):

$$\text{Coils per phase} = \frac{\text{Number of slots}}{\text{Number of phases}} \quad (2.127)$$

i) Slot Pitch: This is the width of a slot measured in degrees. It is given as (Bimbhra, 2004):

$$\text{Slot pitch}, \gamma = \frac{180^0 \times \text{Number of poles}}{\text{Number of slots}} \quad (2.128)$$

j) Pole pitch: This refers to the peripheral distance between identical points on two adjacent poles. A pole pitch is equal to the circumference of the armature divided by the number of poles and it is always equal to 180^0 electrical. It may also be computed in terms of number of slots as follows(Sawhney and Chakrabarti, 1996; Bimbhra, 2004):

$$\text{Pole pitch} = \frac{\text{Number of slots}}{\text{Number of poles}} \quad (2.129)$$

k) Coil pitch: This refers to the distance between two sides of a coil. When the coil pitch is equal to a pole pitch, the winding is called a full pitch winding (Bimbhra, 2004). When this is not the case, the winding is referred to as a fractional-pitch or chorded winding. The coil span is a function of the coil pitch and is given as (Sawhney and Chakrabarti, 1996; Bimbhra, 2004):

$$\text{Coil span} = \text{coil pitch} \times \text{pole pitch} \tag{2.130}$$

It is measured in terms of slots or degrees.

l) Phase spread: This is the number of adjacent slots in any pole section containing coils of the same phase. It is usually given in degrees and is computed as follows (Sawhney and Chakrabarti, 1996; Bimbhra, 2004):

$$\text{Phase spread} = \text{Number of slots per pole per phase} \times \text{slot pitch} \tag{2.131}$$

m) Clock diagram: A diagram that shows the winding arrangement of polyphase ac windings.

2.2.13.2Classification of AC windings

AC windings can be classified from several points of view(Liwschitz-Garik 1950). The following classifications are relevant to this research.

a) Single Phase or Poly-Phase Winding

AC windings are classified as single phase, two phase, three or more phases corresponding to the number of phases of the lines to which they are connected.

b) Single Layer or Double Layer Winding

When the AC winding is designed with one coil side occupying the total slot area in all slots, the winding is referred to as a single layer winding. If the winding is designed in such a way that the slot contains an even number of coil sides in two layers, then the winding is called a double layer winding.

c) Concentric or Distributed Winding

Concentric winding is a winding in which all coils in a coil group have a common center. All coils in a concentric winding have different coil spans and different number of turns. Distributed winding, on the other hand, is a winding in which all phases have equal coils and equal slot space is devoted to all phases (Mittle and Mittal, 1996; Sawhney and Chakrabarti, 1996; Bimbhra, 2004).

d) Integral-Slot or Fractional Slot Winding

When the number of slots per pole per phase is an integer, then the winding is referred to as integral slot winding. In this type of winding, coil groups of all phases have equal number and size of coils and hence all phase windings are symmetrical. A fractional-slot winding is a winding in which the number of slots per pole per phase is a fractional number. In this type of winding, the number of single coils is not the same for all coil groups of any phase.

A discussion of the nature of single and two phase windings is provided in the following sub-sections.

2.2.13.3 Single phase induction machine winding design

The concentric winding is the most widely used for capacitor-run single phase induction machines. In the concentric winding for single phase induction machines, all coils in a pole group have a common center. The coils also have different pitches and different number of turns both on the main and the auxiliary windings. The auxiliary winding is usually designed to have a higher resistance and a lower reactance than the main winding (Mittleand Mittal, 1996). The number of turns on the auxiliary winding is typically calculated as a function of the number of turns in the main winding.

The solution to the winding design problem usually begins with the specification of the following parameters; (Fuchs *et al.,* 1987)

a) Number of stator slots

b) Number of poles

c) Current densities of the main and auxiliary windings

d) Current in the main and auxiliary windings

e) Specific magnetic loading or the air-gap flux density

The goal of winding design is to find the actual number of turns for the main and auxiliary windings and their distribution in slots. For single phase induction machines, sinusoidal winding distribution is normally adopted because it minimizes the harmonic in the air-gap flux wave(Fuchs *et al.*, 1987; Sawhney and Chakrabarti, 1996; Mittle and Mittal, 1996; Bimbhra, 2004). The sinusoidal winding distribution is a distribution in which the turns of the windings located within the slots are distributed in a sinusoidal manner. The following equations define the sinusoidal distribution of the turns of the main winding (Fuchs *et al.,* 1987):

$$N_{CAj} = \frac{N_{PA}\sin\left(\frac{j\pi}{Q_p}\right)}{\sum_{j=1}^{\frac{Q_p-1}{2}}\sin\left(\frac{j\pi}{Q_p}\right)} \; for\; Q_p\; odd \tag{2.132}$$

$$N_{CAj} = \frac{N_{PA}\sin\left(\frac{(2j-1)\pi}{2Q_p}\right)}{\sum_{j=1}^{\frac{Q_p}{2}}\sin\left(\frac{(2j-1)\pi}{2Q_p}\right)} \; for\; Q_p\; even \tag{2.133}$$

Where N_{CAj} is the number of turns in the jth coil of the main winding.$N_{PA}$is the number of turns per pole in the main winding and Q_p is the number of slots per pole.

The winding factor which is the ratio of the geometric and algebraic sums of the induced voltages in a set of distributed coils is given as (Fuchs *et al.,* 1987):

$$K_w = \frac{\sin\left(\frac{\pi}{2}\right)\sum_{j=1}^{q_c} N_{Ci} \sin\left(\frac{\pi Y_{cj}}{2\,Q_p}\right)}{\sum_{j=1}^{q_c} N_{Cj}} \tag{2.134}$$

The concentric winding is single layer and has the same number of coil groups as poles, each group being made up of two or more coils that fit concentrically around one another. If a machine has a specification of 4 poles and 32 slots then such a winding is wound to have four identical coil groups. The maximum number of coils per group is typically approximated to the whole number obtained after dividing the number of slots per pole by 2. The procedure for calculating the turns in various coils of a pole group is as follows (Rosenberg, 1970; Mittle and Mittal, 1996):

a) Obtain the span for various coils

b) Determine the chord or pitch factor of various coils

c) Calculate the number of turns in various coils based on equations (2.132) and (2.133).

The arrangement of the main winding in slots for a 4 poles and 32 slots CRSPIM has the form given in Table 2.3.

Table 2.3: Arrangement of the Main Winding in Slots for a 4-Pole, 32 Slots CRSPIM(Rosenberg, 1970)

Coilgroup	**CoilNumber**	**Slot Number**	**Coil Span**	**Number of turns per coil**
1	1	3 – 6	3	Nm1
	2	2 – 7	5	Nm2
	3	1 – 8	7	Nm3
2	1	14 – 11	3	Nm1
	2	15 - 10	5	Nm2
	3	16 – 9	7	Nm3
3	1	19 – 22	2	Nm1
	2	18 - 23	4	Nm2
	3	17 - 24	6	Nm3
4	1	30 – 27	2	Nm1
	2	31 - 26	4	Nm2
	3	32 – 25	6	Nm3

Nm1 to Nm3 arecalculated using equation (2.132). They are typically different in sinusoidal winding distribution. Winding connection between coil groups may be series or parallel depending on the voltage and current requirements of the machine. The auxiliary winding for the 4 poles and 32 slots motor also consists of four identical coil groups. Like the main winding, the auxiliary winding also has three coils in a coil group but the number of turns is different from the number of turns in the coils of the main winding. The number of turns in the auxiliary winding is usually calculated using the following equation (Mittle and Mittal, 1996):

$$N_a = K \times \frac{k_{wm}}{k_{wa}} \times N_m \tag{2.135}$$

Where$K$ is the transformation ratio between the auxiliary and the main winding and it ranges from 1.5 to 2. k_{wa} is the winding factor of the auxiliary winding and it is usually taken to vary from 0.78 to 0.84. The arrangement of the auxiliary winding in the slots is similar to that of the main winding except that the auxiliary winding is placed at the top of the slots. Its poles are also placed midway between the poles of the main winding (Rosenberg, 1970). In other words, the auxiliary winding is displaced 90^0 electrical degrees from the main winding. The winding diagram for a four pole, 32 slots CRSPIM is given in Figure 2.33.

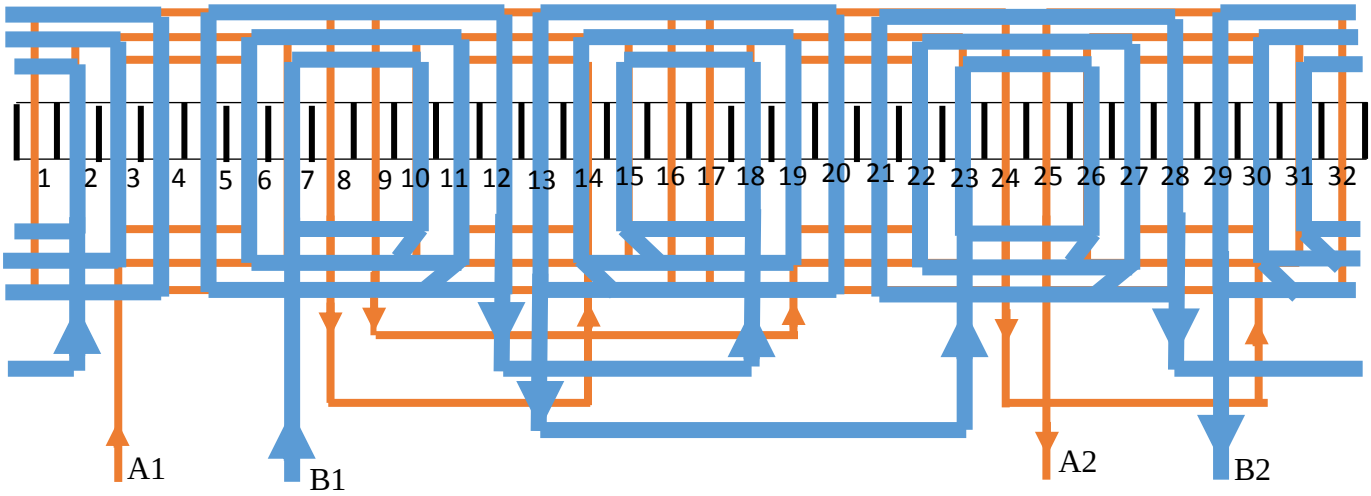


Figure 2.33: Winding Diagram of the Stator of a 4-Pole, 32 slots CRSPIM(Rosenberg, 1970)

In Figure 2.33, the poles of the auxiliary winding are located between two main winding poles to effectively displace the axis of the auxiliary winding 90^0 from the axis of the main winding.

2.2.13.4 Poly-phase double-layer winding

In a poly-phase winding, double layer winding, the number of coils is always equal to the number of slots. If the winding is to be balanced and symmetrical, it is essential that the number of phases is a factor of the number of slots. It is also essential that the number and size of coils of the windings is the same for all phases (Bhimbra, 2004). When the number of slots per pole per

phase is an integer, the winding is referred to as an integral slot winding. If the number of slots per pole per phase is not an integer, the winding is referred to as a fractional-slot winding.

The integral slot winding can either be full pitch or fractional pitch. When it is full pith, the number of slots per pole is the same as the coil pitch or the span of the coil. When the winding is fractional pitch, then the coil pitch is less than the number of slots per pole or the pole pitch. The fractional pitch winding is the most popular type of winding pattern used in poly-phase ac windings because of its advantages over the full pitch integral slot winding. These advantages are as follows; (Bimbhra, 2004)

a) It reduces the copper requirement of the coils that make up the winding

b) It reduces the harmonics in the emf and mmf waveforms of the phases

The coil pitch in poly-phase ac windings generally varies from two-thirds (*i.e.*⅔) of a pole pitch to a full pole pitch. Any coil pitch less than two-thirds of a pole pitch is not used in practice because a chording of more than one-third (⅓) of a pole pitch will significantly reduce the phase voltages (Bimbhra, 2004).

The number of slots per pole per phase determines the number of coils per phase group. It also determines the phase spread of coils in a group. The number of pole phase groups is given as (Liwschitz-Garik, 1950):

$$\text{Number of pole phase groups} = \text{Number of poles} \times \text{Number of phases} \tag{2.136}$$

Poly-phase ac windings are typically designed in such a way that coils of one group in any pole section are in adjacent slots. If the winding is a double layer type, which is commonly the case with poly-phase ac windings, every coil in a coil group has one of its coil-sides in the top half of one slot and the other coil-side in the bottom half of another slot one coil pitch away. Double layer, integral slot, fractional pitch winding has the advantage that it is easier and cheaper to

manufacture than its single layer counterpart. In addition, it increases machine performance (Bimbhra, 2004).

2.2.13.5 Two phase winding layout

A two phase winding is like a three phase winding, or any poly-phase winding for that matter, in all respects except for the number of groups and the connection of the windings (Rosenberg, 1970). The coils of the two phase winding are connected to produce two windings instead of three or more windings. Also, in a two phase winding, the slots per pole are divided into two parts, one part for each phase.

Using equation (2.136), the case of a two phase, four pole machine gives eight pole phase groups. The eight groups are shown in Figure 2.34 where the circle represents the cross-sectional view of the stator of the two phase machine.

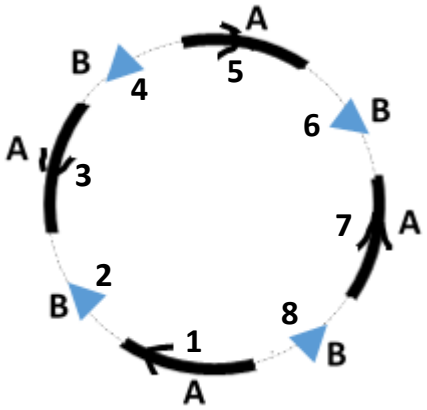


Figure 2.34: One Line Diagram of a Two Phase Four Pole Winding Layout.(Liwschitz-Garik 1950)

In Figure 2.34, a pole phase group is represented by a single line. The eight pole phase groups are numbered 1 – 8 in a clockwise direction. Groups 1, 3, 5 and 7 are coil groups belonging to one of the two phases, say phase A. Coil groups 2, 4, 6 and 8 belong to the second phase i.e. phase B. Coil groups of phase A are indicated by heavy black lines while the coil groups of

phase B are indicated by thin blue lines. The current direction of the individual pole phase groups is indicated by arrows. The arrows show that two consecutive pole phase groups of the same phase lie under poles of different polarity and therefore the current in these pole phase groups flow in different directions. The arrows also show that two alternate pole phase groups of the same phase lie under poles of same polarity and the current in these pole phase groups flow in the same direction as seen in Figure 2.34. This is a rule that applies to all windings regardless of whether it is single phase or poly phase, concentric or distributed as the case may be. The rule guides the designer in determining the manner in which the coil groups of any phase may be connected in series or parallel in order to withstand the voltage to be applied to the windings. (Liwschitz-Garik 1950)For example, a winding may be laid out to have a series-connection for 220V and two-parallel connection for 110V.

In a two phase integral slot winding, the beginning of the phases lie in slots which are half a pole-pitch apart. This implies that the axis of one phase winding is displaced 90^0 electrical degrees from the axis of the other phase winding. (Rosenberg, 1970)

2.3 REVIEW OF SIMILAR WORKS

A review of similar works done in the area of performance improvement of single phase induction machine is presented as follows;

Lee *et al.* (2001) proposed the vector control of the single phase induction machine in which the stator current was decoupled into the flux producing component and the torque producing component so that the speed of the machine was effectively controlled as the load on the machine changes in real-time. The use of the d – q model equations of the single phase induction machine in the stationary reference frame was evident in this work. An equivalent circuit in which stator parameters were referred to the rotor side was proposed. Model equations in the stationary reference frame were subsequently transformed to the synchronously rotating reference frame. The authors used a single phase inverter in which the main and auxiliary windings were connected to each arm of the inverter and their common terminal was connected to the neutral point of the DC link. An additional arm was included for the input stage power factor correction. Result of the work showed that the motor speed was effectively controlled using the q-axis current even though the speed reference was changed at no load while the d-axis current remained constant. With changes in load, the result of the proposed method showed that the torque ripples were reduced when compared to those of the conventional capacitor motor without control. Although the proposed method gave improved performance over that of the conventional system, significant torque ripples were evident during load changes. Moreover, the proposed system requires complex modeling techniques. Motor drive efficiency improvement was not considered in this work.

Mademlis *et al*. (2005) proposed a triac-based optimal control scheme for accomplishing efficiency optimization in single phase induction machines under constant torque operation. A

model of the machine derived using the double revolving field theory and the use of symmetrical components theory was used to analyze the problem of efficiency optimization. An optimal efficiency condition that relates the currents in auxiliary and main windings of the machine was obtained. The input voltage to the machine was then adjusted in accordance to load torque requirements. Expressions for the average torque and total electrical losses were derived in terms of motor parameters, supply frequency and motor slip. By these expressions, an optimal ratio of main winding current to auxiliary winding current at which motor efficiency is maximized is determined and used to control the Triac conduction time and this effectively determined the control input voltage supplied to the machine. Results show that the relative values of motor efficiency increase and loss reduction in the case of the optimal control method over that of the nominal supply system were quite high at light loads but very low under heavy load torque values. The absolute values of motor efficiency under different loads were obscured in the work, making it difficult to quantify, in absolute terms, the value of the motor efficiency under the control method. The proposed method is quite simple and cost-effective. The response time of the controller, in the event of any load disturbance, was quite fast. However, the Triac-based drive introduced voltage and current harmonics thereby producing additional torque pulsations and associated temperature rise in the machine.

A method for sensor-less efficiency maximization control of an inverter driven single phase induction machine was proposed in **Zahedi and Vaez-Zadeh (2009)**. The electrical loss in the machine was modeled into the equivalent circuit derived using the double revolving field theory approach and a thorough efficiency analysis was carried out. The solution adopted consists of the calculation of an optimal value of slip that gives minimum electrical loss at any supply frequency. The control of this optimal slip was achieved by sensing and utilizing the phase

difference between the currents in the main and auxiliary windings. This way, the control methodology achieved efficiency control and speed control simultaneously. Results show that efficiency of the given CRSPIM improved by 5.5% while driving a 2Nm load torque and by 18.1% while driving a 1Nm load torque when the proposed efficiency control scheme is compared to the constant volts per hertz control method in which the same motor was used. Improvements in efficiency and input power consumption were also achieved by using the proposed scheme over the constant volts per hertz control method when motor speed was changed. In this work, however, no comparison was made with respect to the performance of the given CRSPIM when driven conventionally from a fixed voltage source. Moreover, the series-connected capacitor remained in the motor circuit which effectively reduces the reliability of the proposed drive scheme.

Azzolin *et al.* (2012) proposed a decoupling strategy to reduce the value of pulsating torque and current pulsations in a vector-controlled unsymmetrical single phase induction machine. A control law was formulated and used to compensate the coupling terms. Results with and without the decoupling algorithm were compared. Although the proposed solution excludes the series-connected capacitor, significant pulsations were present in the stator current signal owing to the winding asymmetry of the SPIM which will ultimately lead to significant torque pulsations in the machine. Performance results were limited to the stator current in this work and the implementation of the proposed algorithm is complex and expensive.

Mera and Campeanu (2012) proposed a method that improves motor efficiency by varying the value of the capacitor in the auxiliary winding for a given load torque. An optimal value of capacitance that gave maximum efficiency was determined based on an experimental procedure. A CRSPIM designed for two different speeds was used in this work. Four different values of

torque between just below the rated torque and a value near the maximum torque were applied to the machine and it was observed that motor efficiency rises with increase in torque and varies with the capacitor. Maximum efficiency for the given machine was observed to be about 32% for a high torque and about 13% at rated torque in the case of the 2 – pole winding configuration and the capacitor values were 8µF and 5µF respectively. For the 12-pole winding configuration of the same machine, maximum motor efficiency was observed to be about 26% for a high torque and about 17% for rated torque in the case of the 2 – pole winding configuration and the capacitor values were 13µF and 8µF respectively. Although the approach used in this work is simple, the presence of a capacitor in the motor winding circuit increases the overall cost of the system and risks the reliability of the system as well because in the event that the capacitor fails, the system fails as well. In addition, the efficiency improvement is limited by the capacitor control in the proposed method.

In their work, **Asghari and Fallah (2012)** proposed an inverter – based method to optimize the torque and efficiency of the standard capacitor – run single phase induction. The inverter, along with a phase angle controller was used to produce the necessary phase shift required for motor operation. The revolving field method was used for the analysis of the machine and a condition that establishes maximum efficiency and minimum pulsating torque simultaneously across a limited range of motor speed was obtained. The work proposed a non-quadrature optimal phase angle between the voltages of the main and auxiliary winding. The result or work showed that motor efficiency increased from 57.17% to 74.27% when the test motor is operated at rated conditions .A drawback in this work was the lack of consideration for light or non-rated load torques and the presence of significant torque pulsations during steady state operation.

A sensor-less variable speed single phase induction motor drive based on direct rotor field orientation techniques was proposed in **Caruso *et al*.(2012)**. A three-leg voltage source inverter was selected for use with the control strategy. The control strategy uses two independent linear closed-loop control systems that allow for a good torque control. The d – q model equation of the machine in the stationary reference frame was used for the analysis of the motor control system. Upon estimation of the rotor speed and rotor flux vector, proportional plus integral (PI) and PID controllers were used to determine reference voltages to be applied to the inverter in order to synthesize the necessary quadrature voltages to be supplied to the main and auxiliary windings. Results showed that the rotor speed followed its commanded values. Under load variations, from half load to full load torque value, speed control was weak. Flux was not affected by load variations as the rotor flux amplitude was maintained constant still under change of load from half load to full load torque. Consequently, this condition does not make the proposed method energy-efficient. In addition, stator currents produced pulsations because of the asymmetry in the stator windings of the machine.

An optimization method in which the effect of change in core material, rotor slot number and dimensions and stator winding turns and wire diameter on efficiency and torque at rated conditions was studied in **Sobhani *et al.*(2013a)**. Under this method, efficiency at rated load increased by 43% and 21% respectively for a 400W SPIM and 250W SPIM. Considerationswere, however, limited to full load operating point. Light load operation was not considered. Although rated torque of both machines increased significantly, the torque pulsation problem was ignored in the work. In addition, the SPIM model applied is a steady state model that lacks capacity for dynamic operation studies.

Sobhani *et al*.(2013b) proposed the use of intelligent systems such as inductive proximity sensors (IPS) and magnetic field monitoring system (MFMS) to replace the centrifugal switch in the SPIM for increased reliability. In this method, the sensors scans the magnetic field of the motor and then smart devices decide when the capacitor is disconnected. A suitable capacitor that is compatible with the intelligent system was also selected. The proposed system was applied to a motor data and simulation results show that the efficiency and breakdown torque increased by 13.5% and 44% respectively for the given motor data. Reduced starting/acceleration time was credited to the proposed system but the reduction was not quantified. The problem of torque pulsations was not addressed and efficiency considerations at light loads was ignored.

Jang (2013) discussed the model of the vector control strategy used by several researchers for existing single phase induction machines. The work identifies the major problems associated with the vector-controlled SPIM. The research proposed a vector control scheme in which a symmetrical two phase induction motor (TPIM) is advocated to replace the existing SPIM. Simulation results show a very good speed and current control in non-rated conditions. The work calls for an entirely new machine design thereby discounting the existing designs of the single phase machine. Although the proposed solution is viable, it is a very expensive option. In addition, considerations were not given to efficiency in the analysis. Such a scheme as proposed is liable to operate at low efficiency because of constant flux operation. Moreover, the energy saving ability of the proposed scheme is limited because of lack of an energy optimizing strategy.

In their paper, **Jannati*et al.* (2014)**proposed a speed sensorless direct field oriented control of SPIM using extended kalman filter. A d-q model of the unsymmetrical SPIM was used in their analysis. They developed balanced stator voltage equations of the SPIM by applying transformation equations to compensate for the asymmetry between the stator winding

parameters. A kalman filter technique was used to estimate rotor speed instead of using sensors for speed measurement. Although good speed tracking and good dynamic performance of the proposed scheme was obtained, torque pulsations with a value of 10% of rated torque are still evident in steady state. Their study was limited to speed control and torque pulsation treatment at rated torque and no considerations of light load operation. The low efficiency problem was not addressed.

In **Hekmati *et al*. (2014)**,CRSPIM performance under different capacitance values was investigated. The effects of changing the capacitance on certain motor performance characteristics including efficiency and electromagnetic torque and pulsating torque were discussed and analyzed. A control strategy involving a parallel bidirectional switch plus a fixed capacitor along with test motor was simulated to demonstrate the applicability of the analyses. The performance of the proposed scheme was compared with that of a conventional SPIM and the results showed significant reduction in the input current, 88% reduction in torque pulsations and a significant improvement in efficiency at rated conditions. The limitation of this work is that consideration was limited to rated conditions and non-rated conditions was not considered. Moreover, the series-connected capacitor remained in the motor circuit during operation thereby making the proposed drive scheme unreliable.

Hosseini (2016) proposed a method to eliminate torque pulsations near rated load. The proposed method involves the concept of non-orthogonal stator windings in which the optimal angle of shift away from the orthogonal position and capacitance value was calculated to eliminate torque pulsations around the rated torque. The proposed method was applied on a 4 pole, 32 slots CRSPIM data and simulation results showed that by using the existing capacitance value of 5μ and a shift angle of 23.3^0, torque pulsations are eliminated for a load of 1.394Nm near rated load

compared to the existing CRSPIM in which significant torque pulsations exist at the same load. Simulation results also show that the non-orthogonal CRSPIM is capable of generating increased breakdown torque, starting torque and power factor and also reduced input current and ohmic losses in the machine. The problem with this method is that the shift angle of $23.3^0$is not implementable in the existing CRSPIM.

Although different methods have been developed by several researchers in recent years to reduce the level of torque pulsations and to improve the operating efficiency of existing single phase induction machines, none of these methods have eliminated torque pulsations at all loads in these machines. Moreover, energy efficiency improvement functions have not been explored in the vector-controlled drives of these machines. This research has therefore developed an efficiency-optimizing vector-controlled scheme for existing single phase induction machines with a view to improving the torque production and operating efficiency of these machines at non-rated loads under steady state conditions.

CHAPTER THREE

MATERIALS AND METHOD

3.1 INTRODUCTION

A generalized model of the CRSPIM was developed and used to evaluate the performances of the existing CRSPIM. The model was also used to investigate the influence of the spatial angular displacement on the performances of the motor with a view to determining whether there was any spatial angular displacement that exhibited improved performances over those of the standard motor design with a spatial angular displacement of 90^0.The process of applying balanced voltages to the machine is discussed to clarify if non-quadrature angular displacement exhibits performances that are superior to those of the quadrature (i.e. 90^0) angular displacement. A method to improve the performances of the standard or existing CRSPIM was then developed using a pulse width modulated single phaseinverter topology to control voltage supply to the auxiliary winding when it became clear that the performances of the standard motor design with quadrature angular displacement can in fact be improved upon if balanced voltages are applied to its stator windings. The approach for evaluating the performance of the SPIM with respect to torque production under thismethod is also provided with a view to comparing its performance to the performance of the existing line-operated capacitor-run single phase induction machine. A more advanced method of motor performance improvement was proposed and developed owing to the limitations of the first method. This advanced method is the vector-controlled modified SPIM strategy with an efficiency-optimizing function which also utilizes the sinusoidal pulse width modulation (SPWM) technique. The development of this method is also presented in this chapter with a view to comparing performances of the proposed scheme to the performances of the existing line-operated capacitor-run single phase induction machine.

3.2 GENERALIZED MODEL DEVELOPMENT FOR THE CRSPIM

Ageneralized d-q model for the CRSPIM has been derived from first principles in this work. The purpose of deriving this generalized model is to develop a set of equations from where it is possible to observe the influence of auxiliary winding displacement angle,∂ on the torque production and efficiency profile of the machine.Figure 3.1 illustrates the stator windings of a SPIM whose axes are displaced at an arbitrary angle,∂.

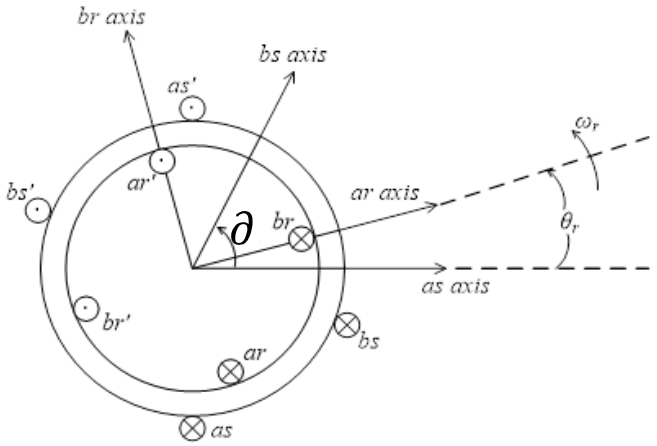


Figure 3.1: Schematic Cross-Section of a SPIM with Arbitrary Angle ∂between the axis of the Stator Windings.

The assumptions stated in section 2.2.2.4 applies here as well. The conductors of the stator and rotor coils are as shown in Figure 3.1.

Figure 3.2 gives the electrical model of the stator and rotor windings. The axis of the '*bs'* winding, that is, the auxiliary winding has been shifted away from the quadrature position. The variables and parameters of each winding are as indicated in Figure 3.2.

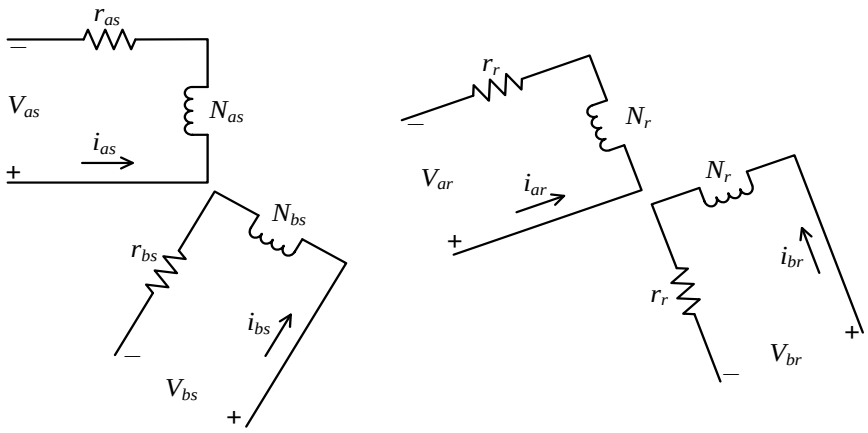


Figure 3.2: Spatial Arrangement of the Stator and Rotor circuits

As shown in Figure 3.2, the main '*as'* winding and auxiliary windings 'bs*'*are non-identical.Both windings areassumed to be sinusoidally distributed and are spaced at an arbitrary angle ∂ apart instead of 90^0 as is the case with the standard designs of the single phase induction machine.The rotor windings are assumed to consistof two identical sinousoidally distributed windings. The parameters and the variables indicated in Figure 3.2 are as defined in section 2.2.2.4:

The voltage equations of the stator and rotor windings can be obtained by the application of Kirchoff's voltage law to the stator and rotor windings illustrated in Figure3.2. These equations are as follows:

$$V_{as} = r_{as}i_{as} + p\lambda_{as} \tag{3.1}$$

$$V_{bs} = r_{bs}i_{bs} + p\lambda_{bs} \tag{3.2}$$

$$V_{ar} = r_r i_{ar} + p\lambda_{ar} \tag{3.3}$$

$$V_{br} = r_r i_{ar} + p\lambda_{br} \tag{3.4}$$

where:

$$p = \frac{d}{dt} \tag{3.5}$$

λdenotes flux linkage of respective windings. The stator and rotor flux linkage equations are as follows;

$$\lambda_{as} = (L_{asas} + L_{las})i_{as} + L_{asbs}i_{bs} + L_{asar}i_{ar} + L_{asbr}i_{br} \tag{3.6}$$

$$\lambda_{bs} = L_{bsas}i_{as} + (L_{bsbs} + L_{lbs})i_{bs} + L_{bsar}i_{ar} + L_{bsbr}i_{br} \tag{3.7}$$

$$\lambda_{ar} = L_{aras}i_{as} + L_{arbs}i_{bs} + (L_{arar} + L_{lr})i_{ar} + L_{arbr}i_{br} \tag{3.8}$$

$$\lambda_{br} = L_{bras}i_{as} + L_{brbs}i_{bs} + L_{brar}i_{ar} + (L_{brbr} + L_{lr})i_{br} \tag{3.9}$$

All the inductances are as defined in section 2.2.2.4.

In matrix notation, equation (3.6) – (3.9) are written as;

$$\begin{bmatrix} \lambda_{as} \\ \lambda_{bs} \\ \lambda_{ar} \\ \lambda_{br} \end{bmatrix} = \begin{bmatrix} L_{asas} + L_{las} & L_{asbs} & L_{asar} & L_{asbr} \\ L_{bsas} & L_{bsbs} + L_{lbs} & L_{bsar} & L_{bsbr} \\ L_{aras} & L_{arbs} & L_{arar} + L_{lr} & L_{arbr} \\ L_{bras} & L_{brbs} & L_{brar} & L_{brbr} + L_{lr} \end{bmatrix} \begin{bmatrix} i_{as} \\ i_{bs} \\ i_{ar} \\ i_{br} \end{bmatrix} \tag{3.10}$$

3.2.1 Derivation of Winding Inductances

The inductances in equation (3.10) are evaluated in this section.The fundamental component of the winding function of the main winding is as given in equation (2.13). For a non-quadrature shift in the auxiliary winding, the fundamental component of the winding function of the auxiliary winding is now givenas:

$$N_{bs}(\theta) = N_{bs}Cos(\theta - \partial) \tag{3.11}$$

Where ∂ is the angle of displacement of the auxiliary winding from the main winding. The spatial arrangement between the main and auxiliary winding may be viewed from the illustration of Figure 3.3.

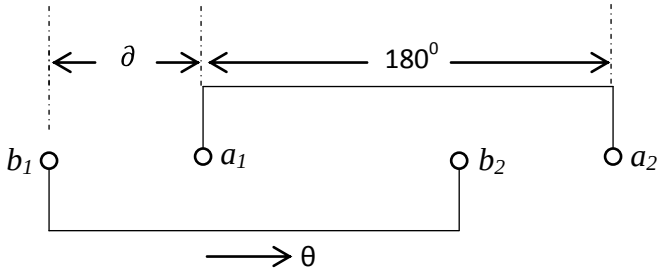


Figure 3.3 Winding Terminal Arrangement of a Two-Coil Single Phase Induction Machine

In Figure 3.3, a_1 and b_1 represent the start terminals of the main and auxiliary winding while a_2 and b_2 represent the end terminals. The b_1 terminal is displaced ∂ electrical degrees away from the a_1 terminal. Each coil spans 180 electrical degrees.

For the rotor windings, the fundamental components of the winding functions are as given in equations (2.15) and (2.16).

3.2.1.1 Stator magnetizing inductances

By applying equation (2.12), the magnetizing inductance of the main winding of the stator is expressed as:

$$L_{asas} = \frac{\mu_0 rL}{g}\int_0^{2\pi}(N_{as}\cos\theta)^2 d\theta \tag{3.12}$$

Equation (3.12) is reduced to:

$$L_{asas} = \frac{\mu_0 rl{N_{as}}^2\pi}{g} \tag{3.13}$$

The magnetizing inductance of the auxiliary winding of the stator is expressed as:

$$L_{bsbs} = \frac{\mu_0 rL}{g}\int_0^{2\pi}(N_{bs}\cos(\theta-\partial))^2 d\theta \tag{3.14}$$

Equation (3.14) is reduced to:

$$L_{bsbs} = \frac{\mu_0 r L {N_{bs}}^2 \pi}{g} \tag{3.15}$$

3.2.1.2 Rotor magnetizing inductances

The magnetizing inductance of the *a* - axis winding of the rotor is expressed as:

$$L_{arar} = \frac{\mu_0 r L}{g} \int_0^{2\pi} (N_r \cos(\theta - \theta_r))^2 d\theta \tag{3.16}$$

Equation (3.16) is reduced to:

$$L_{arar} = \frac{\mu_0 r l {N_r}^2 \pi}{g} \tag{3.17}$$

The magnetizing inductance of the *b* – axis winding of the rotor is expressed as:

$$L_{brbr} = \frac{\mu_0 r L}{g} \int_0^{2\pi} (N_r sin(\theta - \theta_r))^2 d\theta \tag{3.18}$$

Equation (3.18) is reduced to;

$$L_{brbr} = \frac{\mu_0 r L {N_r}^2 \pi}{g} \tag{3.19}$$

3.2.1.3 Stator mutual inductances

The expressions for stator mutual inductances and their solutions are given as follows;

$$L_{asbs} = \frac{\mu_0 r L}{g} \int_0^{2\pi} N_{as} \cos\theta \; x \; N_{bs} \cos(\theta - \partial) \, d\theta \tag{3.20}$$

$$L_{asbs} = \frac{\mu_0 r l N_{as} N_{bs} \pi}{g} \cos\partial \tag{3.21}$$

Similarly,

$$L_{bsas} = \frac{\mu_0 r l N_{as} N_{bs} \pi}{g} \cos\partial \tag{3.22}$$

3.2.1.4 Rotor Mutual Inductances

The expressions for rotor mutual inductances and their solutions are given as follows;

$$L_{arbr} = L_{brar} = \frac{\mu_0 r L}{g} \int_0^{2\pi} N_r \cos(\theta - \theta_r) \; x \; N_r sin(\theta - \theta_r) \, d\theta \tag{3.23}$$

$$L_{arbr} = L_{brar} = 0 \tag{3.24}$$

3.2.1.5 Stator - rotor mutual inductances

The stator-rotor mutual inductances are expressed as follows:

$$L_{asar} = \frac{\mu_0 rL}{g}\int_0^{2\pi} N_{as}\cos\theta \; x \; N_r \cos(\theta - \theta_r)\, d\theta \tag{3.25}$$

$$L_{asar} = \frac{\mu_0 rlN_{as}N_r\pi}{g}\cos\theta_r \tag{3.26}$$

$$L_{asbr} = \frac{\mu_0 rL}{g}\int_0^{2\pi} N_{as}\cos\theta \; x \; N_r sin(\theta - \theta_r)\, d\theta \tag{3.27}$$

$$L_{asbr} = -\frac{\mu_0 rlN_{as}N_r\pi}{g}\sin\theta_r \tag{3.28}$$

$$L_{bsar} = \frac{\mu_0 rL}{g}\int_0^{2\pi} N_{bs}\cos(\theta - \partial) \; x \; N_r \cos(\theta - \theta_r)\, d\theta \tag{3.29}$$

$$L_{bsar} = \frac{\mu_0 rlN_{bs}N_r\pi}{g}\cos(\theta_r - \partial) \tag{3.30}$$

$$L_{bsbr} = \frac{\mu_0 rL}{g}\int_0^{2\pi} N_{bs}\cos(\theta - \partial) \; x \; N_r sin(\theta - \theta_r)\, d\theta \tag{3.31}$$

$$L_{bsbr} = -\frac{\mu_0 rlN_{bs}N_r\pi}{g}\sin(\theta_r - \partial) \tag{3.32}$$

The machine inductances are reduced as follows:

$$L_{asas} = CN_{as}{}^2 \tag{3.33(a))}$$

$$L_{bsbs} = CN_{bs}{}^2 \tag{3.33(b))}$$

$$L_{arar} = CN_r{}^2 \tag{3.33(c))}$$

$$L_{brbr} = CN_r{}^2 \tag{3.33(d))}$$

$$L_{asbs} = L_{bsas} = CN_{as}N_{bs}\cos\partial \tag{3.33(e))}$$

$$L_{arbr} = L_{brar} = 0 \tag{3.33(f))}$$

$$L_{asar} = L_{aras} = CN_{as}N_r\cos\theta_r \tag{3.33(g))}$$

$$L_{asbr} = L_{bras} = -CN_{as}N_r sin\theta_r \tag{3.33(h))}$$

$$L_{bsar} = L_{arbs} = CN_rN_{bs}\cos(\theta_r - \partial) \tag{3.33(i))}$$

$$L_{bsbr} = L_{brbs} = -CN_{bs}N_r\sin(\theta_r - \partial) \tag{3.33(j))}$$

Where $C = \frac{\mu_0 r l \pi}{g}$ (3.34)

If the following identities are defined:

$$L_{mas} = C{N_{as}}^2 \quad (3.35(a))$$

$$L_{mbs} = C{N_{bs}}^2 \quad (3.35(b))$$

$$L_{mr} = C{N_r}^2 \quad (3.35(c))$$

Then it follows that:

$$L_{asas} = L_{mas} \quad (3.36(a))$$

$$L_{bsbs} = L_{mbs} \quad (3.36(b))$$

$$L_{arar} = L_{mr} \quad (3.36(c))$$

$$L_{brbr} = L_{mr} \quad (3.36(d))$$

$$L_{asbs} = L_{bsas} = L_{mas}\frac{N_{bs}}{N_{as}}\cos\partial \quad (3.36(e))$$

$$L_{arbr} = L_{brar} = 0 \quad (3.36(f))$$

$$L_{asar} = L_{aras} = L_{mas}\frac{N_r}{N_{as}}\cos\theta_r \quad (3.36(g))$$

$$L_{asbr} = L_{bras} = -L_{mas}\frac{N_r}{N_{as}}\sin\theta_r \quad (3.36(h))$$

$$L_{bsar} = L_{arbs} = L_{mbs}\frac{N_r}{N_{bs}}\cos(\theta_r - \partial) \quad (3.36(i))$$

$$L_{bsbr} = L_{brbs} = -L_{mbs}\frac{N_r}{N_{bs}}sin(\theta_r - \partial) \quad (3.36(j))$$

Equations (3.36 (a) – (j)) reveal that some of the inductances are functions of the spatial angular displacement ∂ between the stator windings. The inductance matrix in equation (3.10) is therefore re-written as:

$$\boldsymbol{L} = \begin{bmatrix} L_{mas} + L_{las} & L_{mas}\frac{N_{bs}}{N_{as}}\cos\partial & L_{mas}\frac{N_r}{N_{as}}\cos\theta_r & -L_{mas}\frac{N_r}{N_{as}}\sin\theta_r \\ L_{mas}\frac{N_{bs}}{N_{as}}\cos\partial & L_{mbs} + L_{lbs} & L_{mbs}\frac{N_r}{N_{bs}}\cos(\theta_r - \partial) & -L_{mbs}\frac{N_r}{N_{bs}}sin(\theta_r - \partial) \\ L_{mas}\frac{N_r}{N_{as}}\cos\theta_r & L_{mbs}\frac{N_r}{N_{bs}}\cos(\theta_r - \partial) & L_{mr} + L_{lr} & 0 \\ -L_{mas}\frac{N_r}{N_{as}}\sin\theta_r & -L_{mbs}\frac{N_r}{N_{bs}}sin(\theta_r - \partial) & 0 & L_{mr} + L_{lr} \end{bmatrix} \tag{3.37}$$

If equation (3.37) is expressed in the form of equation (2.10), then:

$$\boldsymbol{L_s} = \begin{bmatrix} L_{mas} & L_{mas}\frac{N_{bs}}{N_{as}}\cos\partial \\ L_{mas}\frac{N_{bs}}{N_{as}}\cos\partial & L_{mbs} \end{bmatrix} + \begin{bmatrix} L_{las} & 0 \\ 0 & L_{lbs} \end{bmatrix} \tag{3.38(a))}$$

$$\boldsymbol{L_{sr}} = \begin{bmatrix} L_{mas}\frac{N_r}{N_{as}}\cos\theta_r & -L_{mas}\frac{N_r}{N_{as}}\sin\theta_r \\ L_{mbs}\frac{N_r}{N_{bs}}\cos(\theta_r - \partial) & -L_{mbs}\frac{N_r}{N_{bs}}sin(\theta_r - \partial) \end{bmatrix} \tag{3.38(b))}$$

$$(\mathbf{L_{sr}})^{\mathbf{T}} = \begin{bmatrix} L_{mas}\frac{N_r}{N_{as}}\cos\theta_r & L_{mbs}\frac{N_r}{N_{bs}}\cos(\theta_r - \partial) \\ -L_{mas}\frac{N_r}{N_{as}}\sin\theta_r & -L_{mbs}\frac{N_r}{N_{bs}}sin(\theta_r - \partial) \end{bmatrix} \tag{3.38(c))}$$

$$\boldsymbol{L_r} = \begin{bmatrix} L_{mr} & 0 \\ 0 & L_{mr} \end{bmatrix} + \begin{bmatrix} L_{lr} & 0 \\ 0 & L_{lr} \end{bmatrix} \tag{3.38(d))}$$

The turn's transformation follows next.

3.2.2 Turn's Transformation

In order to simplify analysis, all rotor variables and the variables of the auxiliary winding are referred to the stator main winding by appropriate turn's ratio. The following equations accomplish this transformation:

$$i'_{ar} = \frac{N_r}{N_{as}} i_{ar} \tag{3.39(a))}$$

$$i'_{br} = \frac{N_r}{N_{as}} i_{br} \quad (3.39(b))$$

$$r'_r = \left(\frac{N_{as}}{N_r}\right)^2 r_r \quad (3.39(c))$$

$$V'_{ar} = \frac{N_{as}}{N_r} V_{ar} \quad (3.39(d))$$

$$V'_{br} = \frac{N_{as}}{N_r} V_{br} \quad (3.39(e))$$

$$\lambda'_{ar} = \frac{N_{as}}{N_r} \lambda_{ar} \quad (3.39(f))$$

$$\lambda'_{br} = \frac{N_{as}}{N_r} \lambda_{br} \quad (3.39(g))$$

$$\boldsymbol{L}'_{sr} = \frac{N_{as}}{N_r} \boldsymbol{L}_{sr} \quad (3.39(h))$$

$$\boldsymbol{L}'_r = \left(\frac{N_{as}}{N_r}\right)^2 \boldsymbol{L}_r \quad (3.39(i))$$

$$L'_{lr} = \left(\frac{N_{as}}{N_r}\right)^2 L_{lr} \quad (3.39(j))$$

Substituting for the variables V_{bs} V_{ar}, V_{br}, I_{bs}, I_{ar}, I_{br}, $\lambda_{bs}\lambda_{ar}$ and λ_{br} in equations (3.2) – (3.4) using their equivalents in equations (3.39 (a) - (e)), the expressions for the voltage equations of the auxiliary winding and rotor windings with variables and parameters referred to the main winding are obtained as:

$$V'_{bs} = r'_{bs} i'_{bs} + p\lambda'_{bs} \quad (3.40(a))$$

$$V_{ar}{}' = r'_r i'_{ar} + p\lambda'_{ar} \quad (3.40(b))$$

$$V'_{br} = r'_r i'_{br} + p\lambda'_{br} \quad (3.40(c))$$

The primed quantities are quantities referred to the main winding. The equations of the inductances referred to the main stator winding are obtained by applying equations (3.39(h) – (j)) to equations (3.38 (a) - (d)) and are as given as:

$$\boldsymbol{L_s} = \begin{bmatrix} L_{mas} & L_{mas}\cos\partial \\ L_{mas}\cos\partial & L_{mas} \end{bmatrix} + \begin{bmatrix} L_{las} & 0 \\ 0 & L'_{lbs} \end{bmatrix} \quad (3.41(a))$$

$$\boldsymbol{L'_{sr}} = \begin{bmatrix} L_{mas}\cos\theta_r & -L_{mas}\sin\theta_r \\ L_{mas}\cos(\theta_r - \partial) & -L_{mas}sin(\theta_r - \partial) \end{bmatrix} \quad (3.41(b))$$

$$(\mathbf{L'_{sr}})^{\mathbf{T}} = \begin{bmatrix} L_{mas}\cos\theta_r & L_{mas}\cos(\theta_r - \partial) \\ -L_{mas}\sin\theta_r & -L_{mas}sin(\theta_r - \partial) \end{bmatrix} \quad (3.41(c))$$

$$\boldsymbol{L'_r} = \begin{bmatrix} L_{mas} & 0 \\ 0 & L_{mas} \end{bmatrix} + \begin{bmatrix} L'_{lr} & 0 \\ 0 & L'_{lr} \end{bmatrix} \quad (3.41(d))$$

The referred inductance matrix is therefore expressed as;

$$\boldsymbol{L'} = \begin{bmatrix} L_{mas} + L_{las} & L_{mas}\cos\partial & L_{mas}\cos\theta_r & -L_{mas}\sin\theta_r \\ L_{mas}\cos\partial & L_{mas} + L'_{lbs} & L_{mas}\cos(\theta_r - \partial) & -L_{mas}sin(\theta_r - \partial) \\ L_{mas}\cos\theta_r & L_{mas}\cos(\theta_r - \partial) & L_{mas} + L'_{lr} & 0 \\ -L_{mas}\sin\theta_r & -L_{mas}sin(\theta_r - \partial) & 0 & L_{mas} + L'_{lr} \end{bmatrix} \quad (3.42)$$

Using equations (2.10) and the expressions of equations (3.39 (a) – (b)) and (3.39(d) – (h)), the referred flux linkage matrix, in compact form, is as given as:

$$\begin{bmatrix} \boldsymbol{\lambda'}_{abs} \\ \boldsymbol{\lambda'}_{abr} \end{bmatrix} = \begin{bmatrix} \mathbf{L'_s} & \mathbf{L'_{sr}} \\ (\mathbf{L'_{sr}})^{\mathbf{T}} & \mathbf{L'_r} \end{bmatrix} \begin{bmatrix} \boldsymbol{i'}_{abs} \\ \boldsymbol{i'}_{abr} \end{bmatrix} \quad (3.43)$$

Where:

$$\boldsymbol{\lambda'}_{abs} = \begin{bmatrix} \lambda_{as} \\ \lambda'_{bs} \end{bmatrix} \quad (3.44(a))$$

$$\boldsymbol{\lambda'}_{abr} = \begin{bmatrix} \lambda'_{ar} \\ \lambda'_{br} \end{bmatrix} \quad (3.44(b))$$

$$\mathbf{i'}_{abs} = \begin{bmatrix} \mathrm{i}_{as} \\ \mathrm{i}'_{bs} \end{bmatrix} \quad (3.45(a))$$

$$\mathbf{i'}_{abr} = \begin{bmatrix} \mathrm{i}'_{ar} \\ \mathrm{i}'_{br} \end{bmatrix} \quad (3.45(b))$$

The voltage equations (3.1) and (3.40 (a) - (c)) with respect to equations (3.42) and (3.43) are difficult to solve because of the time-varying inductances between the stator and the rotor as seen from equations (3.41 (b) and (c)). The equations are non–linear differential equations whose solutions are simplified by the use of the reference frame transformation technique.

3.2.3 Stationary Reference frame Transformation of Stator Variables

Application of equation (2.21) to equations (3.1) and (3.40(a)) yields the following;

$$\boldsymbol{K_s V}_{abs} = \boldsymbol{K}_s \boldsymbol{r}_{abs} \boldsymbol{i}_{abs} + \boldsymbol{K}_s p \boldsymbol{\lambda}_{abs} \tag{3.46}$$

Simplifying equation (3.46) further yields:

$$\boldsymbol{V}_{qds} = \boldsymbol{K}_s \boldsymbol{r}_{abs} \boldsymbol{K_s}^{-1} \boldsymbol{i}_{qds} + K_s p\left[\boldsymbol{K_s}^{-1} \boldsymbol{\lambda}_{qds}\right] \tag{3.47}$$

Where:

$$\boldsymbol{V}_{qds} = \begin{bmatrix} V_{qs} \\ V'_{ds} \end{bmatrix} \tag{3.48}$$

$$\boldsymbol{r}_{abs} = \begin{bmatrix} r_{as} & 0 \\ o & r'_{bs} \end{bmatrix} \tag{3.49}$$

$$\boldsymbol{\lambda}_{qds} = \begin{bmatrix} \lambda_{qs} \\ \lambda'_{ds} \end{bmatrix} \tag{3.50}$$

$$\boldsymbol{i}_{qds} = \begin{bmatrix} i_{qs} \\ i'_{ds} \end{bmatrix} \tag{3.51}$$

In expanded form, equation (3.47) is written as;

$$\begin{bmatrix} V_{qs} \\ V'_{ds} \end{bmatrix} =$$

$$\begin{bmatrix} \cos\theta & \sin\theta \\ \sin\theta & -\cos\theta \end{bmatrix} \begin{bmatrix} r_{as} & 0 \\ o & r_{bs} \end{bmatrix} \begin{bmatrix} \cos\theta & \sin\theta \\ \sin\theta & -\cos\theta \end{bmatrix} \begin{bmatrix} i_{qs} \\ i_{ds} \end{bmatrix} + \begin{bmatrix} \cos\theta & \sin\theta \\ \sin\theta & -\cos\theta \end{bmatrix} p \left[\begin{bmatrix} \cos\theta & \sin\theta \\ \sin\theta & -\cos\theta \end{bmatrix} \begin{bmatrix} \lambda_{qs} \\ \lambda_{ds} \end{bmatrix} \right] \tag{3.52}$$

Which is reduced to:

$$\begin{bmatrix} V_{qs} \\ V'_{ds} \end{bmatrix} = \begin{bmatrix} \frac{(r_{as}+r'_{bs})}{2} + \frac{(r_{as}-r'_{bs})}{2}\cos 2\theta & \frac{(r_{as}-r'_{bs})}{2}\sin 2\theta \\ \frac{(r_{as}-r'_{bs})}{2}\sin 2\theta & \frac{(r_{as}+r'_{bs})}{2} - \frac{(r_{as}-r'_{bs})}{2}\cos 2\theta \end{bmatrix} \begin{bmatrix} i_{qs} \\ i'_{ds} \end{bmatrix} + \omega \begin{bmatrix} \lambda'_{ds} \\ -\lambda_{qs} \end{bmatrix} + p \begin{bmatrix} \lambda_{qs} \\ \lambda'_{ds} \end{bmatrix} \tag{3.53}$$

In the stationary reference frame whererereference frame speed, $\omega = 0$ and hence $\theta = 0$ according to equation (2.24), the stator voltage equations are given as:

$$V_{qs} = r_{as} i_{qs} + p\lambda_{qs} \tag{3.54(a))}$$

$$V'_{ds} = r'_{bs} i'_{ds} + p\lambda'_{ds} \tag{3.54(b))}$$

Using equations (2.21) and (2.23), the q – d voltages in the stationary reference frame are obtained as:

$$V_{qs} = V_{as} \tag{3.55}$$

$$V'_{ds} = -V'_{bs} \tag{3.56}$$

Similarly, the q – d currents in the stationary reference frame are obtained as:

$$i_{qs} = i_{as} \tag{3.57}$$

$$i'_{ds} = -i_{bs} \tag{3.58}$$

Appropriate modifications with respect to the CRSPIMis made to the voltage equation of the auxiliary winding represented by equation (3.54(b)). Figure 3.4 shows the configuration of the stator windings of the existing design of the CRSPIM.

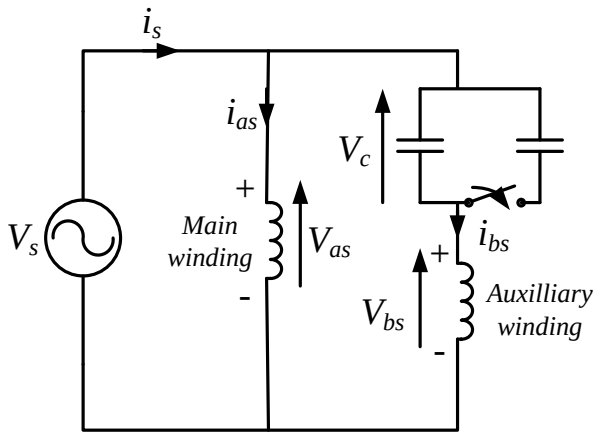


Figure 3.4: Schematic Representation of Configuration of the Stator Windings of the CRSPIM

In Figure 3.4, V_s is a sinusoidal voltage source. Therefore,

$$V_s = V_m \cos \omega t \tag{3.59}$$

Where V_m is the peak value of the source voltage and ω is the angular frequency of the source voltage. From Figure 3.4, the following equations are obtained:

$$V_{as} = V_s \tag{3.60}$$

$$V'_{bs} = V_s - V_c \tag{3.61}$$

$$i'_{bs} = CpV_c \tag{3.62}$$

where V_c is the voltage across the capacitors. V_{as} is the main winding voltage and V'_{bs} is the auxiliary winding voltage. i_{as} and i'_{bs} are the currents flowing in the main and auxiliary windings. C is the effective capacitance of the start and run capacitors.

3.2.4 Stationary Reference frame Transformation of Rotor Variables

Application of equations (2.26) and (2.27) to equations (3.3) and (3.4) yields:

$$\boldsymbol{V}_{qdr} = \boldsymbol{K}_r \boldsymbol{r}'_r \boldsymbol{K}_r^{-1} \boldsymbol{i}_{qdr} + \boldsymbol{K}_r p\left[\boldsymbol{K}_r^{-1} \boldsymbol{\lambda}_{qdr}\right] \tag{3.63}$$

Equation (3.63) reduces to;

$$\begin{bmatrix} V'_{qr} \\ V'_{dr} \end{bmatrix} = \begin{bmatrix} r'_r & 0 \\ 0 & r'_r \end{bmatrix} \begin{bmatrix} i'_{qr} \\ i'_{dr} \end{bmatrix} + (\omega - \omega_r) \begin{bmatrix} \lambda'_{dr} \\ -\lambda'_{qr} \end{bmatrix} + p \begin{bmatrix} \lambda'_{qr} \\ \lambda'_{dr} \end{bmatrix} \quad (3.64)$$

in the stationary reference frame. The rotor voltage equations are therefore written as:

$$V'_{qr} = r'_r i'_{qr} - \omega_r \lambda'_{dr} + p\lambda'_{qr} \quad (3.65(a))$$

$$V'_{dr} = r'_r i'_{dr} + \omega_r \lambda'_{dr} + p\lambda'_{dr} \quad (3.65(b))$$

V'_{qr} and V'_{dr} are both equal to zero because the rotor windings of the SPIM are short-circuited.

3.2.5 Transformation of Flux Linkages

The flux linkage equation (3.43) is re-written as follows:

$$\boldsymbol{\lambda}'_{abs} = \boldsymbol{L}'_s \boldsymbol{i}'_{abs} + \boldsymbol{L}'_{sr} \boldsymbol{i}'_{abr} \quad (3.66(a))$$

$$\boldsymbol{\lambda}'_{abr} = (\boldsymbol{L}'_{sr})^T \boldsymbol{i}'_{abs} + \boldsymbol{L}'_r \boldsymbol{i}'_{abr} \quad (3.66(b))$$

Application of equations (2.21), (2.26) and their inverse to equations (3.66 (a) and (b)) yields:

$$\begin{bmatrix} \boldsymbol{\lambda}'_{qds} \\ \boldsymbol{\lambda}'_{qdr} \end{bmatrix} = \begin{bmatrix} \boldsymbol{K_s L'_s K_s^{-1}} & \boldsymbol{K_s L'_{sr} K_r^{-1}} \\ \boldsymbol{K_r (L'_{sr})^T K_s^{-1}} & \boldsymbol{K_r L'_r K_r^{-1}} \end{bmatrix} \begin{bmatrix} \boldsymbol{i}'_{qds} \\ \boldsymbol{i}'_{qdr} \end{bmatrix} \quad (3.67)$$

Equation (3.67) reduces to:

$$\begin{bmatrix} \lambda_{qs} \\ \lambda'_{ds} \\ \lambda'_{qr} \\ \lambda'_{dr} \end{bmatrix} = \begin{bmatrix} L_{mas} + L_{las} & -L_{mas}cos\partial & L_{mas} & 0 \\ -L_{mas}cos\partial & L_{mas} + L'_{lbs} & -L_{mas}cos\,\partial & L_{mas}\sin\partial \\ L_{mas} & -L_{mas}cos\,\partial & L_{mas} + L'_{lr} & 0 \\ 0 & L_{mas}\sin\partial & 0 & L_{mas} + L'_{lr} \end{bmatrix} \begin{bmatrix} i_{qs} \\ i'_{ds} \\ i'_{qr} \\ i'_{dr} \end{bmatrix} \quad (3.68)$$

in the stationary reference frame.

The flux linkage equations are therefore written out as follows:

$$\lambda_{qs} = (L_{mas} + L_{las}) i_{qs} - L_{mas}cos\partial i'_{ds} + L_{mas} i'_{qr} \quad (3.69\ (a))$$

$$\lambda'_{ds} = -L_{mas}\cos\partial\, i_{qs} + (L_{mas} + L'_{lbs}) i'_{ds} - L_{mas}cos\,\partial i'_{qr} + L_{mas}\sin\partial i'_{dr} \quad (3.69\ (b))$$

$$\lambda'_{qr} = L_{mas} i_{qs} - L_{mas} cos\,\partial i'_{ds} + (L_{mas} + L'_{lr}) i'_{qr} \quad (3.69\ (c))$$

$$\lambda'_{dr} = L_{mas} \sin\partial\, i'_{ds} + (L_{mas} + L'_{lr}) i'_{dr} \quad (3.69\ (d))$$

Equations (3.69(a)-(d)) are re-arranged in the following form;

$$\lambda_{qs} = L_{las} i_{qs} + L_{mas}\left(i_{qs} + i'_{qr}\right) - L_{mas} \cos\partial\, i'_{ds} \quad (3.70\ (a))$$

$$\lambda'_{qr} = L'_{lr} i'_{qr} + L_{mas}(i_{qs} + i'_{qr}) - L_{mas} \cos\partial\, i'_{ds} \quad (3.70\ (b))$$

$$\lambda'_{ds} = L'_{lbs} i'_{ds} + L_{mas} \sin\partial\, (i'_{ds} + i'_{dr}) + L_{mas}(1 - \sin\partial) i'_{ds} - L_{mas} \cos\partial\, (i_{qs} + i'_{qr}) \quad (3.70(c))$$

$$\lambda'_{dr} = L'_{lr} i'_{dr} + L_{mas} \sin\partial\, (i'_{ds} + i'_{dr}) + L_{mas}(1 - \sin\partial) i'_{dr} \quad (3.70(d))$$

3.2.6 Equivalent Circuit of the SPIM with Non-Quadrature Winding

The equivalent circuit of the SPIM with non-quadrature winding was then derived from equations (3.54 (a)-(b)),(3.65 (a)-(b))and (3.70 (a)-(d))and is provided in Figure 3.5.

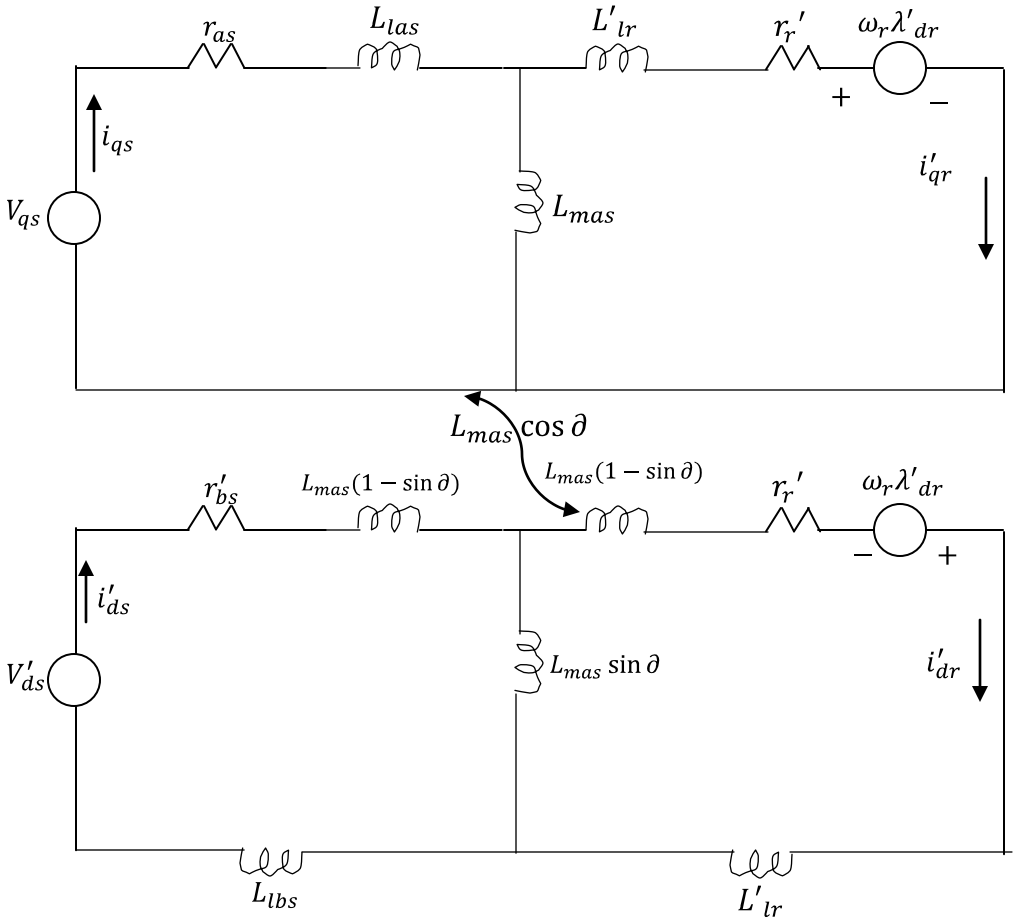


Figure 3.5: Equivalent Circuit of a SPIM with Non-Quadrature Windings

3.2.7 Torque Equation

Utilizing equations (2.19), (2.25), (2.27) and element (2,1) of equation (3.67), the generalized torque expression is obtainedas follows:

$$T_e = \frac{P}{2}\left(\begin{bmatrix}\cos\theta & \sin\theta \\ \sin\theta & -\cos\theta\end{bmatrix}\begin{bmatrix}i_{qs} \\ i'_{ds}\end{bmatrix}\right)^T \frac{d}{d\theta_r}\begin{bmatrix}L_{mas}\cos\theta_r & L_{mas}\cos(\theta_r-\partial) \\ -L_{mas}\sin\theta_r & -L_{mas}sin(\theta_r-\partial)\end{bmatrix}\begin{bmatrix}\cos\sigma & \sin\sigma \\ \sin\sigma & -\cos\sigma\end{bmatrix}\begin{bmatrix}i'_{qr} \\ i'_{dr}\end{bmatrix} \tag{3.71}$$

Simplifying equation (3.71) in the stationary reference frame results in the following equation;

$$T_e = \frac{P}{2}L_{mas}\left(i'_{dr}i_{qs} - i'_{ds}i'_{qr}\sin\partial - i'_{ds}i'_{dr}\cos\partial\right) \tag{3.72}$$

3.2.8 Generalized Steady State Model of the CRSPIM Using HBT.

Utilizing the Harmonic balance technique (HBT) and equation (3.59), the following are true:

$$V_{qs} = V_m \cos(\omega t + \varphi) = Re\left[\bar{V}_{qs} e^{j\omega t}\right] \tag{3.73}$$

$$\bar{V}_{qs} = V_m e^{j\varphi} \tag{3.74}$$

$\bar{V}_{qs}$ is the reference voltage phasor with $\varphi = 0$. $\bar{V}_{qs}$ is same as the peak value of the supply voltage. The other variables of both the stator and rotor are expressed in terms of their phasors as follows:

$$V'_{ds} = Re\left[\bar{V}'_{ds} e^{j\omega_e t}\right] \tag{3.75 (a))}$$

$$V'_{c} = Re\left[\bar{V}'_{c} e^{j\omega_e t}\right] \tag{3.75 (b))}$$

$$V'_{qr} = Re\left[\bar{V}'_{qr} e^{j\omega_e t}\right] = 0 \tag{3.75 (c))}$$

$$V'_{dr} = Re\left[\bar{V}'_{dr} e^{j\omega_e t}\right] = 0 \tag{3.75 (d))}$$

$$\lambda_{qs} = Re\left[\bar{\lambda}_{qs} e^{j\omega_e t}\right] \tag{3.75 (e))}$$

$$\lambda'_{ds} = Re\left[\bar{\lambda}'_{ds} e^{j\omega_e t}\right] \tag{3.75 (f))}$$

$$\lambda'_{qr} = Re\left[\bar{\lambda}'_{qr} e^{j\omega_e t}\right] \tag{3.75 (g))}$$

$$\lambda'_{dr} = Re\left[\bar{\lambda}'_{dr} e^{j\omega_e t}\right] \tag{3.75 (h))}$$

$$i_{qs} = Re\left[\bar{\imath}_{qs} e^{j\omega_e t}\right] \tag{3.75 (i))}$$

$$i'_{ds} = Re\left[\bar{\imath}'_{ds} e^{j\omega_e t}\right] \tag{3.75 (j))}$$

$$i'_{qr} = Re\left[\bar{\imath}'_{qr} e^{j\omega_e t}\right] \tag{3.75 (k))}$$

$$i'_{dr} = Re\left[\bar{\imath}'_{dr} e^{j\omega_e t}\right] \tag{3.75 (l))}$$

With equations (3.73) and (3.75 (a) - (l)) applied to the variables in equations (3.54 (a) - (b)), (3.61), (3.62) and (3.65 (a) - (b)) and then applying the linearity and differentiation rules of the HBT, the following equations are obtained:

$$\bar{V}_{qs} = r_{as}\bar{\imath}_{qs} + j\omega_e\bar{\lambda}_{qs} + p\bar{\lambda}_{qs} \quad (3.76\ (a))$$

$$\bar{V}'_{ds} = r'_{bs}\bar{\imath}'_{ds} + j\omega_e\bar{\lambda}_{ds} + p\bar{\lambda}'_{ds} - \bar{V}'_c \quad (3.76\ (b))$$

$$C'p\bar{V}'_c + \mathrm{j}\omega_e C'\bar{V}'_c = -\bar{\imath}'_{ds} \quad (3.76\ (c))$$

$$0 = r'_r\bar{\imath}'_{qr} - \omega_r\bar{\lambda}'_{dr} + j\omega_e\bar{\lambda}_{qr} + p\bar{\lambda}'_{qr} \quad (3.76\ (d))$$

$$0 = r'_r\bar{\imath}'_{dr} + \omega_r\bar{\lambda}'_{qr} + j\omega_e\bar{\lambda}_{dr} + p\bar{\lambda}'_{dr} \quad (3.76\ (e))$$

At steady state,

$$p\bar{F} = 0 \quad (3.77)$$

where F represents voltage, current or flux linkage. The generalized steady state voltage equations of the CRSPIM are therefore given as follows:

$$\bar{V}_{qs} = r_{as}\bar{\imath}_{qs} + j\omega_e\bar{\lambda}_{qs} \quad (3.78\ (a))$$

$$\bar{V}'_{ds} = r'_{bs}\bar{\imath}'_{ds} + j\omega_e\bar{\lambda}_{ds} - \bar{V}'_c \quad (3.78\ (b))$$

$$\mathrm{j}\omega_e C'\bar{V}'_c = -\bar{\imath}'_{ds} \quad (3.78\ (c))$$

$$0 = r'_r\bar{\imath}'_{qr} - \omega_r\bar{\lambda}'_{dr} + j\omega_e\bar{\lambda}_{qr} \quad (3.78\ (d))$$

$$0 = r'_r\bar{\imath}'_{dr} + \omega_r\bar{\lambda}'_{qr} + j\omega_e\bar{\lambda}_{dr} \quad (3.78\ (e))$$

Applying HBT to the flux linkage equations 3.70 (a) – (d) yields the following;

$$\bar{\lambda}_{qs} = L_{las}\bar{\imath}_{qs} + L_{mas}\left(\bar{\imath}_{qs} + \bar{\imath}'_{qr}\right) - L_{mas}\cos\partial\,\bar{\imath}'_{ds} \quad (3.79\ (a))$$

$$\bar{\lambda}'_{qr} = L'_{lr}\bar{\imath}'_{qr} + L_{mas}(\bar{\imath}_{qs} + \bar{\imath}'_{qr}) - L_{mas}\cos\partial\,\bar{\imath}'_{ds} \quad (3.79\ (b))$$

$$\bar{\lambda}'_{ds} = L'_{lbs}\bar{\imath}'_{ds} + L_{mas}\sin\partial\left(\bar{\imath}'_{ds} + \bar{\imath}'_{dr}\right) + L_{mas}(1 - \sin\partial)\bar{\imath}'_{ds} - L_{mas}\cos\partial\,(\bar{\imath}_{qs} + \bar{\imath}'_{qr}) \quad (3.79\ (c))$$

$$\bar{\lambda}'_{dr} = L'_{lr}\bar{\imath}'_{dr} + L_{mas}\sin\partial\,(\bar{\imath}'_{ds} + \bar{\imath}'_{dr}) + L_{mas}(1 - \sin\partial)\bar{\imath}'_{dr} \quad (3.79\ (d))$$

The application of HBT to the torque expression of equation (3.72) yields the average and pulsating torque expressions of the generalized CRSPIM model. The expressions are as follows:

$$T_{avg} = \frac{P}{4} L_{mas} Re\left[\overline{\imath}'_{dr}\overline{\imath}^{*}_{qs} - \overline{\imath}'_{ds}\overline{\imath}'^{*}_{qr} \sin\partial - \overline{\imath}'_{ds}\overline{\imath}'_{dr} \cos\partial\right] \quad (3.80\ (a))$$

$$T_{puls} = \frac{P}{4} L_{mas} Re\left[\left[\overline{\imath}'_{dr}\overline{\imath}_{qs} - \overline{\imath}'_{ds}\overline{\imath}'_{qr} \sin\partial - \overline{\imath}'_{ds}\overline{\imath}'_{dr} \cos\partial\right] e^{j2\omega_e t}\right] \quad (3.80\ (b))$$

Where T_{avg} and T_{puls} are the average and pulsating torque components respectively. The magnitude of the torque pulsations is obtained from equation (3.80(b)) as:

$$\left|T_{puls}\right| = \frac{P}{4} L_{mas} \left|\left[\overline{\imath}'_{dr}\overline{\imath}_{qs} - \overline{\imath}'_{ds}\overline{\imath}'_{qr} \sin\partial - \overline{\imath}'_{ds}\overline{\imath}'_{dr} \cos\partial\right] e^{j2\omega_e t}\right| \quad (3.80\ (c))$$

Where * refers to complex conjugate

When equations (3.79(a)-(d)) are substituted for flux linkages in the voltage equations of (3.78(a)-(e)), the generalized steady state voltage equations are obtained as:

$$\overline{V}_{qs} = \left(r_{as} + j\frac{\omega_e}{\omega_b} X_{as}\right)\overline{\imath}_{qs} + j\frac{\omega_e}{\omega_b} X_{mas}\overline{\imath}'_{qr} - j\frac{\omega_e}{\omega_b} X_{mas} \cos\partial\, \overline{\imath}'_{ds} \quad (3.81(a))$$

$$\overline{V}'_{ds} = \left(r'_{bs} + j\frac{\omega_e}{\omega_b} X'_{bs} - j\frac{\omega_b}{\omega_e} X'_{c}\right)\overline{\imath}'_{ds} + j\frac{\omega_e}{\omega_b} X_{mas} \sin\partial\, \widetilde{\imath}'_{dr} - j\frac{\omega_e}{\omega_b} X_{mas} \cos\partial\, \overline{\imath}_{qs} -$$

$$j\frac{\omega_e}{\omega_b} X_{mas} \cos\partial\, \overline{\imath}'_{qr} \quad (3.81(b))$$

$$0 = \left(r'_r + j\frac{\omega_e}{\omega_b} X'_r\right)\overline{\imath}'_{qr} + j\frac{\omega_e}{\omega_b} X_{mas}\overline{\imath}_{qs} - j\frac{\omega_e}{\omega_b} X_{mas} \cos\partial\, \overline{\imath}'_{ds} - \frac{\omega_r}{\omega_b}\left(X'_r\overline{\imath}'_{dr} + X_{mas} \sin\partial\, \overline{\imath}'_{ds}\right) \quad (3.81(c))$$

$$0 = \left(r'_r + j\frac{\omega_e}{\omega_b} X'_r\right)\overline{\imath}'_{dr} + j\frac{\omega_e}{\omega_b} X_{mas} \sin\partial\, \overline{\imath}'_{ds} + \frac{\omega_r}{\omega_b}\left(X'_r\overline{\imath}'_{qr} + X_{mas}\overline{\imath}_{qs} - X_{mas} \cos\partial\, \overline{\imath}'_{ds}\right) \quad (3.81(d))$$

Where:

$$X_{as} = X_{mas} + X_{las} \quad (3.82\ (a))$$

$$X_{bs} = X_{mas} + X_{lbs} \quad (3.82\ (b))$$

$$X'_c = \frac{1}{\omega_e C'} \quad (3.82\ (c))$$

$$X_r = X_{mas} + X_{lr} \quad (3.82\ (d))$$

ω_e is the electrical frequency of the voltage supply and ω_b is the base electrical frequency used to convert inductances to reactances. The voltage equations (3.81 (a)- (d)) are written in matrix form as follows:

$$\begin{bmatrix} \overline{V}_{qs} \\ \overline{V'}_{ds} \\ 0 \\ 0 \end{bmatrix} = \begin{bmatrix} r_{as} + j\frac{\omega_e}{\omega_b}X_{as} & -j\frac{\omega_e}{\omega_b}X_{mas}\cos\partial & j\frac{\omega_e}{\omega_b}X_{mas} & 0 \\ -j\frac{\omega_e}{\omega_b}X_{mas}\cos\partial & (r'_{bs} + j(\frac{\omega_e}{\omega_b}X'_{bs} - \frac{\omega_b}{\omega_e}X_c) & -j\frac{\omega_e}{\omega_b}X_{mas}\cos\partial & j\frac{\omega_e}{\omega_b}X_{mas}\sin\partial \\ j\frac{\omega_e}{\omega_b}X_{mas} & -(j\frac{\omega_e}{\omega_b}X_{mas}\cos\partial + \frac{\omega_r}{\omega_b}X_{mas}\sin\partial) & r'_r + j\frac{\omega_e}{\omega_b}X'_r & -\frac{\omega_r}{\omega_b}X'_r \\ \frac{\omega_r}{\omega_b}X_{mas} & j\frac{\omega_e}{\omega_b}X_{mas}\sin\partial - \frac{\omega_r}{\omega_b}X_{mas}\cos\partial & \frac{\omega_r}{\omega_b}X'_r & r'_r + j\frac{\omega_e}{\omega_b}X'_r \end{bmatrix} \begin{bmatrix} \overline{i}_{qs} \\ \overline{i'}_{ds} \\ \overline{i'}_{qr} \\ \overline{i'}_{dr} \end{bmatrix} \quad (3.83)$$

Equations (3.54(a) - (b)), (3.61), (3.65(a) – (b)), (3.70(a) – (d)), and (3.72) represent the new dynamic model of the CRSPIM whose stator windings are spatially displaced at an arbitrary angle ∂. For convenience, the equations are stated as follows;

$$V_{qs} = r_{as}i_{qs} + p\lambda_{qs} \quad (3.84(a))$$

$$V'_{ds} = r'_{bs}i'_{ds} + p\lambda'_{ds} \quad (3.84(b))$$

$$V'_{ds} = V_s - V'_c \quad (3.84(c))$$

$$V'_{qr} = r'_r i'_{qr} - \omega_r \lambda'_{dr} + p\lambda'_{qr} \quad (3.84(d))$$

$$V'_{dr} = r'_r i'_{dr} + \omega_r \lambda'_{dr} + p\lambda'_{dr} \quad (3.84(e))$$

$$\lambda_{qs} = L_{las}i_{qs} + L_{mas}(i_{qs} + i'_{qr}) - L_{mas}\cos\partial\, i'_{ds} \quad (3.84(f))$$

$$\lambda'_{qr} = L'_{lr}i'_{qr} + L_{mas}(i_{qs} + i'_{qr}) - L_{mas}\cos\partial\, i'_{ds} \quad (3.84(g))$$

$$\lambda'_{ds} = L'_{lbs}i'_{ds} + L_{mas}\sin\partial\,(i'_{ds} + i'_{dr}) + L_{mas}(1 - \sin\partial)i'_{ds} - L_{mas}\cos\partial\,(i_{qs} + i'_{qr}) \quad (3.84(h))$$

$$\lambda'_{dr} = L'_{lr} i'_{dr} + L_{mas} \sin\partial\,(i'_{ds} + i'_{dr}) + L_{mas}(1 - \sin\partial) i'_{dr} \qquad (3.84(i))$$

$$T_e = \frac{P}{2} L_{mas}\left(i'_{dr} i_{qs} - i'_{ds} i'_{qr} \sin\partial - i'_{ds} i'_{dr} \cos\partial\right) \qquad (3.84\ (j))$$

With∂ equated to 90^0 in the newly developeddynamic model, the dynamic model of the conventional single phase induction machine can be deduced.A variant of the modeldeducible from equations (3.84(a)-(j)) is given in equation (2.31). The differences being that:

a) the rotor variables and the *d* – axis stator variables are referred to the main winding

b) the turn's ratio $\frac{N_d}{N_q}$ and its reciprocal have been cancelled from the rotor voltage equationsas a consequence of referring variables to the main winding.

This modeling approach eliminates the d-axis mutual inductance (i.e. L_{mbs} or L_{md}) completely with the advantage that it reduces the number of parameters required to characterize the machine.Equations (3.80(a) – (b)) and equations (3.83) represent the new steady state model of the CRSPIM whose stator windings are spatially displaced at an arbitrary angle ∂ otherwise referred to as the generalized CRSPIM model.

3.3 MODEL VALIDATION

The generalized CRSPIM model was used to evaluate the dynamic and steady state performances of the existing CRSPIM 1 by setting ∂ to $90^0$and using the motordata in Table A.1.Simulation results obtained were then compared with the results obtained in(Ong, 1998) and (Krause *et al*, 2002). The dynamic voltages, currents, speed and torque produced in the motor are compared. Also compared, are the steady state torque and efficiency of the machine under no – load and load conditions.

The harmonic balance technique wasused for steady state analysis in this work as opposed to the technique of symmetrical components used in (Ong,1998) and (Krause *et al*,2002). The dynamic

characteristics were obtained by solving equations (3.84(a)–(j)) in the MATLAB/Simulinkenvironment. The equations that solve for winding currents in the dynamic model are derived from equations (3.84 (f) – (i)) and are given in equations (B.5) – (B.8) where λ_{mqc}, λ_{mdc} and λ_{mdr} are dummy variables. The flow chart that describes the solution of the dynamic equations is provided in Figures 3.6. The simulink model constructed for the solution of the dynamic model is given in Figure 3.7. The flow chart that describes the solution of the steady state equations is provided in Figure3.8.

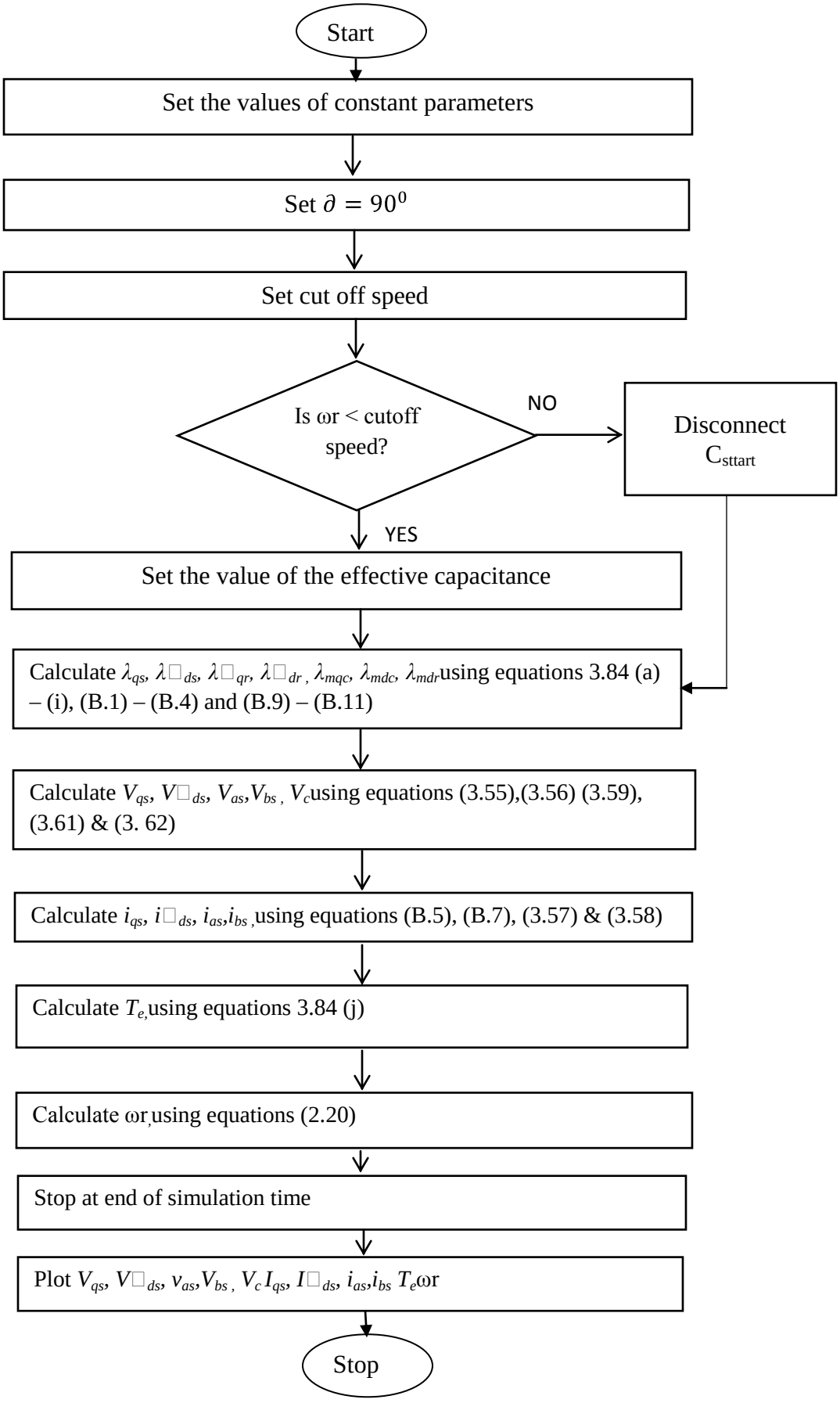


Figure 3.6: Flow Chart for the Solution of the Dynamic Model

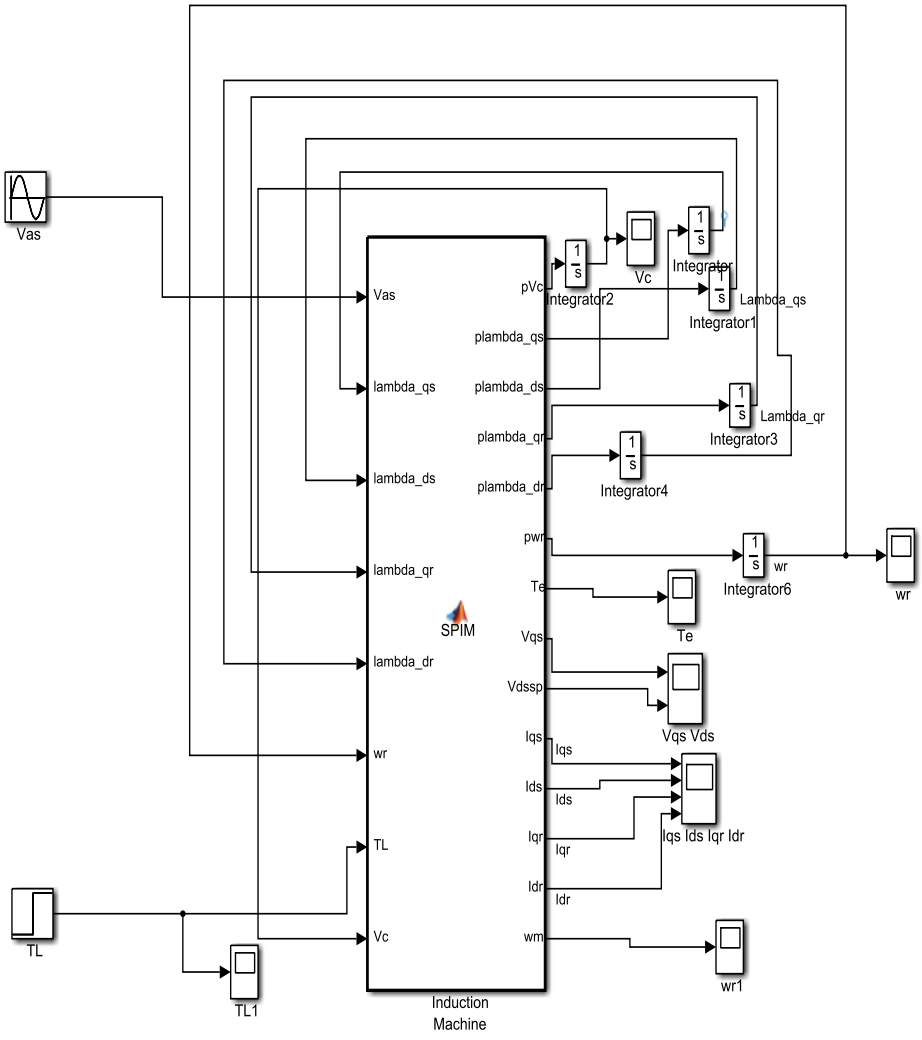


Figure 3.7: Simulink Model

The steady state performances were obtained by solving equation (3.83) for currents and then calculating the motor speed, magnitude of main and auxiliary windingcurrents, mechanical power output, electrical power input, phase angle of currents and the efficiency of the machine using the following equations:

$$\omega_r = \omega_e(1 - s) \tag{3.85}$$

$$|I_{qs}| = |a + jb| \tag{3.86}$$

$$|I_{ds}| = |c + jd| \tag{3.87}$$

Mechanical power output, $P_{out} = T_{avg} \times \omega_r$ (3.88)

$$\emptyset_{qs} = arctan\left(\frac{b}{a}\right) \quad (3.89)$$

$$\emptyset_{ds} = arctan\left(\frac{d}{c}\right) \quad (3.90)$$

$$power\ input = Re\left(V_{qs}I^*_{qs} + V_{ds}I^*_{ds}\right) \quad (3.91)$$

Efficiency $= \frac{power\ output}{power\ input}$ (3.92)

Where $\emptyset_{qs}$ and $\emptyset_{ds}$ are respectively, the phase angles of currents in the main and auxiliary windings. S is the slip of the machine. $|I_{qs}|$and $|I_{ds}|$are the magnitudes of current in the main and auxiliary windings respectively. Variables *a* and *b* are the real and imaginary parts respectively of the main winding current phasor and they are obtained from the first row of the current matrix expressed in Appendix B. Variables c and *d* are the real and imaginary parts respectively of the auxiliary winding current phasor and they are obtained from the second row of the current matrix. Theaverage torque and the magnitude of pulsating torque are calculated from equations (3.80(a) and (c)) respectively. A comprehensive assessment of the dynamic and steady state operation of the CRSPIMis provided in chapter five.

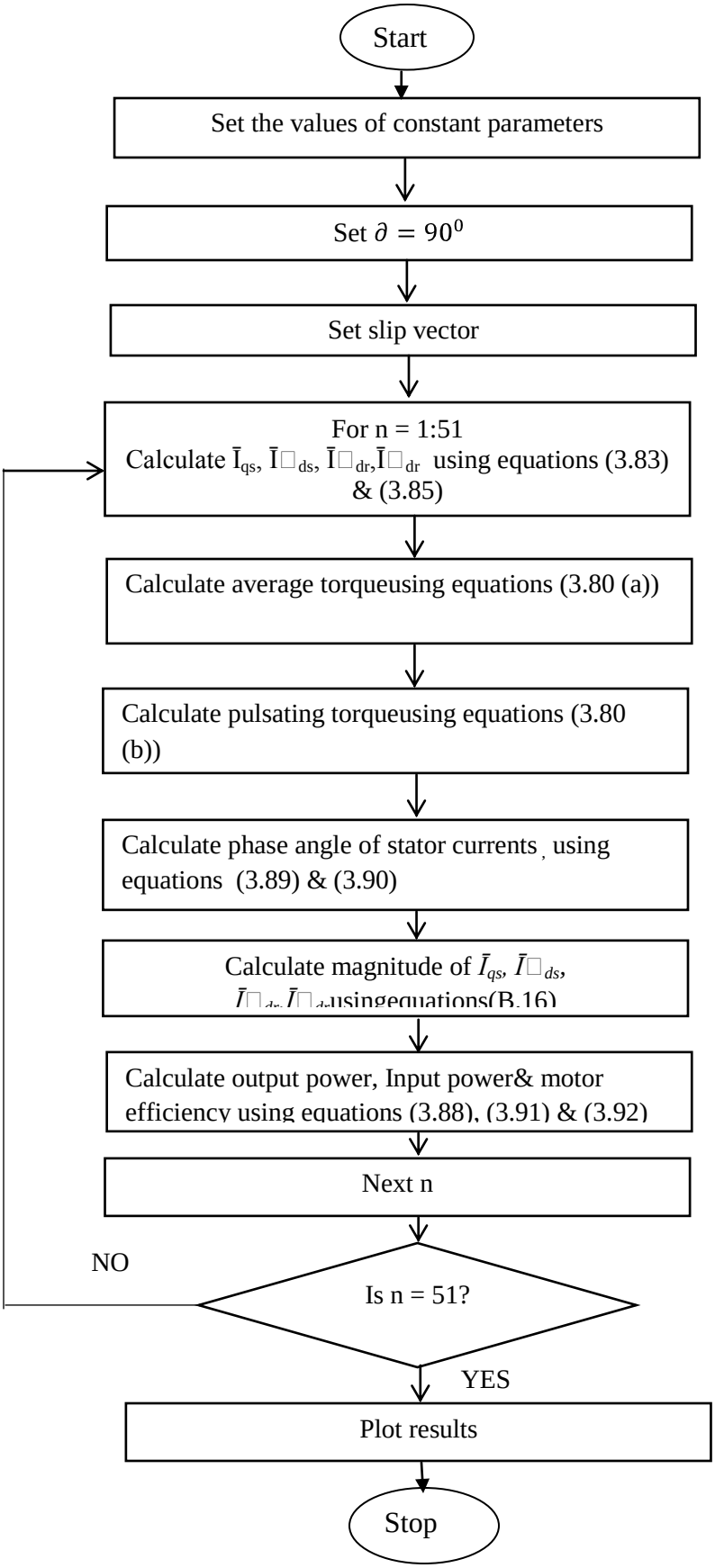


Figure 3.8: Flow Chart for the Solution of the Equations of the Steady State Model

3.4 INFLUENCE OF SPATIAL ANGLE ∂ ON THE TORQUE PRODUCTION

The average torque, magnitude of pulsating torque and efficiency of the CRSPIM for different displacement angles between 0 and 180^0 was investigated by solving the new model for these performances across the entire motor speed range. A range of displacement angles that gave comparable motor performance to that of the standard capacitor – run motor was identified to be$50^0 – 80^0$. However, CRSPIM 1 whose data is given in Table A.1 is a 24 slots, 4 pole machine having a slot angle of 30^0.The only implementable spatial angle in the identified range is $60^0$and therefore considerations for torque and efficiency improvement have been limited to the displacement angle of 60^0. Motor performances for this case have been compared with the performances of the standard motor with a displacement angle of 90^0 with respect to average torque,magnitude of pulsating torque and efficiency. The graphical results are provided in section 4.2 and they were obtained using equations (3.80 (a)), (3.80 (c))and (3.92) respectively.

In order to clear any doubt as to whether the 60^0 spatial angular displacement indeed has any advantage over the standard motor design, the condition for balanced motor operation was applied to the generalizedmodel of the CRSPIMin order to find out the best case performance scenario for both the 60^0 and 90^0 winding configuration particularly with respect to torque production in the machine. Consequently, the theory treated in section 2.2.2.10 was applied to advance the investigations of motor performance with a view to finding out the potential advantage, if any, that the 60^0 winding configuration might have when compared to the conventional 90^0 winding configuration. By applying the condition for balanced motor operation to the steady state model, it was possible to observe the best case performance scenario for both the 60^0 and 90^0winding configuration and therefore to decide which spatial angular displacement to retain going forward. The magnitude of torque pulsations is a very important factor that helped

to decide which winding configuration is superior because motor performance deteriorates with the increase in its value. Moreover, the presenceof torque pulsations complicates efforts to control the machine. The process of applying balanced condition to the 60^0 and 90^0winding configurations is discussed in the following section.

3.4.1 Application of Balanced Condition to the 60^0 and 90^0 Configurations for Best Torque Performance

Equations (2.22) and (2.23) were utilized in order to examinethe effects of imposing balanced currents in the stator windings of the single phase induction machine. The steps taken to study these effects are outlined in the following section.

3.4.1.1 Steps taken to study the effects of imposing balanced currents in the stator windings of the single phase induction machine.

a) The condition for balanced currents states that the stator currents must have a phase difference of $(\pi - \partial)$ and that their magnitudes must be in inverse proportion to the ratio of the effective turns of the windings. Therefore, the steady state voltage equations (3.83) was operated upon by applying the following equation:

$$\bar{\imath}_{ds} = \frac{\bar{\imath}_{qs}}{a} e^{j(\pi-\partial)} \tag{3.93}$$

Where

$$a = \frac{N_a}{N_m} \tag{3.94}$$

$\bar{\imath}_{ds}$ and $\bar{\imath}_{qs}$ are the peak values of the auxiliary and main winding currents respectively. $e^{j(\pi-\partial)}$ is an operator to revolve $\bar{\imath}_{qs}$ by $(\pi - \partial)$.

b) The resulting steady state equation of the single phase induction machine is as follows:

$$\begin{bmatrix} \overline{V}_{qs} \\ 0 \\ 0 \\ 0 \end{bmatrix}$$

$$= \begin{bmatrix} \left(r_{as} + j\frac{\omega_e}{\omega_b}X_{as}\right) - j\frac{\omega_e}{a\omega_b}X_{mas}\cos\partial\,(e^{j(\pi-\partial)}) & j\frac{\omega_e}{\omega_b}X_{mas} & 0 & 0 \\ -j\frac{\omega_e}{\omega_b}X_{mas}\cos\partial + \frac{1}{a}\left(r'_{bs} + j\left(\frac{\omega_e}{\omega_b}X'_{bs}\right)\right)(e^{j(\pi-\partial)}) & -j\frac{\omega_e}{\omega_b}X_{mas}\cos\partial & j\frac{\omega_e}{\omega_b}X_{mas}\sin\partial & -1 \\ j\frac{\omega_e}{\omega_b}X_{mas} - \frac{1}{a}(j\frac{\omega_e}{\omega_b}X_{mas}\cos\partial + \frac{\omega_r}{\omega_b}X_{mas}\sin\partial)(e^{j(\pi-\partial)}) & r'_r + j\frac{\omega_e}{\omega_b}X'_r & -\frac{\omega_r}{\omega_b}X'_r & 0 \\ \frac{\omega_r}{\omega_b}X_{mas} + \frac{1}{a}\left(j\frac{\omega_e}{\omega_b}X_{mas}\sin\partial - \frac{\omega_r}{\omega_b}X_{mas}\cos\partial\right)(e^{j(\pi-\partial)}) & \frac{\omega_r}{\omega_b}X'_r & r'_r + j\frac{\omega_e}{\omega_b}X'_r & 0 \end{bmatrix} \begin{bmatrix} \overline{i}_{qs} \\ \overline{i}'_{qr} \\ \overline{i}'_{dr} \\ \overline{V}'_{ds} \end{bmatrix}$$

(3.95)

Equation (3.95) is indicative of efforts to eliminate the run capacitor from the auxiliary winding and estimate a voltage, $\overline{V}'_{ds}$ to be injected on the auxiliary winding. The series capacitive impedance in (3.83) has been eliminated in the equation (3.95). This is because the supply of balanced currents obviates the need for a capacitor in the auxiliary winding circuit. The voltage $\overline{V}'_{ds}$ was calculated to determine the voltage required to supply a current to the auxiliary winding that enforces compliance with the condition for balanced operation of the machine.

c) The effects of the imposition of balanced currents on the torque production in the machine for the two different winding configurations are given in section 4.3. The calculated auxiliary winding voltage and its phase angle are given in section4.3 as well.

A method to improve the performancesof the standard or existing CRSPIM in the light of the foregoing analysis was therefore realized. The method is developed next.

3.5 DEVELOPMENT OF APWM INVERTER DRIVE FOR STANDARD SPIM TORQUE PERFORMANCE IMPROVEMENTS

Fundamental theory of the single phase machine with quadrature stator windings suggests that if the windings turns ratio can be made equal to the inverse ratio of stator currents and the stator currents can be set 90^0 apart in time throughout entire motor speed range, then it is possible to improve motor performance. In particular, this means that the average torque in the machine can be increased while the torque pulsations can be significantly reduced if not completely eliminated. This research has applied the analysis treated in section *2.2.2.9* to demonstrate the applicability of the method of using a pulse width modulated inverter to supply balanced voltages to the stator windings of the existing single phase induction machine in order to improve its performance. The realization involves the use of an inverter topology and associated controller that will enable the supply of a voltage whose amplitude and phase vary with motor speedin an effort to produce an auxiliary winding current whose phase lead is 90^0 with respect to the main winding current.

The single phase inverter topology shown in Figure 2.25 was selected. In this arrangement, the main winding receives power directly from the mains supply. The auxiliary winding is supplied by the single phase inverter. This topology was upgraded as shown in Figure 3.9. In this figure, the main ac voltage is rectified to dc and then the rectified dc voltage is filtered before feeding the inverter. The speed signal was used to calculate a reference voltage. This reference voltage is compared with the actual voltage supplied to the auxiliary winding and the error signal is processed by a PID controller to generate the PWM signals required to switch the devices of the inverter in order to synthesize the desired output to be injected into the auxiliary phase winding. This output is a voltage whose amplitude and phase is proportional to the machine speed in compliance with the condition for balanced currents in the main and auxiliary windings. The

scheme was realized in MATLAB/Simulink environment. It was applied to two different machines whose data are provided in Tables A.1 and A.2 in Appendix A. The machine data are referred to as Machine 1 and Machine 2 respectively. The model equations of the rectifier, filter, inverter and that of the single phase induction machine are provided in sections 3.5.1 – 3.5.3.

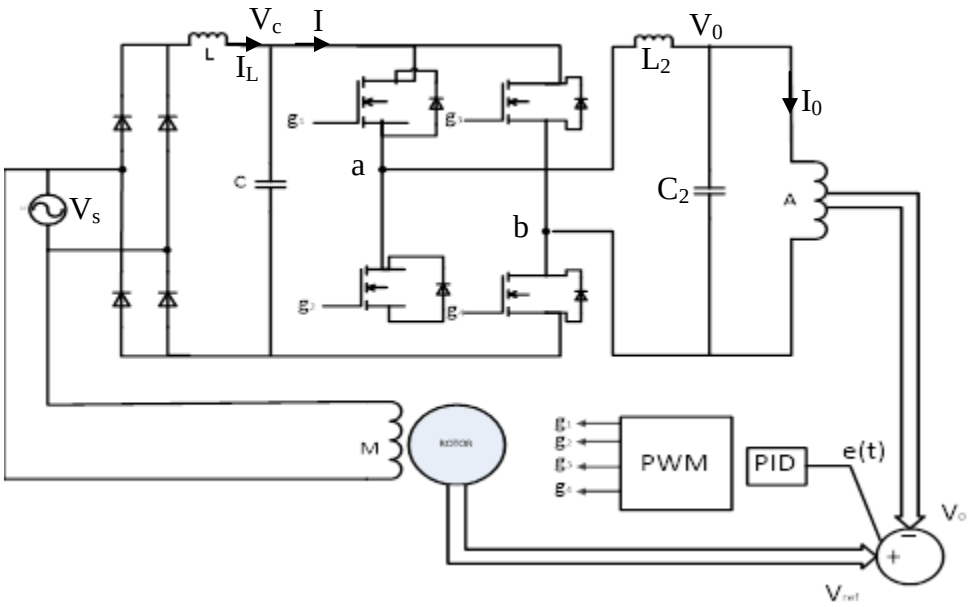


Figure 3.9: Pulse Width Modulated Inverter-Drive

3.5.1 Model Equations of the Rectifier and its Filter

The model equations of the rectifier and its filter are obtained from Figure 3.9 and are given as;

$$V_c = V_s - L\frac{dI_L}{dt} \qquad (3.96(a))$$

$$C\frac{dV_c}{dt} = I_L - I \qquad (3.96\ (b))$$

Where V_c is the d.c voltage across the capacitor. V_s is the source voltage. I_L and I are the inductor current and input current to the inverter while L and C are inductance and capacitance of the input filter components.

3.5.2 Model Equations of the Inverter and its Filter

The model equations of the inverter and its filter are obtained from Figure 3.9 and are given as;

$$V_0 = V_{ab} - L_2 \frac{dI}{dt} \quad (3.97\ (a))$$

$$C_2 \frac{dV_0}{dt} = I - I_a \quad (3.97\ (b))$$

V_0 is the fundamental output voltage of the inverter. I_a is the inverter output current while L_2 and C_2 are the inductance and capacitance of the output filter components. The inverter output voltage V_{ab} is as given in equation (2.86):

$$V_{ab} = V_C(S_{ap} - S_{bp}) \quad (3.98)$$

The value of therectifier and inverter filter component values were calculated from equations (2.95) – (2.97). These values are tabulated in Tables 3.1 and 3.2 for Machine 1 and Machine 2 respectively.

Table 3.1: Drive Circuit Pameters of Machine 1

Parameters	**Values**
V_{c1}	200V
L	0.004mH
C	0.18F
L_2	0.04mH
C_2	1800μF
f_C	600Hz
f_S	2kHz
Kpwm	1

Table 3.2: Drive Circuit Pameters of Machine 2

Parameters	**Values**
V_{c2}	400V
L	0.003mH
C	0.18F
L_2	0.03mH
C_2	1800μF
f_C	700Hz
f_S	2kHz
Kpwm	1

The modulating signal in this scheme is the output of the PID controller and it has the form of equation (2.90). The inverter switches are pulse width modulated with this modulating signal and a carrier triangular wave having a frequency of 2kHz and amagnitude of 1. The switching frequency of 2kHz was chosen because it helps, along with the filter components, to remove the harmonics present in the output voltage of the inverter phases while minimizing the switching losses in the inverter.

3.5.3 Model of the Conventional Single Phase Induction Machine

By setting ∂ to 90^0 in model equations (3.84), the following equations are obtained.

$$V_{qs} = r_{as}i_{qs} + p\lambda_{qs} \quad (3.99\ (a))$$

$$V'_{ds} = r'_{bs}i'_{ds} + p\lambda'_{ds} \quad (3.99\ (b))$$

$$V'_{qr} = r'_{r}i'_{qr} - \omega_r\lambda'_{dr} + p\lambda'_{qr} \quad (3.99\ (c))$$

$$V'_{dr} = r'_{r}i'_{dr} + \omega_r\lambda'_{dr} + p\lambda'_{dr} \quad (3.99\ (d))$$

$$\lambda_{qs} = L_{las}i_{qs} + L_{mas}\left(i_{qs} + i'_{qr}\right) \quad (3.99\ (e))$$

$$\lambda'_{qr} = L'_{lr}i'_{qr} + L_{mas}(i_{qs} + i'_{qr}) \quad (3.99\ (f))$$

$$\lambda'_{ds} = L_{lbs}i'_{ds} + L_{mas}(i'_{ds} + i'_{dr}) \quad (3.99\ (g))$$

$$\lambda'_{dr} = L'_{lr}i'_{dr} + L_{mas}(i'_{ds} + i'_{dr}) \quad (3.99\ (h))$$

$$T_e = \frac{P}{2}L_{mas}\left(i'_{dr}i_{qs} - i'_{ds}i'_{qr}\right) \quad (3.99\ (i))$$

3.6 DEVELOPMENT OF A PID CONTROLLER FOR THE INVERTER DRIVE

To develop the controller for the machine drive, it is necessary to model the drive system and obtain the expression for the closed loop transfer function in terms of the PID controller gains. The gains are then calculated and fine-tuned based on the MATLAB pidtool command. A guide

on the way to use the pidtool command is found in(Control system toolbox user's guide, 2013a). The modeling of the PWM inverter drive system is presented in this section.

3.6.1 Modeling of the Single Phase PWM Inverter Drive

The single phase PWM inverter drive model is given in Figure 3.10

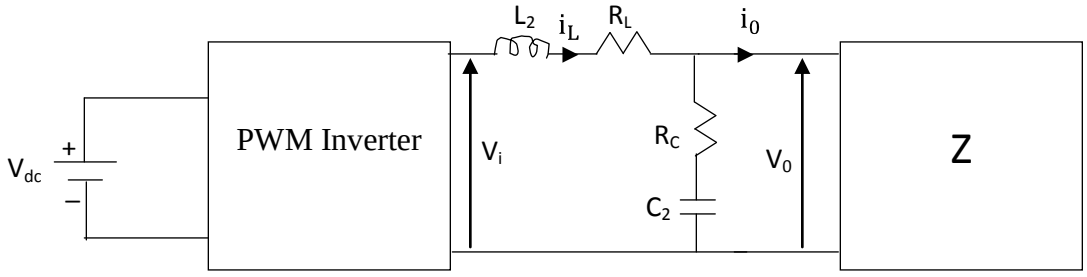


Figure 3.10: Single Phase PWM Inverter Drive Model

The equations that describe the circuit behavior may be obtained from Figure 3.10 and is expressed as:

$$V_i(t) = L_2 \frac{di_L(t)}{dt} + i_L R_L + V_0(t) \tag{3.100}$$

$$i_L(t) = C_2 \frac{dV_{c2}(t)}{dt} + i_0(t) \tag{3.101}$$

$$V_0(t) = V_{c2}(t) + C_2 \frac{dV_{c2}(t)}{dt} R_c \tag{3.102}$$

Equation (3.101) assumes that the circuit is loaded (with Z as the load impedance) and a load current of i_0 flows in the load circuit. $R_L$and$R_c$are the equivalent series resistances (ESRs) of the inductor and capacitor. The state space equation of the single phase inverter of Figure 3.10 is obtained from equations (3.100)-(3.102) and is expressed as:

$$\begin{bmatrix} \dot{i}_L(t) \\ \dot{V}_{c2}(t) \end{bmatrix} = \begin{bmatrix} \frac{Z(R_L+R_c)-R_L R_c}{L(Z+R_c)} & -\frac{Z}{L(Z+R_c)} \\ \frac{1}{C\left(1+\frac{R_c}{Z}\right)} & -\frac{1}{ZC\left(1+\frac{R_c}{Z}\right)} \end{bmatrix} \begin{bmatrix} i_L(t) \\ V_{c2}(t) \end{bmatrix} + \begin{bmatrix} \frac{1}{L} \\ 0 \end{bmatrix} V_i(t) \tag{3.103}$$

$$V_0(t) = \begin{bmatrix} \frac{ZR_c}{Z+R_c} & \frac{Z}{Z+R_c} \end{bmatrix} \begin{bmatrix} i_L(t) \\ V_{c2}(t) \end{bmatrix} \tag{3.104}$$

$$V_i(t) = V_i u(t) \tag{3.105}$$

Where:

$$u(t) = \begin{Bmatrix} 1 & V_i(t) = V_{dc} \\ 0 & V_i(t) = 0 \\ -1 & V_i(t) = -V_{dc} \end{Bmatrix} \quad (3.106)$$

V_C is the input dc source voltage. $\dot{i_L}(t)$ and $\dot{V}_{c2}(t)$ are the derivatives of the inductor current and capacitor voltage respectively. ESRs are often neglected in the analysis because they have very small values. If the ESRs of the inductor and capacitor are neglected, then a simplified model of the single phase inverter can be obtained as given in Figure 3.11.

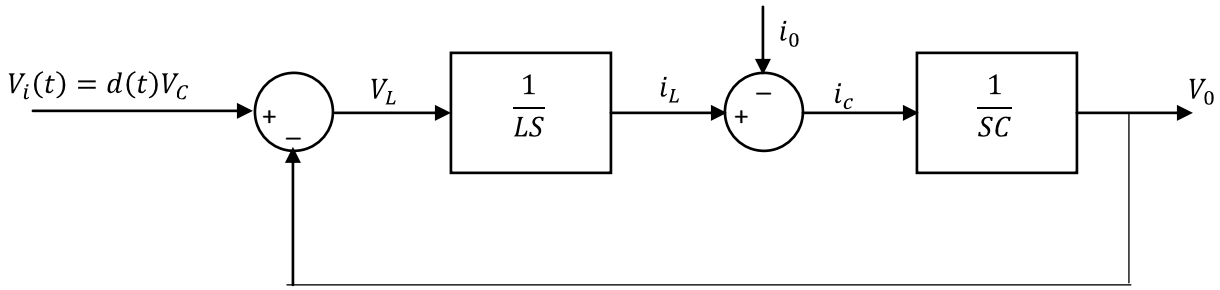


Figure 3.11: A Simplified Model of the PWM Single Phase Inverter Drive

$d(t)V_C$ is the average value of $V_i(t)$ and $d(t)$ is the sinusoidal reference signal required to create a desired output voltage. The model of the single phase inverter drive was utilized to obtain a single loop controller subsystem in the manner described in section 3.6.2.

3.6.2 Controller Structure for a Single Phase Inverter Drive

The system in Figure 3.11 is an open loop system whose output is a voltage and the control objective is to regulate the output voltage to its reference value with zero steady state error without overshoot and with a fast response. Such objectives can be achieved by introducing a PID controller in a closed loop arrangement of the type shown in Figure 3.12.

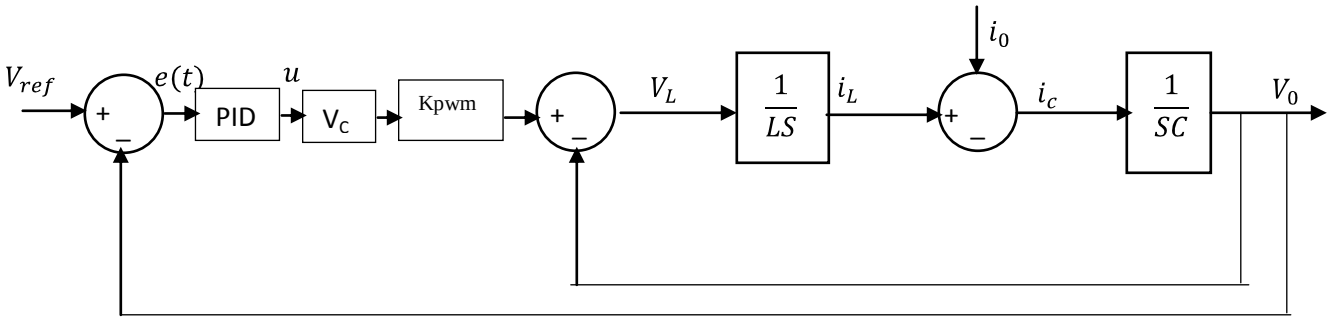


Figure 3.12: Closed Loop Control of the Single Phase Inverter Drive

In Figure 3.12, the reference command V_{ref} is compared with V_0 and the error signal $e(t)$ is generated. The controller processes the error signal and provides the control signal u. The PID controller uses the error signal to generate the proportional, integral and derivative actions according to equation (2.98). The closed loop transfer function of the system in Figure 3.12 was computed and is expressed as;

$$TF_{CL} = \frac{k_D V_C K_{pwm} s^2 + V_C K_{pwm} k_p s + V_C K_{pwm} k_i}{LCs^3 + V_C K_{pwm} k_d s^2 + (V_C K_{pwm} k_p + 1)s + V_C K_{pwm} k_i} \quad (3.107)$$

Frequency response design method was employed in order to determine the parameters of the PID controller. In determining the parameters of the controller, the bandwidth, ω_b was selected to be 1000Hz in order to ensure a fast response and to guarantee tracking of the sinusoidal reference voltage. Other specifications are percentage overshoot of 0.01 and a phase margin of greater than 60^0 to ensure system stability. The steps taken to design the controller is outlined as follows;

a) Set Ki to zero
b) Calculate damping ratio for the specified value of percentage overshoot using equation (2.100)
c) Calculate the natural frequency ω_n corresponding to the chosen bandwidth using equation (2.101).

d) Using the values of ζ and ω_n obtained, determine the denominator of a second order transfer function that meets the given specifications and compare with the denominator of equation (3.107).

e) Calculate values of k_p and k_d

f) Fine-tune k_p, k_i and k_D by adjusting their values as necessary using MATLAB pidtool command until the desired specifications are met.

3.6.3 Controller Parameters

The values obtained for k_p, k_i and k_D using the steps outlined in section 3.6.2 are 0.07646, 4.6678 and 0.00031312 respectively for the scheme to drive Machine 1, designated as system 1.The values obtained for k_p, k_i and k_D are 0.050425, 3.5344 and 0.00017985 respectively for the scheme to drive Machine 2, designated as system 2. The corresponding closed loop transfer functions of system 1 and system 2 were calculated using the values in Tables 3.1, 3.2 and the controller parameters. The closed loop transfer functions are expressed respectively as;

$$G(s)_1 = \frac{6958s^2+1.699e06s+1.037e08}{s^3+6958s^2+1.81e06s+1.037e08} \quad (3.108)$$

$$G(s)_2 = \frac{7993s^2+2.241e06s+1.571e08}{s^3+7993s^2+2.352e06s+1.571e08} \quad (3.109)$$

The bode plots of the closed loop systems are given in Figures 3.13 and 3.14. The bandwidth,$\omega_b$of the closed loop systems 1 and 2 are approximately 5700 and 6500 rad/s respectively. The magnitude and phase of the closed loop transfer functions are unity and 0^0 respectively at the fundamental frequencies,ω_0 of 377rad/s and 314 rads/s respectively for systems 1 and 2.

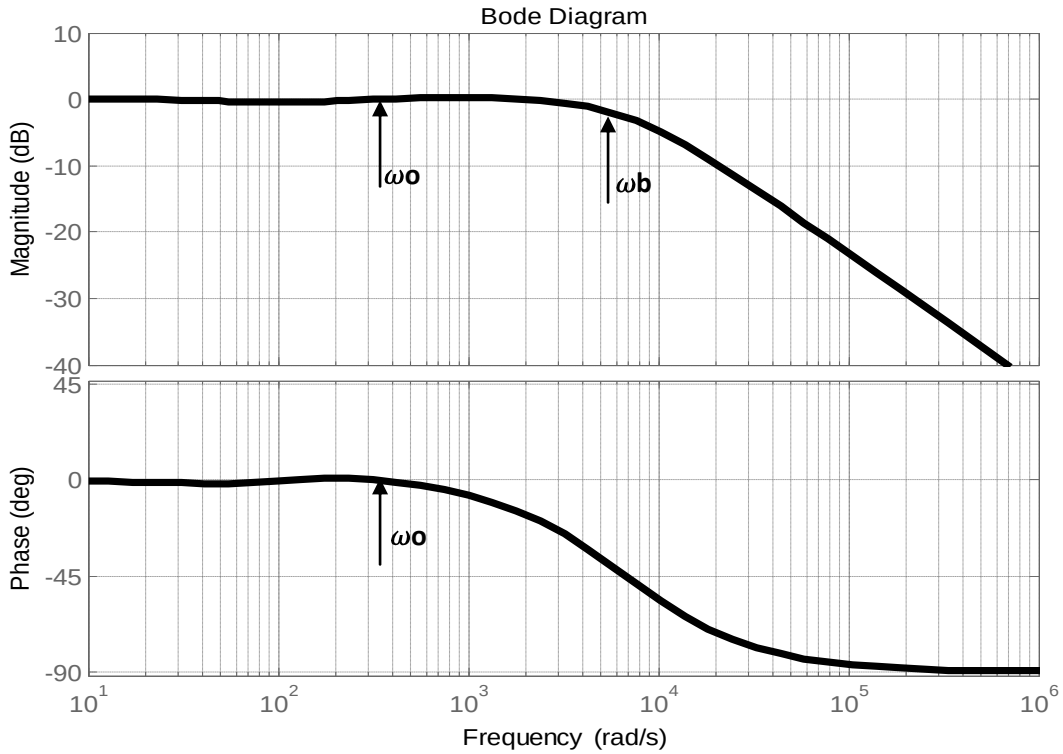


Figure 3.13: Closed Loop Frequency Response for System 1

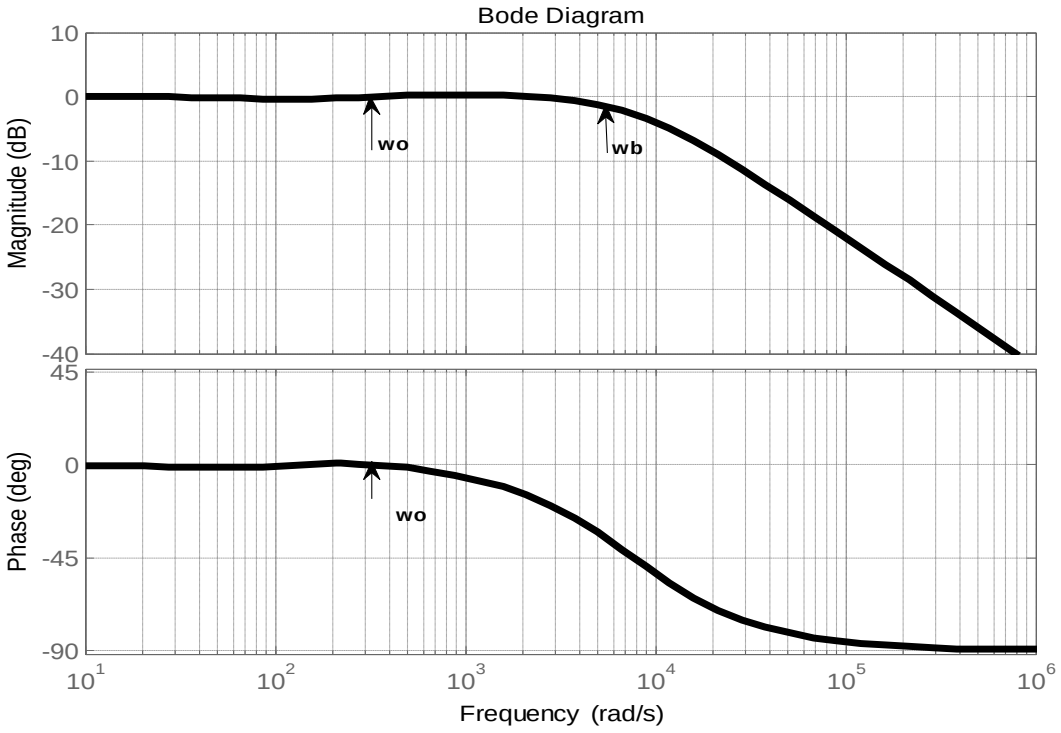


Figure 3.14: Closed Loop Frequency Response for System 2

3.6.4 Computation of Reference Voltage

Equations (2.68) and (2.70) were utilized to compute the phase and magnitude of the reference voltage. The motor parameters applied for Machine 1 and Machine 2 are obtained from Tables A.1 and A.2 respectively. The reference voltage, V_{ref} was therefore constructed as follows:

$$V_{ref} = |V_a| sin\emptyset_a \tag{3.110}$$

3.6.5 Flow Chart

The Simulink program reads the reference input signal and the feedback output voltage signal. It then calculates the error between the two signals and produces PWM pulses to control the inverter switches. The flow chart of the solution is given in Figure 3.15.

Simulation results are provided in section 4.4. The results show the effects of the scheme of Figure 3.9 on the electromagnetic torque produced in Machines 1 and 2. Simulation results of the SPWM algorithm, reference voltage, inverter fundamental output voltage and winding currents are also presented in section 4.4.

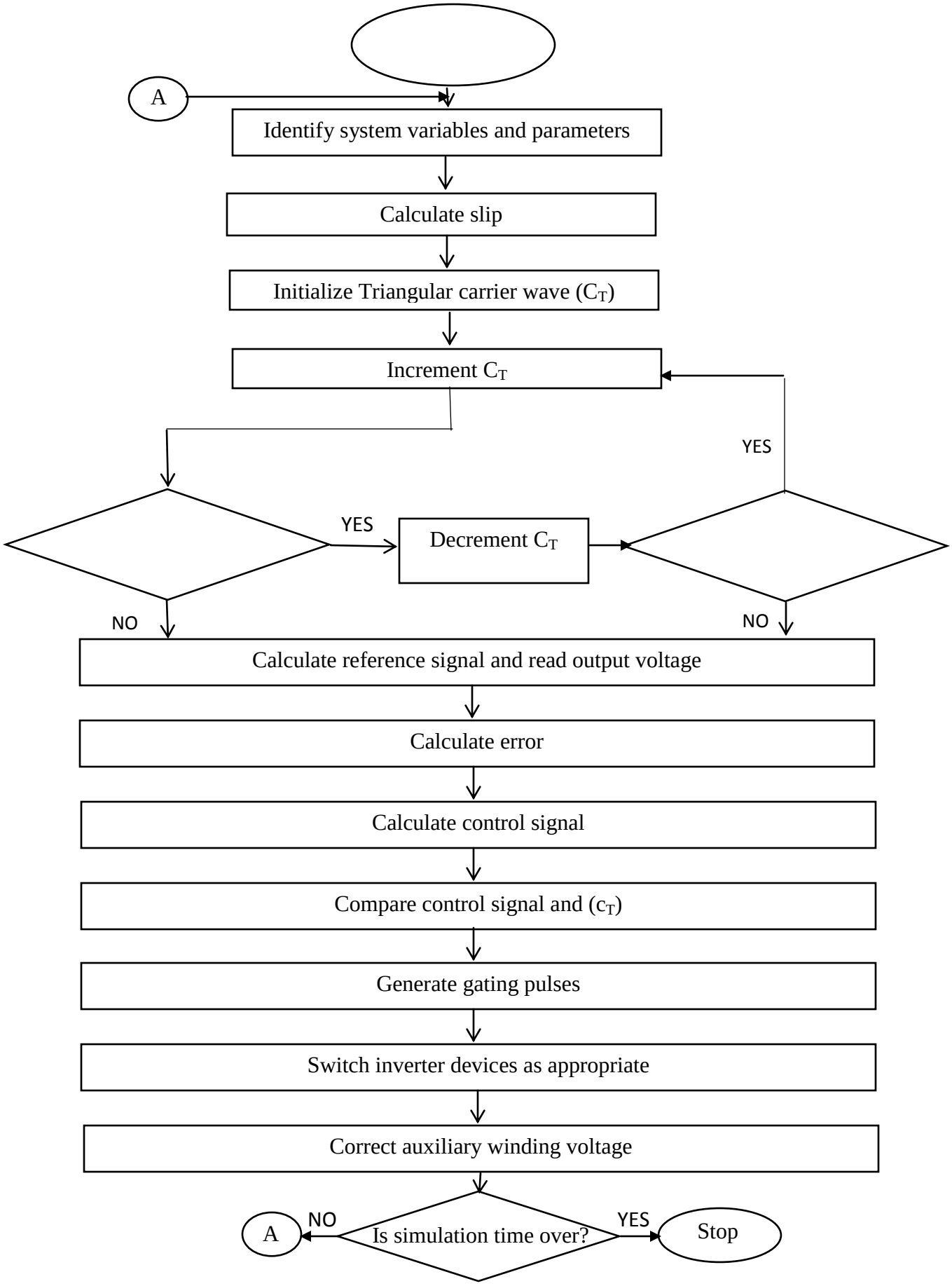


Figure 3.15: Flow Chart of the Control Algorithm

The condensed simulink program used to implement the flow chart of Figure 3.15 is given in

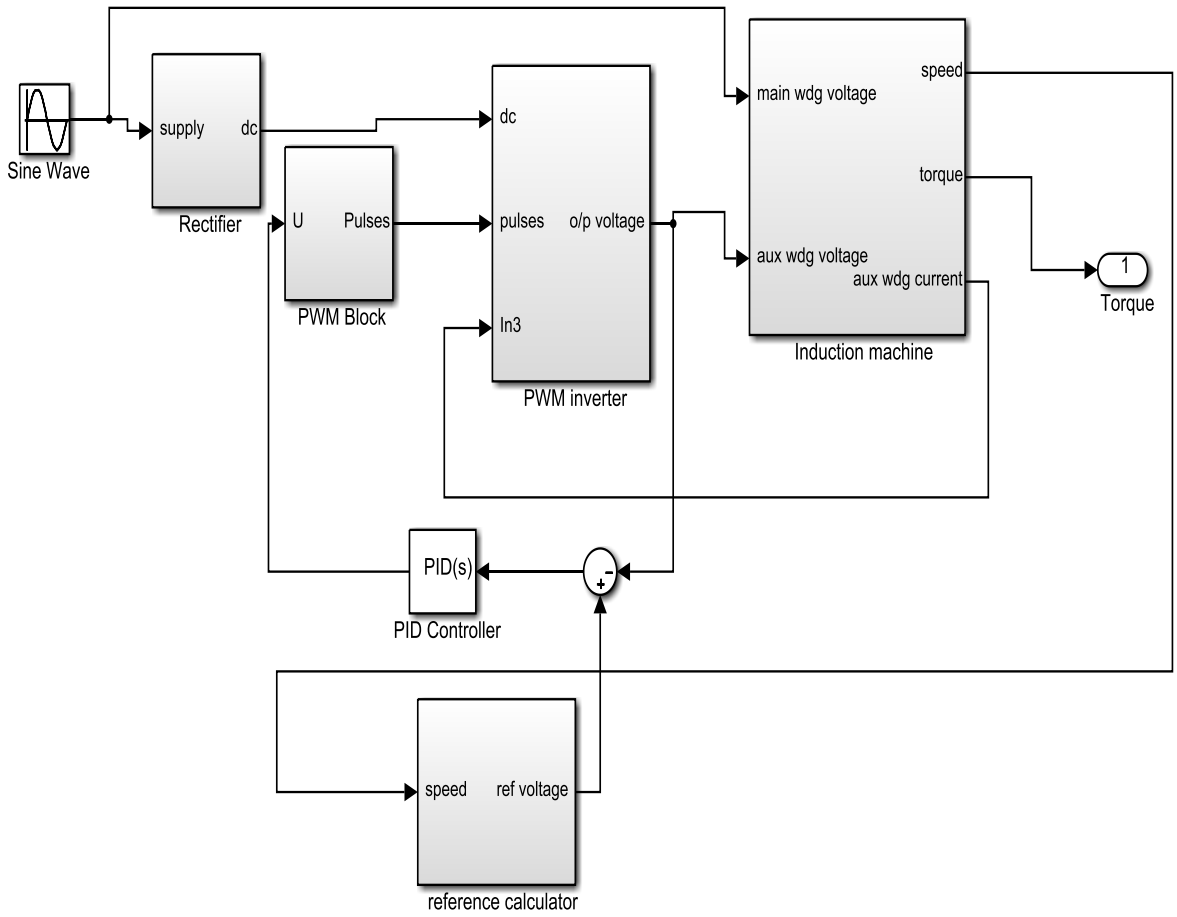


Figure 3.16. An expanded view of each block is given in Figures 3.17 – 3.21.

Figure 3.16: Simulink Realization of the PWM Inverter-Driven SPIM

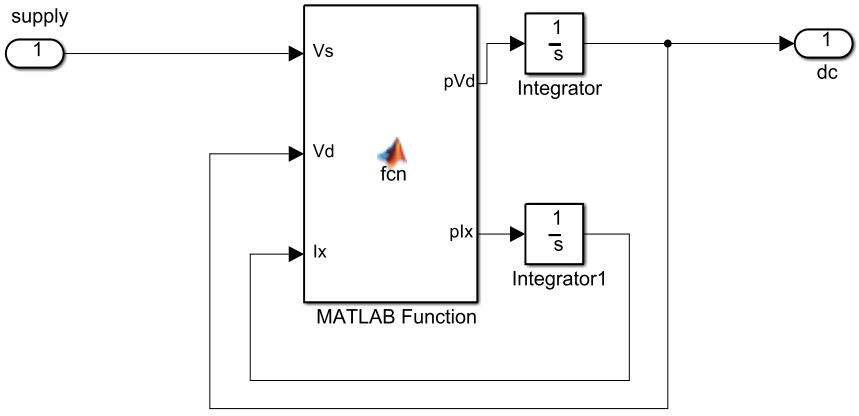


Figure 3.17: Rectifier Block

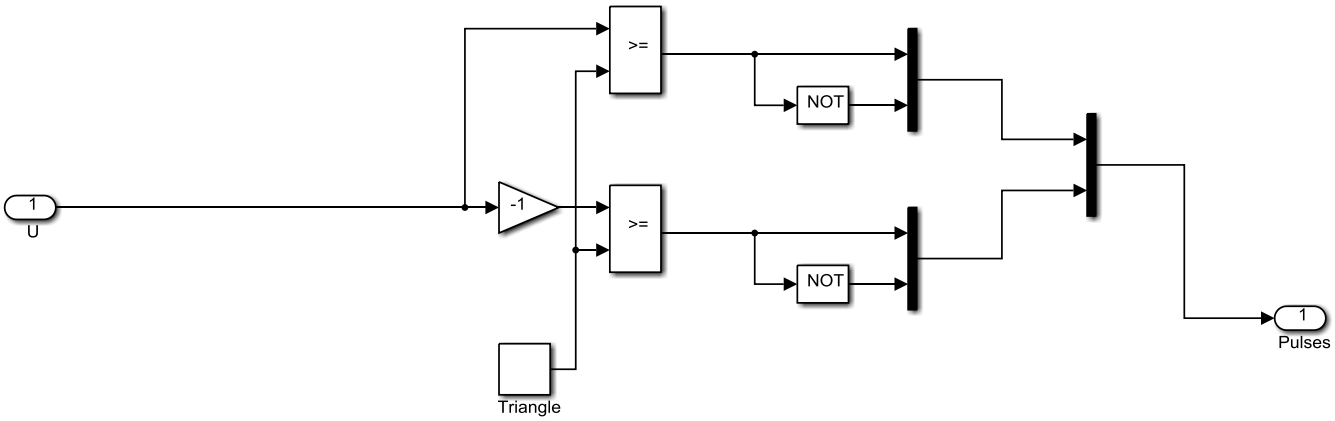


Figure 3.18: PWM Block

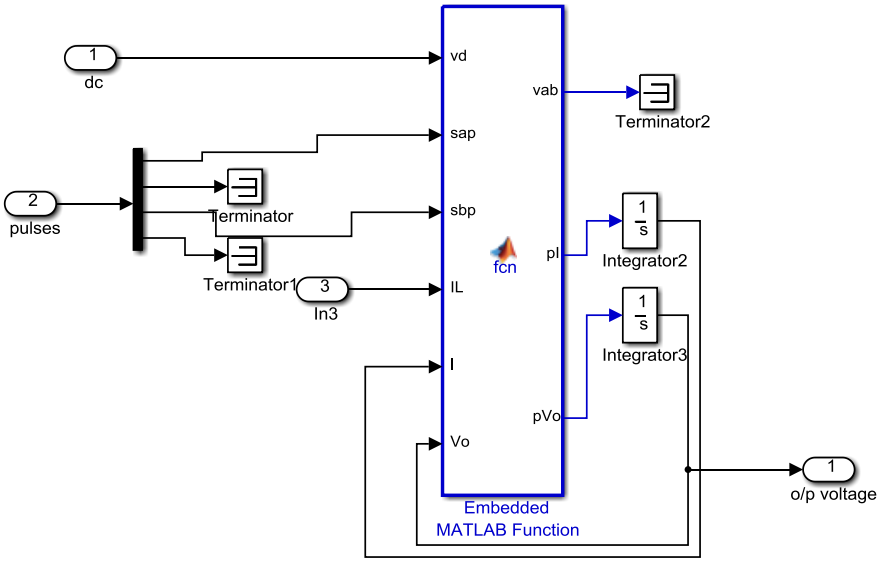


Figure 3.19: Inverter Block

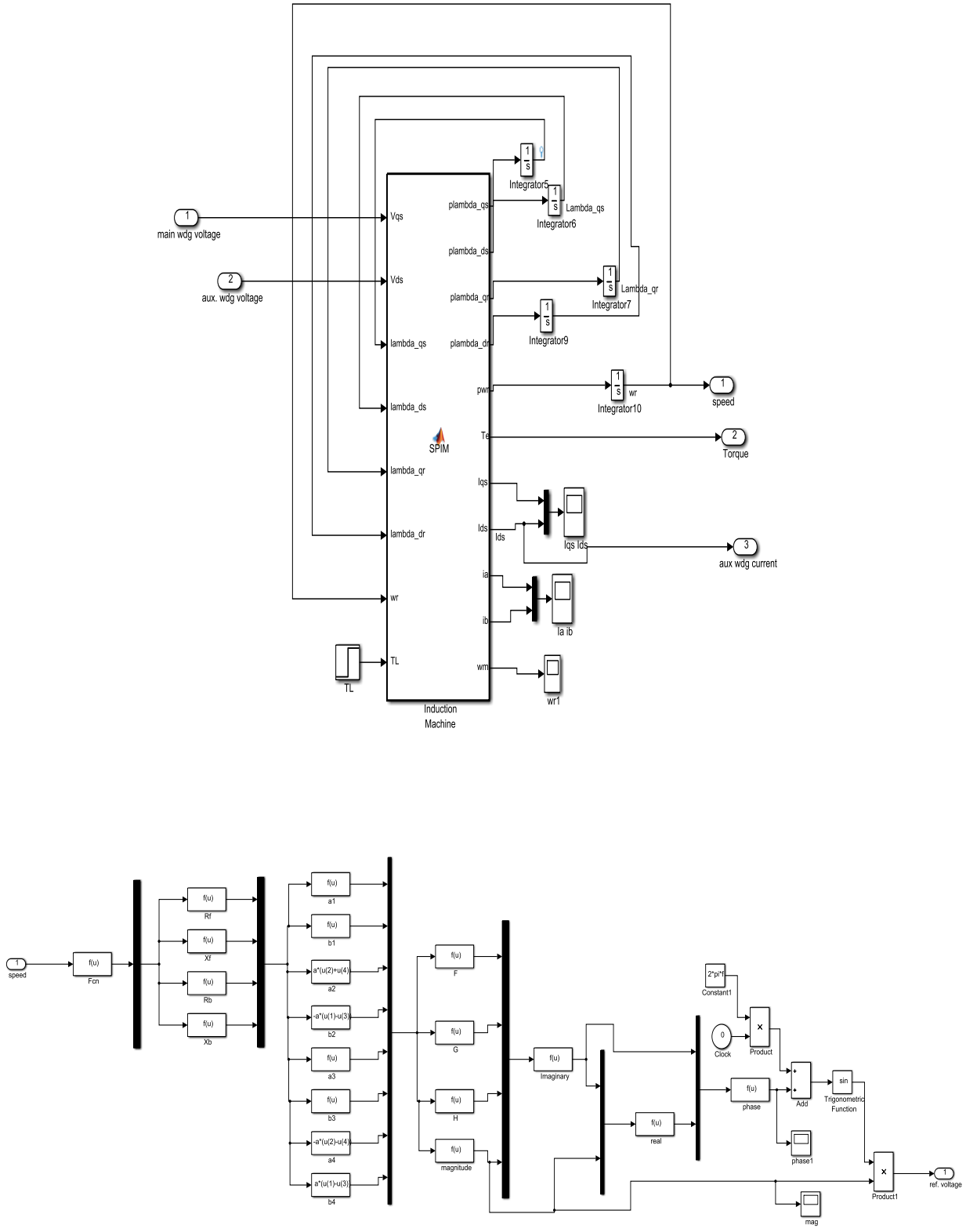


Figure 3.20: Single Phase Induction Machine Block

Figure 3.21: Reference Voltage Computation Block

3.7 PROBLEM WITH THE METHOD OF USING A PULSE WIDTH MODULATED INVERTER AND A PID CONTROLLER

There exists a substantial amount of torque pulsations in steady state in the machines driven by the method of using a pulse width modulated inverter and a PID controller.The reason is because the auxiliary and main winding currents of Machines 1 and 2 are not balanced. This means that the phase lead of the auxiliary winding current with respect to the main winding current is not 90^0 and the ratio of the magnitude of the main winding current to the auxiliary winding current is not the same as the winding turn's ratio. A review of the works of Jang (2013) and Jannati *et al.* (2014) gives good reasons to believe that this problem is caused by the asymmetry or unbalance in the main and auxiliary winding parameters.In his effort to supply balanced currents and voltages and to eliminate asymmetry,Jang (2013)utilized the vector control strategy and obtaineda newly designed symmetrical two phase induction motor. His result showed good current control which promises to eliminate torque pulsations. Jannati *et al.* (2014) also utilized the vector control strategy but in addition, they used transformation matrices to compensate for the asymmetry between the main and auxiliary windings in efforts to supply balanced currents and voltages and to eliminate asymmetry in the windings of the SPIM. Their efforts, however, did not eliminate the torque pulsations. In view of the insight from the work of these researchers, a second method utilizing a pulse width modulatedtwo-phase, two leg inverter topology and an efficiency-optimizing vector-controlled modified-SPIM is proposed in this work. In this segment of the research, the modified SPIM is viewed as an existing SPIM but with its auxiliary winding re-designed to have identical parameters as those of the main winding. The idea is to retrofit the existing single phase induction machine and indeed the huge population of such single phase machines operating globally for residential, commercial and industrial applications. The

retrofitting concept calls for a symmetrical winding design of the stator windings of existing single phase induction machines to produce improved machines referred to, in this research, as modified-SPIMs. To proceed therefore, the model of the modified SPIM is developed first and is presented in the next section. Secondly, a sinusoidal PWM open loop strategy is developed for the modified SPIM in order to test its performance when driven by a two phase two leg inverter. The two-phase, two leg inverter topology was selected because it is cheap and it has an excellent ability to supply balanced two phase voltages and currents. The open loop strategy was then upgraded to a closed loop vector control scheme. The development of the vector-controlled drive scheme with its associated efficiency-optimizing function is provided in subsequent sections. The performance of the modified SPIM under the proposed schemewas evaluatedand comparedto the performance of the existing capacitor-run single phase induction machine.

3.8 MODEL OF THE MODIFIED SINGLE PHASE INDUCTION MACHINE

A model for the modified single phase induction machine was obtained directly from the generalized CRSPIM model.The stator windings of the modified SPIM, by the proposed re-design, have identical parameters. The parameters are the winding resistance, leakage inductance and the number of turns of each winding. As a corollary, the stator windings are also balanced because their parameters are identical. The dynamic and steady state models, in the stationary reference frame, of the modified single phase induction machine are obtained if the following equations are imposed on the model equations (3.84 (a), (b), (d) - (j)) and (3.83).

$$\partial = 90^0 \tag{3.111}$$

$$N_{as} = N_{bs} = N_s \tag{3.112}$$

$$r_{as} = r'_{bs} = r_{bs}\frac{N_{as}}{N_{bs}} = r_s \tag{3.113}$$

$$l_{las} = l'_{lbs} = l_{lbs}\frac{N_{as}}{N_{bs}} = l_{ls} \tag{3.114}$$

Where N_s, r_s and l_{ls} are the number of turns, winding resistance and leakage inductance of each stator winding.

The resulting dynamic model of the modified SPIM is given by the following set of equations:

$$V_{qs} = r_s i_{qs} + p\lambda_{qs} \quad (3.115(a))$$

$$V_{ds} = r_s i_{ds} + p\lambda_{ds} \quad (3.115(b))$$

$$V'_{qr} = r'_r i'_{qr} - \omega_r \lambda'_{dr} + p\lambda'_{qr} \quad (3.115\ (c))$$

$$V'_{dr} = r'_r i'_{dr} + \omega_r \lambda'_{qr} + p\lambda'_{dr} \quad (3.115\ (d))$$

$$\lambda_{qs} = L_{ls} i_{qs} + L_{mas}\left(i_{qs} + i'_{qr}\right) \quad (3.115\ (e))$$

$$\lambda'_{qr} = L'_{lr} i'_{qr} + L_{mas}(i_{qs} + i'_{qr}) \quad (3.115\ (f))$$

$$\lambda_{ds} = L'_{ls} i_{ds} + L_{mas}(i_{ds} + i'_{dr}) \quad (3.115\ (g))$$

$$\lambda'_{dr} = L'_{lr} i'_{dr} + L_{mas}(i_{ds} + i'_{dr}) \quad (3.115\ (h))$$

$$T_e = \frac{P}{2} L_{mas}\left(i'_{dr} i_{qs} - i_{ds} i'_{qr}\right) \quad (3.115\ (i))$$

The steady state model, on the other hand, is given as follows:

$$\begin{bmatrix} \overline{V}_{qs} \\ \overline{V}_{ds} \\ \overline{V}'_{qr} \\ \overline{V}'_{dr} \end{bmatrix} = \begin{bmatrix} r_s + j\frac{\omega_e}{\omega_b} X_s & 0 & j\frac{\omega_e}{\omega_b} X_{mas} & 0 \\ 0 & r_s + j\frac{\omega_e}{\omega_b} X_s & 0 & j\frac{\omega_e}{\omega_b} X_{mas} \\ j\frac{\omega_e}{\omega_b} X_{mas} & -\frac{\omega_r}{\omega_b} X_{mas} & r'_r + j\frac{\omega_e}{\omega_b} X'_r & -\frac{\omega_r}{\omega_b} X'_r \\ \frac{\omega_r}{\omega_b} X_{mas} & j\frac{\omega_e}{\omega_b} X_{mas} & \frac{\omega_r}{\omega_b} X'_r & r'_r + j\frac{\omega_e}{\omega_b} X'_r \end{bmatrix} \begin{bmatrix} \overline{i}_{qs} \\ \overline{i}_{ds} \\ \overline{i}'_{qr} \\ \overline{i}'_{dr} \end{bmatrix} \quad (3.116)$$

3.9 DEVELOPMENT OF A SINUSOIDAL PWM OPEN LOOP INVERTER DRIVE STRATEGY FOR THE MODIFIED SPIM

An open loop sinusoidal PWM control strategy was developed in which the following sinusoidal modulating signals:

$$m_{ap} = M\cos(\omega_m t + \emptyset_m) \quad (3.117)$$

$$m_{bp} = M\cos(\omega_m t + \emptyset_m - \frac{\pi}{2}) \quad (3.118)$$

are used to synthesize two independent voltages of fixed frequency and amplitude but phase shifted by 90^0 from each other at the output of a two phase two leg inverter. $\omega_m$is the angular frequency, $\emptyset_m$ is phase angle and M is the modulating index. The modulating index is chosen in such a way that the synthesized output voltage is equal to the rated voltage of the existing SPIM. For the purpose of analysis, the inverter is supplied with dc voltage and the output voltages are used to drive the modified SPIM as shown in the circuit arrangement of Figure 3.22.

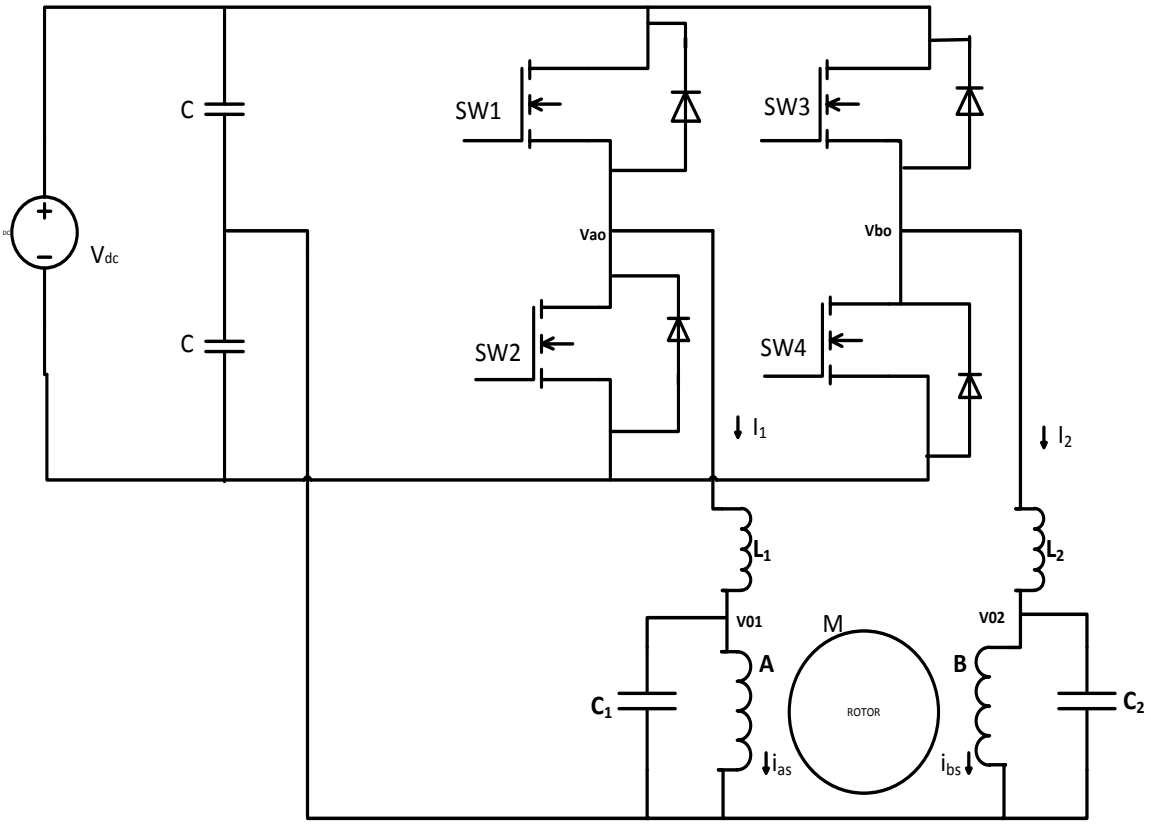


Figure 3.22: Two Phase Two Leg Inverter Topology Connected to the Modified SPIM

The model equations of the inverter and the output LC filters are provided in the next two subsections.

3.9.1 Model Equations of the Inverter and its Filters

The model equations of the inverter and its filters were obtained from Figure 3.22 and are given as:

$$V_{01} = V_{ao} - L_1 \frac{dI_1}{dt} \quad (3.119(a))$$

$$C_1 \frac{dV_{01}}{dt} = I_1 - i_{as} \quad (3.119(b))$$

$$V_{02} = V_{bo} - L_2 \frac{dI_2}{dt} \quad (3.119(c))$$

$$C_2 \frac{dV_{02}}{dt} = I_2 - i_{bs} \quad (3.119(d))$$

V_{01}andV_{02} are the fundamental output voltages of phases *A* and *B* respectively. L_1, $C_1$and L_2, $C_2$are the inductance and capacitance of the output filter components of phases A and B respectively. $V_{ao}$and V_{bo} are the pole voltages of the inverter. Again, from Figure 3.22 the pole voltages with respect to the neutral point 'o' are determined as:

$$V_{ao} = \frac{V_{dc}}{2}(2S_{ap} - 1) \quad (3.120\ (a))$$

$$V_{bo} = \frac{V_{dc}}{2}(2S_{bp} - 1) \quad (3.120\ (b))$$

$V_{ao}$and V_{bo} are the high frequency output voltages of the inverter phases. $V_{dc}$is the dc input to the inverter.

The inverter switches were pulse width modulated with the modulating signals of equations (3.117) and (3.118) for phases A and B respectively and a carrier triangular wave having a frequency of 1kHz. The switching frequency of 1kHz was chosen because it helps, along with the filter components, to remove the harmonics present in the output voltage of the inverter phases while minimizing the switching losses in the inverter. $V_{as}$and V_{bs}being the voltages applied to the phase windings of the modified SPIM are the fundamental output voltages of the inverter phases A and B. Equations (3.119 (a)-(d)),(3.120)and (2.79) were utilized along with

equations (3.115 (a)-(i))in order to implement the arrangement of Figure 3.22 in MATLAB/Simulink environment. The simulation results of machine performance with respect to torque production are presented in section 4.5. The modulating signals, inverter fundamental output voltages and winding currents are also presented in section 4.5. The two test motor data for CRSPIM 1 and CRSPIM 2 presented in Tables A.1 and A.2 respectively were modified to satisfy the condition for balanced stator windings. The data given in Tables 3.3 and 3.4 are the modified data for CRSPIM 1 and CRSPIM 2 in respect of the implementation of their respective modified SPIM model. This type of modification to the data of the existing CRSPIM was previously done in (Krause *et al*, 2013). The models are referred to as modified SPIM 1 and modified SPIM 2. The values of the dc voltageand filter components computed from equations (2.79) and (2.97) respectively for the drivesof modified SPIM 1 and modified SPIM 2 are presented in Tables 3.5 and 3.6.

Table 3.3: Parameters of the Modified SPIM 1

Parameters	**Values**
Turn's ratio	1
Main and Auxiliary winding resistance	2.02
Main and Auxiliary winding leakage Inductance	7.4mH
Rotor leakage inductance	5.6mH
Rotor resistance	4.12
Mutual Inductance	0.1772H

Table 3.4: Parameters of the Modified SPIM 2

Parameters	**Values**
Turn's ratio	1
Main and Auxiliary winding resistance	4
Main and Auxiliary winding leakage Inductance	0.0203H
Rotor leakage inductance	0.0304H
Rotor resistance	3.61
Mutual Inductance	0.1954H
Core loss resistance	910

Table 3.5: DC Voltage and Filter Component Values for the Drive of Modified SPIM 1

Parameters	**Values**
V_{dc}	350V
m_A	0.8
$L_1 = L_2$	0.003mH
$C_1 = C_2$	0.18F
f_C	700Hz
f_S	1kHz

Table 3.6: DC Voltage and Filter Component Values for the Drive of Modified SPIM 2

Parameters	**Values**
V_{dc}	650V
m_A	0.8
$L_1 = L_2$	0.003mH
$C_1 = C_2$	0.18F
f_C	700Hz
f_S	1kHz

The open loop control scheme was realized in MATLAB/Simulink platform. The Simulink implementation of the system of Figure 3.22 is shown in Figure 3.23.

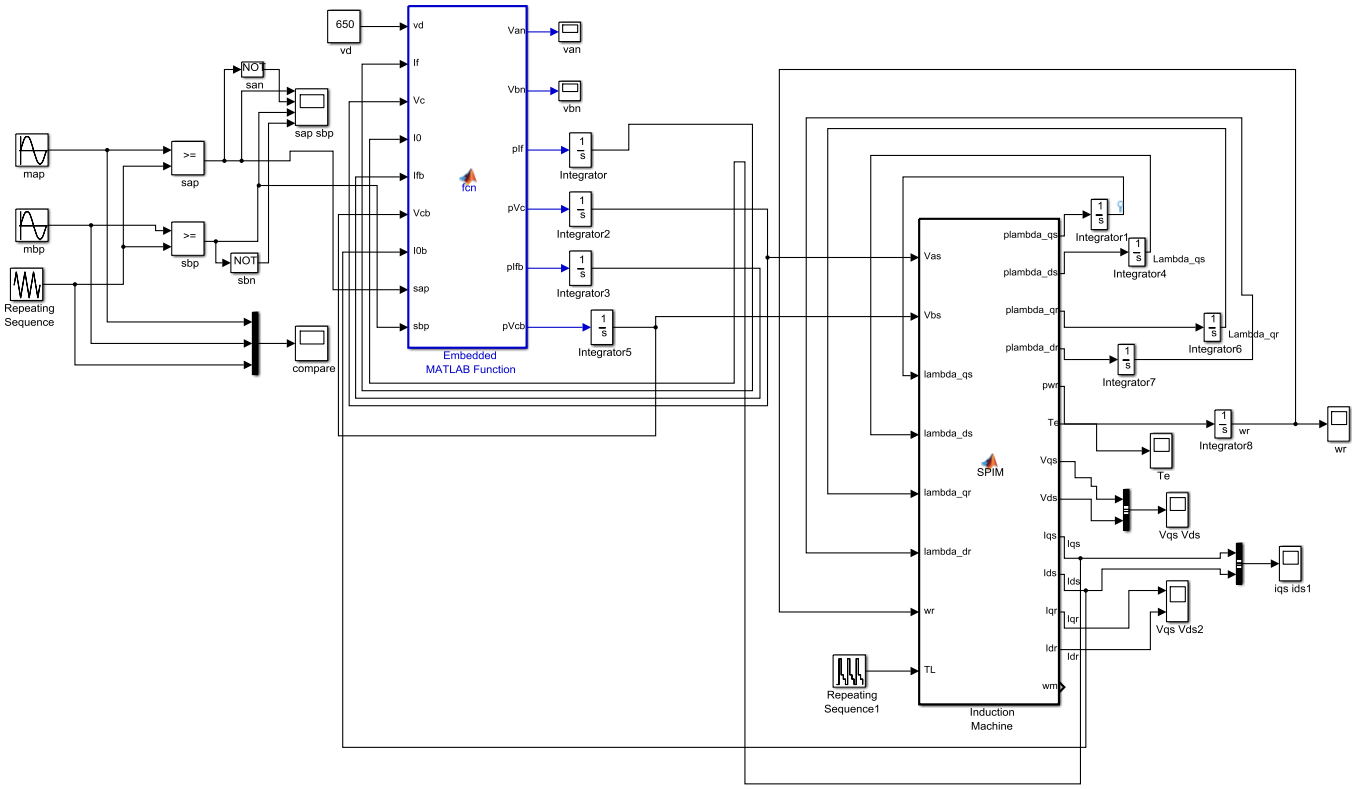


Figure 3.23: Simulink Implementation of the Open Loop Control of Inverter-Driven Modified SPIM

3.10 DEVELOPMENT OF CLOSED LOOP CONTROL STRATEGY FOR THE MODIFIEDSPIM

The control or modulating signals applied to the inverter drive developed in the previous section were assumed and are therefore external to the drive system. The result of the drive strategy, however, makes a strong case for a very effective solution to the problem of torque pulsation in the existing CRSPIM. The results showed that torque pulsations can be successfully eliminated at steady state if:

a) The parameters of the auxiliary winding are made identical to those of the main winding as demonstrated in the modifications made to Tables A.1 and A.2 resulting in corresponding Tables 3.3 and 3.4 respectively.

b) Two independent voltages and currents of equal magnitude and frequency but phase shifted 90^0 apart in time are applied to the two identical windings.

In keeping with this philosophy, a better control strategy was developed. This strategy is a closed loop control strategy in which the modulating signals are computed or derived from within the drive system and are then used to control the inverter output voltages in order to drive the modified SPIM. Such a strategy is a high performance motor drive strategy commonly referred to as the vector control strategy and is developed for the modified SPIM in section 3.10.2. Before the development of the vector control drive scheme, it is necessary to transform the model of the modified single phase induction machine from the stationary reference frame to the synchronous reference frame. This transformation is developed in the subsection 3.10.1.

3.10.1 Transformation of the Modified SPIM Model Equations from Stationary to Synchronous Reference Frame

Vector control strategy requires the transformation of machine variables such as voltages, currents and flux linkages to the synchronously rotating reference frame in order to transform these sinusoidal quantities into equivalent DC quantities. The dynamic model equations (3.115 (a)-(i)) are transformed to their equivalent equations in the synchronous reference frame. The transformation of the stator voltage equations, rotor voltage equations, flux linkage equations and the torque equation is done in this section.

3.10.1.1 Transformation of stator voltage equation

The application of Park's transformation equation (2.21)to equations (3.115(a) - (b)), gives the following equation;

$$({}^{s}\mathbf{K}_{\mathrm{s}}^{\mathrm{e}})\boldsymbol{V}^{s}{}_{qds} = ({}^{s}\mathbf{K}_{\mathrm{s}}^{\mathrm{e}})\boldsymbol{r}_{s}\boldsymbol{i}_{qds}^{s} + ({}^{s}\mathbf{K}_{\mathrm{s}}^{\mathrm{e}})p\boldsymbol{\lambda}_{qds}^{s} \tag{3.121}$$

Simplifying equation (3.121) and applying equation (2.25) gives the following equation;

$$\boldsymbol{V}^{\boldsymbol{e}}_{qds} = (^{\mathbf{s}}\mathbf{K}^{\mathbf{e}}_{\mathbf{s}})\boldsymbol{r}_s(^{\mathbf{s}}\mathbf{K}^{\mathbf{e}}_{\mathbf{s}})^{-1}\boldsymbol{i}^{\boldsymbol{e}}_{qds} + (^{\mathbf{s}}\mathbf{K}^{\mathbf{e}}_{\mathbf{s}})p\left[(^{\mathbf{s}}\mathbf{K}^{\mathbf{e}}_{\mathbf{s}})^{-1}\boldsymbol{\lambda}^{\boldsymbol{e}}_{qds}\right] \quad (3.122)$$

Where the superscripts *'s'*and *'e'* indicate stationary and synchronous reference frames respectively. The transformation matrix ($^{\mathbf{s}}\mathbf{K}^{\mathbf{e}}_{\mathbf{s}}$) is as given in equation (2.109). The solution of equation (3.122) is given as;

$$V^e_{qs} = r_s i^e_{qs} + \omega_e \lambda^e_{ds} + p\lambda^e_{qs} \quad (3.123(a))$$

$$V^e_{ds} = r_s i^e_{ds} - \omega_e \lambda^e_{qs} + p\lambda^e_{ds} \quad (3.123(b))$$

Equations (3.123 (a) – (b)) give the equivalent stator voltage equations of the modified SPIM in the synchronous reference frame.

3.10.1.2Transformation of rotor voltage equations

The rotor variables in the synchronous reference frame obtainedby applying equations (2.26) and (2.27) to equations (3.115 (c) - (d)).The following compact equation results:

$$\boldsymbol{V}'^{\boldsymbol{e}}_{qdr} = (^{\mathbf{s}}\mathbf{K}^{\mathbf{e}}_{\mathrm{r}})r'_r(^{\mathbf{s}}\mathbf{K}^{\mathbf{e}}_{\mathrm{r}})^{-1}\boldsymbol{i}'^{\boldsymbol{e}}_{qdr} - \omega_r(^{\mathbf{s}}\mathbf{K}^{\mathbf{e}}_{\mathrm{r}})\left[(^{\mathbf{s}}\mathbf{K}^{\mathbf{e}}_{\mathrm{r}})^{-1}\boldsymbol{\lambda}'^{\boldsymbol{e}}_{dqr}\right] + (^{\mathbf{s}}\mathbf{K}^{\mathbf{e}}_{\mathrm{r}})p\left[(^{\mathbf{s}}\mathbf{K}^{\mathbf{e}}_{\mathrm{r}})^{-1}\boldsymbol{\lambda}'^{\boldsymbol{e}}_{qdr}\right] \quad (3.124)$$

The solution of equation (3.124) is given as;

$$V'^e_{qr} = r'_r i'^e_{qr} + (\omega_e - \omega_r)\lambda'^e_{dr} + p\lambda'^e_{qr} \quad (3.125\ (a))$$

$$V'^e_{dr} = r'_r i'^e_{dr} - (\omega_e - \omega_r)\lambda'^e_{qr} + p\lambda'^e_{dr} \quad (3.125(b))$$

Equations (3.125(a) – (b)) give the equivalent rotor voltage equations of the modified SPIM in the synchronous reference frame.

3.10.1.3Transformation of flux linkages

When the Park's transformation equations (2.21), (2.25) (2.26) and (2.27) are applied to equations (3.115(e)-(h)), the following equation results:

$$\begin{bmatrix}\boldsymbol{\lambda}^{\boldsymbol{e}}_{qds}\\ \boldsymbol{\lambda}'^{\boldsymbol{e}}_{qdr}\end{bmatrix} = \begin{bmatrix}(^{\mathbf{s}}\mathbf{K}^{\mathbf{e}}_{\mathbf{s}})\boldsymbol{L}'_{\boldsymbol{s}}(^{\mathbf{s}}\mathbf{K}^{\mathbf{e}}_{\mathbf{s}})^{-1} & (^{\mathbf{s}}\mathbf{K}^{\mathbf{e}}_{\mathbf{s}})\boldsymbol{L}'_{\boldsymbol{sr}}(^{\mathbf{s}}\mathbf{K}^{\mathbf{e}}_{\mathrm{r}})^{-1}\\ (^{\mathbf{s}}\mathbf{K}^{\mathbf{e}}_{\mathrm{r}})(\boldsymbol{L}'_{\boldsymbol{sr}})^{\boldsymbol{T}}(^{\mathbf{s}}\mathbf{K}^{\mathbf{e}}_{\mathbf{s}})^{-1} & (^{\mathbf{s}}\mathbf{K}^{\mathbf{e}}_{\mathrm{r}})\boldsymbol{L}'_{\boldsymbol{r}}(^{\mathbf{s}}\mathbf{K}^{\mathbf{e}}_{\mathrm{r}})^{-1}\end{bmatrix}\begin{bmatrix}\boldsymbol{i}^{\boldsymbol{e}}_{qds}\\ \boldsymbol{i}'^{\boldsymbol{e}}_{qdr}\end{bmatrix} \quad (3.126)$$

The solution of equation (3.126) is given as;

$$\lambda_{qs}^{e} = L_{ls} i_{qs}^{e} + L_{mas}\left(i_{qs}^{e} + i'^{e}{}_{qr}\right) \quad (3.127(a))$$

$$\lambda_{ds}^{e} = L'_{ls} i_{ds}^{e} + L_{mas}\left(i_{ds}^{e} + i'^{e}{}_{dr}\right) \quad (3.127\ (b))$$

$$\lambda_{qr}'^{e} = L'_{lr} i_{qr}'^{e} + L_{mas}(i_{qs}^{e} + i_{qr}'^{e}) \quad (3.127(c))$$

$$\lambda_{dr}'^{e} = L'_{lr} i_{dr}'^{e} + L_{mas}\left(i_{ds}^{e} + i'^{e}{}_{dr}\right) \quad (3.127\ (d))$$

Equations (3.127 (a) – (d)) give the equivalent flux linkage equations of the modified SPIM in the synchronous reference frame.

3.10.1.4 Transformation of torque equation

Equation (3.115 (i)) was transformed to its synchronous reference frame equivalent by first substituting for the rotor currents, i'_{qr} and i'_{dr} using equations (3.115 (f) and (h)). Thereafter, equations (2.25) and (2.27) were applied to it to yield the following:

$$T_e = \frac{P}{2}\frac{L_{mas}}{L'_r}\left(\lambda'^{e}{}_{dr} i^{e}{}_{qs} - \lambda'^{e}{}_{qr} i^{e}{}_{ds}\right) \quad (3.128)$$

Where:

$$L'_r = L'_{lr} + L_{mas} \quad (3.129)$$

Equation (3.128) gives the equivalent torque equation of the modified SPIM in the synchronousreference frame.

3.10.2 Development of the Vector Control Scheme

The development of the vector control scheme for the modified single phase induction motor is presented in this subsection. The indirect rotor flux oriented vector control scheme is selected because the scheme avoids the complicated task of rotor flux measurement and instead allows for a convenient method of estimating the angular position of the rotor flux using the stator currents.

3.10.2.1 Formulation of the rotor flux oriented vector control scheme

The rotor flux oriented vector control scheme is derived from the dynamic equations of the modified single phase induction machine in the synchronously rotating reference frame. The synchronous reference frame model of the modified single phase induction machine was utilized for the purpose of formulating the control scheme. The equations were obtained in section 3.10.1 and are written as follows;

$$V^{e}{}_{qs} = r_s i^{e}{}_{qs} + \omega_e \lambda^{e}{}_{ds} + p\lambda^{e}{}_{qs} \quad (3.130\ (a))$$

$$V^{e}{}_{ds} = r_s i^{e}{}_{ds} - \omega_e \lambda^{e}{}_{qs} + p\lambda^{e}{}_{ds} \quad (3.130\ (b))$$

$$V'^{e}{}_{qr} = r'_r i'^{e}{}_{qr} + (\omega_e - \omega_r)\lambda'^{e}{}_{dr} + p\lambda'^{e}{}_{qr} \quad (3.130\ (c))$$

$$V'^{e}{}_{dr} = r'_r i'^{e}{}_{dr} - (\omega_e - \omega_r)\lambda'^{e}{}_{qr} + p\lambda'^{e}{}_{dr} \quad (3.130\ (d))$$

$$\lambda'^{e}{}_{qs} = L_s i^{e}{}_{qs} + L_{mas} i'^{e}{}_{qr} \quad (3.130\ (e))$$

$$\lambda'^{e}{}_{ds} = L_s i^{e}{}_{ds} + L_{mas} i'^{e}{}_{dr} \quad (3.130\ (f))$$

$$\lambda'^{e}{}_{qr} = L_r i'^{e}{}_{qr} + L_{mas} i^{e}{}_{qs} \quad (3.130\ (g))$$

$$\lambda'^{e}{}_{dr} = L_r i'^{e}{}_{dr} + L_{mas} i^{e}{}_{ds} \quad (3.130\ (h))$$

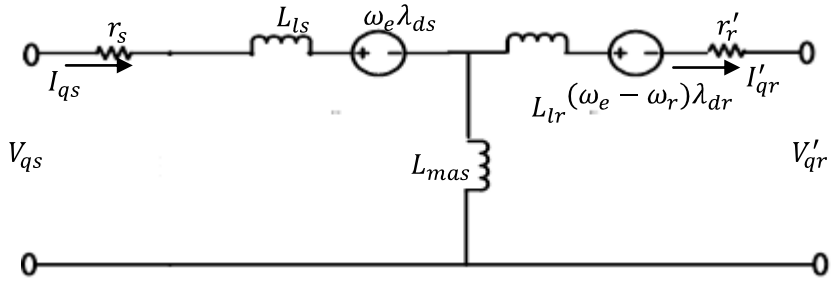
$$T_e = \frac{P}{2}\frac{L_{mas}}{L_r}\left(\lambda'^{e}{}_{dr} i^{e}{}_{qs} - \lambda'^{e}{}_{qr} i^{e}{}_{ds}\right) \quad (3.130\ (i))$$

where:

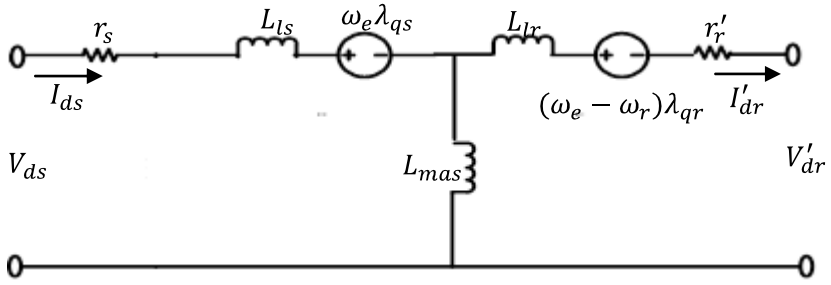
$$L_s = L_{ls} + L_{mas} \quad (3.131)$$

V_{qs}andV_{ds} are the voltages applied to the stator windings in the q – d reference frame. $i_{qs}$and i_{ds} are the q – d axes currents in the stator windings. i'_{qr} and i'_{dr} are respectively the currents in the q – d axis rotor windings. λ_{qs}andλ_{ds} are the flux linkages of the stator windings respectively. λ'_{qr}andλ'_{dr} are the flux linkages of the rotor windings. The superscript *e* indicates that the equations are associated with the synchronously rotating reference frame.

The equivalent circuit of the modified SPIM was derived from equations (3.130(a)-(h)) and is given in Figure 3.24 (a) – (b).



(a) q - axis



(b) d - axis

Figure 3.24: Modified Single Phase Induction Motor q-d axes Equivalent Circuits

With the *d*-axis of the synchronous reference frame aligned with rotor flux, the *q*-axis component of the rotor flux and the rotor flux magnitude are then given as follows:

$$\lambda_{qr}'^{e} = 0 \qquad (3.132\ (a))$$

$$\lambda_{r}'^{e} = \lambda_{dr}'^{e}. \qquad (3.132(b))$$

Applying Equations 3.132 (a)-(b) to rotor voltage equations (3.130 (c)-(d)) gives the following equations:

$$0 = r_r' i_{qr}'^{e} + \omega_{sl}\lambda_{r}'^{e} \qquad (3.133\ (a))$$

$$0 = r_r' i_{dr}'^{e} + p\lambda_{r}'^{e} \qquad (3.133\ (b))$$

Where:

$$\omega_{sl} = \omega_e - \omega_r \quad (3.134)$$

$\omega_{sl}$is defined as the slip frequency. Expressions for rotor currents are obtained from equations(3.130 (g) and (h)) and are given as:

$$i'^{e}_{dr} = \frac{\lambda'^{e}_{dr} - L_{mas} i^{e}_{ds}}{L_r} \quad (3.135\ (a))$$

$$i'^{e}_{qr} = \frac{\lambda'^{e}_{qr} - L_{mas} i^{e}_{qs}}{L_r} \quad (3.135\ (b))$$

With the alignment of the rotor flux, the rotor current equations are modified as follows:

$$i'^{e}_{dr} = \frac{\lambda'^{e}_{r} - L_{mas} i^{e}_{ds}}{L_r} \quad (3.136\ (a))$$

$$i'^{e}_{qr} = \frac{-L_{mas} i^{e}_{qs}}{L_r} \quad (3.136\ (b))$$

Slip frequency may be written from equations (3.133 (a)) and (3.136 (b))as:

$$\omega_{sl} = \frac{r'_r L_{mas} i^{e}_{qs}}{L'_r \lambda'^{e}_{r}} \quad (3.137)$$

From equation (3.133 (b)) and (3.136 (a)), the following is obtained;

$$p\lambda'^{e}_{r} + \frac{r'_r}{L'_r} \lambda'^{e}_{r} = \frac{r'_r L_{mas} i^{e}_{ds}}{L'_r} \quad (3.138)$$

The expression of torque from equation (3.130(i)) after applying equations (3.132 (a) – (b)).is reduced to;

$$T_e = \frac{P}{2} \frac{L_{mas}}{L_r} \left(\lambda'^{e}_{r} i^{e}_{qs} \right) \quad (3.139)$$

Equation (3.139) illustrates that torque produced in the machine is a linear function of the q-axis component of the stator current i^{e}_{qs}. The torque and flux are controlled by i^{e}_{qs} and i^{e}_{ds} respectively. Equations (3.138) and (3.139) show the relationships between these quantities. The two phase inverter can only synthesize the stator voltages and not the stator currents and therefore a relationship that relates stator voltages V^{e}_{qs} and V^{e}_{qs} to currents i^{e}_{qs} and i^{e}_{ds} and the rotor

flux was obtained by applying equations (3.130 (e), (f)) and (3.136 (a) - (b)) to (3.130 (a) – (b)). The relationship is given as:

$$(r_s + pL_x)i_{qs}^e = V_{qs}^e - \omega_e(L_x i_{ds}^e + \frac{L_{mas}}{{L'_r}^2}\lambda'^e_r) \quad (3.140\text{ (a)})$$

$$(r_s + pL_x)i_{ds}^e = V_{ds}^e - \frac{L_{mas}}{L'_r}p\lambda'^e{}_r + \omega_e L_x i_{qs}^e \quad (3.140\text{ (b)})$$

Where:

$$L_x = L_s - \frac{{L_{mas}}^2}{L'_r} \quad (3.141)$$

Equations (3.140 (a) and (b)) represent a non-linear system for which V_{qs}^e and V_{ds}^e are inputs and i_{qs}^e and i_{ds}^e are outputs. The dynamics of i_{qs}^e and $i_{ds}^e$are de-coupled by defining two new control inputs σ_{qs} and σ_{ds}such that:

$$\sigma_{qs} = V_{qs}^e - \omega_e(L_x i_{ds}^e + \frac{L_{mas}}{{L'_r}^2}\lambda'^e_r) \quad (3.142)$$

$$\sigma_{ds} = V_{ds}^e - \frac{L_{mas}}{L'_r}p\lambda'^e_r + \omega_e L_x i_{qs}^e \quad (3.143)$$

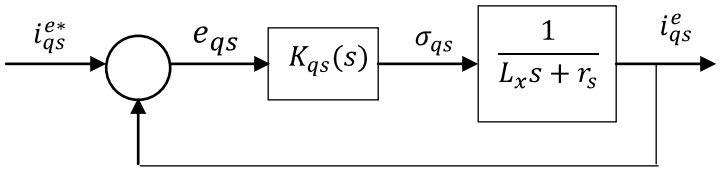
Where σ_{qs} and σ_{ds} are defined as;

$$\sigma_{qs} = (r_s + pL_x)i_{qs}^e \quad (3.144)$$

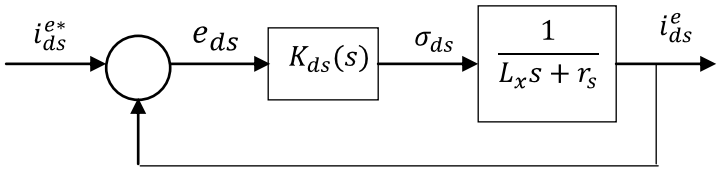
$$\sigma_{ds} = (r_s + pL_x)i_{ds}^e \quad (3.145)$$

3.10.2.2 Controller design

Equation (3.144) represents a subsystem that controls i_{qs}^e by σ_{qs} while equation (3.145) gives a subsystem that controls $i_{ds}^e$by σ_{ds}. σ_{qs} andσ_{ds} are obtained in simulation from two PI controllers, $K_{qs}(s)$ and $K_{ds}(s)$ as illustrated in Figure 3.25 (a) - (b).



(a) q-axis current control



(b) d-axis current control

Figure 3.25: Control Block Diagram for Stator Current Control

As seen in Figure 3.25, $K_{qs}(s)$ processes the error e_{qs} between $i_{qs}^{e}$and its reference and provides σ_{qs} while $K_{ds}(s)$ processes the error e_{ds} between $i_{ds}^{e}$and its reference and provides σ_{ds}. The PI controller is chosen because it guarantees that the actual currents track their references with zero steady state error. Based on the block diagram of Figure 3.25, the control system loop gain, G_{OLi} is given as;

$$G_{OLi} = \left(\frac{k_p s + k_i}{s}\right)\left(\frac{1}{L_x s + r_s}\right) \tag{3.146}$$

Equation (3.146) simplifies to;

$$G_{OLi} = \frac{k_p}{L_x s}\left(\frac{s + \frac{k_i}{k_p}}{s + \frac{r_s}{L_x}}\right) \tag{3.147}$$

Using the pole cancellation method to determine the controller gains, the following equations are deduced from equation (3.147):

$$\frac{k_i}{k_p} = \frac{r_s}{L_x} \tag{3.148}$$

$$\frac{k_p}{L_x} = \frac{1}{\tau_i} \tag{3.149}$$

Where τ_i is the desired time constant of the closed loop system. The closed loop transfer functions of the systems in Figure 3.25 (a) and (b) are therefore given as:

$$\frac{i_{qs}^e}{i_{qs}^{e*}} = \frac{1}{\tau_i s+1} \tag{3.150}$$

$$\frac{i_{ds}^e}{i_{ds}^{e*}} = \frac{1}{\tau_i s+1} \tag{3.151}$$

i_{qs}^{e*}andi_{ds}^{e*}arethe reference values of the q and d-axis stator currents respectively. The time constant is chosen such that the bandwidth of the closed loop control system is 10 times smaller than the switching frequency of the inverter. This choice allows for a fast current control response. The control block diagram of the flux control system is obtained from equation (3.138) and given in Figure 3.26.

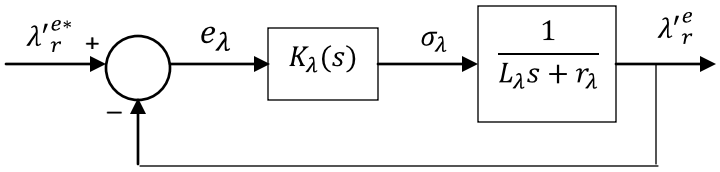


Figure 3.26: Control Block Diagram for Rotor Flux Control

Similar to the current control, the flux controller gains are obtained as;

$$\frac{k_i}{k_p} = \frac{r_\lambda}{L_\lambda} \tag{3.152}$$

$$\frac{k_p}{L_\lambda} = \frac{1}{\tau_i} \tag{3.153}$$

where:

$$L_\lambda = \frac{L_r}{L_{ms} r_r'} \tag{3.154}$$

$$r_\lambda = \frac{1}{L_{ms}} \tag{3.155}$$

The control block diagram of the speed control system is given in Figure 3.27 and it is based on the machine dynamics given equation (2.20).

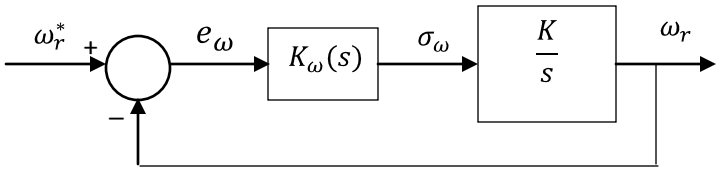


Figure 3.27: Control Block Diagram for Speed Control

The open loop gain of the speed control system is obtained from Figure 3.27 and is given as;

$$G_{OL\omega} = \frac{k_\omega K}{s} \tag{3.156}$$

$$K = \frac{P}{2J} \tag{3.157}$$

$K_\omega(s)$ is a PI controller and hence equation (3.156) is expanded to give:

$$G_{OL\omega} = \frac{k_{i\omega} K\left(1+\frac{k_{p\omega} s}{k_{i\omega}}\right)}{s^2} \tag{3.158}$$

The determination of the controller gains is done by noting that the magnitude of the open loop gain is unity at the cross-over frequency ω_c. Therefore,

$$\left|\frac{k_{i\omega} K\left(1+\frac{k_{p\omega} s}{k_{i\omega}}\right)}{s^2}\right| s = j\omega_c \quad = 1 \tag{3.159}$$

and the phase angle is given by;

$$\angle\left(\frac{k_{i\omega} K\left(1+\frac{k_{p\omega} s}{k_{i\omega}}\right)}{s^2}\right) = -180^0 + \varphi_{PM} \tag{3.160}$$

The time constant of the speed control loop system is chosen to be an order of magnitude less than the time constant of the *q*-axis current control loop because the speed control loop should be

slower than the q-axis current control loop. $\varphi_{PM}$is the phase margin of the speed control system and is chosen to be at least 60^0 to guarantee the stability of the system.

The supply voltages in the synchronous reference frame are then calculated based on equations (3.142) and (3.143) and are given as:

$$V_{qs}^{e} = \sigma_{qs} + \omega_e(L_x i_{qs}^{e} + \frac{L_{mas}}{L'^{2}_{r}}\lambda'^{e}_{r}) \tag{3.161}$$

$$V_{ds}^{e} = \sigma_{ds} + \frac{L_{mas}}{L'_{r}} p\lambda'^{e}_{r} - \omega_e L_x i_{qs}^{e} \tag{3.162}$$

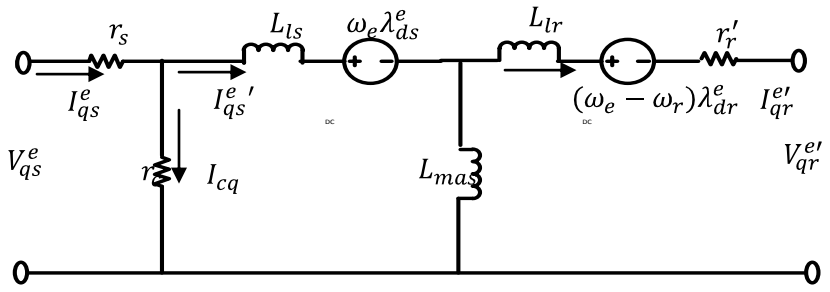
Equations (3.161) and (3.162) are DC quantities which when transformed to the stationary reference frame yields the fundamental sinusoidal voltages of the stator windings. The control or modulating signals are obtained by scaling down this fundamental voltage component. The control signals were supplied to the PWM inverter to synthesize the stator voltages required to generate the desired rotor flux and torque in the machine. The control objective is to regulate the rotor flux and the torque to their commanded values. Since the required stator voltages are not directly related to flux and speed or torque, the strategy adopted is to regulate the rotor flux and rotor speed or torque through some controllers and the output of the controllers now give the reference values for the q and d axes stator currents. The actual q and d axes stator currents are then regulated to their references. The values of K_p and K_i for the q and d-axis currents, flux and speed controllers were calculated using equations (3.148)-(3.149), (3.152)-(3.153) and (3.159)-(3.160) respectively and then fine-tuned using the control systems tool box in MATLAB to give 1000 and 0.2 respectively for the current controllers, 100 and 50 respectively for the flux controller and finally 100 and 1000 for the speed controller.

To improve efficiency of operation, the rotor flux was regulatedin the desired operating range. By regulating the flux in the machine, drive efficiency is increased and the machine operates in an energy-efficient manner. The maximization of efficiency by regulating flux in the machine is

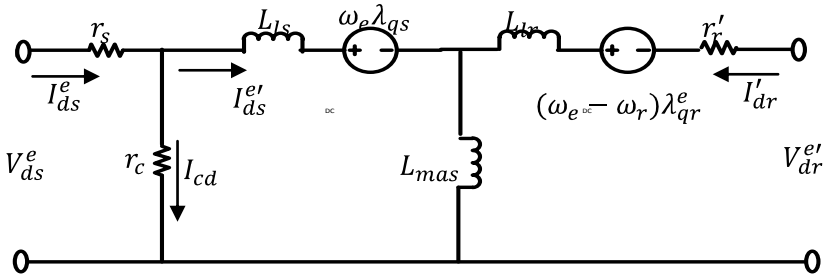
the objective of the proposed efficiency optimizing technique which has been integrated to the vector control strategy described. The development of the efficiency optimizing technique is discussed in the next section.

3.11 DEVELOPMENT OF THE PROPOSED EFFICIENCY OPTIMIZING SCHEME

The objective of the efficiency optimizing technique is to regulate the flux magnitude such that minimum losses occur while maintaining a desired torque. Essentially, the air gap flux is variable when the load is changing as opposed to the case of the CRSPIM in which the flux is constant regardless of changes in load. The modified single phase induction machine equivalent circuit is now redrawn as given in Figures 3.28 (a) and (b) to account for the core loss resistance, r_c. As a result, the voltage, flux linkage and torque equations of the machine are reformulated to account for the effect of the core loss resistance.



(a) q - axis



(b) d - axis

Figure 3.28: Modified Single Phase Induction Motor q-d Axes Equivalent Circuits with Core Loss Resistance

The following voltage, flux linkage and current equations are obtained from the equivalent circuits of Figures 3.28 (a) and (b).

a) Voltage Equations

$$V_{qs}^{e} = r_s i_{qs}^{e\prime} + \mathrm{k}\omega_e \lambda_{ds}^{e} + kp\lambda_{qs}^{e} \tag{3.163}$$

$$V_{ds}^{e} = r_s i_{ds}^{e\prime} - \mathrm{k}\omega_e \lambda_{qs}^{e} + kp\lambda_{ds}^{e} \tag{3.164}$$

$$0 = r_r{}' i_{qr}^{e\prime} + (\omega_e - \omega_r)\lambda_{dr}^{e\prime} + p\lambda_{qr}^{e\prime} \tag{3.165}$$

$$0 = r_r{}' i_{dr}^{e\prime} - (\omega_e - \omega_r)\lambda_{qr}^{e\prime} + p\lambda_{dr}^{e\prime} \tag{3.166}$$

b) Current Equations

The currents$i_{cq}$and i_{cd} flowing through the core loss branches are obtained from the equivalent circuits are given as;

$$i_{cq} = i_{qs}^{e} - i_{qs}^{e\prime} \tag{3.167}$$

$$i_{cd} = i_{ds}^{e} - i_{ds}^{e\prime} \tag{3.168}$$

$$i_{cq} = \frac{V_{qs}^{e}}{kr_c} \tag{3.169}$$

$$i_{cd} = \frac{V_{ds}^{e}}{kr_c} \tag{3.170}$$

$$k = 1 + \frac{r_s}{r_c} \tag{3.171}$$

Currents $i_{qs}^{e\prime}$ and $i_{ds}^{e\prime}$ are the torque currents responsible for producing electromagnetic torque in the machine as seen from the equivalent circuit of Figure 3.28 (a) and (b).

3.11.1 Voltage Equations in Steady State

Voltage equations in steady state are obtained by setting operator *p* to zero in equations (3.163) - (3.166). The steady state voltage equations are therefore given in matrix form as;

$$\begin{bmatrix} V_{qs} \\ V_{ds} \\ 0 \\ 0 \end{bmatrix} = \begin{bmatrix} r_s & \mathrm{k}\omega_e L_s & 0 & \mathrm{k}\omega_e L_m \\ -\mathrm{k}\omega_e L_s & r_s & -\mathrm{k}\omega_e L_m & 0 \\ 0 & \omega_{sl} L_m & r'_r & \omega_{sl} L_r \\ -\omega_{sl} L_m & 0 & -\omega_{sl} L_r & r'_r \end{bmatrix} \begin{bmatrix} i'_{qs} \\ i'_{ds} \\ i'_{qr} \\ i'_{dr} \end{bmatrix} \tag{3.172}$$

When equations (3.132 (a) – (b))are applied to equation (3.172), the resulting matrix equation is given as:

$$\begin{bmatrix} V_{qs} \\ V_{ds} \\ 0 \\ 0 \end{bmatrix} = \begin{bmatrix} r_s & \mathrm{k}\omega_e L_s & 0 & \mathrm{k}\omega_e L_m \\ -\mathrm{k}\omega_e L_s & r_s & -\mathrm{k}\omega_e L_m & 0 \\ 0 & \omega_{sl} L_m & r'_r & \omega_{sl} L_r \\ 0 & 0 & 0 & r'_r \end{bmatrix} \begin{bmatrix} i'_{qs} \\ i'_{ds} \\ i'_{qr} \\ i'_{dr} \end{bmatrix} \tag{3.173}$$

Rotor currents i'_{qr} and i'_{dr} are obtained from equation (3.173) as;

$$i'_{qr} = \frac{-\omega_{sl}\lambda'_r}{r'_r} \tag{3.174}$$

$$i'_{dr} = 0 \tag{3.175}$$

A relationship between core resistance branch currentsi_{cq}, i_{cd} and torque currents are obtained from equations (3.167) - (3.171) and given as:

$$\begin{bmatrix} i_{cq} \\ i_{ds} \end{bmatrix} = \begin{bmatrix} \frac{r_s}{kr_c} & \frac{\omega_e L_s}{r_c} \\ -\frac{\omega_e L_x}{r_c} & \frac{r_s}{kr_c} \end{bmatrix} \begin{bmatrix} i'_{qs} \\ i'_{ds} \end{bmatrix} \tag{3.176}$$

Relationships between the applied stator currents and torque currents are obtained from equations (3.167), (3.168) and (3.176) and given as:

$$\begin{bmatrix} i_{qs} \\ i_{ds} \end{bmatrix} = \begin{bmatrix} (1 + \frac{r_s}{kr_c}) & \frac{\omega_e L_s}{r_c} \\ -\frac{\omega_e L_x}{r_c} & (1 + \frac{r_s}{kr_c}) \end{bmatrix} \begin{bmatrix} i'_{qs} \\ i'_{ds} \end{bmatrix} \tag{3.177}$$

$$\begin{bmatrix} i'_{qs} \\ i'_{ds} \end{bmatrix} = \frac{1}{\left[1+\frac{r_s}{kr_c}\right]^2 + \frac{\omega_e^2 L_x L_s}{r_c^2}} \begin{bmatrix} (1 + \frac{r_s}{kr_c}) & -\frac{\omega_e L_s}{r_c} \\ \frac{\omega_e L_x}{r_c} & (1 + \frac{r_s}{kr_c}) \end{bmatrix} \begin{bmatrix} i_{qs} \\ i_{ds} \end{bmatrix} \tag{3.178}$$

3.11.2 Electrical Power Loss

The electrical power loss is the sum of the copper and core losses in the machine and is obtained from the equivalent circuits as:

$$P_L = r_s\left(i_{qs}^2 + i_{ds}^2\right) + r'_r\left(i_{qr}^2 + i_{dr}^2\right) + r_c(i_{cq}^2 + i_{cd}^2) \tag{3.179}$$

When equations (3.130 (g)-(h)), (3.176), (3.177), (3.132(b)) and (3.139) are applied to (3.179), the electrical power loss in the modified single phase induction machine is obtained as;

$$P_L = \frac{L_m^2 T_e^2 + \lambda'^2_{rr} k_t^2}{L_m^2 k_t^2 \lambda'_{rr}} A + \lambda'_{rr} B + C \tag{3.180}$$

Where:

$$A = r_s + \frac{L_m^2 r_r}{L_r^2} + \frac{r^2 + k^2 \omega_e^2 L_x^2}{r_c k} + \frac{2 r_s^2}{k r_c} \tag{3.181}$$

$$B = \frac{(r_r + \omega_r^2 L_r^2) k L_m^2}{r_c L_r^4} - \frac{r_r}{L_r^2} + \frac{2}{r_c L_r} (k L_x L_r \omega_e \omega_r - r_r r) \tag{3.182}$$

$$C = \frac{2 L_m T_e}{k_t r_c L_r} [(\omega_r L_r r + k \omega_e r_r L_x) + r_s \omega_e)] \tag{3.183}$$

$$\lambda'_{rr} = \lambda'^2_r \tag{3.184}$$

$$k_t = \frac{P}{2} \frac{L_{ms}}{L_r} \tag{3.185}$$

The criterion for minimum loss is obtained by differentiating equation (3.180) with respect to the square of the flux and is given as;

$$\frac{dP_L}{d\lambda'_{rr}} = \lambda'^2_{rr} k_t^2 A + L_m^2 k_t^2 \lambda'^2_{rr} B - L_m^2 T_e^2 A = 0 \tag{3.186}$$

Equation (3.186) is solved to obtain the optimum value of rotor flux for minimum loss and hence maximum efficiency. The optimum flux is obtained and given as:

$$\lambda'_r = \sqrt{\frac{T_e L_m}{k_t}} \sqrt[4]{\frac{A}{A + \left(\frac{L_m}{k_t}\right)^2 B}} \tag{3.187}$$

Equation (3.187) gives the value of the optimum flux in the machine for a given load torque and speed. The equation suggests that it is possible to minimize total losses in the machine and thereby maximize efficiency at a given speed and for a given load torque within the carrying capacity of the machine.

Equation (3.180) was used to examine the variation of rotor flux with electrical loss for different load torques at rated speed for the modified SPIM. The variation of flux with efficiency of

machine for the same load torques at rated speed was also examined using equation (3.180) and the following equation:

$$\text{Efficiency} = \frac{\text{Power output}}{\text{Power output+electrical power loss}} \tag{3.188}$$

Equation 3.188) gives the efficiency as a function of electrical power loss in the machine.

Figure 3.29 shows the block diagram of the efficiency-optimizing vector controlled drive system for the modified single phase induction machine. For the purpose of analysis, the DC side of the inverter is assumed to be supplied from a rectified AC voltage source. The AC side of the inverter is interfaced with the stator terminals of the modified SPIM. The inverter supplies orthogonal voltages and currents to the machine and controls the voltage such that the flux is regulated at its optimum value for each load torque. The voltage control in turn permits control of the machine power. The torque command is the output of the speed control loop. When the machine drive is in operation, flux is produced in the machine. The flux is regulated to its optimum value by regulating the *d*-axis stator current. This regulation ensures linear control of torque by the *q*-axis stator current. A flux model receives stator currents i_{qs}^{e}, i_{ds}^{e} and speed ω_r and delivers the flux λ_r', supply frequency ω_e and the corresponding angular position θ_e, as shown in Figure 3.29, to ensure proper vector alignment and transformation of stationary reference frame variables to synchronously rotating reference frame variables thereby keeping the integrity of the control system. $\lambda_r'$is used as a feedback signal for flux regulation. $\theta_e$is used in the transformation block while $\omega_e$is utilized in the decoupling block to decouple the dynamics of i_{qs}^{e} and i_{ds}^{e}.The flow chart for the realization of the scheme is shown in Figure 3.30. Finally, the Simulink implementation of the proposed drive method is shown in Figure 3.31.Simulation results of the proposed drive scheme is provided in section 4.7.

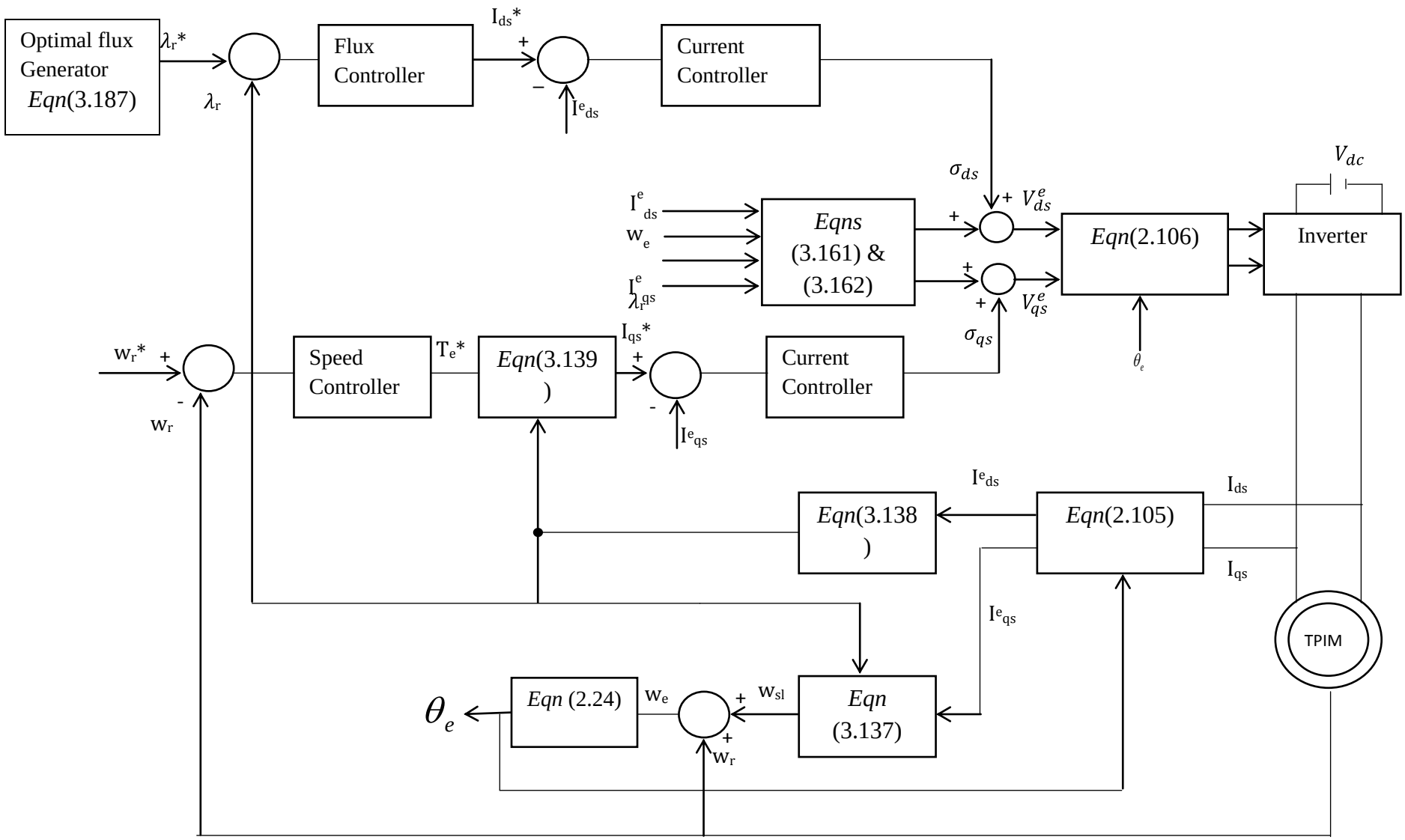


Figure 3.29: Block Diagram of Vector Control Strategy with Efficiency-Optimizing Function

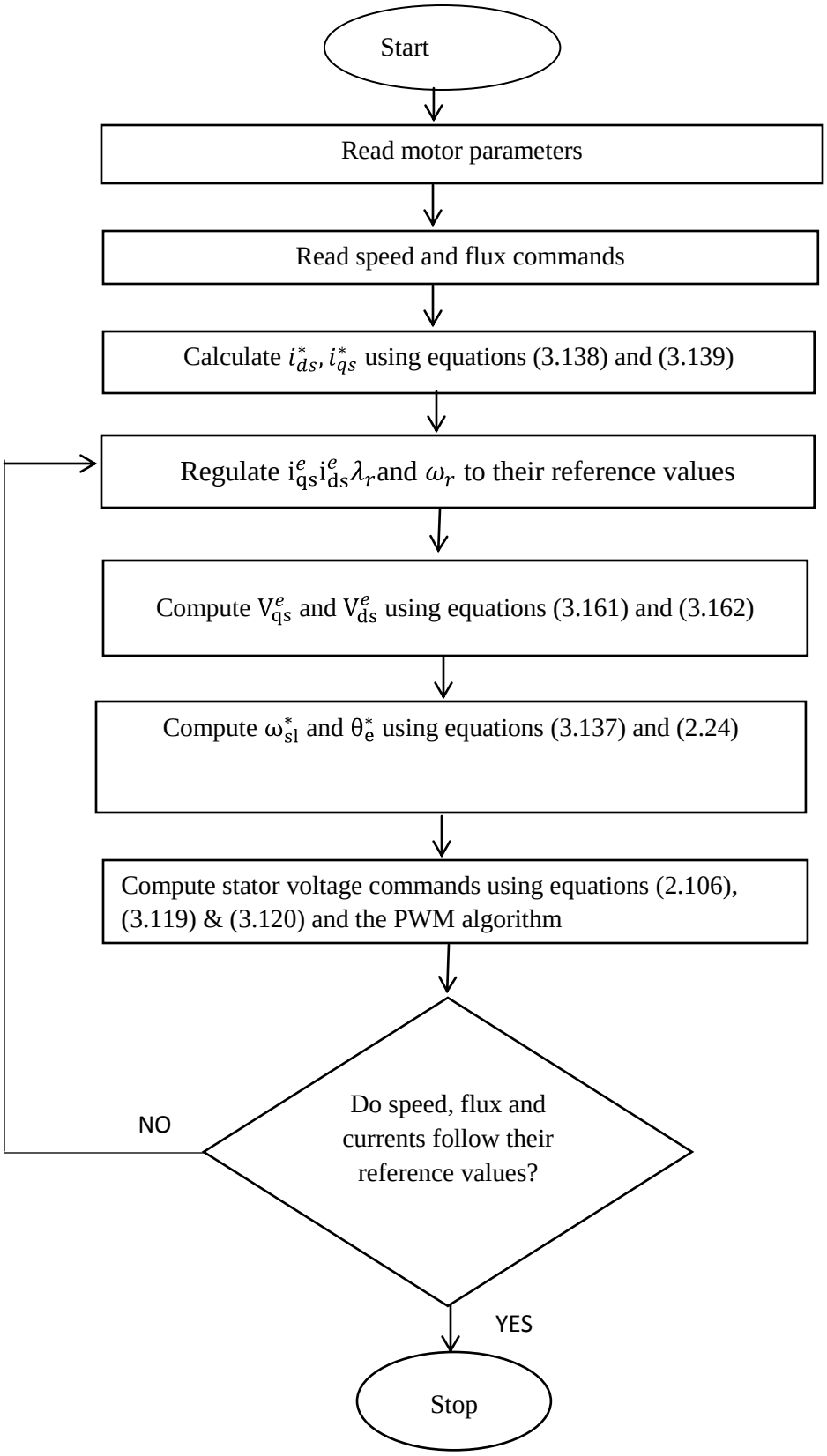


Figure 3.30: Flow Chart for the Indirect Vector-Controlled Induction Motor

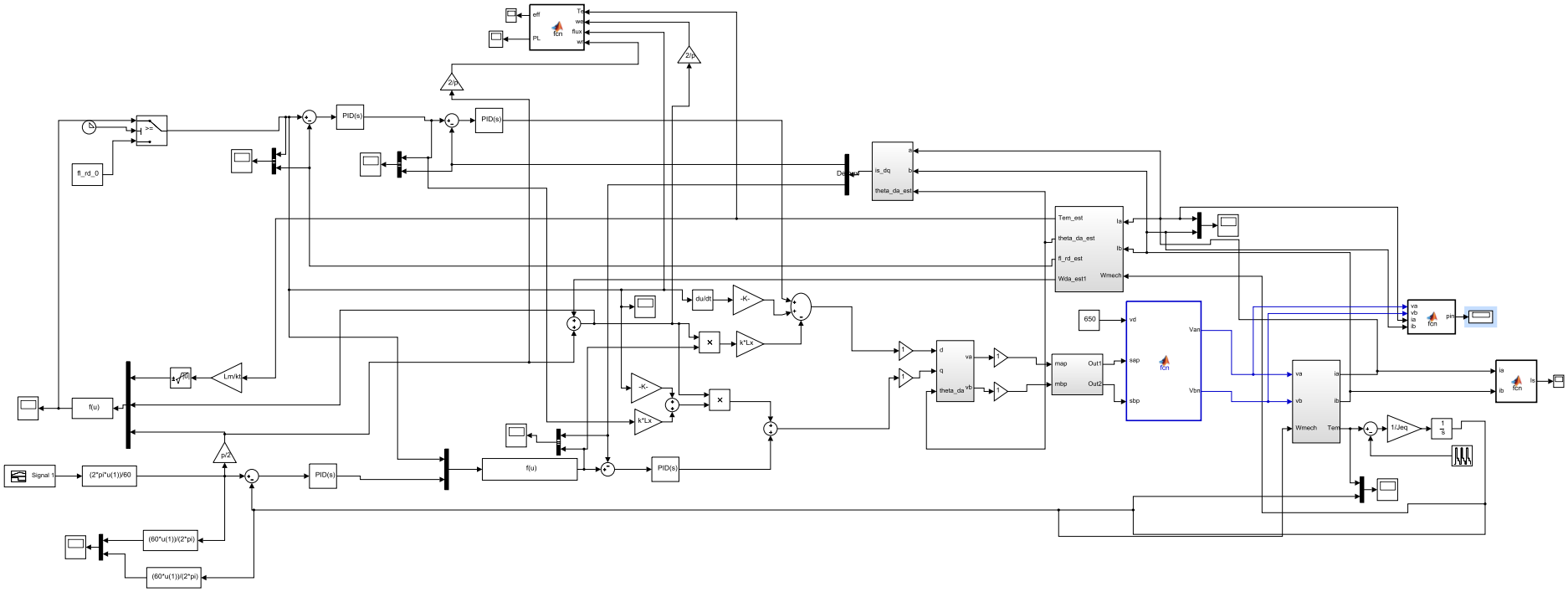


Figure 3.31: Simulink Implementation of the Efficiency-Optimizing Vector- Controlled Modified SPIM

3.12 MODIFIED SPIM WINDING LAYOUT

It is proposed for the modified SPIM to have a two phase, double layer, fractional pitch integral slot winding instead of the concentric winding of the existing CRSPIM. This is because the two phase, double layer, fractional pitch integral slot winding allows two identical windings to be equally distributed in stator slots thereby forming two balanced windings. This type of winding distribution reduces the copper requirement of the coils that make up the winding and it also reduces the harmonics in the *e.m.f* and *m.m.f* waveforms of the phases. Coil group connections in the two phase winding are like the group connections in the concentric winding. The development of the winding layout of the two phase, double layer, fractional pitch integral slot winding for the modified SPIM having a 4 pole and 32 slots as the original machine is presented in the next section.

3.12.1 Development of Modified SPIM Winding Layout Design

The Modified SPIM is an existing SPIM in which the auxiliary winding is removed and replaced with a new winding whose characteristics are identical to those of the main winding. In addition, the concentric winding layout of the existing machine is changed for a distributed winding, specifically a double layer, fractional pitch integral slot winding in this work. The design therefore, focuses on a new winding layout for the existing SPIM. It does not focus on computing the number of turns, winding resistance, leakage inductance and size of the new winding. This is because these parameters are known ab initio from the parameters of the existing main winding. For the purpose of this research, the values of the parameters of the new winding have been obtained directly from the main winding data of Table A.2. In this work, the main winding of the existing SPIM is referred to as Phase *A* winding while the new winding is

referred to as Phase *B* winding. The design of the winding layout is provided in the following section.

3.12.1.1 Design of modified SPIM winding layout

The modified SPIM winding layout is a double layer winding in which the number of coils is equal to the number of slots. The number and size of coils of the Phase A winding is the same as those for the Phase B winding. The number of stator slots and the number of poles are obtained from the architecture of the existing machine. The steps followed in the development of the winding layout are outlined below.

Step 1: Assign coils to Phase A and Phase B

Step2: Determine coil connections per phase

Step 3: Establish the direction of current in coil sides

The assignment of coils to Phases A and B is described in the following section.

3.12.1.2 Assignment of coils to phases A and B

Assigning coils to phases A and B is carried out through the steps outlinedas follows;

a) Find the number of slots per pole per phase using equation (2.126)
b) Equate the number of slots per pole per phase to the number of coils per group
c) Compute the number of coils per phase using equation (2.127)
d) Compute the number of groups per phase using equation (2.128)
e) Compute the slot angular pitchusing equation (2.129)
f) Select slot 1 as the beginning of Phase A winding
g) Compute the slot number for the beginning of Phase B winding.
h) Compute pole pitch using equation (2.130)
i) Select coil pitch

j) Compute coil span using equation (2.131)

k) Compute phase spread using equation (2.132)

l) Develop the winding table, clock diagram and the actual winding layout.

CHAPTER FOUR

RESULTS AND DISCUSSION

4.1 DYNAMIC AND STEADY STATE SIMULATION OF THE CRSPIM

Simulation results of the dynamic and steady state behavior of the CRSPIM is provided in this section. The results illustrates the voltages, currents, speed, electromagnetic torque and efficiency in the motor.

4.1.1 Simulation Results of the Dynamic Behavior of the CRSPIM

Simulation results of the dynamic behavior of the CRSPIM is provided in this section. The simulation results of the dynamic behavior of the CRSPIM are givenin Figure 4.1 and Figures 4.2 – 4.3. Figure 4.1 compares favorably well with simulations results in Krause *et al*, (2002) while Figures 4.2 – 4.3 compare favorable well with simulation results in Ong, (1998).

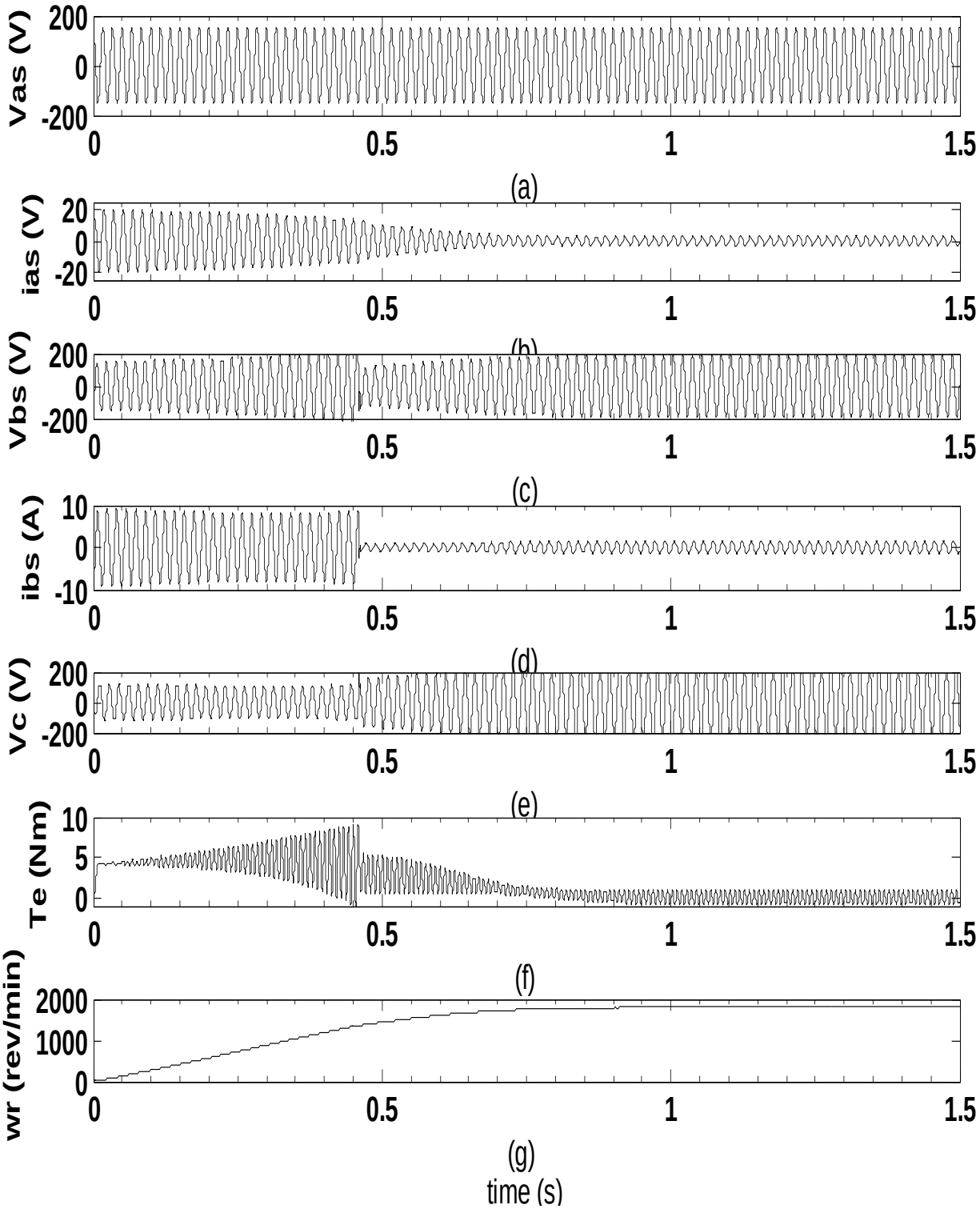


Figure 4.1: Machine Variables of the CRSPIM under No-Load

The voltages V_{as} and V_{bs} across the main and auxiliary windings respectively are shown in Figure 4.1 (a) and (c).They are sinusoidal functions of time. The currentsi_{as} and i_{bs}flowingin the main and auxiliary windings are shown in Figure 4.1 (b) and (d)respectively.They are sinusoidal functions of time as well. Figure 4.1 (e)shows the voltage across the run capacitor. It can be observed that the magnitude of the voltage starts to increase from the time the centrifugal switch is opened and reaches a peak value of about 200V.Before the centrifugal switch is opened, the voltage is lower because the effective series capacitance in the auxiliary winding is the sum of the capacitance of the start and run capacitors and the combined capacitive impedance is low. When the switch opens, the start capacitor is disconnected from the auxiliary winding circuit. The instantaneous value of the electromagnetic torque in the machine is shown in Figures 4.1 (f) when the machine is not loaded and Figure 4.2 (d) when the machine is loaded. The torque is seen to have a starting torque value of approximately 4Nm. There is a high amount of torque pulsations during the starting time between 0 and 0.46s while the centrifugal switch is still closed. After the switch is opened, the pulsations reduce considerably but are still verysignificant after the motor attains steady state. The torque in the machine is seen to rise when load is applied to the machine. Step inputs of 1Nm and0.5Nm were applied at 1.5s and 1.75 s respectively of simulation time to simulate load conditions. A step input of 1Nmwas again applied at 2 sand the load was removed at 2.25 s as shown in in Figure 4.2 (c). Figures 4.1 (g) and 4.3 (a) show the start-up speed characteristics of the machine. The motor speed can be seen to increase from zero to 1800 rev/minon no- load in Figure 4.1 (g). The corresponding $q - d$ reference frame variables V_{qs} and V_{ds} are shown in Figure 4.2 (a) and (b) respectively.

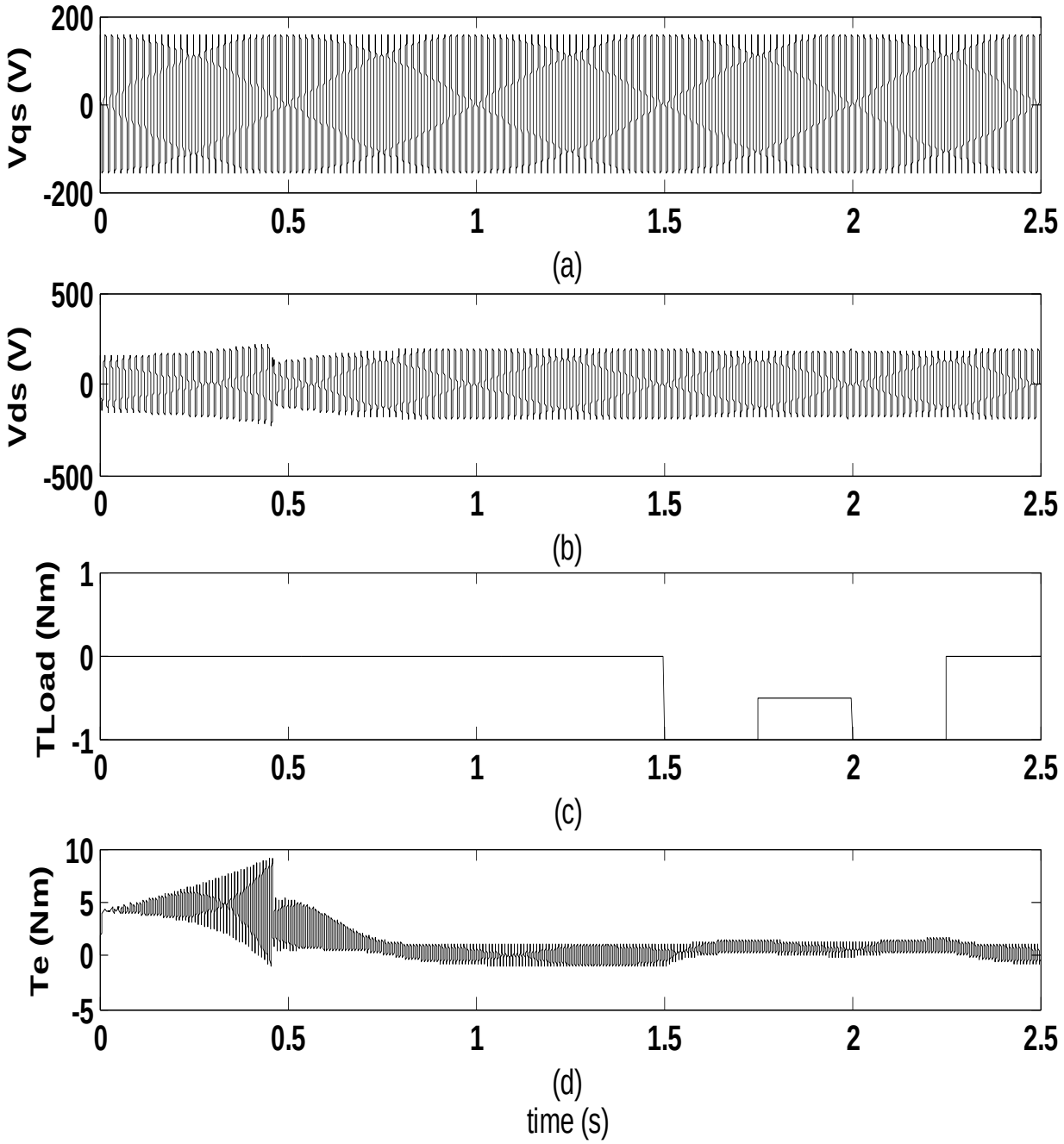


Figure 4.2: Starting Characteristics and Load Response of the CRSPIM showing Vqs, Vds, TLoad and Te.

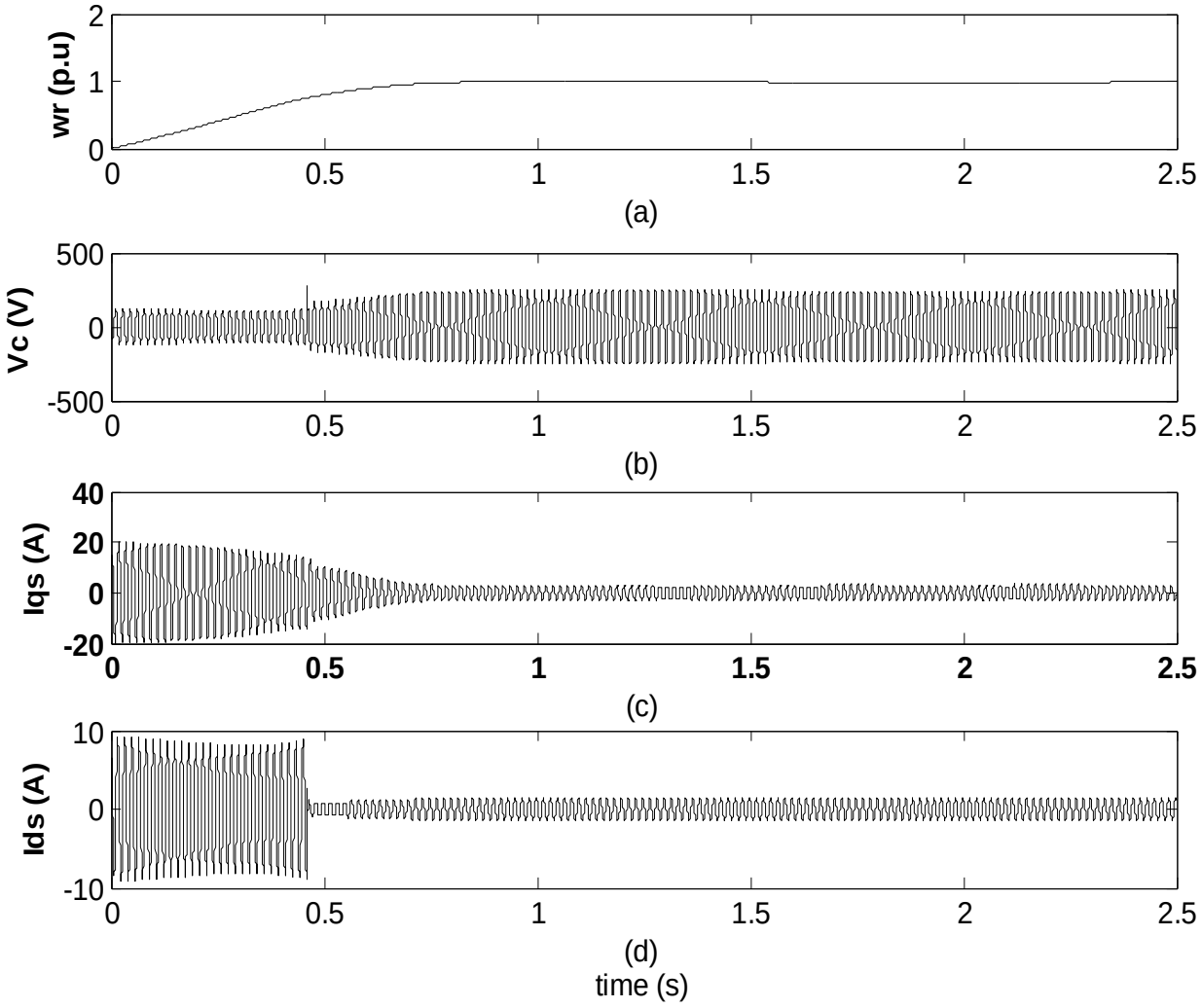


Figure 4.3: Starting Characteristics and Load Response of the CRSPIM showing ωr, Vc, Iqs and Ids.

The corresponding $q - d$ reference frame variables I_{qs} and I_{ds} are shown in Figure 4.3 (c) and (d) respectively. It can be observed in Figure 4.3 (c) and (d) that the value of the currents is high between 0 and 0.46 s before the centrifugal switch opens. This situation causes high copper losses in the windings thereby decreasing efficiency at low speeds. Motor speed can be seen to increase from zero to 1p.uon load in Figure 4.3 (a).The speed is seen to drop with load and then rise again when the load is removed. The motor is seen to reach steady state value after about 1 s.

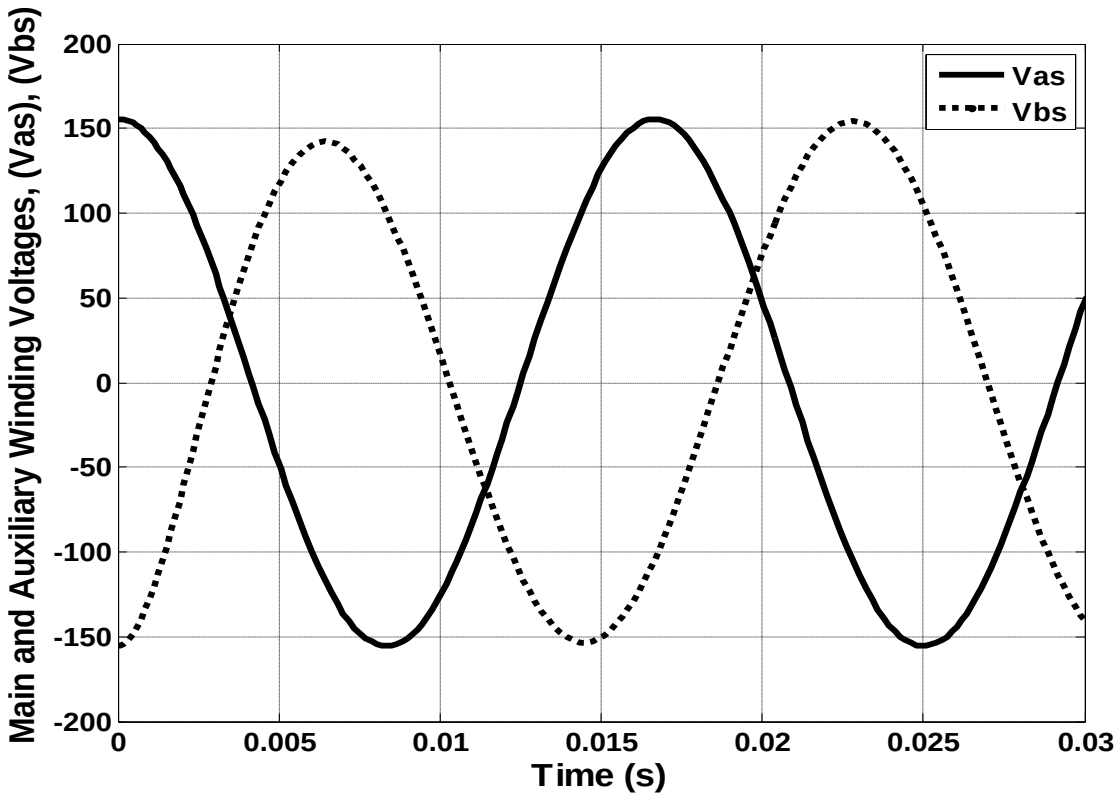


Figure 4.4: Waveform of Voltages across the Main and Auxiliary Windings in about 2 Periods

Figures 4.1 (a) and (c) are reproduced for time values of 0 to 0.03 s in Figure 4.4 where the two voltages have been plotted on the same axis. It can be observed that the voltages across the two windings are unequal in magnitude and the phase angle between them is not 90^0. Figures 4.1 (b) and (d) are reproduced for time values of 0 to 0.03 s in Figure 4.5 where the two current signals have been plotted on the same axis. It can be observed that the currentsin the two windings are unequal in magnitude and the phase angle between them is not 90^0 as well.

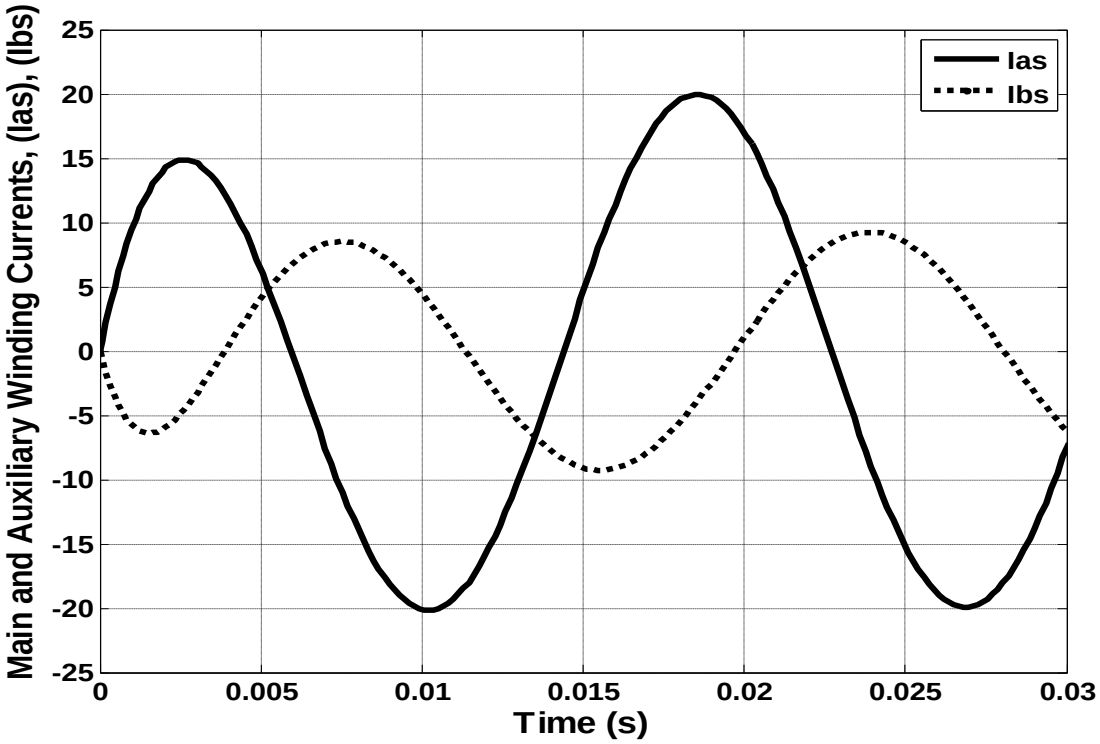


Figure 4.5: Waveform of Currents in the Main and Auxiliary Windings of the Stator in about 2 Periods

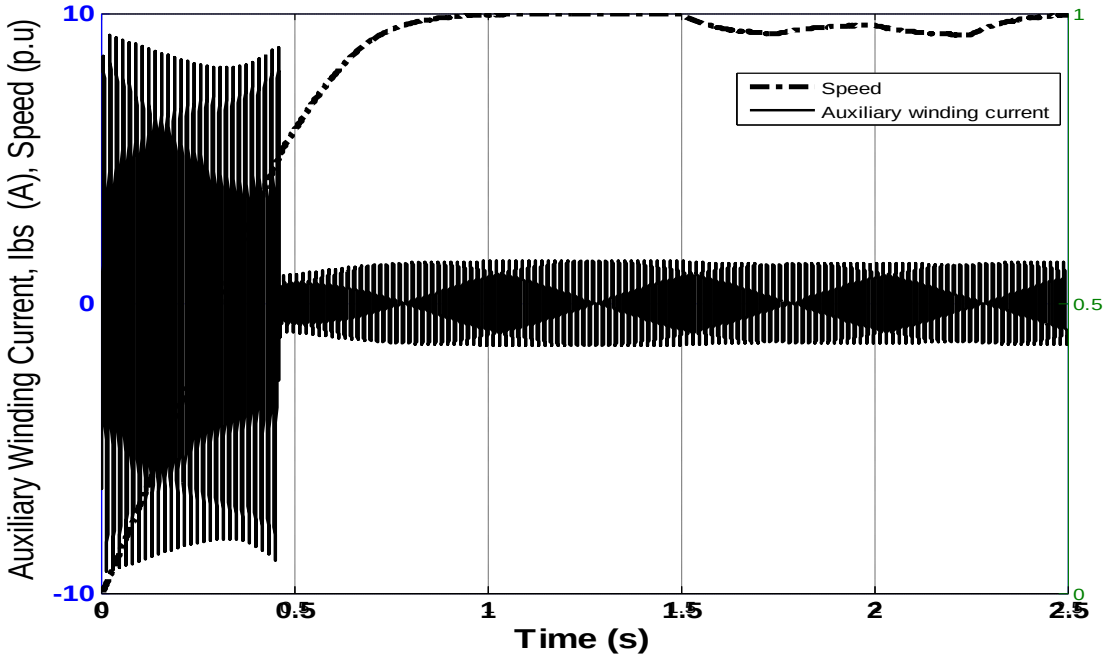


Figure 4.6: Rotor Speed Super-Imposed on Current Flowing in the Auxiliary Winding

The effect of the opening of the centrifugal switch can be observed in Figure 4.6. The currentflowing in the auxiliary winding is seen to drop after the switch is opened at 0.46 s when the motor speed has attained a value of 75% of synchronous speed.

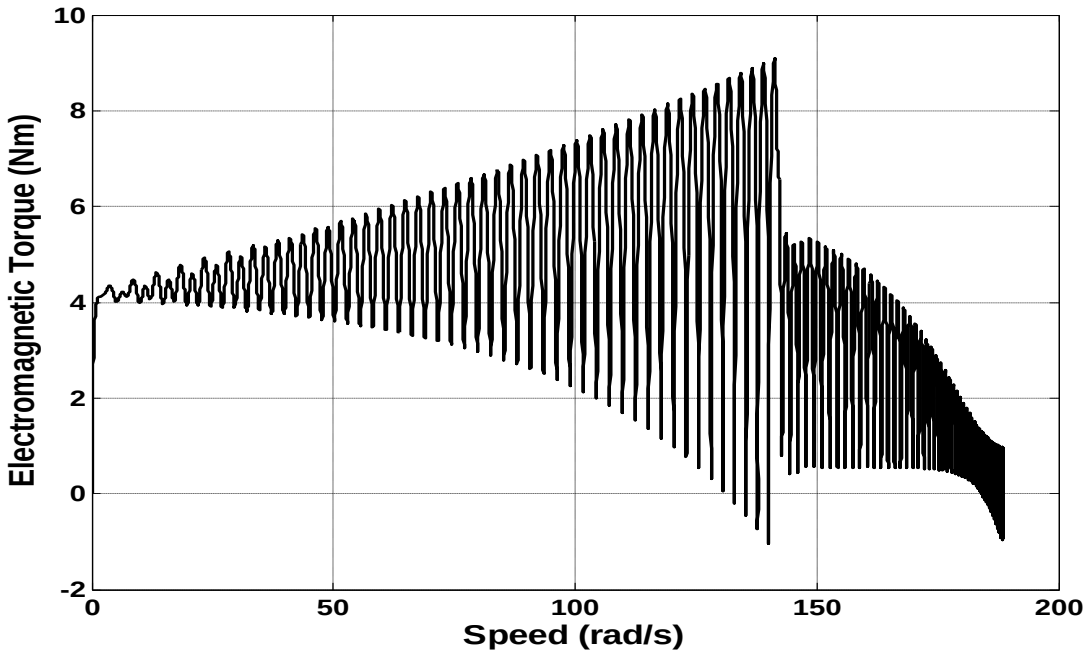
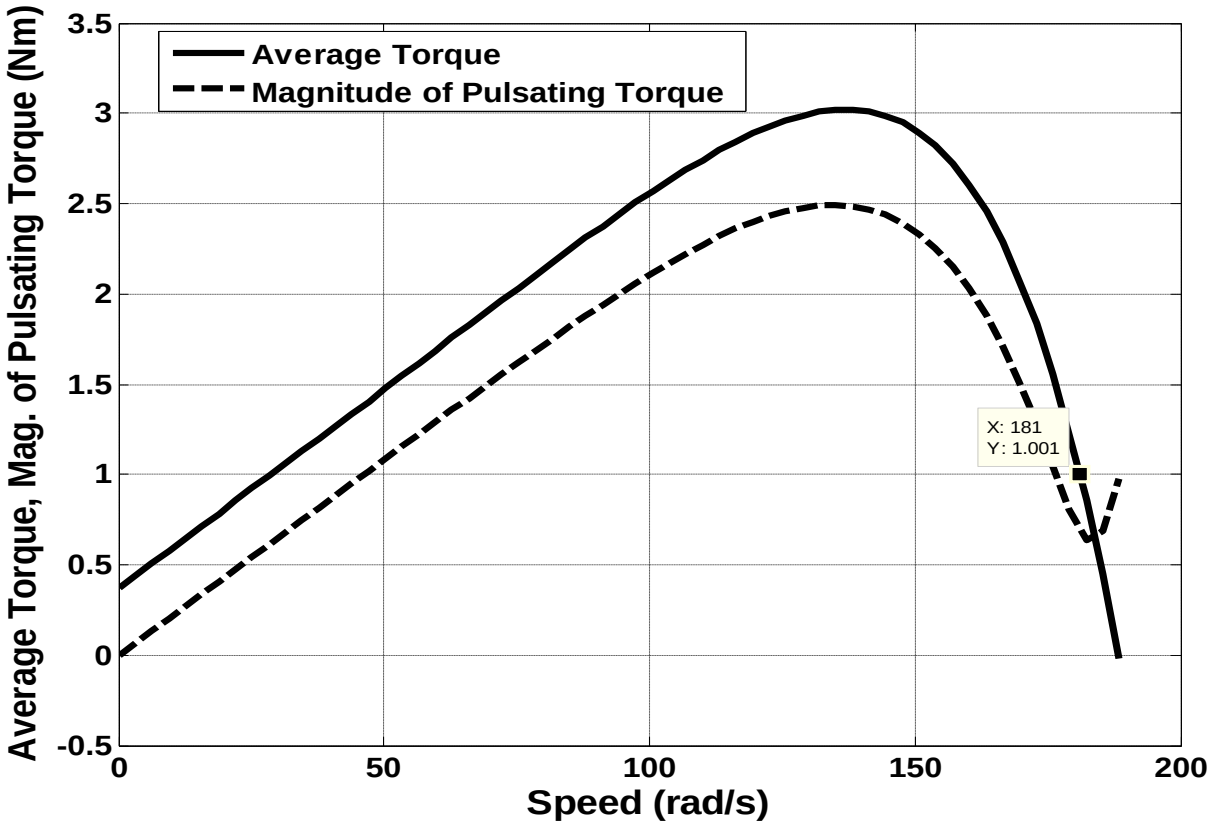


Figure 4.7: Dynamic Torque - Speed Characteristics of the CRSPIM

Figure 4.7 shows the dynamic torque speed characteristics of the CRSPIM. The torque production is clearly seen as the motor runs from zero speed to synchronous speed. The torque pulsations that cause noise and vibration in the machine can be clearly seen as well. The pulsations continue to increase until about 75% of synchronous speed when the switch is disconnected. After the switch is disconnected, the pulsations reduce in magnitude and reach a minimum value near rated speed of 181rad/s (or 1728 rev/min).

4.1.2 Simulation Results of the Steady State Behavior of the CRSPIM

The steady state performance of the CRSPIM is depicted in Figures 4.8 – 4.10. Figure4.8 compares favorably well with simulation result in Krause *et al*, (2002). Figures 4.9 - 4.10



compare favorably well with simulation results in Ong, (1998).

Figure 4.8: Torque – Speed Characteristics

The average torque of the machine through-out the motor speed range is shown in Figure 4.8 with only the run-capacitor present in the auxiliary winding circuit. The starting torque is observed to be 0.3761Nm. The value is lower than the rated torque of 1Nm. This explains why another capacitor is used to raise the value of the starting torque to about 4Nm as observed in the dynamic torque characteristics of the motor. The value of the average torque is seen to increase with motor speed and reaches a maximum of 3.02 Nm. The value of the average torque then decreases to zero Nm at synchronous speed. The magnitude of the pulsating torque is plotted against motor speed in the same figure. It can be observed that the magnitude of the pulsating torque increases from zero to a maximum value of 2.49Nm and then reduces to 0.6888 Nm at rated conditions. The minimum value of the pulsating torque magnitude can be observed to occur at same speed as the rated torque.

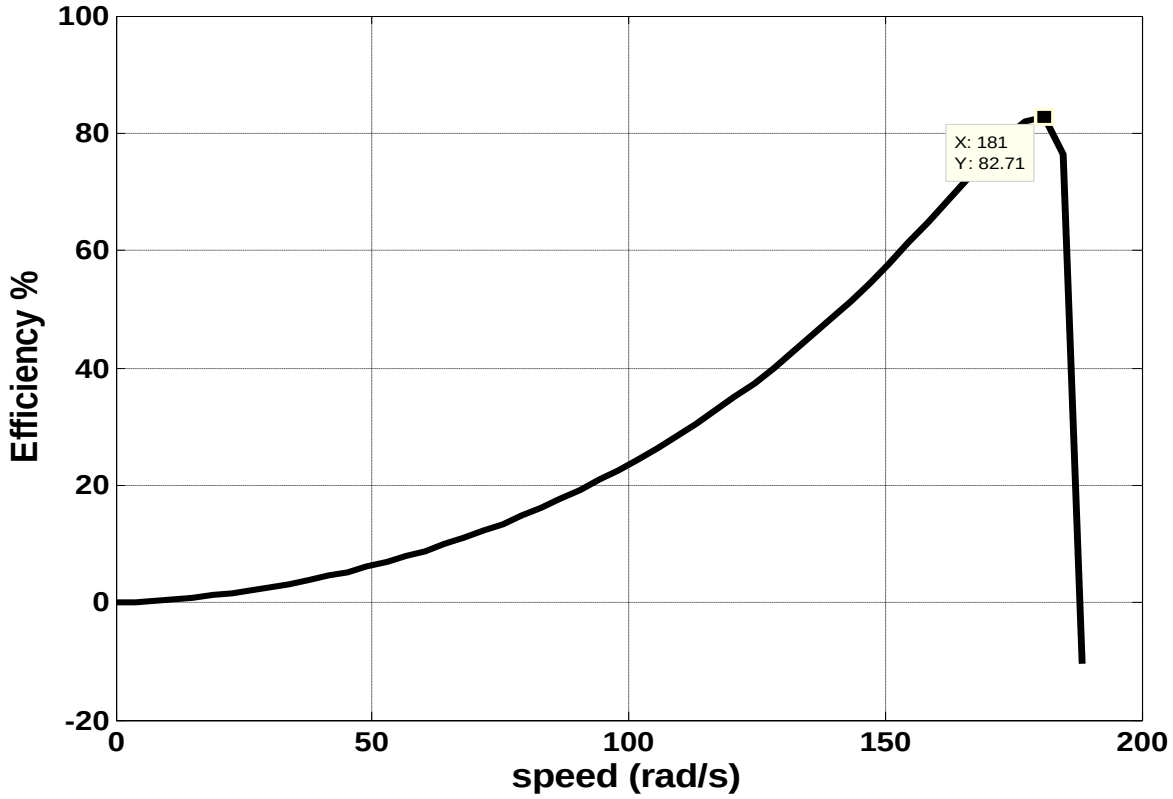


Figure 4.9: Efficiency versus Speed

The efficiency of the motor is plotted against motor speed in Figure 4.9.The motor efficiency has a maximum value of 82.71% which occurs at rated motor conditions. Below rated conditions, the efficiency is observed to fall rapidly. The phase angles of currents in the main and auxiliary windings are plotted against rotor speed in Figure 4.10. It can be observed that the difference in phase angles is close to 90^0at the rated operating point and this explains why rated operating point is the point of best performances in the machine.

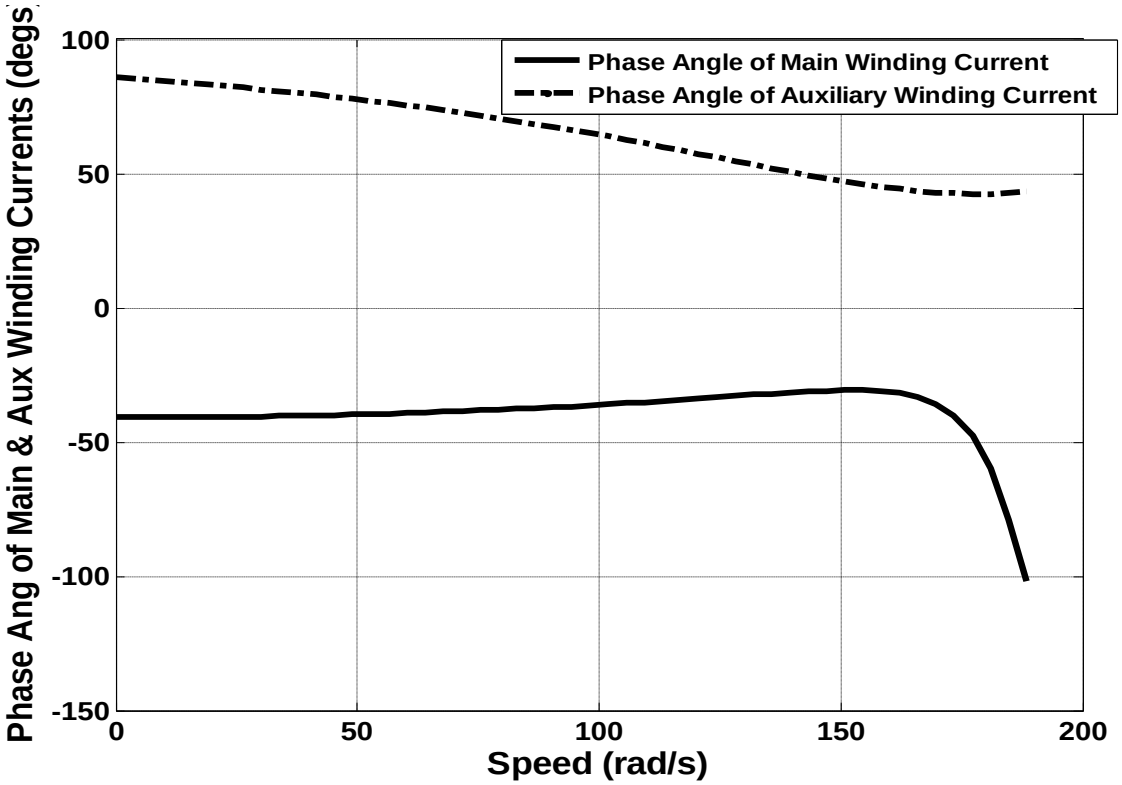


Figure 4.10: Phase Angle of Currents in Main and Auxiliary Winding versus Speed

4.2 INFLUENCE OF DISPLACEMENT ANGLE ∂ ON THE TORQUE PRODUCTION AND EFFICIENCY PROFILE OF THE CRSPIM

The graphs of average torque, magnitude of torque pulsations and efficiency in the CRSPIM with ∂ set between 0^0 and 180^0 are provided in Figures 4.11 – 4.13. The results of comparison between motor performances for the case of displacement angle 60^0 and the performances of the standard motor with a displacement angle of 90^0 with respect to torque production and efficiency are given in Figures 4.14 – 4.16.

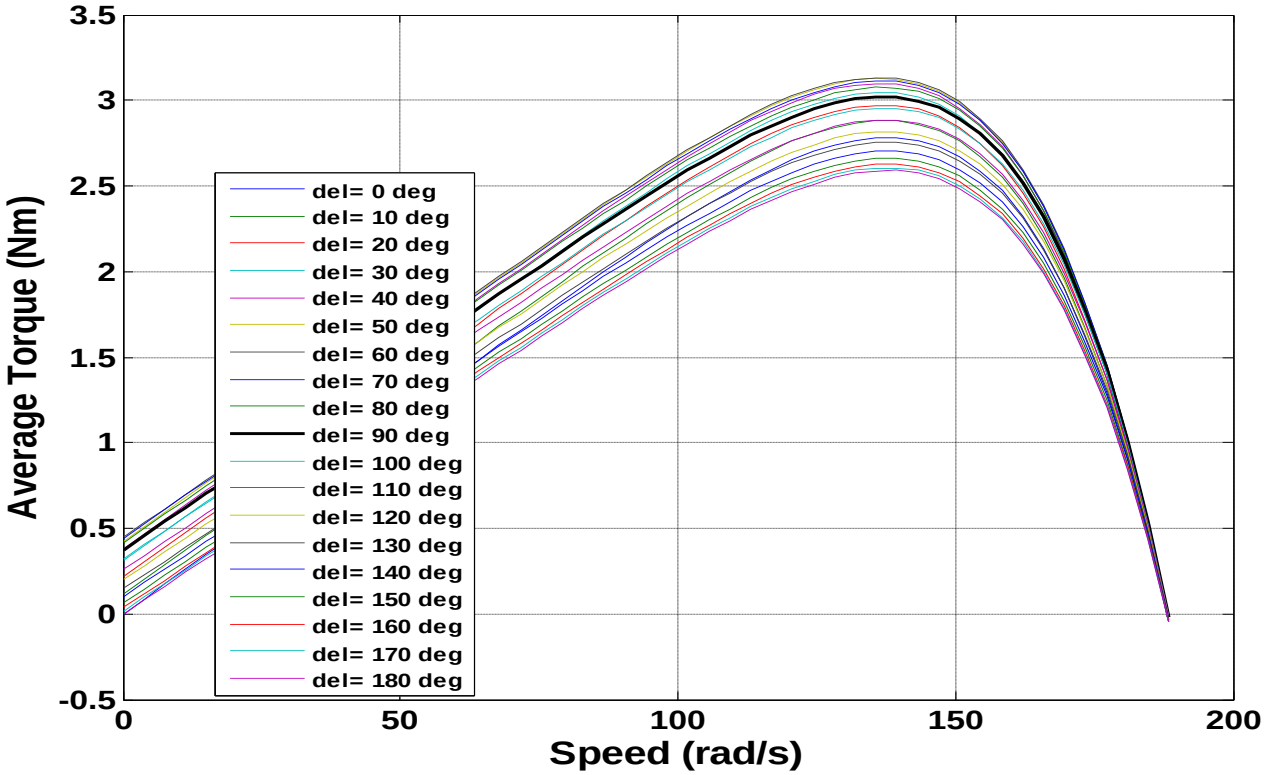
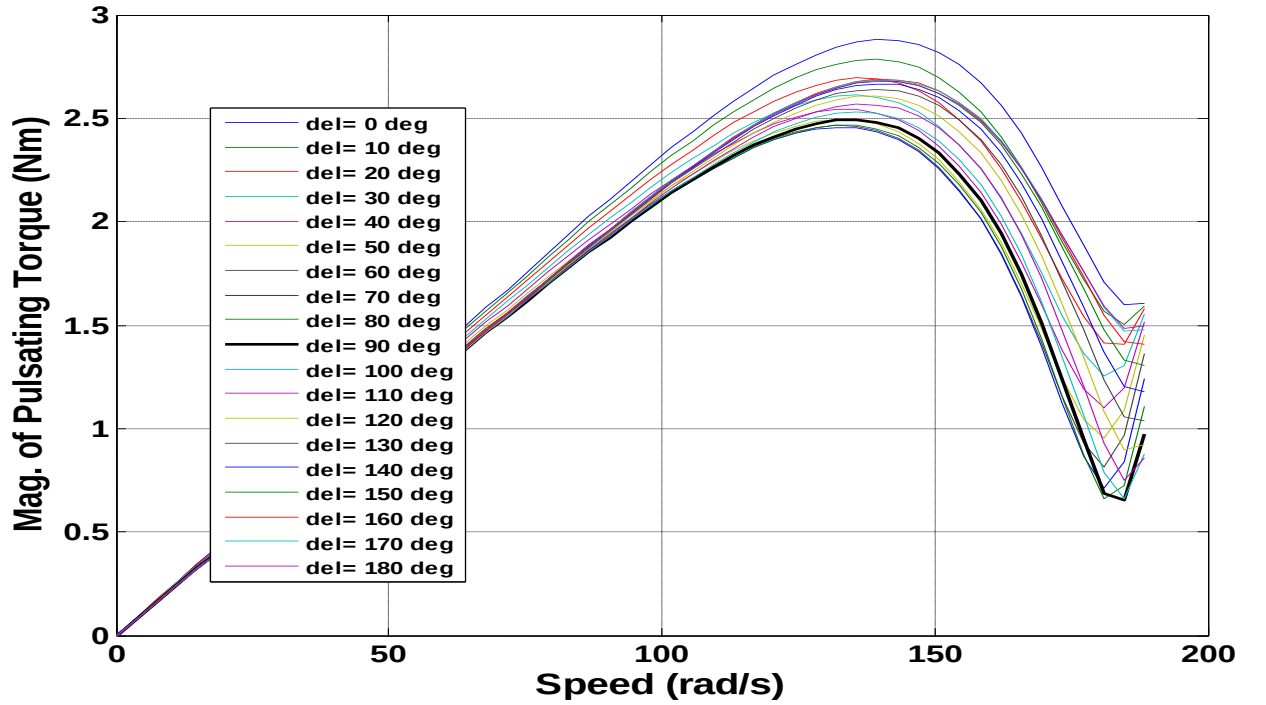


Figure 4.11: Average Torque versus Motor speed for ∂ between 0^0 and 180^0

Figure 4.11showsthat the range of angular displacements that give higher values of average



torque than that of 90^0 is 50^0 - 80^0.

Figure 4.12: Pulsating Torque Magnitude versus Motor speed for ∂ between 0^0 and 180^0

Figure 4.12showsthat the range of angular displacements that give marginally lower magnitudes of torque pulsations than that of 90^0 is 60^0 - 80^0.

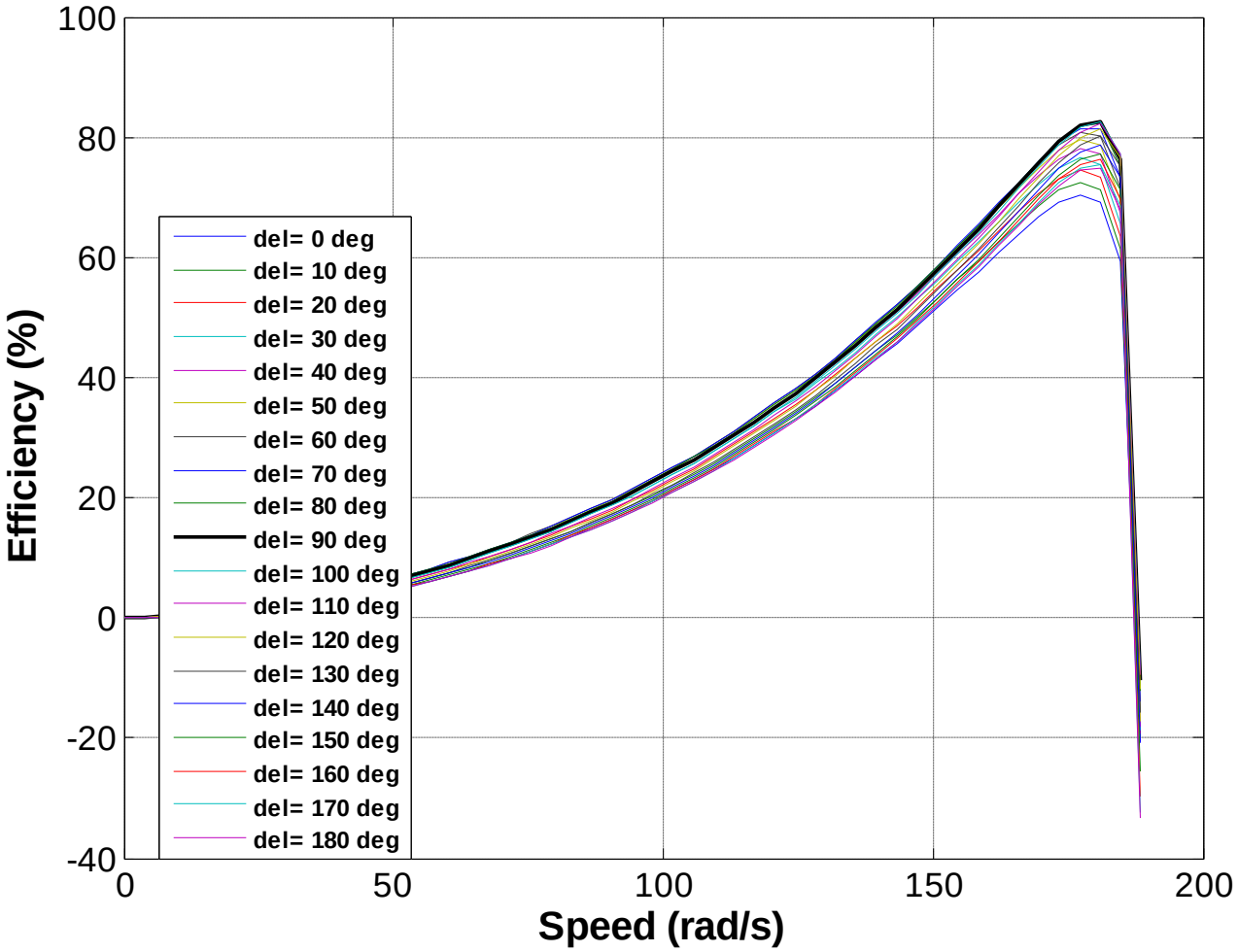


Figure 4.13: Efficiency versus Motor speed for ∂ between 0^0 and 180^0

Figure 4.13shows that the range of angular displacements that give marginally higher values of efficiency than that of 90^0in the low speed range is 60^0 - 80^0.

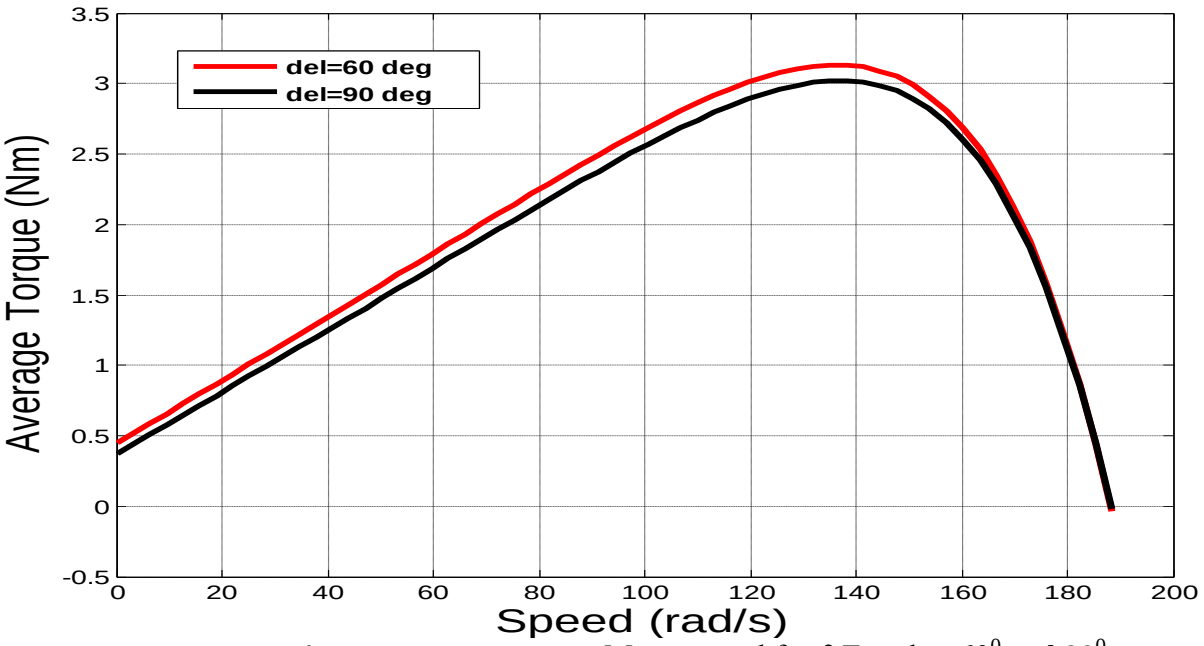
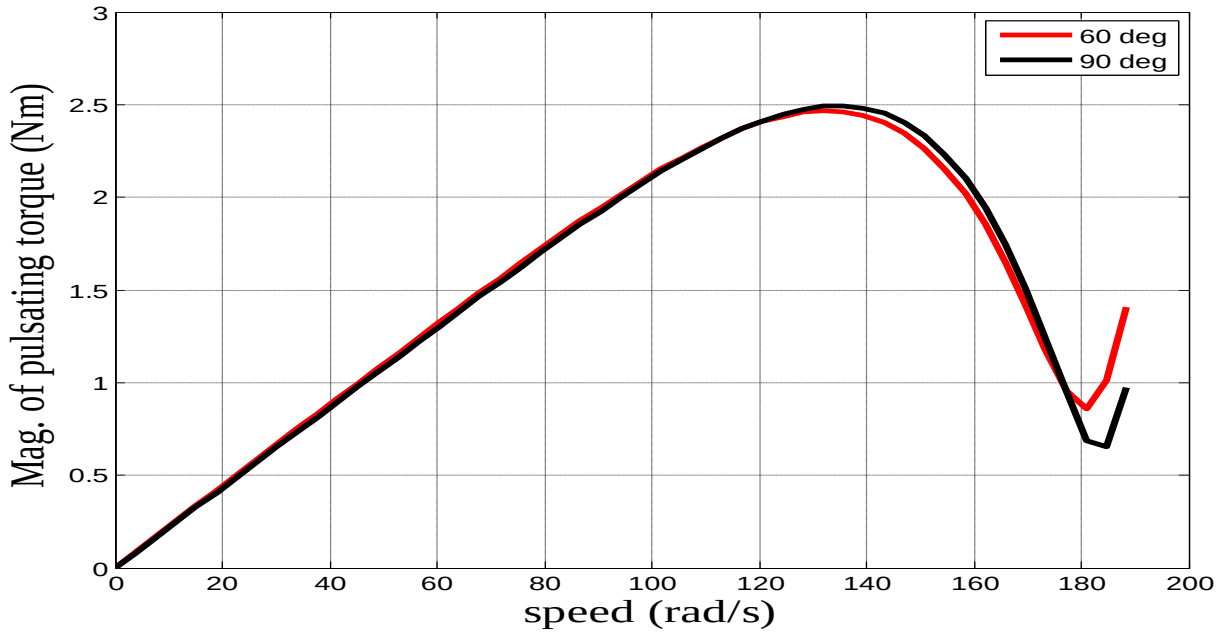


Figure 4.14: Average Torque versus Motor speed for ∂ Equal to 60^0 and 90^0

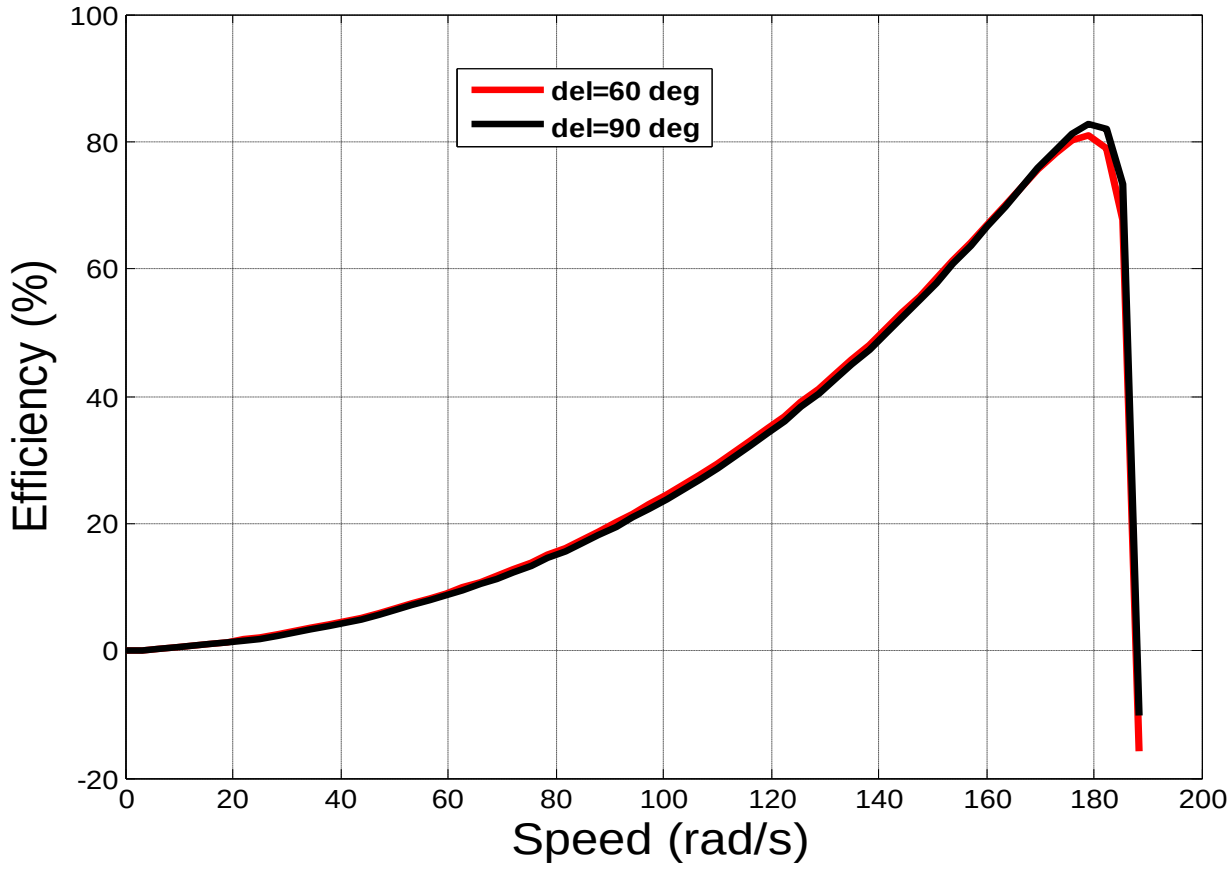
Figure 4.14 shows that there is a marginal increase in average torque from 0 to about 180 rad/s or 1719 rpm for the case when $\boldsymbol{\partial}$ is 60^0. From this point to synchronous speed (i.e. 188.52 rad/s) however, the characteristics remain the same for the two cases. It should be observed that the



starting torques for the 60^0 and 90^0 cases are 0.4478Nm and 0.3761Nm respectively.

Figure 4.15: Pulsating Torque Magnitude versus Motor Speed for ∂ Equal to 60^0 and 90^0

With respect to pulsating torque, a marginal reduction in the magnitude of pulsating torque can be observed in Figure 4.15 for the case when ∂ is 60^0 compared to that of the standard motor design between 117 and 177 rad/s. At rated speed (i.e. 181 rad/s), however, the magnitude of the torque pulsations in the case of the standard motor design is lower than that of the case when ∂ =



60^0 thereby exhibiting a better performance in this regard.

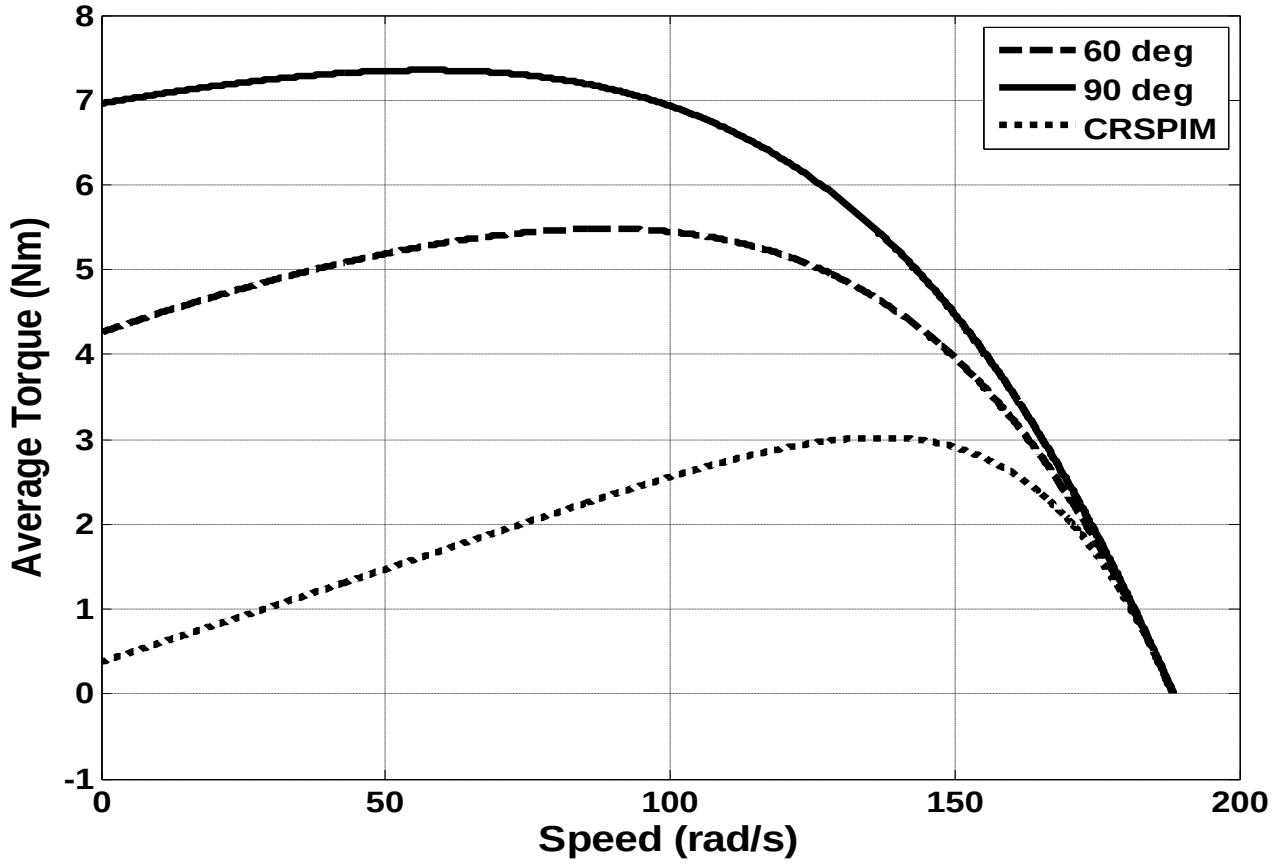
Figure 4.16: Efficiency versus Motor Speed for ∂ Equal to 60^0 and 90^0

Figure 4.16 shows that there is a marginal improvement in efficiency as well over that of the standard motor between 0 and 167 rad/sfor the case when $\partial$is 60^0. At full load operating point (i.e. rated condition) however, the efficiency is higher in the conventional motor design when ∂ is 90^0. At this point, the value of efficiencies are 82.7% and 80.9% respectively for the case when $\partial$is 90^0 and 60^0.

4.3 EFFECTS OF APPLYING BALANCED CONDITION TO THE 60^0 AND 90^0 CONFIGURATIONS FOR BEST TORQUE PERFORMANCE.

The effects of applying balanced condition to the 60^0 and 90^0 single phase induction motor windingconfigurations for best torque performance is presented in this section.

Graphical results of the average torque and the magnitude of pulsating torque are provided. The calculated peak values of the auxiliary winding voltage $\overline{V}'_{ds}$ and the values of its phase angle are

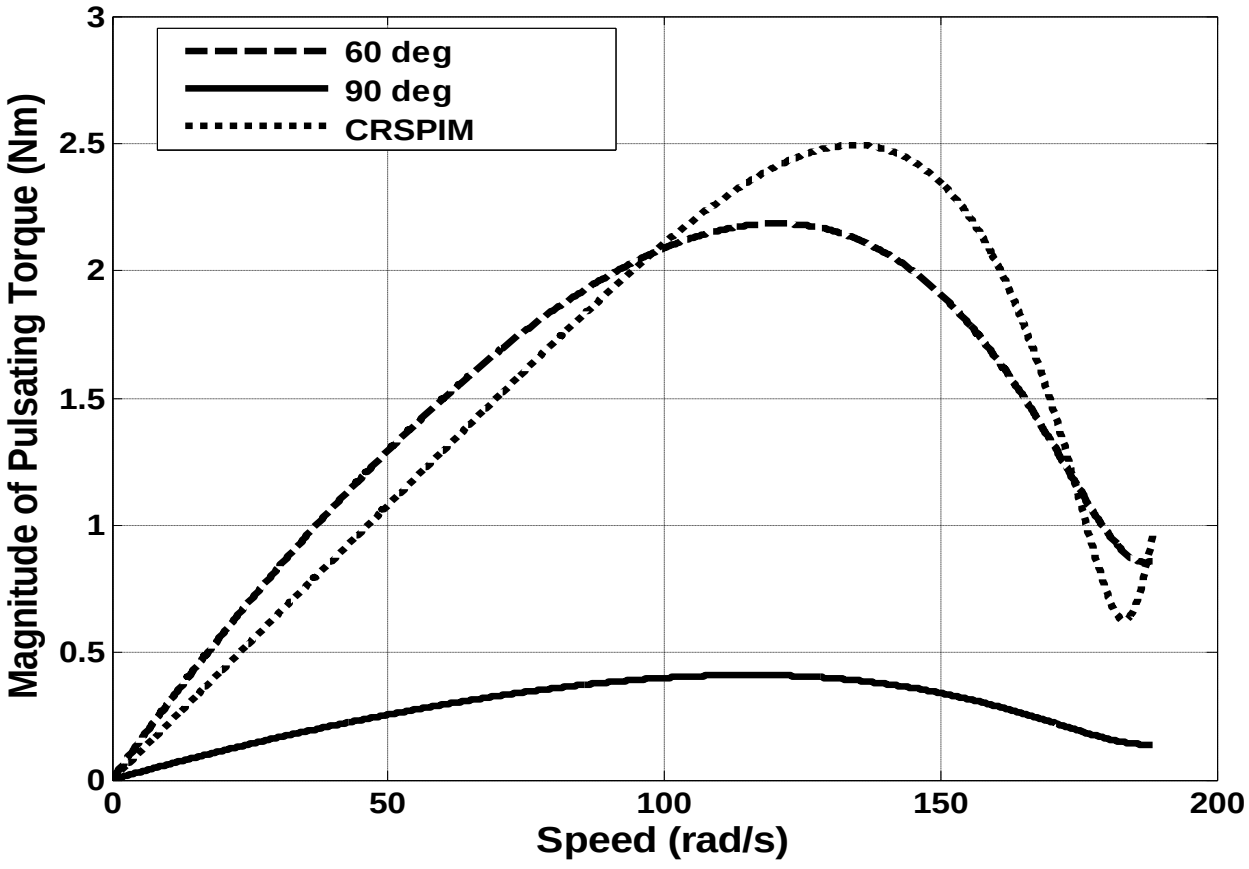


also given in this section.

Figure 4.17: Average Torque versus Motor Speed

With balanced current flowing in the stator windings of the machine, it can be observed in Figure 4.17 that the useful or average torque in the machine is significantly higher in the 90^0 case than in the 60^0 case. The starting torque for the 90^0 case is 7N while the starting torque is seen to be 4.3N for the 60^0. For the conventional CRSPIM with $\partial = 90^0$and without balanced current flowing in the stator, the starting torque value has risen from a low of 0.3761Nm when it is line operated. The values of average torque for all cases converge at rated load torque value (i.e. 1Nm) of the machine.

The magnitude of torque pulsations for three cases is plotted against motor speed in the Figure 4.18. It is clear that the 90^0 case has significantly reduced pulsations in the electromagnetic torque across the entire motor speed range compared to the 60^0 case. It is interesting to note that when balanced condition is imposed on the machine operation, the torque pulsations are



significantly reduced from their levels in the CRSPIM as observed in Figure 4.18. In particular, for the best case of 90^0 winding configuration, the magnitude of torque pulsations which was 0.6888Nm in the CRSPIM at rated conditions has reduced to 0.14Nm.

Figure 4.18: Magnitude of Torque Pulsations versus Motor Speed

The import of the improvement in torque production is that the machine acceleration time will significantly reduce with the effect that the motor efficiency, durability and the motor's ability to operate more quietly will increase.

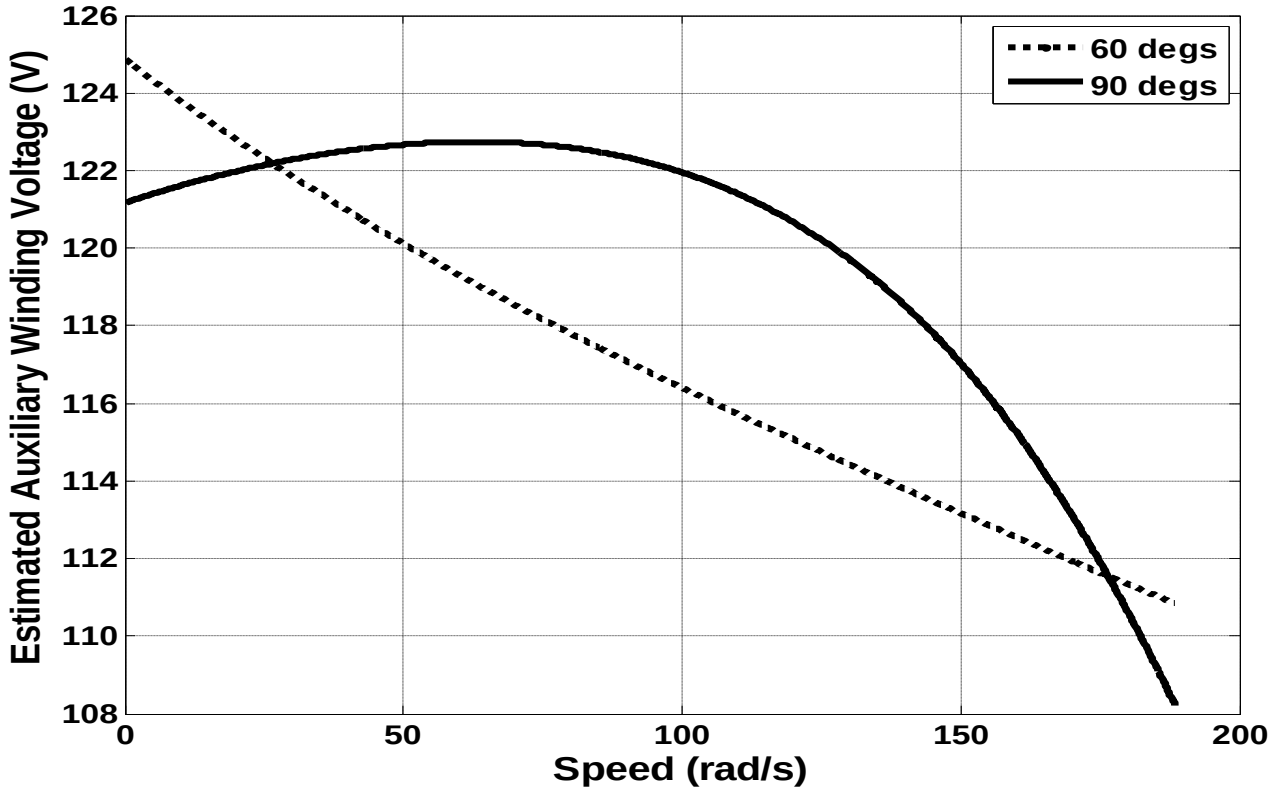


Figure 4.19: Estimated Auxiliary Winding Voltage versus Speed

Figure 4.19 shows the plot of the peak value of the auxiliary winding voltage across the entire motor speed range for the two cases under investigation. It is evident that the voltages vary in magnitude as the motor speed increases from 0 to 188.5 rad/s. The curve corresponding to the spatial angle of 90^0 gives a better performance because its starting and running values are lower

and therefore safer for the motor than those of the curve corresponding to the spatial angle of 60^0.

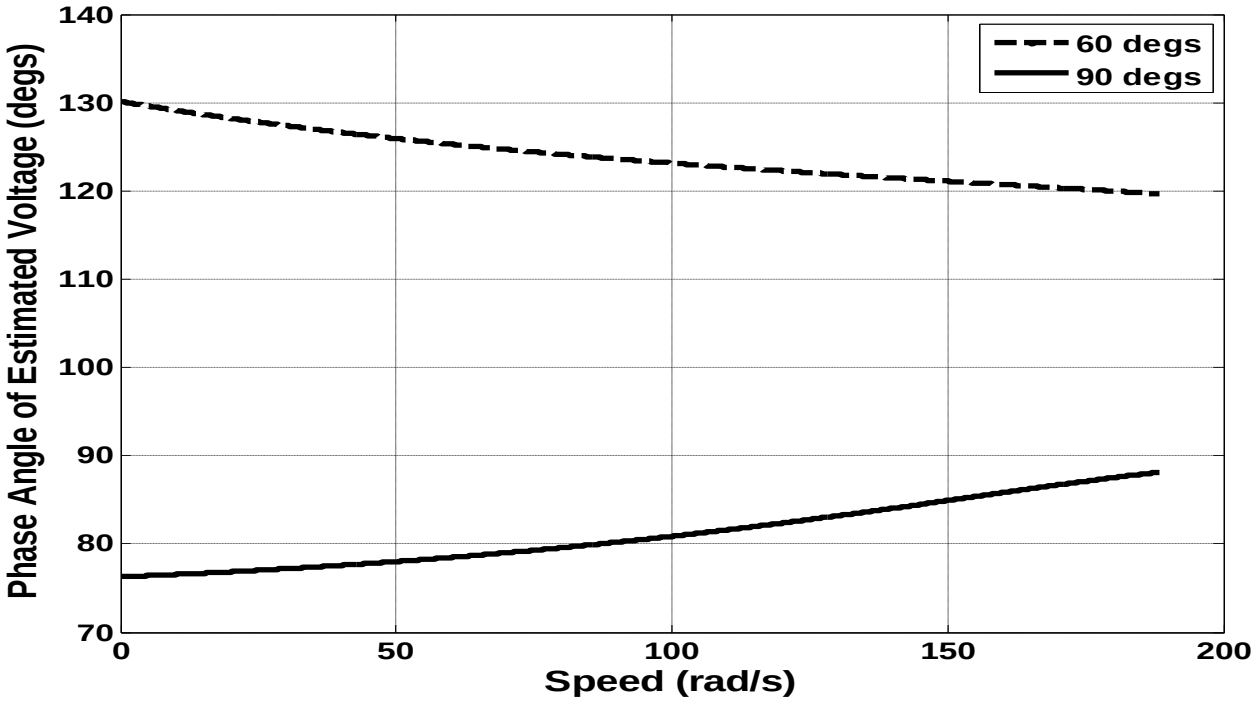


Figure 4.20: Estimated Auxiliary Winding Phase Angle

The phase angles of the voltages also vary with motor speed from 0 to 188.5 rad/s as observed in Figure 4.20. Figures 4.19 and 4.20 are indicative of the need to construct a reference voltage whose magnitude and phase vary with the motor speed.

4.4 SIMULATION RESULTS OF PULSE WIDTH MODULATED INVERTER DRIVE USING A PID CONTROLLER

Figure 4.21 gives the dynamic torque production of the 110V, 60Hz motor referred to as Machine 1 when the scheme of Figure 3.9 is applied to the machine. The total simulation run time is 3s and a rated load of 1Nm was applied at a time of 2s.

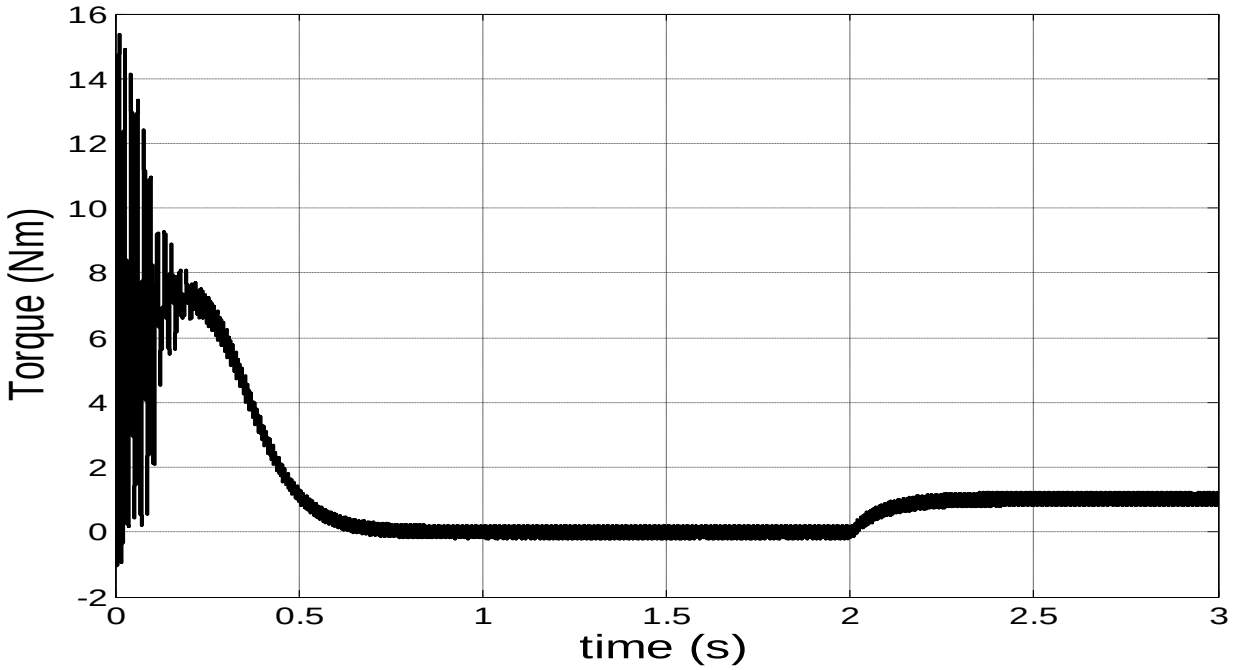
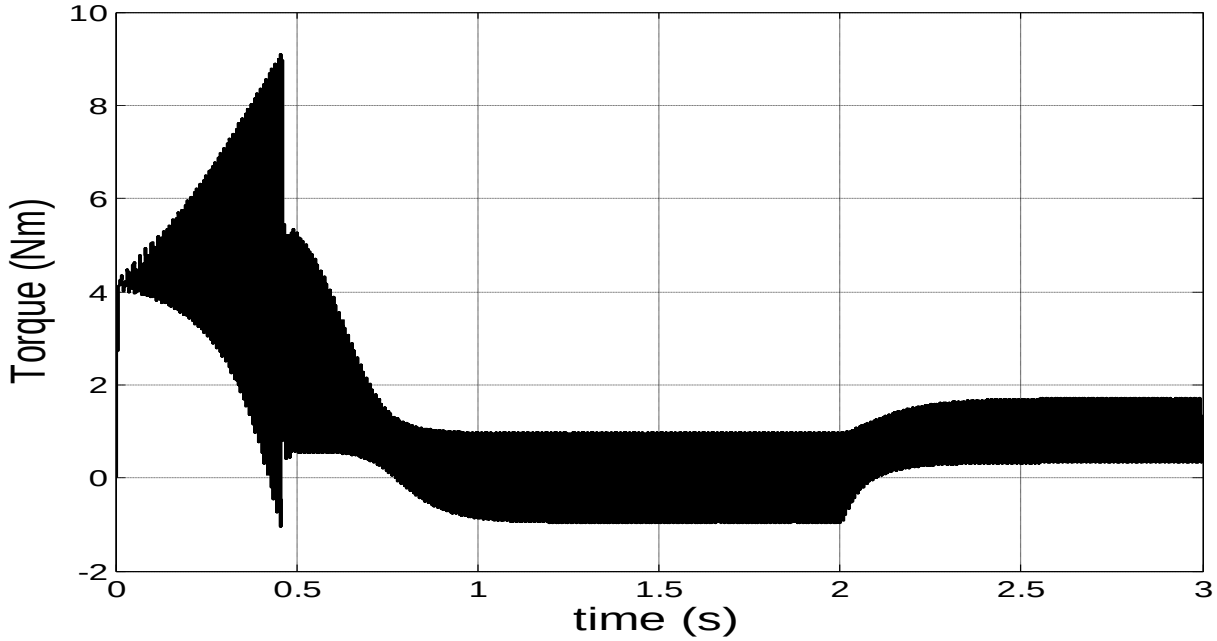


Figure 4.21: Dynamic Torque Production in the Inverter-driven Machine 1

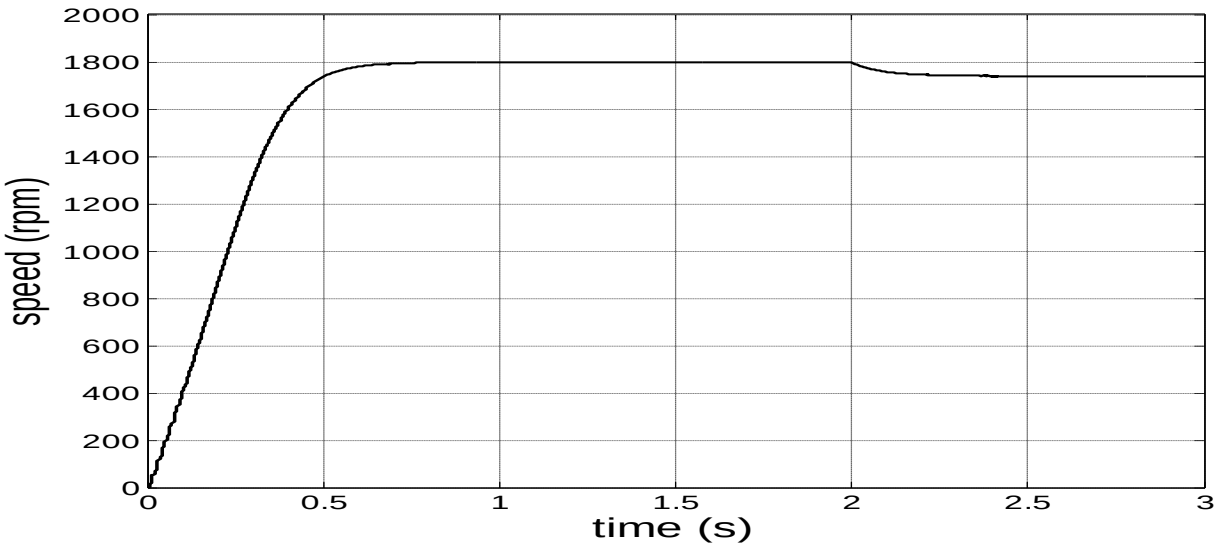
It can be observed in Figure 4.21 that the average starting torque is approximately 7Nm and that the torque pulsations have reduced significantly when compared to those of the capacitor-run



machine of Figure 4.22.

Figure 4.22: Dynamic Torque Production in the Capacitor-Run Machine1

In Figure 4.22, the starting torque is seen to be 4Nm. The starting torque in the machine subjected to the inverter drive is 75% higher than the starting torque of the capacitor-run machine. In addition, the torque pulsations can be observed to be lower in Figure 4.21 than they are in Figure 4.22. The peak to peak magnitude of the torque pulsations in the existing CRSPIM of Figure 4.22is1.4Nm at rated load. This value reduced to 0.4Nm in the inverter-driven machine as evident in Figure 4.21. This reduction represents an improvement of 71% over the level of



torque pulsations in the existing CRSPIM.

Figure 4.23: Speed versus Time Characteristics of the Inverter-Driven Machine 1

The graph of Figure 4.23 clearly shows that the machine accelerates from rest and reaches steady state speed in 0.7s. The speed is seen to drop to 1730 rpmat a time of 2s after the load was applied. The gain in average starting torque increases the acceleration time of the machine with the consequence that the machine reaches steady state at time 0.7s down from 1s as seen in

Figures 4.23 and 4.24 for theinverter-driven machine and capacitor-run machine respectively. This represents a 30% improvement in starting time of the machine. The broader implication of the reduction in acceleration time is that the machine runs up to steady state more efficiently.

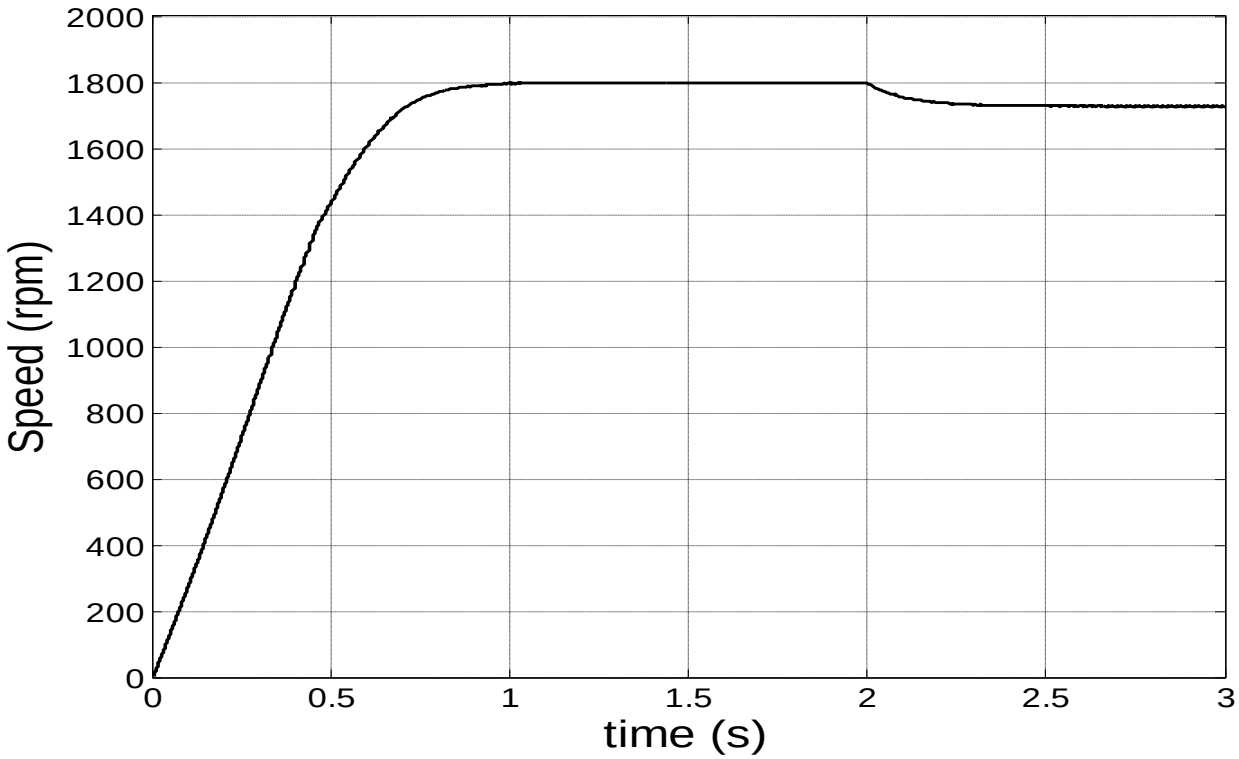


Figure 4.24: Speed versus Time Characteristics of the Capacitor-Run Machine 1

The corresponding graphs for the 220V, 50Hz motor referred to as Machine 2 are given in Figures 4.25 – 4.28.

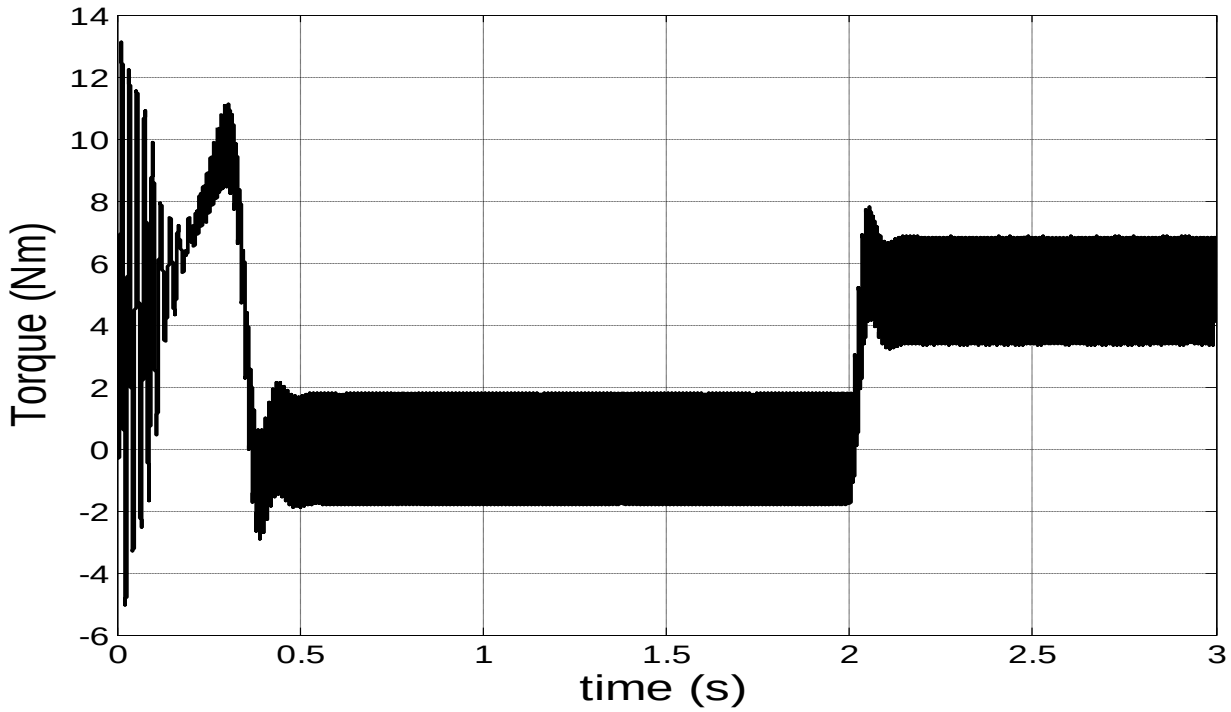


Figure 4.25: Dynamic Torque Production in Inverter-Driven Machine 2

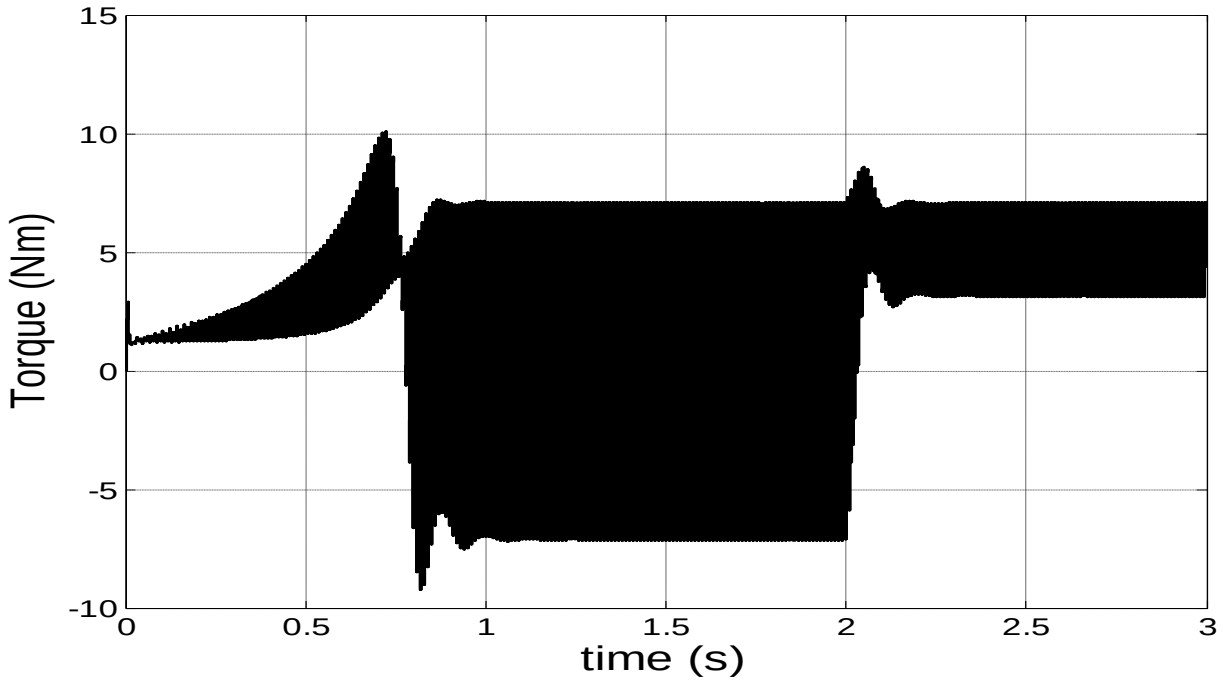
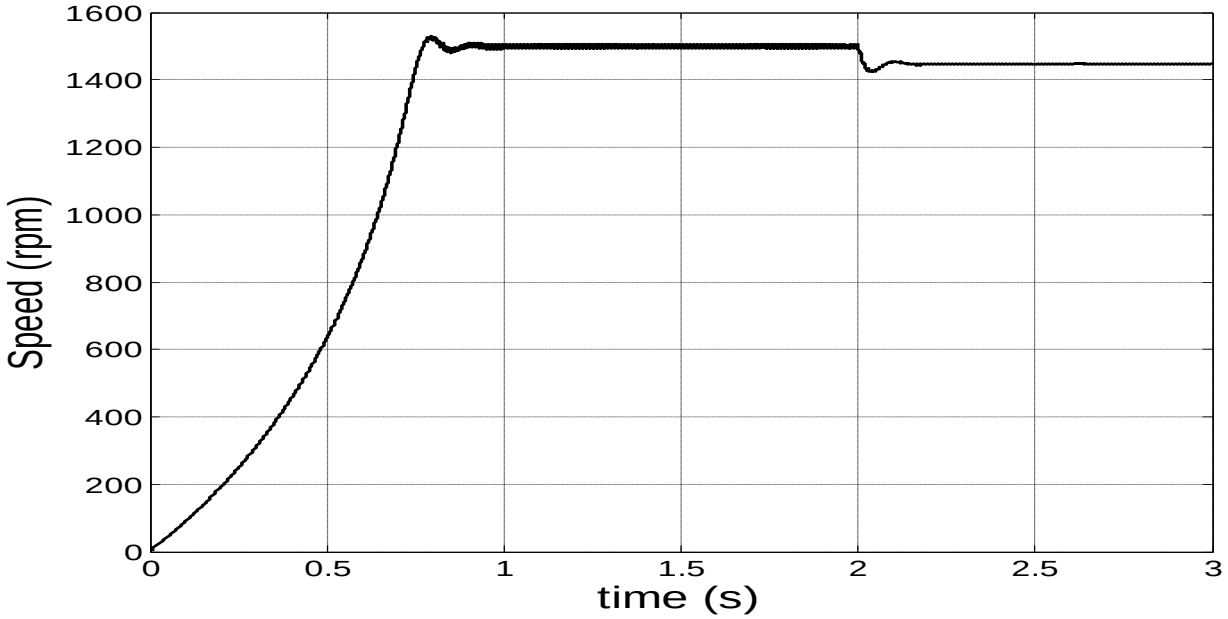


Figure 4.26: Dynamic Torque Production in the Capacitor-Run Machine 2

The starting torque in Figure 4.25 is approximately 6Nm. This represents a 400% increase over the starting torque of 1.2Nm as observed in Figure 4.26. The peak to peak magnitude of the torque pulsations is3.4Nm at rated load in Figure 4.25. This represents an improvement of 15% reduction

in torque pulsations over that of Figure 4.26. It can be observed that the torque pulsations are as

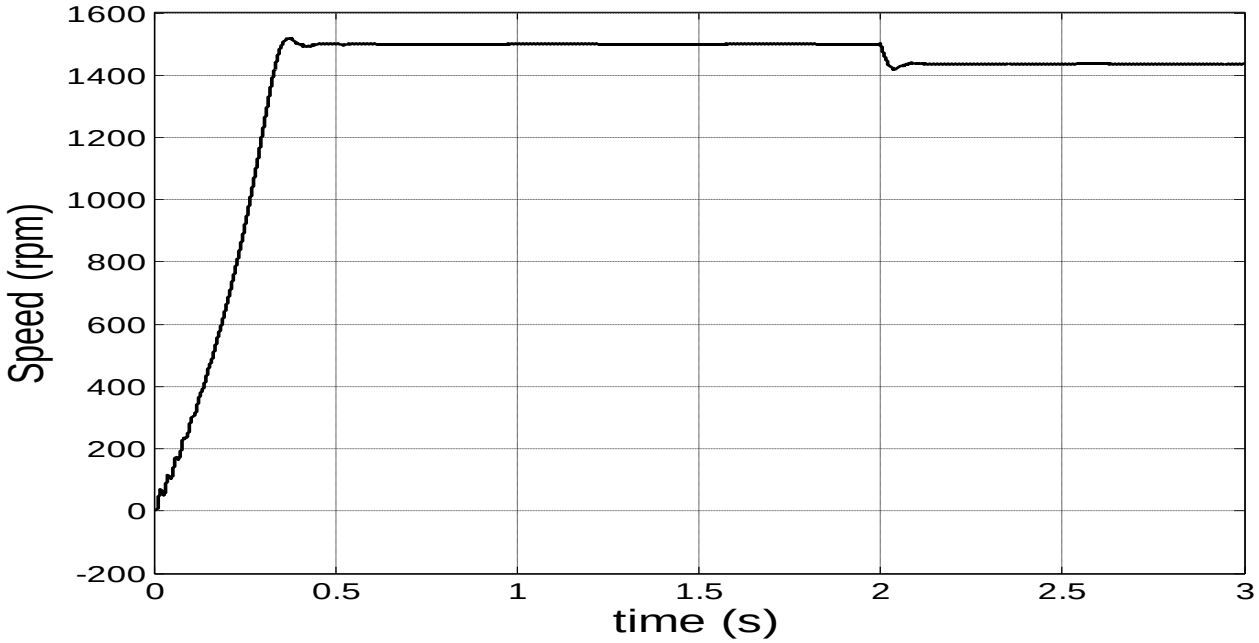


high as 14Nm peak to peak when the capacitor-run machine is not loaded at steady state.

Figure 4.27 Speed versus Time Characteristics of the Capacitor-Run Machine 2

Figure 4.28: Speed versus Time Characteristics of the Inverter-Driven Machine 2

It can be seen in Figures 4.27 and 4.28 that the acceleretion time of Machine 2 reduces from 0.85s to 0.5s when the inverter drive is applied. This represents a 41% improvement in acceleretion time of the machine. The speed of the motor is seen to drop to 1447 rpmat a time of



2s after the load was applied.

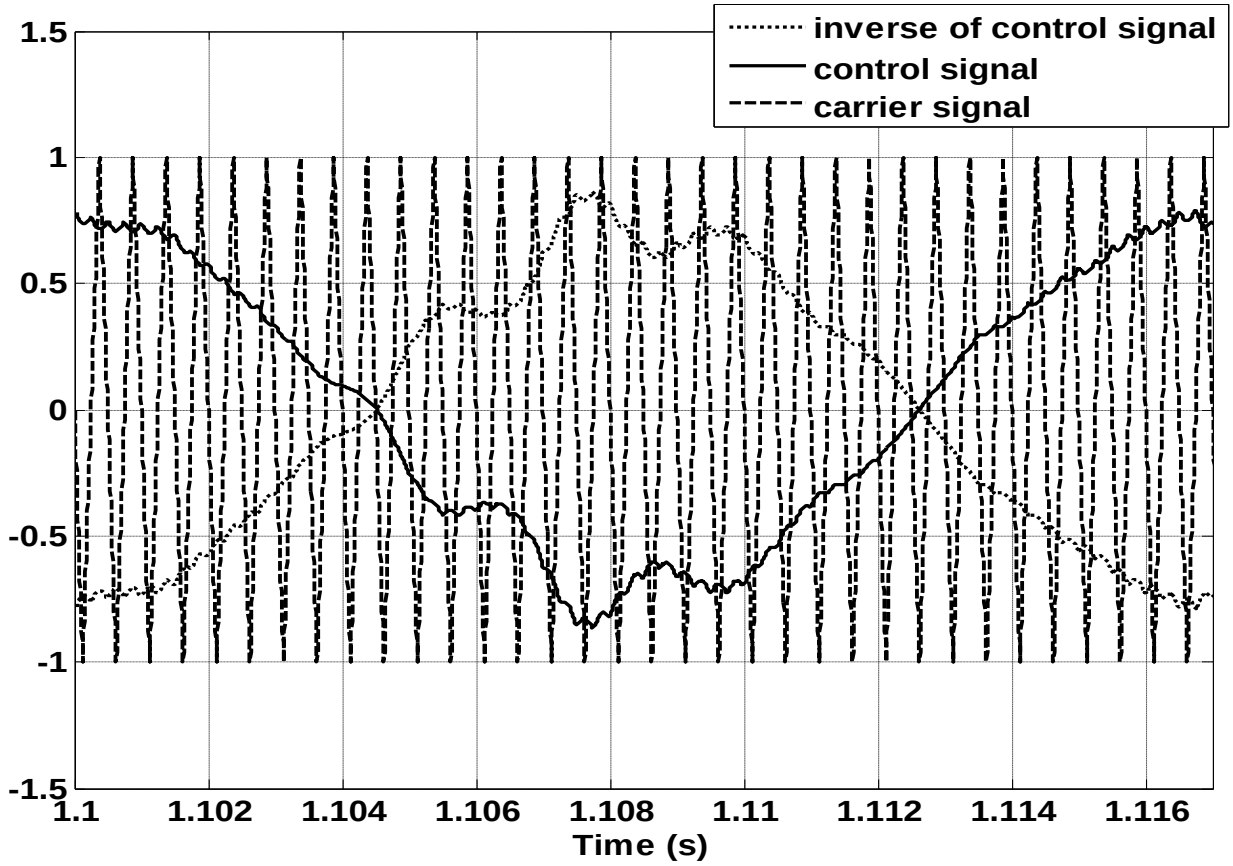


Figure 4.29: Sine–Triangular Wave Comparison of the Inverter Drive of Machine 1

Figure 4.29shows the sinusoidal modulating or control signals and the triangular carrier wave for one period of the control signal. The point of intersection between the sinusoidal signals and the triangular carrier wave determine the switching instants of the semiconductor devices of the inverter.

The result of the sine –triangular wave comparison is the set of pulses given in Figure 4.30and these pulses control the switching of the devices to the effect that the inverter synthesizes an output voltage similar to the reference voltage.

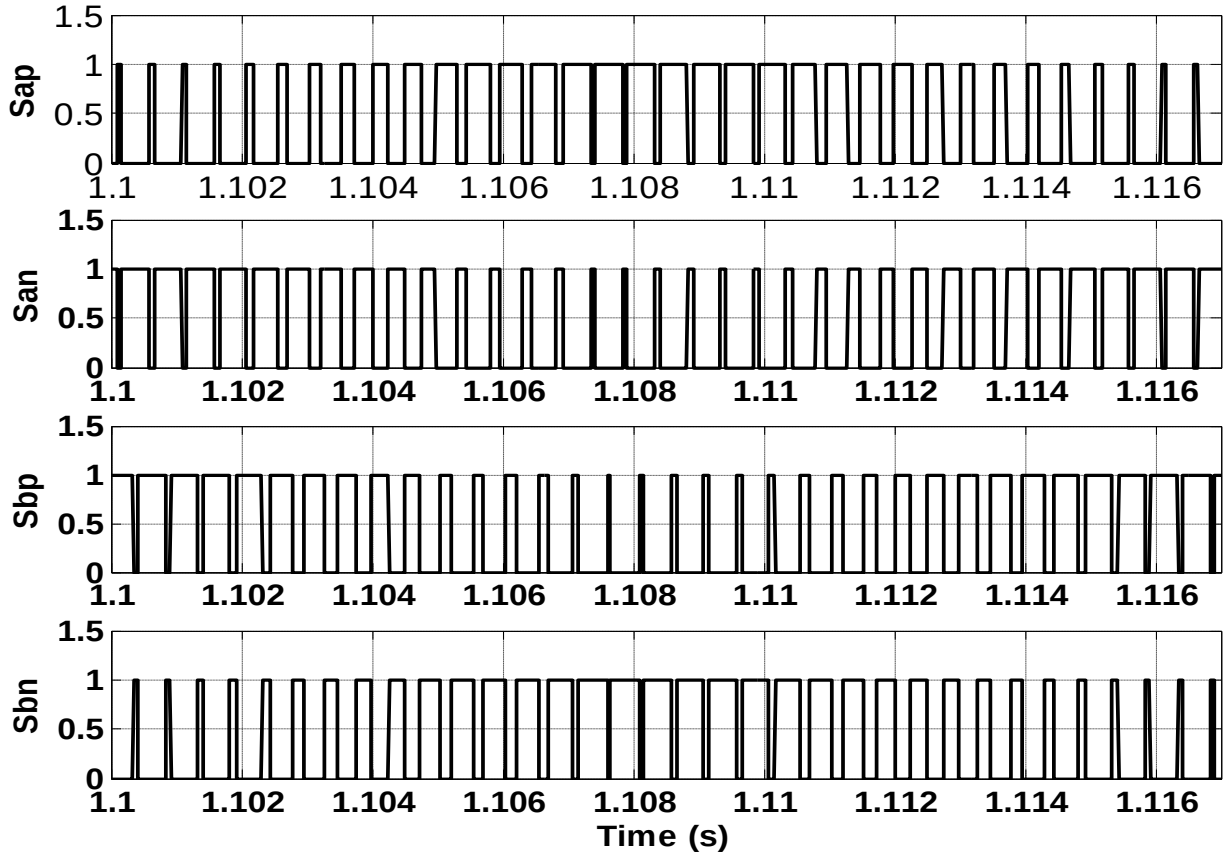


Figure 4.30: Switching Functions of the Inverter Drive of Machine 1

Figure 4.30 shows the switching functions of the inverter as obtained from the PWM algorithm in the time shown on the graph. It can be seen that the pulses have varying widths and this variation is in accordance with the amplitude of the control signal.

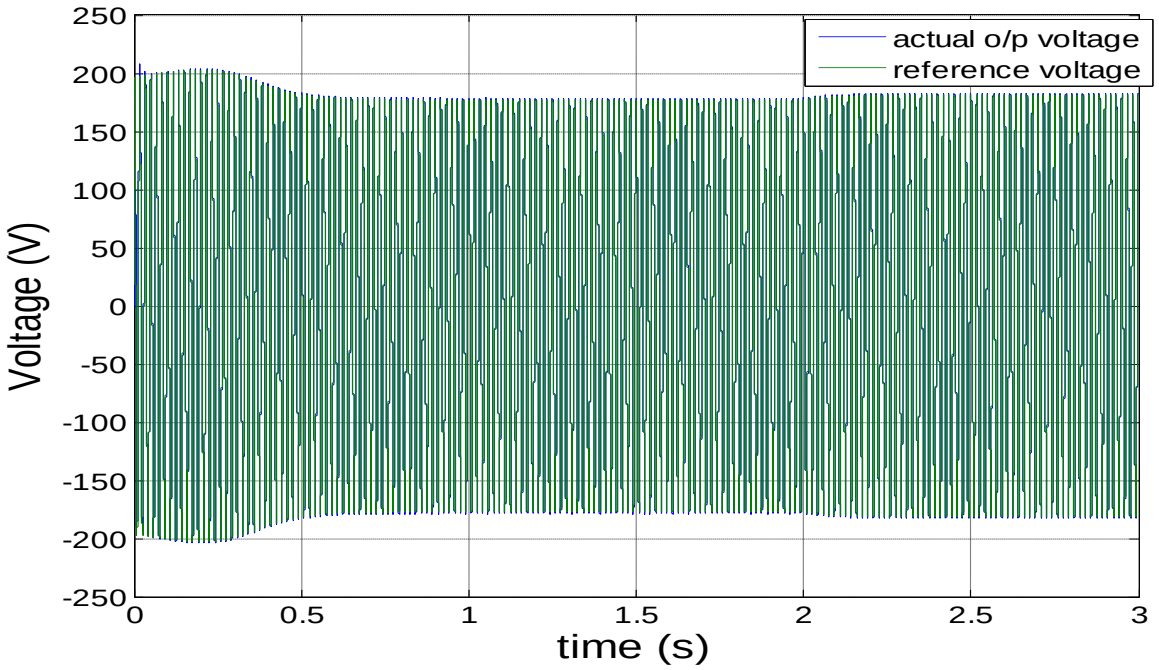
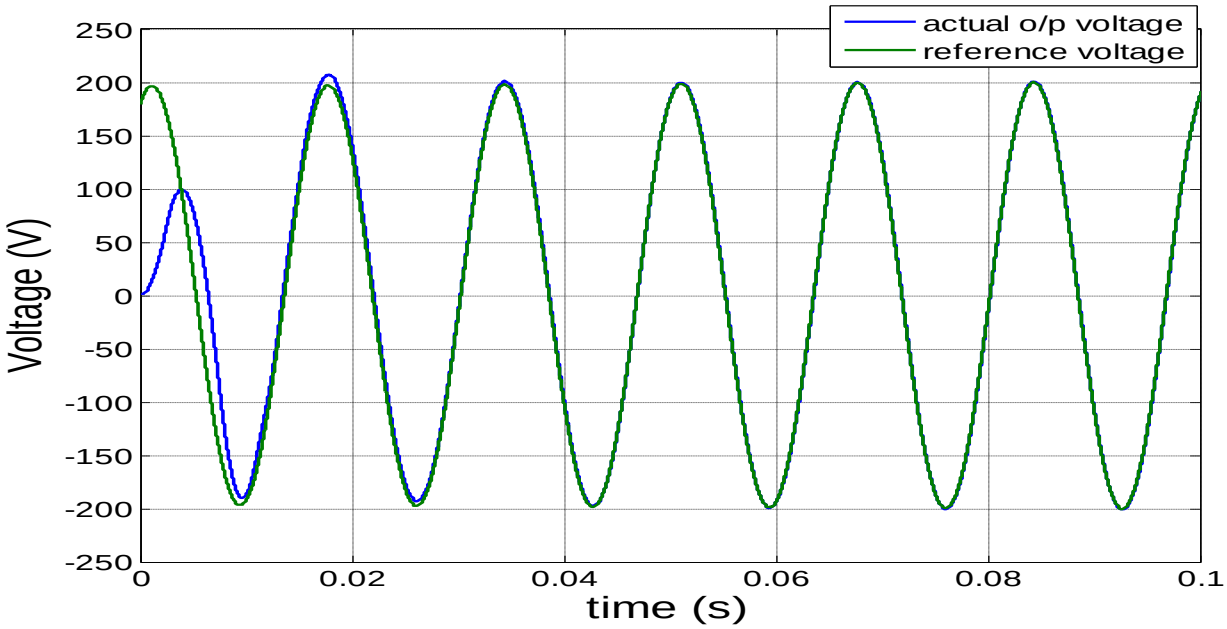


Figure 4.31: Actual Inverter Output Voltage and Reference Voltageversus Time

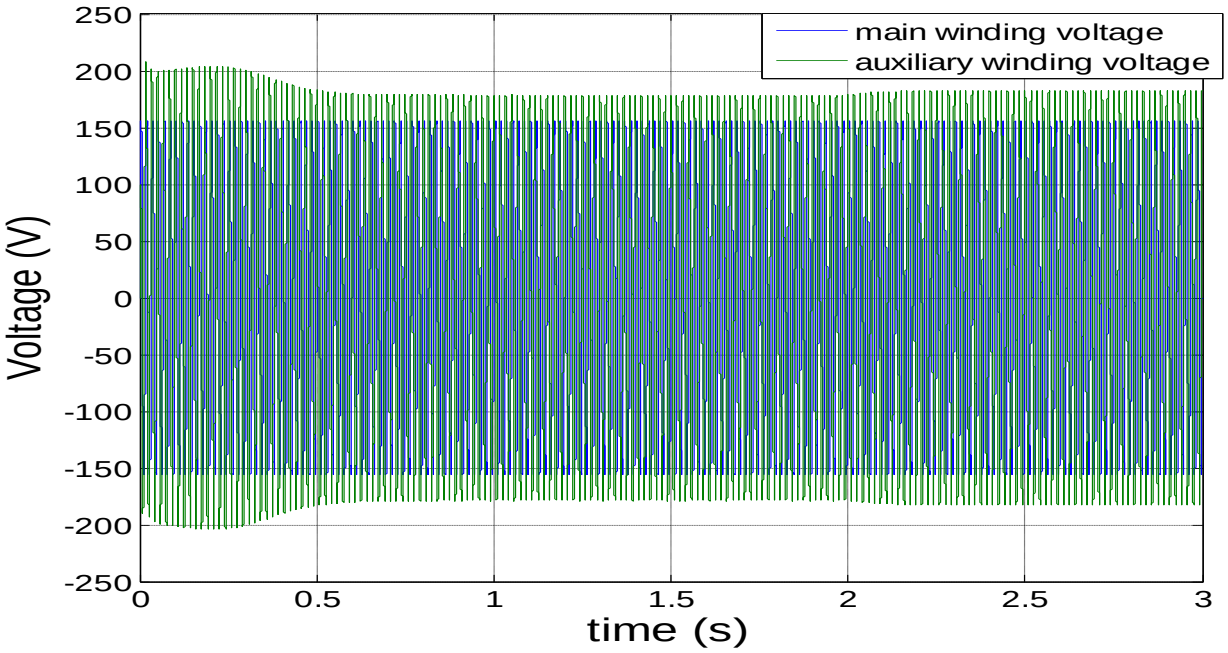
The actual inverter output voltage is superimposed on the reference voltage in Figure 4.31 for ease of comparison. It can be observed that the output voltage is identical to the reference voltage. This similarity is due to the PID controller action. The voltage is seen to vary in



amplitude as motor accelerates from rest to steady state.

Figure 4.32: Reference and Actual Auxiliary Winding Voltage between 0 and 0.1s for Machine 1

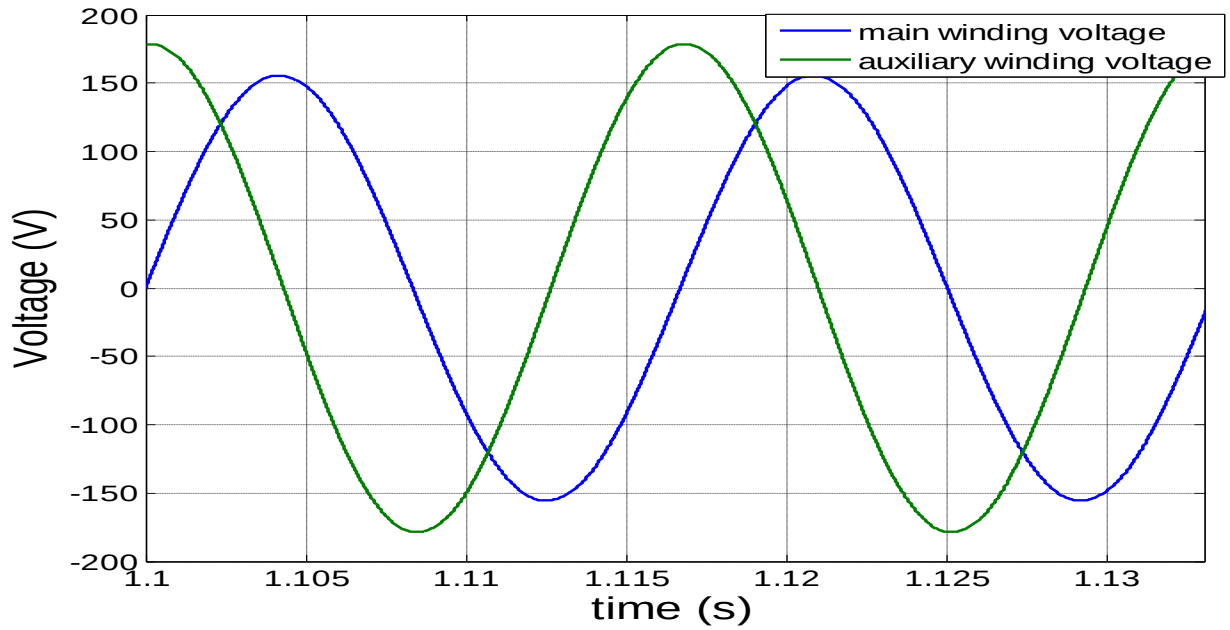
The graph of Figure 4.31 has been reproduced in Figure 4.32 but between 0 and 0.1s in order to show the effect of the PID controller on the inverter output voltage. The actual inverter output voltage is seen to track the reference faithfully from a time of about 0.02s. The import of this



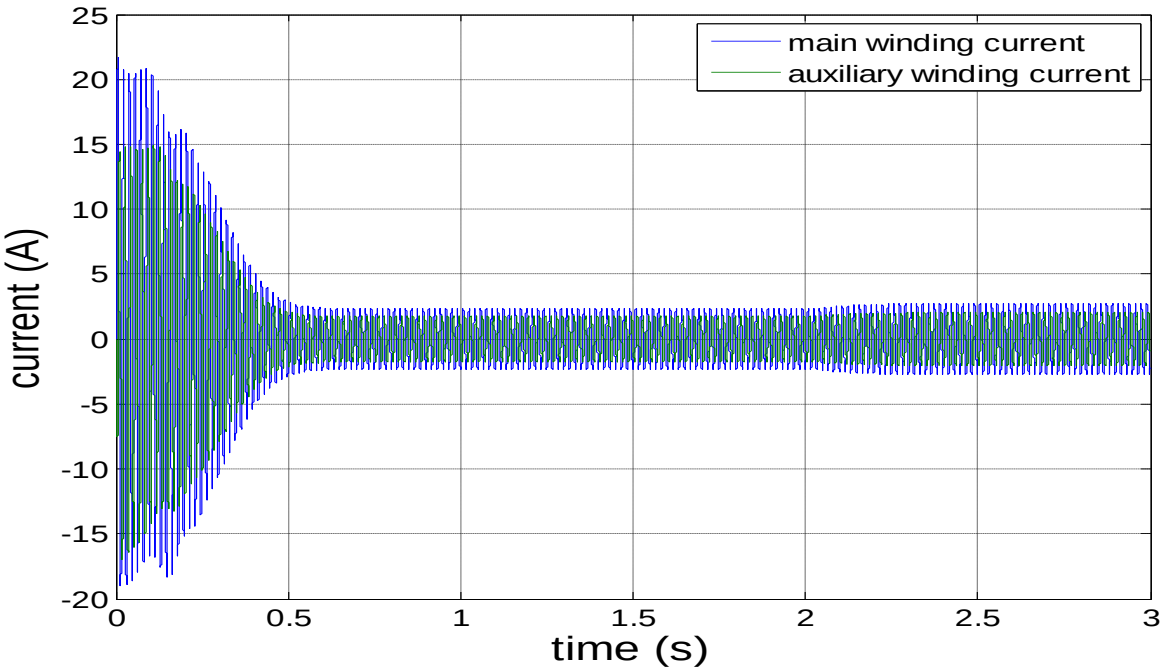
reference tracking is seen in Figure 4.33 and 4.34.

Figure 4.33: Main Winding Voltage and Auxiliary Winding Voltage for Machine 1

Figure 4.34: Main Winding Voltage and Auxiliary Winding Voltage in 2 Periods for Machine1



Figures 4.33 and 4.34 show the main winding voltage and the auxiliary winding voltage which is the same as the inverter output voltage plotted together. Figure 4.33 represents the voltages for the total simulation time while Figure 4.34 presents the same voltages for the period between 1.1s and 1.14s. It can be seen that the auxiliary winding voltage leads the main winding voltage by an angle of 90^0 and that its amplitude is about 1.18 times greater than that of the main winding voltage. This result verifies the analysis given in section 2.2.2.9. The controller is therefore able to command the inverter to supply balanced voltages to the stator windings of the single phase induction machine. This controller action in conjunction with the action of the pulse width modulated inverter explains the reason why there is a significant reduction in the torque pulsations of the machine as seen in Figures 4.21 and 4.22. The reason why the pulsations are not completely eliminated can be seen in the waveforms of the main and auxiliary winding currents. These waveforms are shown in Figures 4.35 and 4.36. Figure 4.35 shows the waveforms of the main and auxiliary winding currents together for the total simulation time. Figure 4.36, on the



other hand, shows the same waveforms in the time between 1.1s and 1.14s

Figure 4.35: Main Winding Current and Auxiliary Winding Current for Machine1

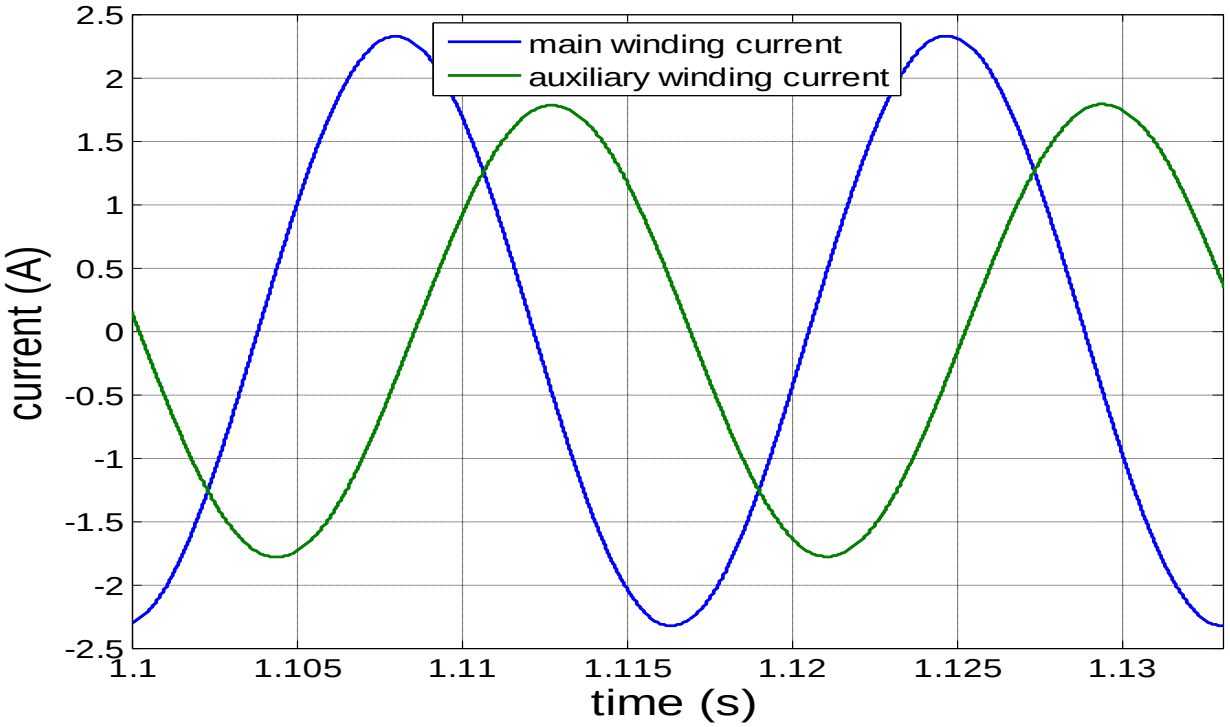


Figure 4.36: Main Winding Current and Auxiliary Winding Current for Machine 1 between 1.1s and 1.13s.

It can be observed in Figure 4.36 that the auxiliary and main winding currents unlike the voltages, are not balanced. The phase lead of the auxiliary winding current is not 90^0 and the ratio of the amplitude of the main winding currents to the auxiliary winding current is approximately 1.3 instead of 1.18. This explains why the torque pulsations are not eliminated. The graphs of Figures 4.37 – 4.44 apply to Machine 2. The explanations given for the results of simulation with respect to Machine 1 also apply to Machine 2.

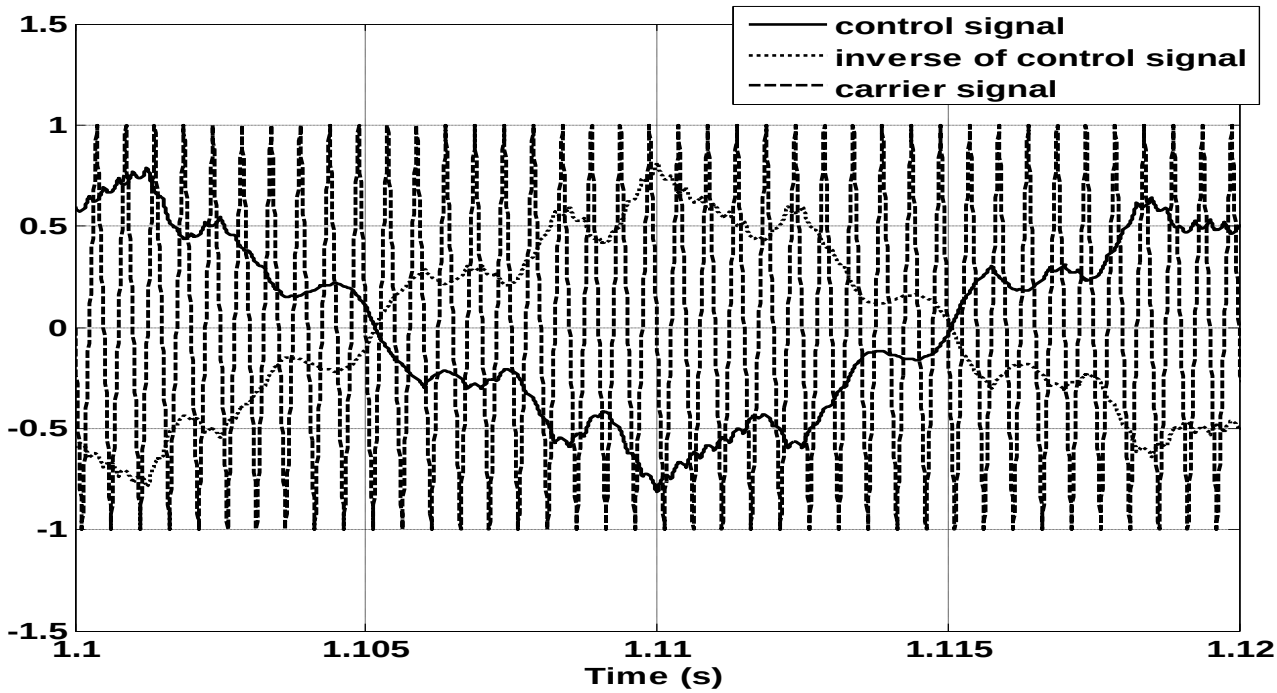
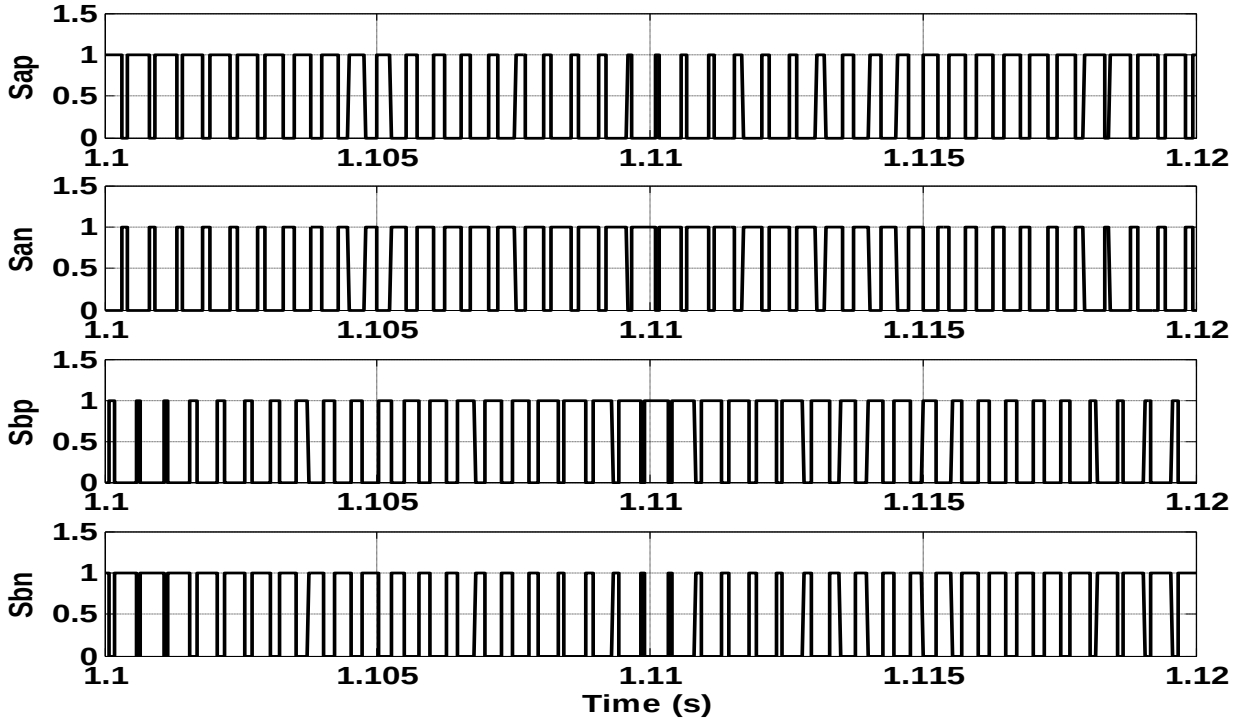


Figure 4.37: Sine–Triangular Wave Comparison of the Inverter Drive of Machine 2

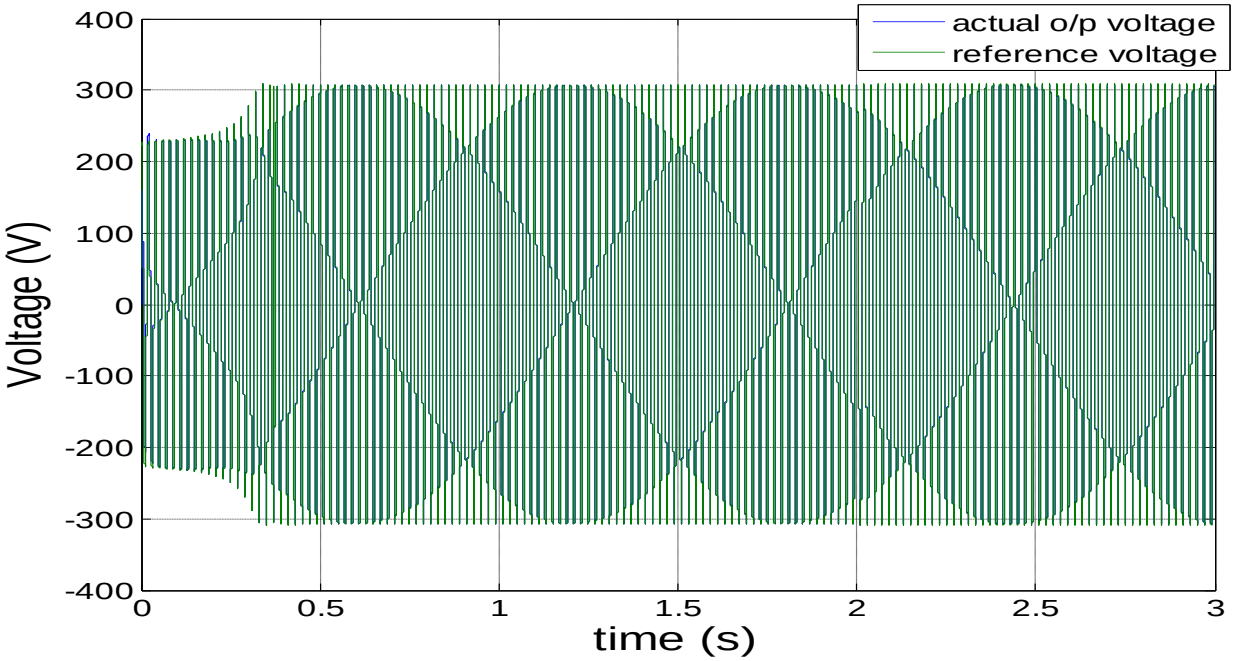
Figure 4.37shows the sinusoidal modulating or control signals and the triangular carrier wave for



one period of the control signal.

Figure 4.38: Switching Functions of the Inverter Drive for Machine 2

The PWM switching signals for the inverter drive of Machine 2 can be observed in Figure 4.38. The output voltage of the inverter is seen to be identical to the reference voltage in Figure 4.39



and 4.40.

Figure 4.39: Reference and Actual Auxiliary Winding Voltage for Inverter Drive of Machine 2

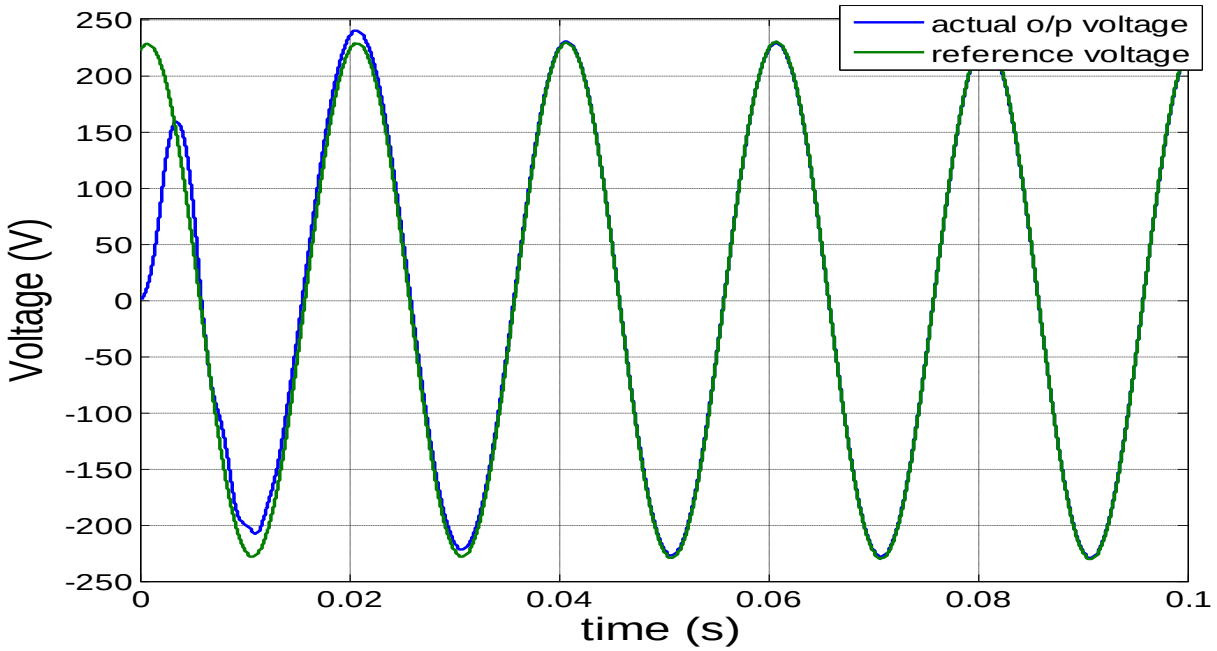


Figure 4.40: Reference and Actual Auxiliary Winding Voltage between 0 and 0.1s for Machine 2

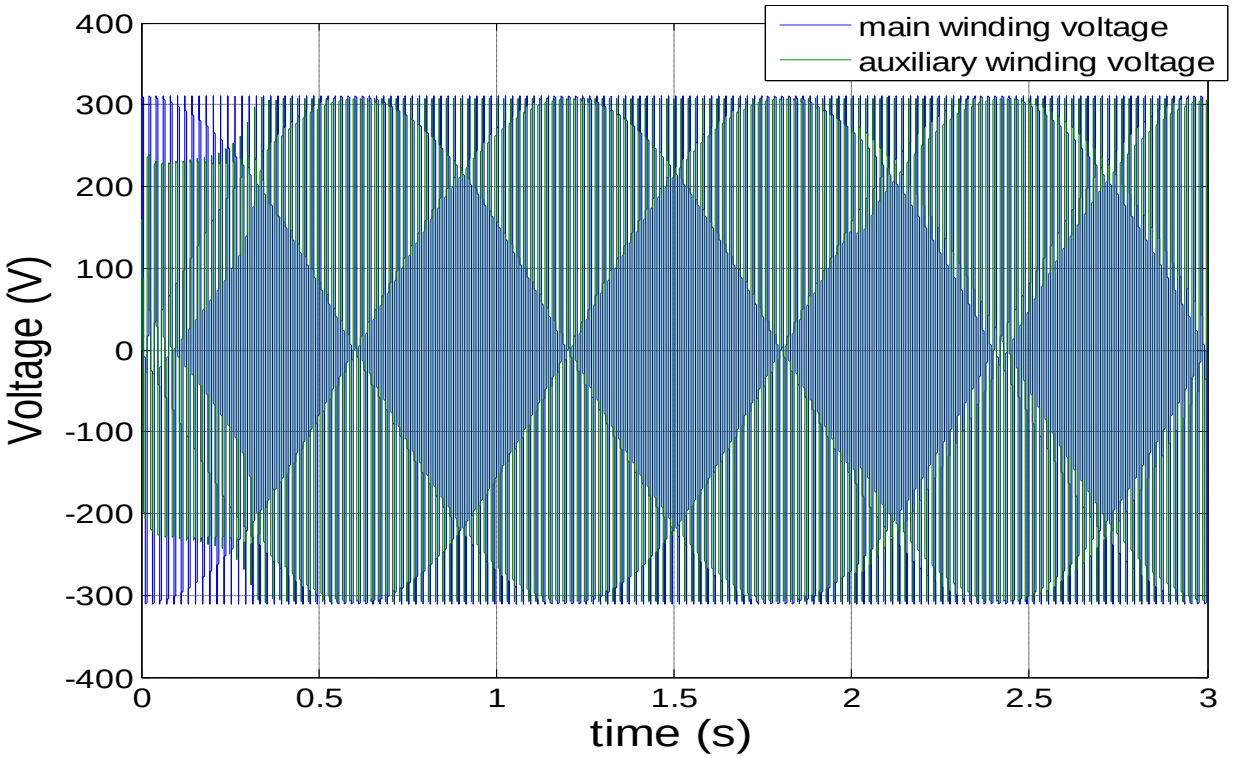


Figure 4.41: Main Winding Voltage and Auxiliary Winding Voltage for Machine 2

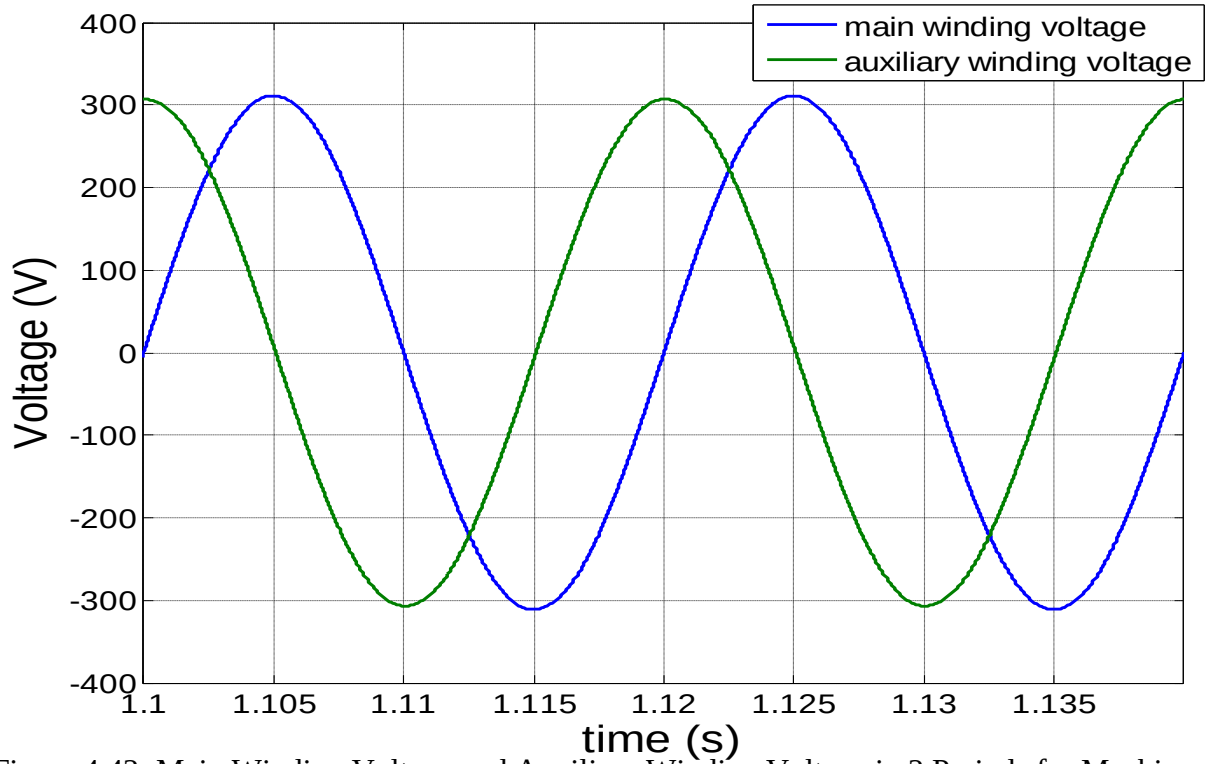
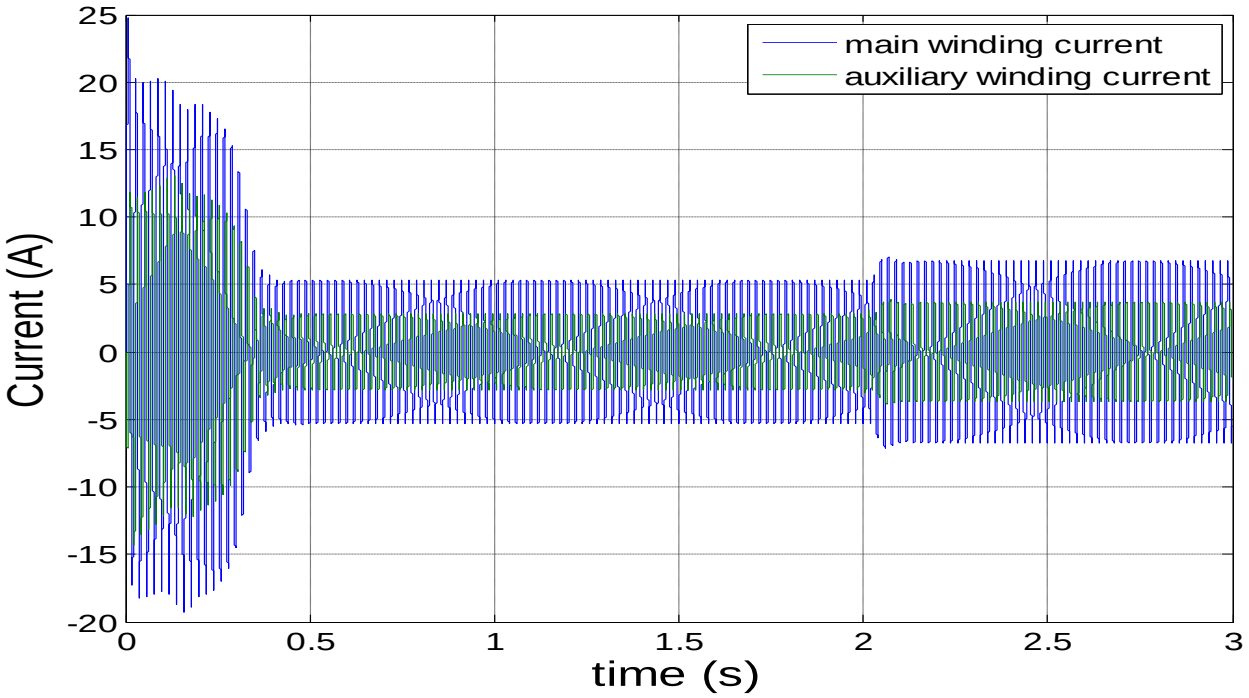


Figure 4.42: Main Winding Voltage and Auxiliary Winding Voltage in 2 Periods for Machine

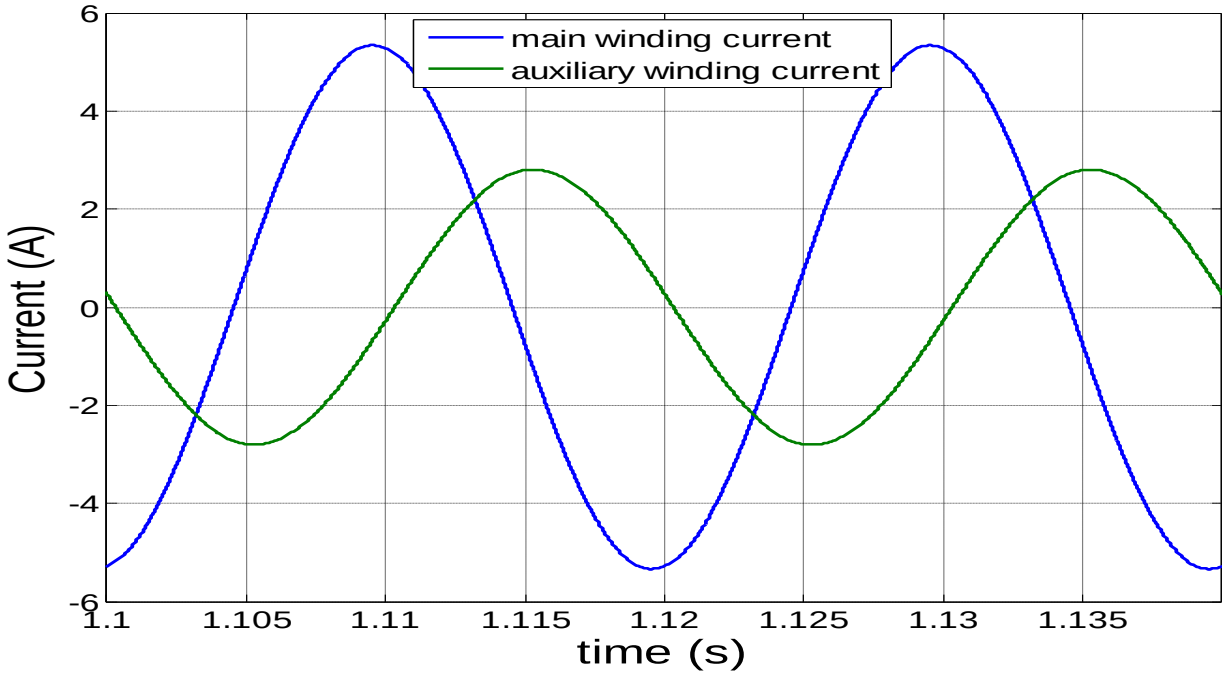
Figures 4.41 and 4.42 show that the main and auxiliary winding voltages are also balanced due to the controller action. Like the inverter drive of Machine 1, Figures 4.43 and 4.44 show the



winding currents to be unbalanced and hence torque pulsations are also not eliminated in Machine 2.

Figure 4.43: Main Winding Current and Auxiliary Winding Current for Machine 2

Figure 4.44: Main Winding Current versus Auxiliary Winding Current in 2 Periods for Machine2



4.5 SIMULATION RESULTS OF THE OPEN LOOP CONTROL STRATEGY

This section presents the results of the simulation of the Sinusoidal PWM open loop two phase inverter drive system of Figure 3.23. The dynamic torque performance results for the modified SPIM is discussed in relation to the dynamic torque performance results of the existing machine when driven conventionally and when driven by the drive scheme of Figure 3.9.

4.5.1 Dynamic Torque Performances of the Modified Single Phase Induction Machine

This subsection presents the results of the open loop control strategy of the inverter-driven modified SPIM. Figure 4.45provides the electromagnetic torque produced in the modified SPIM 1 when driven from a two phase two leg inverter under the sinusoidal PWM open loop control in the MATLAB/Simulink environment. The simulation run time was 3s and a rated load of 1Nm was applied at a time of 2s. Compared with the performances of the inverter drive schemeof Figure 3.9 and those of the machine when driven conventionally with a fixed voltage source and series-connected capacitors, it can be seen that the electromagnetic torque produced in the modified SPIM driven from a two phase two leg inverter exhibits zero torque pulsations in the steady state when the machine is not loaded and when it is loaded to its rated load of 1Nm. It can also be observed that the torque pulsations are significantly reduced in the modified SPIM during the acceleration time when the machine runs up to steady state compared to the torque pulsations in the existing machine when operating under the method of using a PWM Inverter Drive and a PID Controller as shown in Figure 4.21 and when line-operated as shown in Figure 4.22.

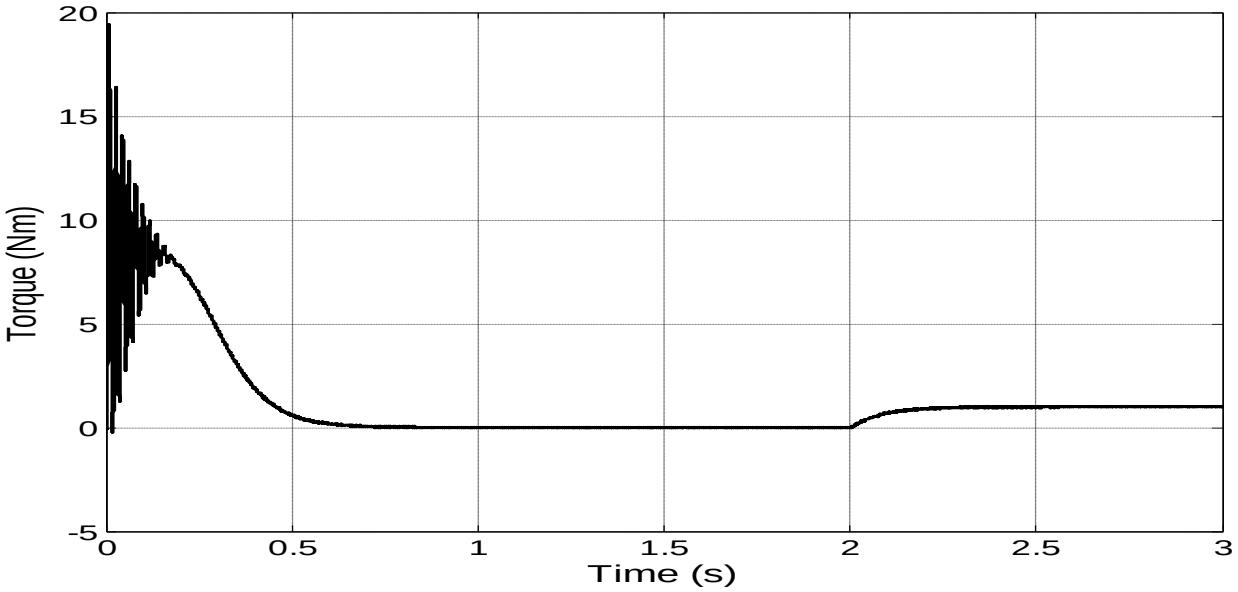


Figure 4.45: Dynamic Torque of the Inverter-Driven Modified SPIM 1 with Open Loop Control

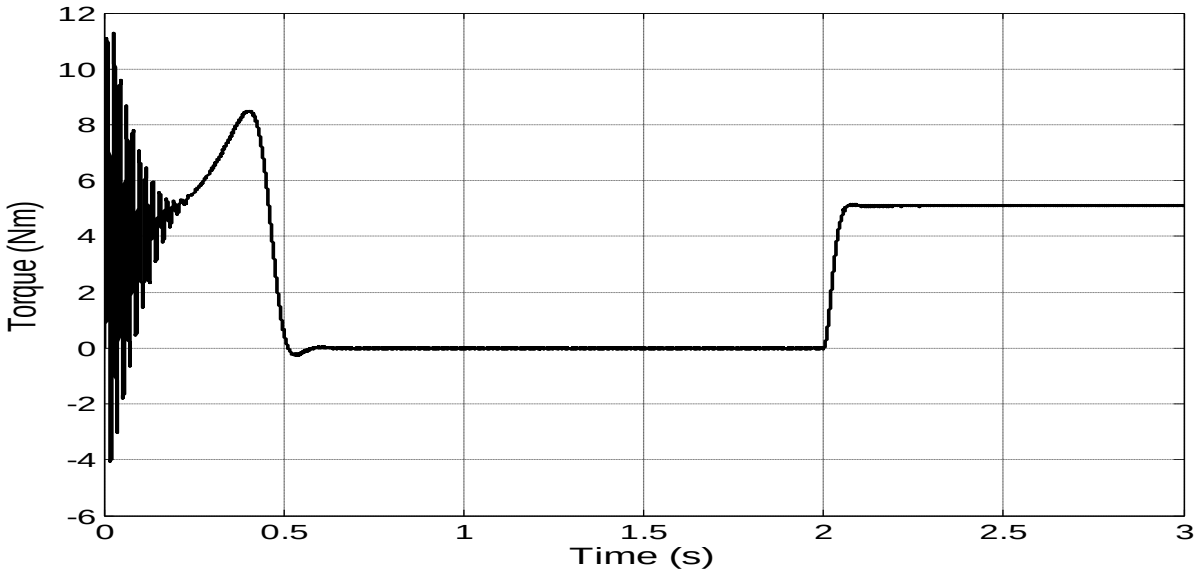


Figure 4.46: Dynamic Torque of the Inverter-Driven Modified SPIM 2 with Open Loop Control

Figure 4.46 gives the electromagnetic torque produced in the modified SPIM 2 when driven from a two phase two leg inverter under the sinusoidal PWM open loop control in the MATLAB/Simulink environment. The simulation run time was 3s and a rated load of 5.1Nm was applied at a time of 2s. Compared with the performances of the existing machine when the existing machine is driven under the method of using a PWM Inverter Drive and a PID

Controller and when the existing machine is line-operated with series-connected capacitors, it can be seen that the electromagnetic torque produced in the modified SPIM driven from a two phase two leg inverter exhibits zero torque pulsations in the steady state when the machine is not loaded and when it is loaded to its rated load of 5.1Nm. It can also be observed that the torque pulsations are significantly reduced in the modified SPIM during the acceleration time when the machine runs up to steady state compared to the torque pulsations in the existing machine when it is operating under the drive scheme of Figure 3.9 as shown in Figure 4.25 and when it is line-operated as shown in Figure 4.26.

It is clear from Figures 4.45and4.46 that the modified SPIM driven from a two leg two phase inverter under the sinusoidal PWM open loop control exhibits significantly improved torque performance over that of the existing CRSPIM. Figure 4.47shows the sinusoidal modulating or control signals and the triangular carrier wave for one period of the control signal. The point of intersection between the sinusoidal signals and the triangular carrier wave determine the switching instants of the semiconductor devices of the inverter. The result of the sine –triangular comparison is the set of pulses shown in Figure 4.48 which control the switching of the devices in such a manner that the inverter synthesizes an output similar to the control signal.

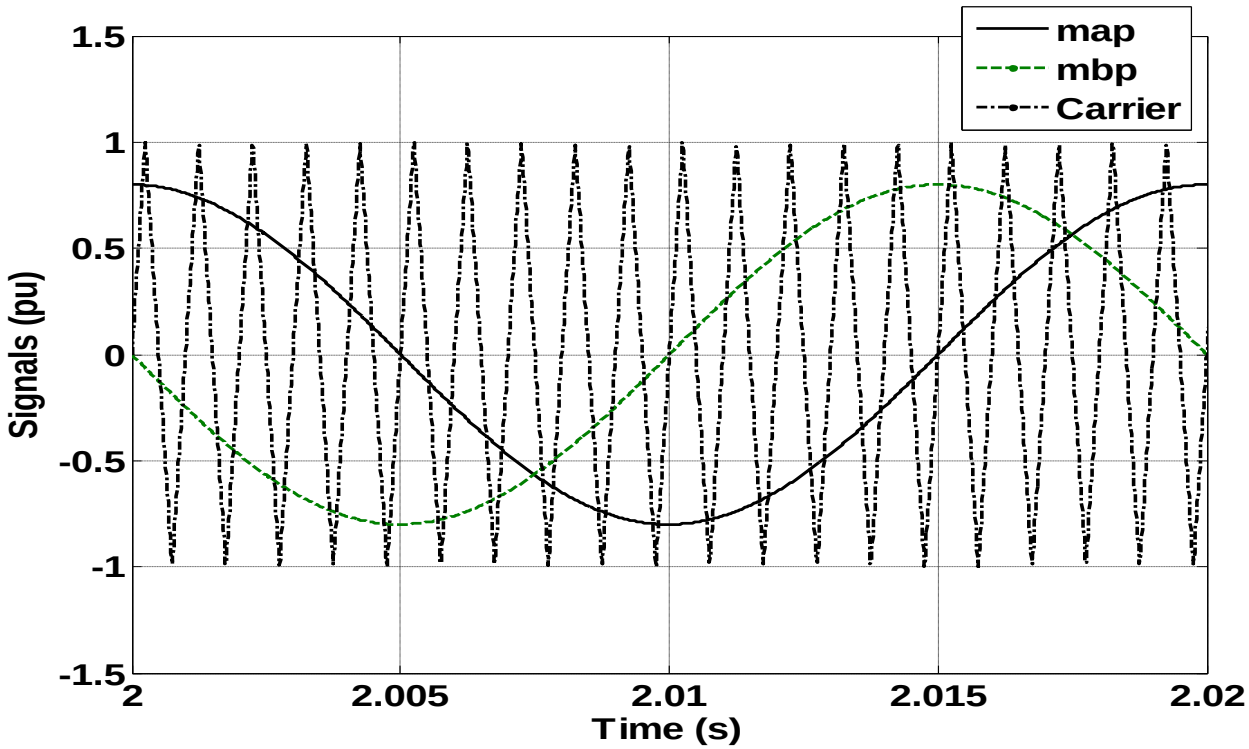
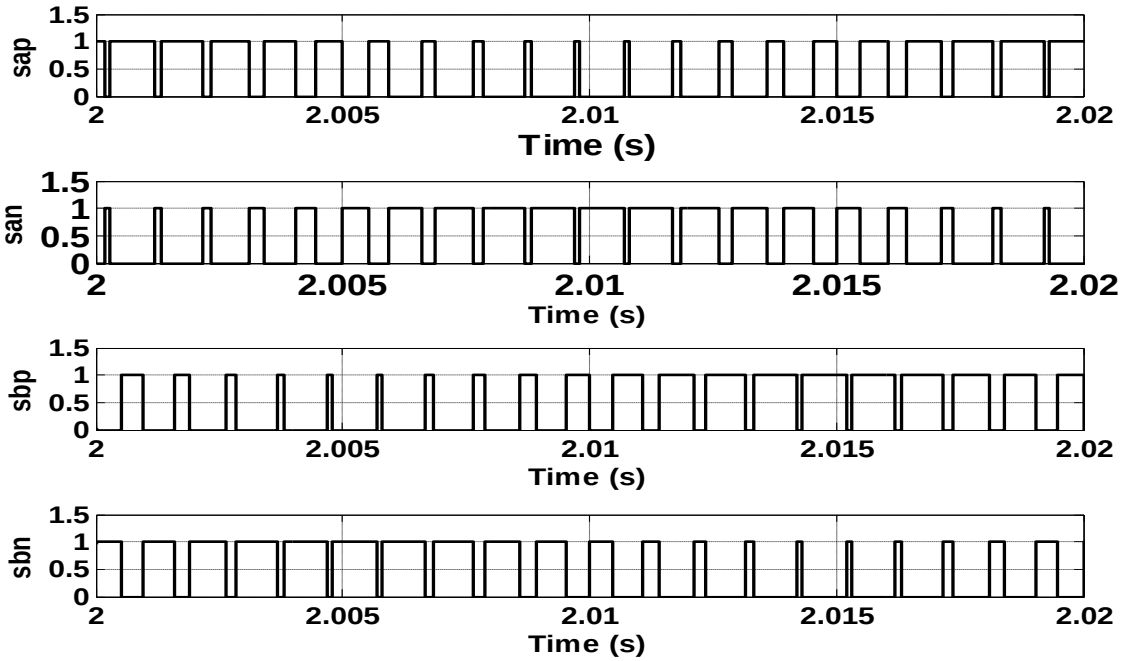


Figure 4.47: Sine–Triangular Wave Comparison of the Inverter Drive of the Modified SPIM2

Figure 4.48 shows the switching functions of the inverter as obtained from the PWM algorithm in a period of the modulating signal. It can be observed that the pulses have varying width and this variation is in accordance with the amplitude of the control signal.



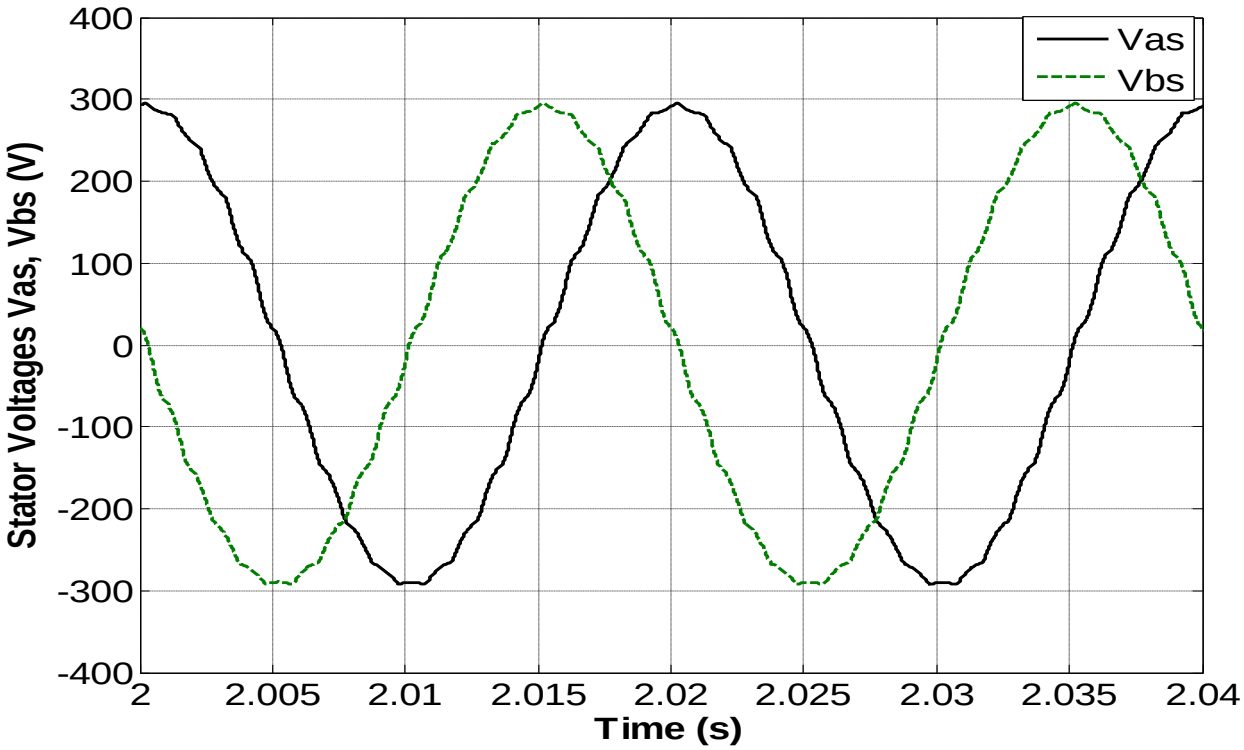
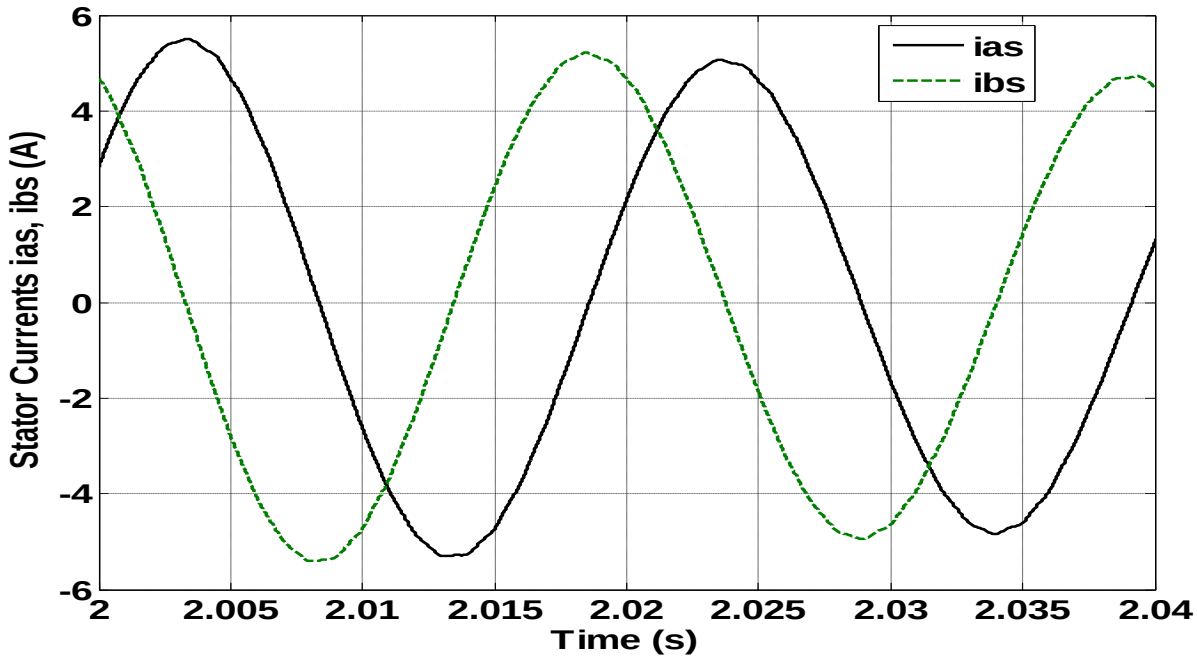


Figure 4.48 Switching Functions of the Inverter Drive of Modified SPIM 2

Figure 4.49: Stator Winding Voltages of Modified SPIM 2 over 2 Periods

Figure 4.49 shows the stator winding voltages V_{as} and V_{bs}supplied by the two phase inverter for the period between 2s and 2.04s. It can be seen that the winding voltages are 90^0 apart in time and that their magnitudes are equal. In other words, the voltages are balanced. Figure 4.50 shows the corresponding currents in the two stator windings. It can be observed that the stator winding currents are balanced as well. The supply of balanced voltages and currents to



symmetrical or balanced windings on the stator explains why the torque pulsations are eliminatedin steady state.

Figure 4.50: Stator Winding Currents in the Modified SPIM 2 for 2 Periods.

4.6 VARIATION OF ROTOR FLUX WITH ELECTRICAL LOSS AND EFFICIENCY IN THE MODIFIED SPIM

Figure 4.51 shows the result of investigation of the variation of rotor flux with electrical loss in the machine for three different load torques at rated speed for the modified SPIM with its parameters as provided in Table 3.4.

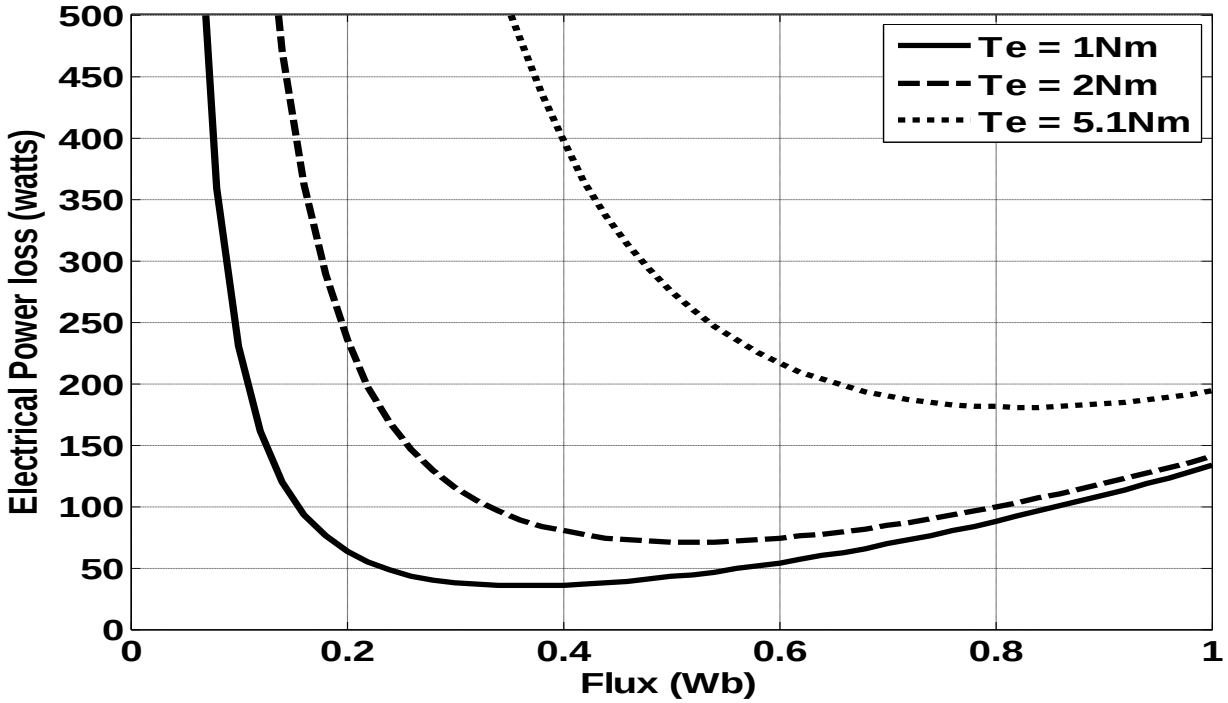


Figure 4.51: Electrical Power Loss versus Flux at Rated Speed for Rated, 2Nm and 1Nm Load Torques

It can be observed in Figure 4.51 that for a given rated speed, the electrical power loss increases with load torque on the machine. This is because copper loss increases as load on the machine increases. Figure 4.51 also shows that there is an optimum flux for which electrical loss in the

machine is minimized and therefore for which efficiency is maximized for a given load torque and rated speed. In particular, the optimal flux and corresponding minimum loss for loads of 5.1Nm, 2Nm and 1Nm are respectively (0.82Wb, 180.63W), (0.52Wb, 70.85W) and (0.36Wb, 35.43W).

The graph of efficiency versus flux in the machine is depicted in Figure 4.52. It can be seen that for the three different load torques considered, although there are different optimum flux values, the maximum efficiency is the same. The value of the efficiency is 81.05% for all the three load torques at rated speed.

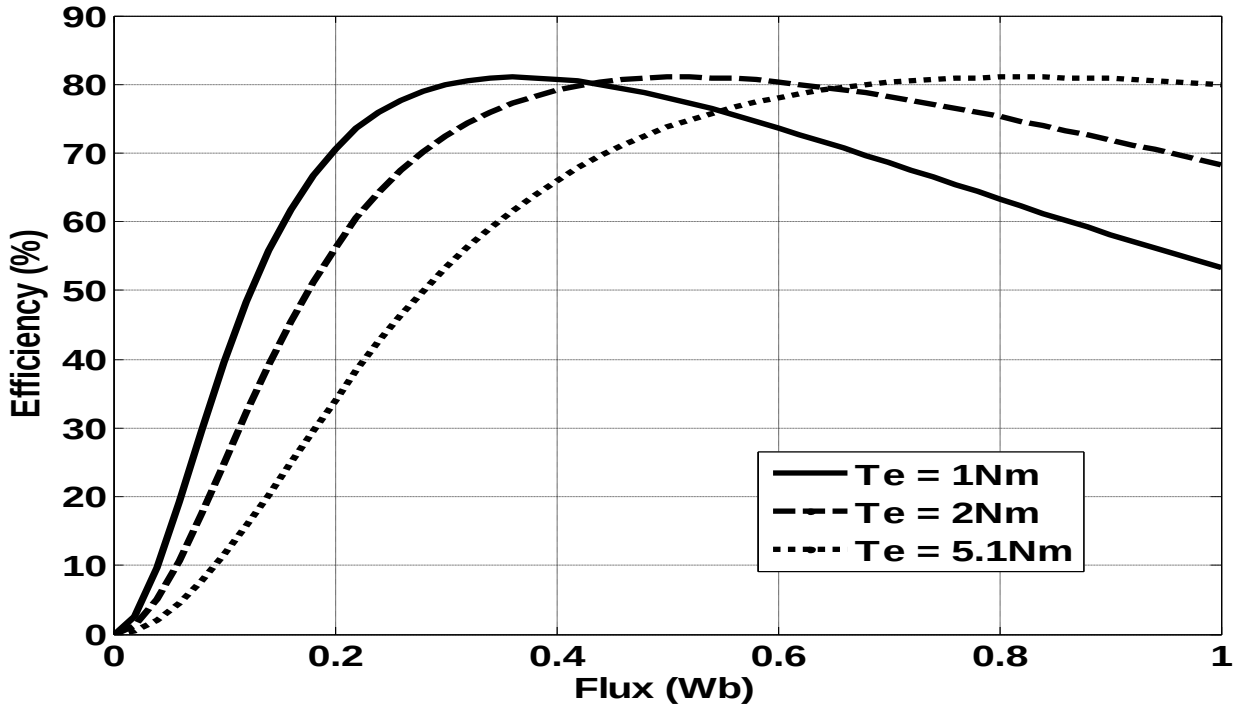


Figure 4.52: Efficiency versus Flux for for Rated, 2Nm and 1Nm Load Torques

4.7 SIMULATION RESULTS OF THE EFFICIENCY OPTIMIZING VECTOR-CONTROLLED STRATEGY

This section presents the simulation results of the modified SPIM performance under the efficiency-optimizingvector controlledscheme of Figure 3.29. In order to evaluate the effect of this scheme on motor performance, rated load of 5.1Nm was first applied on the machine at steady state. The load was then reduced to 2Nm and then to 1Nm at a steady state motor speed of 1447 rpm. This pattern is chosen because it is of interest in this work to compare the performance of the modified SPIM under the proposed scheme to the performance of the existing CRSPIM at rated load and at non-rated loads or light loads. It is noted that the existing CRSPIM performs poorly under light loads or non-rated conditions. Figure 4.53 shows the load torque applied on the existing CRSPIM and the modified SPIM.

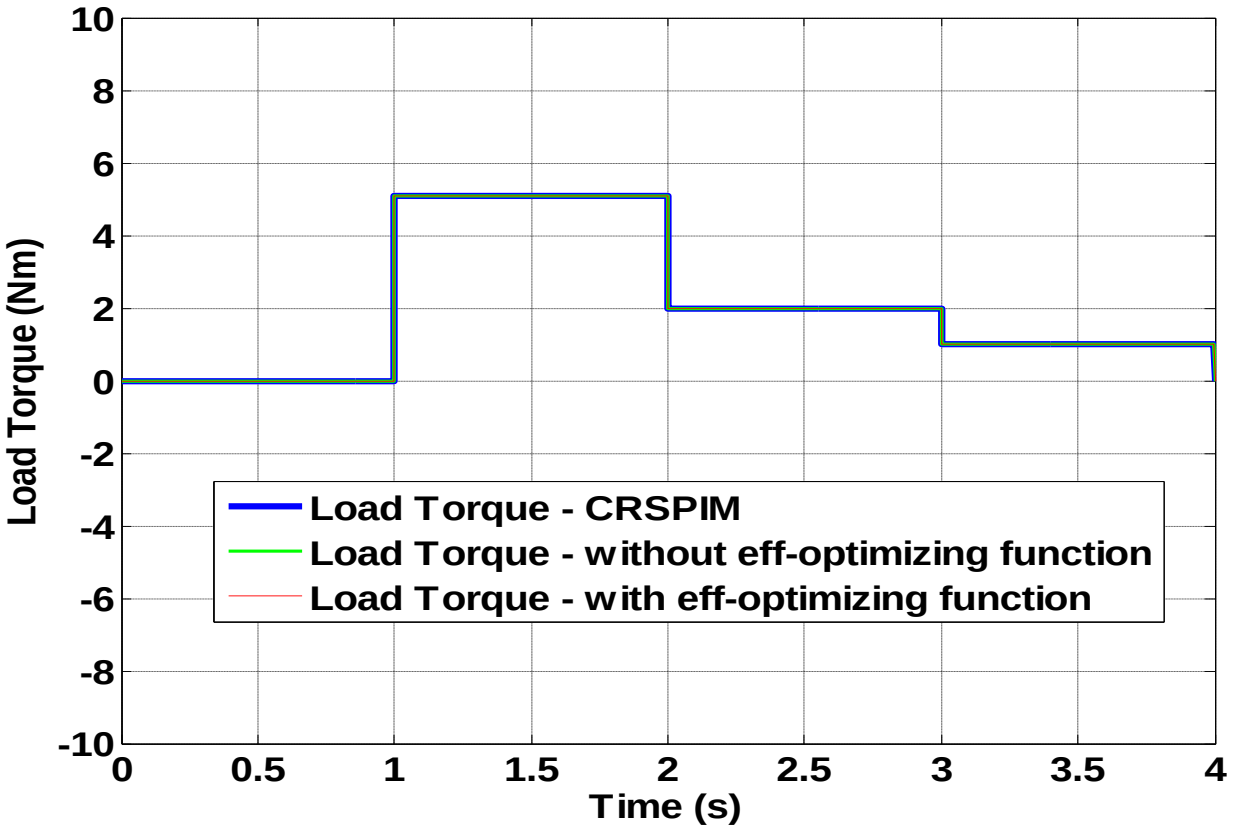
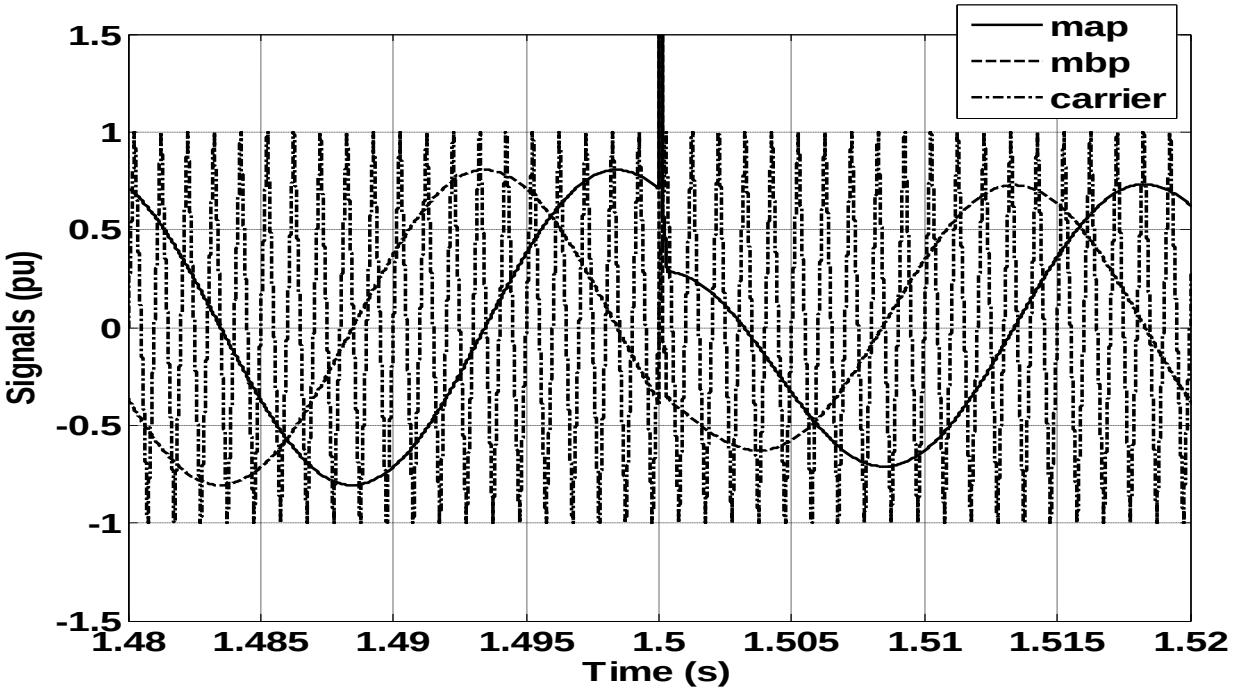


Figure 4.53: Load Torque Applied to the CRSPIM 2 and the Modified SPIM2

It can be seen that a rated load of 5.1Nm was applied on the machine at steady state at a time of 1s and this load remained on the machine until a time of 2s at which time the load is changed to 2Nm. The 2Nm load was applied for 1s. Finally, the load was reduced to 1Nm at 3s and the 1Nm load remained on the machine until the end of simulation time of 4s. During this time, the electrical torque produced in the machines is same as the applied load torque in accordance with equation (2.20). The efficiency-optimizing function was initiated at a time of 1.5s. The total run time was 4s. The performances of the modified SPIM with and without the efficiency-optimizing function are compared with the performances of the existing machine in the same Figures. The performances of interest are the electromagnetic torque produced, speed, flux, electrical power loss, efficiency and the input power to the machines.

Figure 4.54shows the sinusoidal modulating or control signals and the triangular carrier wave for two periods of the two control signals. It can be observed that the modulating signals are 90^0 apart in time. The application of these modulating signals to the pulse width modulated two phase inverter produces a balanced set of two phase voltages. The two phase voltages as synthesized by the two phase inverter are as given in Figure 4.55. A transient is noticeable at the



time of initiation of the efficiency-optimizing function.

Figure 4.54*:* Sine–Triangular Wave Comparison of the Vector-Controlled Drive of the Modified SPIM 2

Figures 4.55 shows a balanced set of two phase voltages V_{as} and V_{bs} supplied to the stator windings by the two phase inverter. The voltages are given for the period between 1.48s and 1.52s. It is seen that the winding voltages are 90^0 apart in time and that their magnitudes are equal. When these voltages are supplied to the symmetrical windings of the modified SPIM, they produce a balanced set of two phase currents i_{as} and i_{bs}. These currents are shown in Figure 4.56.

It can be observed that the stator winding currents are balanced. Transients are also noticeable at the time of initiation of the efficiency-optimizing function.

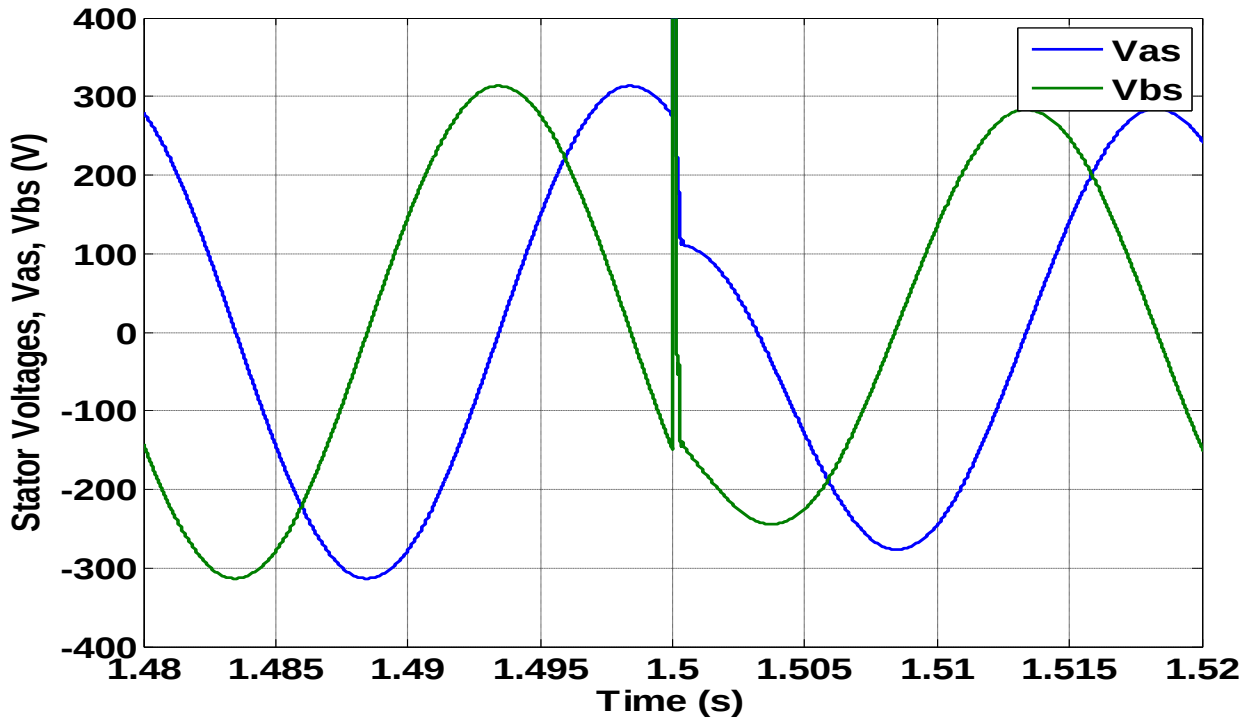
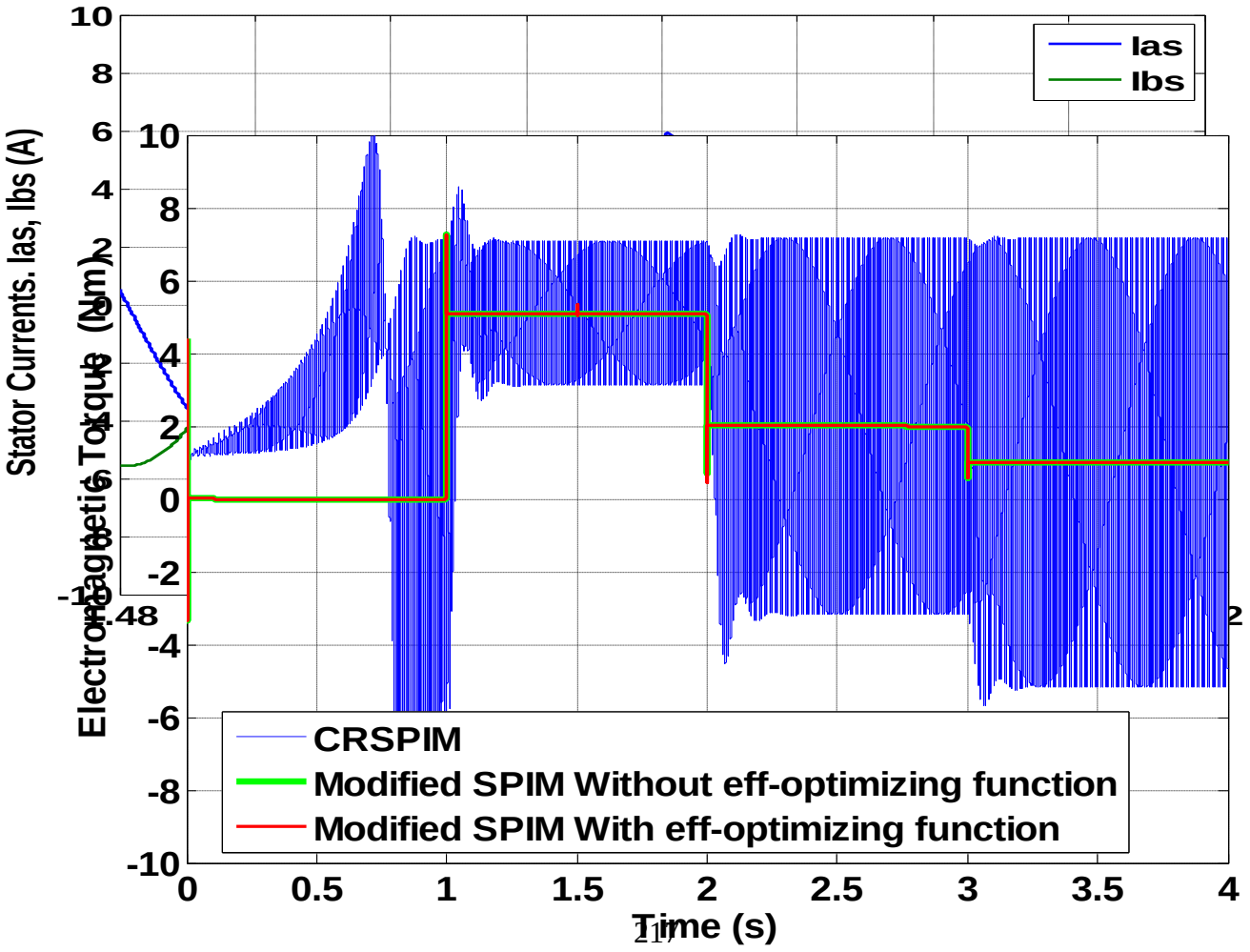


Figure 4.55: Stator Winding Voltages in the Modified SPIM 2 for 2 Periods

Figure 4.56: Stator Winding Currents in the Modified SPIM 2 for 2 Periods

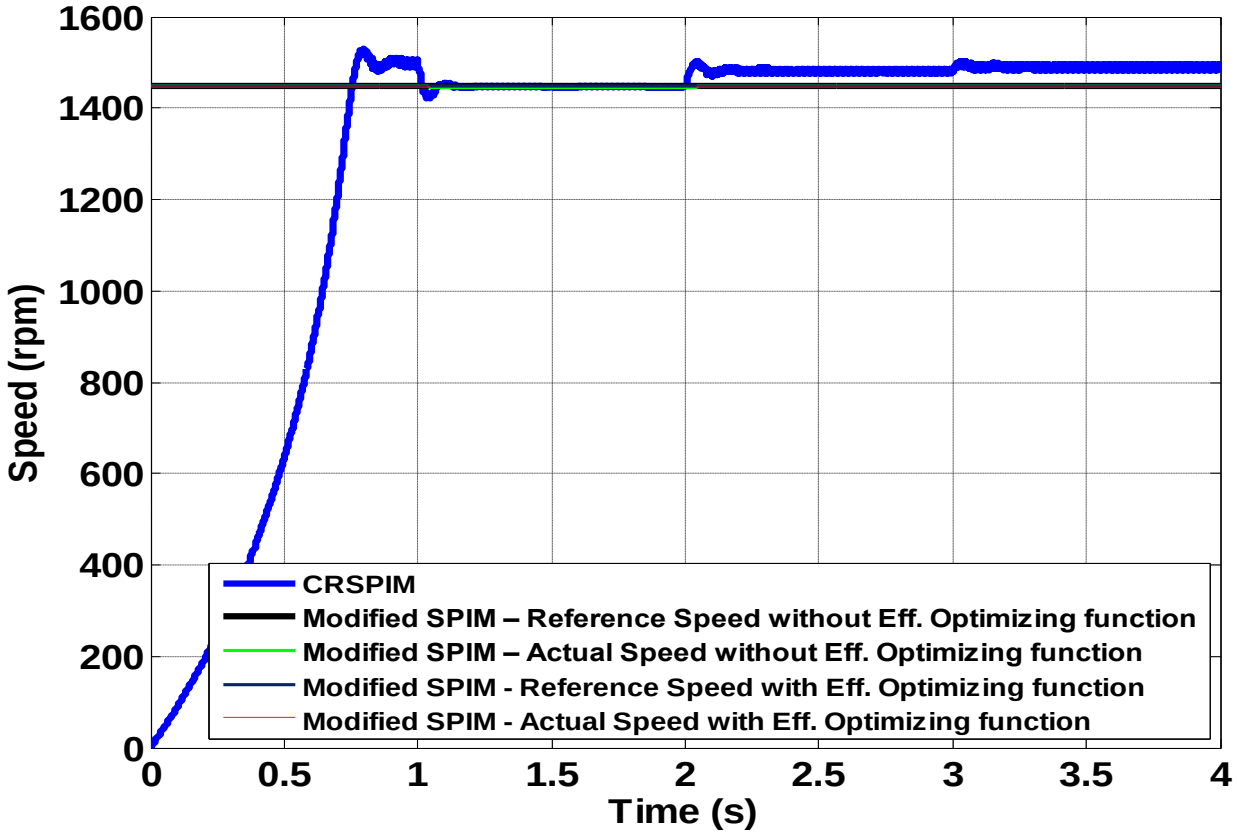
Figure 4.57 shows the electromagnetic torque produced in the existing CRSPIM and the modified SPIM upon application of 5.1Nm, 2Nm and 1Nm loads at 1s, 2s and 3s respectively. It can be observed that torque pulsations are present in the CRSPIM and they increase as load reduces on the machine. This is due to the asymmetry in the stator windings and the application of unbalanced voltages and currents to the windings. It can be observed also, that there are no pulsations in the torque produced in the modified SPIM and this is consistent with the result of



the open loop PWM control of the modified SPIM given in section 4.5. The pulsations are eliminated because of the symmetry in the windings of the modified SPIM and the application of balanced currents to the modified windings.

Figure 4.57: Electromagnetic Torque Produced in the CRSPIM 2and the Modified SPIM 2

Figure 4.58 shows the rated speed command and actual motor speed with time, of the vector-controlled modified SPIM at steady state speed of 1447 rpm. It can be observed that motor speed remained constant at 1447 rpm regardless of changes in load torque. This is due to the speed controller action. The figure also shows the speed of the CRSPIM with time. It can be observed that CRSPIM accelerates from rest to steady state speed of 1500 rpm in a time of 0.85s. The speed reduces to 1447 rpm when rated load of 5.1Nm is applied. It, however, rises to 1480 rpm and 1492 rpm after the load on the machine is dropped to 2Nm and 1Nm respectively. The line operated CRSPIM's speed is uncontrolled. The vector-controlled Modified SPIM, on the other hand, has a robust speed control. With speed command input, motor speed is set to rated speed



and acceleration time is reduced to zero.

Figure 4.58 Speed with Time in the CRSPIM 2 and the Modified SPIM 2

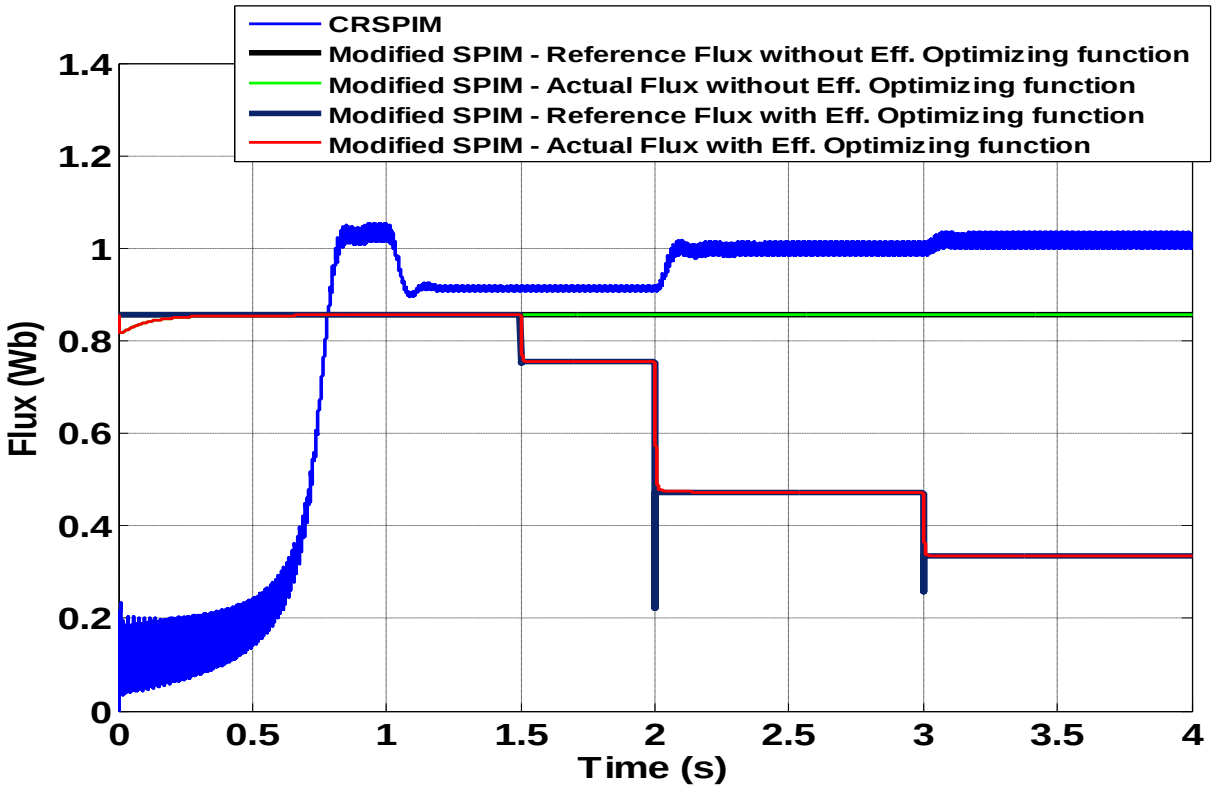
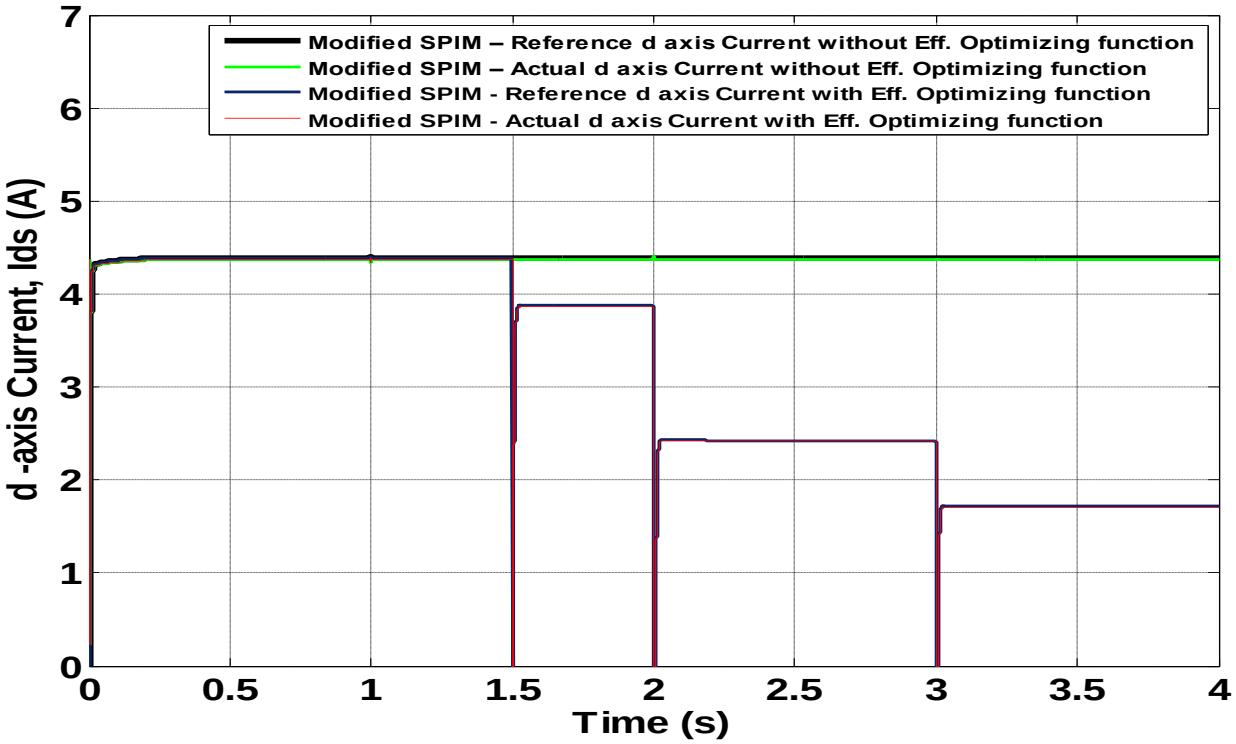


Figure 4.59: Flux in the CRSPIM 2 and the Vector-Controlled Modified SPIM 2 with Time

Figure 4.59 shows the flux in the machines. It is seen that the flux in the vector-controlled modified SPIM without the efficiency-optimizing function remains constant at value of 0.85Wb and it is independent of the load applied on the machine. With the efficiency-optimization scheme initiated in the vector-controlled modified SPIM, it is seen that the flux is regulated to its optimal value for each load torque. The optimal flux when driving the 5.1Nm load is seen to be 0.76Wb. When driving a 2Nm load, the optimal flux is 0.48Wb while optimal flux at 1Nm load is 0.34Wb. These values are significantly lower than the values of flux levels in the CRSPIM for the corresponding loads as seen in the figure. The flux in the CRSPIM is steady at approximately 0.9Wb with rated load applied to the motor. The flux level rises to 1Wb when the load on the

machine is reduced to 2Nm. The level of flux increases slightly above 1Wb when the applied load is further reduced to 1Nm. The reduction in flux levels between the CRSPIM and the



vector-controlled modified SPIM at loads of 5.1Nm, 2Nm and 1Nm is 21%, 55% and 68% respectively. The actual flux in the modified SPIM can be seen to follow its reference faithfully. Pulsations can be observed in the flux of the CRSPIM with time as the machine accelerates to steady state.

Figure 4.60: Reference and Actual d-axis Current in the Vector-Controlled Modified SPIM 2

Figure 4.60 depicts the *d*-axis stator current before and after the efficiency-optimizing function is initiated. The value of the *d*-axis stator current is constant at 4.4A in steady state and it is independent of load on the machine without the efficiency-optimizing function. When this function is initiated however, as with the flux in the machine, the *d*-axis stator current is seen to now vary with load torque. The value has reduced to 3.85A from 4.4A for the rated load and

correspondingly reduced to 2.43A and 1.72A for the 2Nm and 1Nm load respectively. Transients are noticeable at the instant of initiation of the efficiency-optimizing function. Transients are also noticeable at the instant of change in load torque.

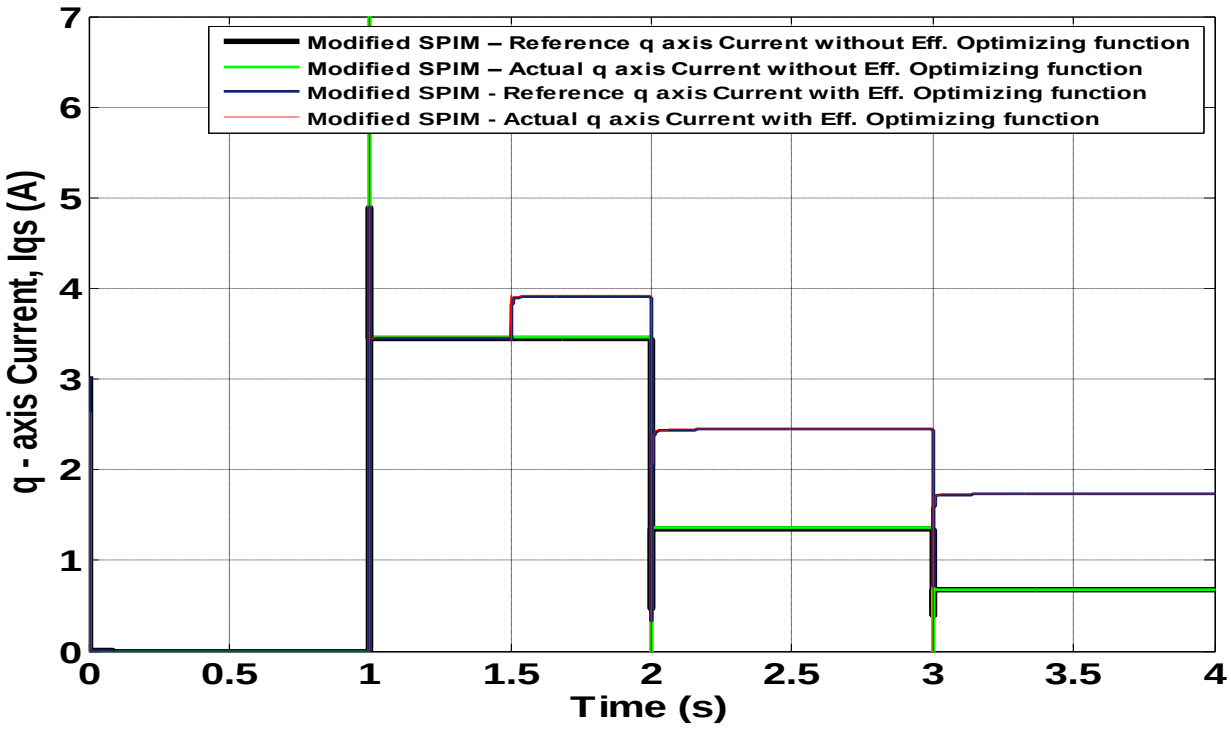


Figure 4.61: Reference and Actual q-axis Current in the Vector-Controlled Modified SPIM 2

Figure 4.61 gives the *q*-axis stator current of the vector-controlled modified SPIM. The values of the *q*-axis currents change with load torque with and without the efficiency-optimizing function. The value is, however, higher in the case after the efficiency–optimizing function is initiated. It can be seen in Figure 4.61 that the *q*-axis stator current increased to 3.9A from 3.4A for the rated load. For the 2Nm and 1Nm loads, the *q*-axis stator current increased from 1.36A to 2.4A and

from 0.68A to 1.72A respectively. The reason for this is because the *q*-axis current is inversely proportional to the flux in the machine in accordance with equation (3.139).

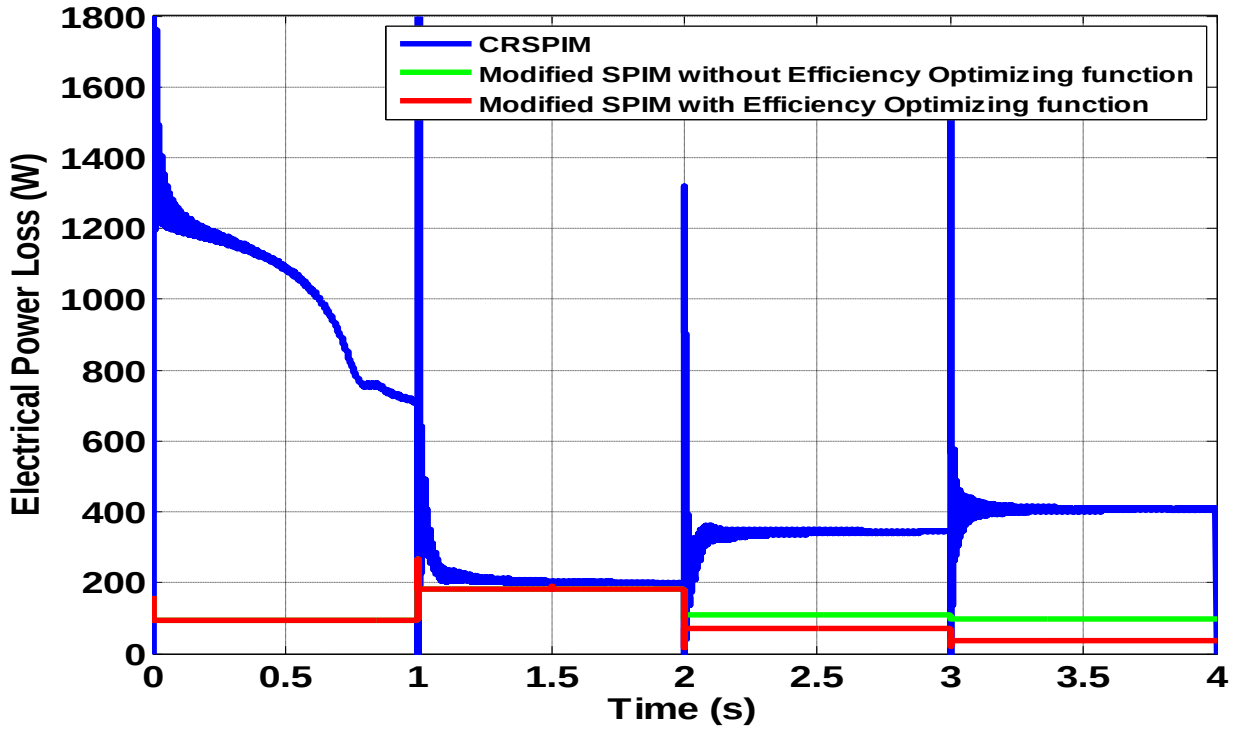
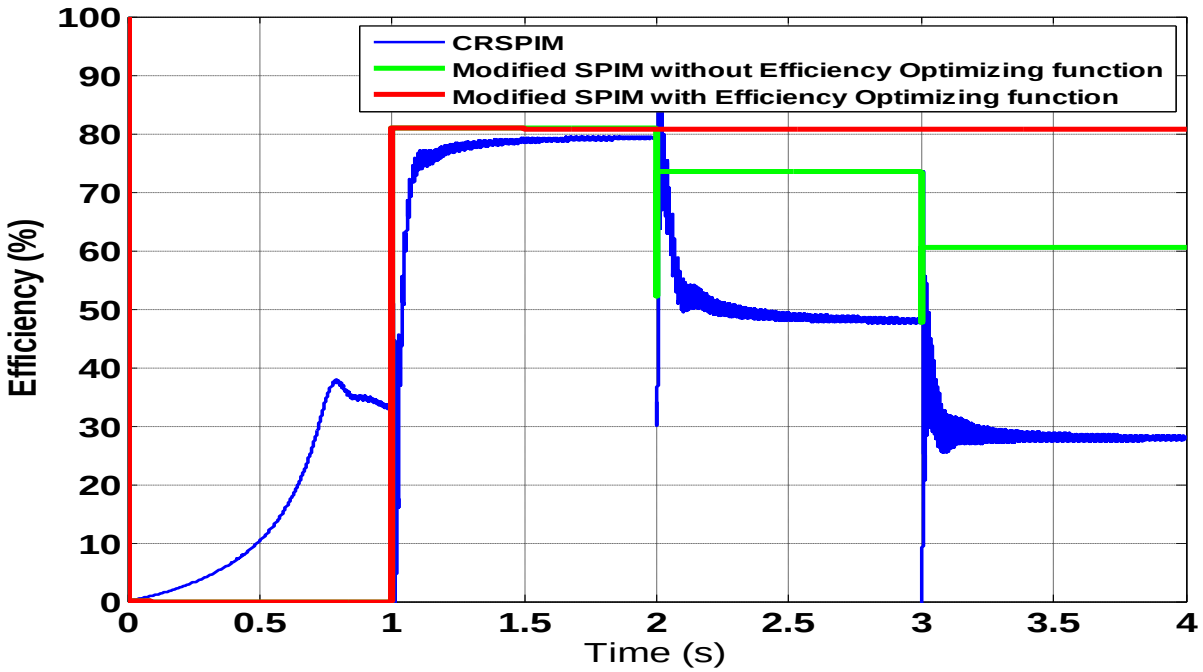


Figure 4.62: Electrical Power Loss in the CRSPIM and the Vector-Controlled Modified SPIM 2 with Time

The electrical loss in the existing CRSPIM is shown in Figure 4.62.It can be observed that the total loss is highest at the time of starting, reaching about 1200W. The loss reduces as the motor accelerates with no-load applied. At steady state however, it increases with reducing load. The electrical loss in the CRSPIM when driving rated load, 2Nm and 1Nm at steady state is 200 W, 340 W and 410 W respectively. For the vector-controlled modified SPIM however, the electrical power loss at no-load is extremely low. The value is 80W.At steady state when driving loads of 5.1Nm, 2Nm and 1Nm, the value of the lossis 182 W, 110 W and 100 W respectively without the efficiency-optimizing function. The total loss is seen to reduce as load on the machine reduces because copper loss is proportional to the load current. The electrical loss at rated speed for the 5.1Nm load torque, 2Nm and 1Nm load after the initiation of the optimizing function is also

depicted in Figure 4.62. It can be observed that the electrical power loss when driving the 5.1Nm load increased only slightly to 184W after the initiation of the efficiency-optimizing function. There is a very significant drop in total electrical loss for light loads of 2Nm and 1Nm as the electrical loss dropped from 110W to 73W and from 100W to 37W after initiating the efficiency optimizing function respectively for the 2Nm and 1Nm loads. Comparing the loss levels of the modified SPIM under the proposed efficiency-optimizing vector control scheme to those of the CRSPIM, it is seen that the reduction in loss levels is 79% and 91% for the 2Nm and 1Nm loads respectively with respect to the loss levels in the CRSPIM at the corresponding loads. For rated load of 5.1Nm, the electrical loss is less by 8% in the efficiency-optimizing vector-controlled



modified SPIM when compared to the electrical loss in the CRSPIM. The additional reduction in electrical loss at light loads occurs because core losses in the machine have been minimized as a consequence of the reduction of flux levels in the machine to optimal levels for each load.

Figure 4.63: Efficiency in the CRSPIM 2 and the Vector-Controlled Modified SPIM 2 with Time

The efficiency at rated speed for the 5.1Nm, 2Nm and 1Nm load in steady state for both the modified SPIM and the CRSPIM is given in Figure 4.63. It can be observed that the efficiency of the vector-controlled modified SPIM when driving loads of 5.1Nm, 2Nm and 1Nm without the efficiency-optimizing function is 81%, 73.5% and 61% respectively. These values are higher than the values of the efficiency of the CRSPIM at corresponding loads. It can be observed that the efficiency of the CRSPIM at rated load of 5.1Nm is 79.3%. While carrying loads of 2Nm and 1Nm, the CRSPIM has efficiency of 47% and 28% respectively. The improvement in efficiency is attributable to the change in machine winding parameters and the action of the inverter to produce stator voltages and currents of equal magnitude and phase difference of 90^0. Figure 4.63 also shows the effect of the initiation of the efficiency-optimizing function on the vector-controlled modified SPIM. The efficiency of the machine under the proposed drive scheme is maximized to a level of 80.8% regardless of the load torque. The value of the machine efficiency drops slightly by 0.2% after the initiation of the efficiency-optimizing function for the rated load of 5.1Nm. For this load, the value of efficiency is 1.5% higher in the vector-controlled modified SPIM than in the CRSPIM. This improvement is not as significant as the improvement in efficiency for light loads of 2Nm and 1Nm. The improvements are 33.8% and 52.8% respectively for the 2Nm and 1Nm loads in the efficiency-optimizing vector-controlled modified SPIM over the efficiency of the CRSPIM when driving the same loads.

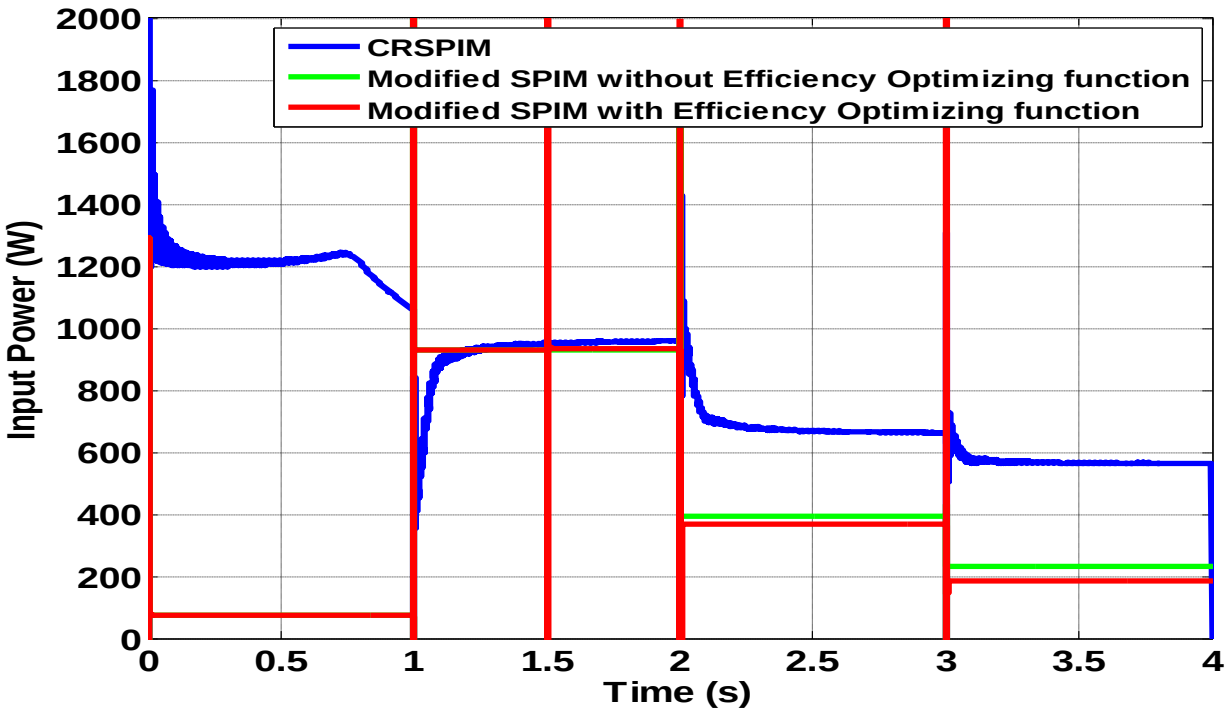
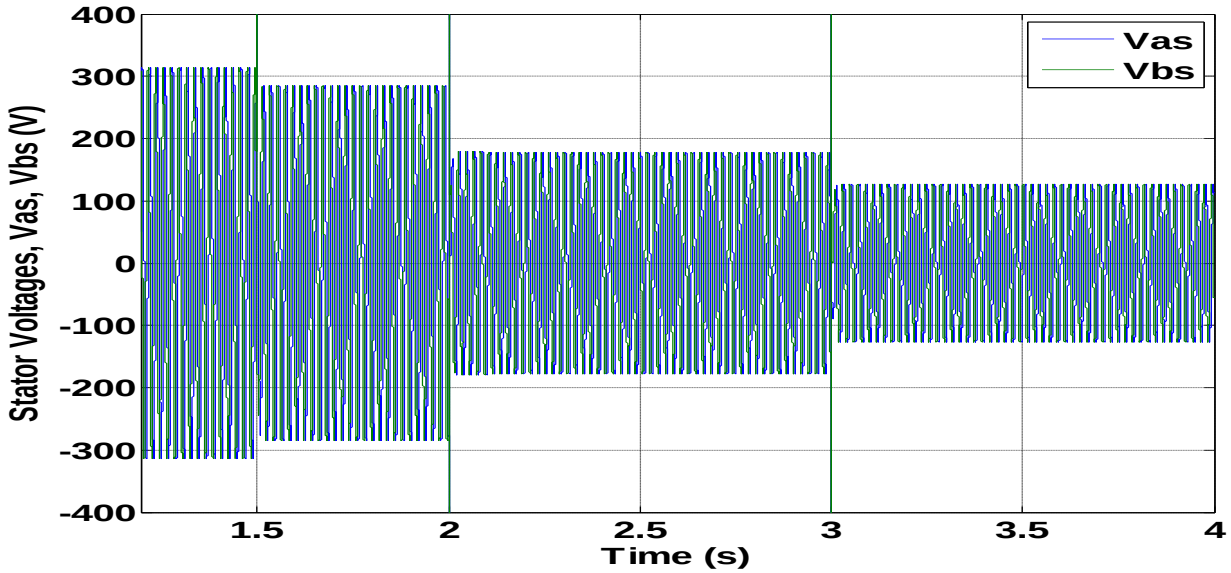


Figure 4.64: Input Power in the CRSPIM 2 and the Vector-Controlled Modified SPIM 2 with Time

The input power in the CRSPIM and the vector-controlled modified SPIM is shown in Figure 4.64. It can be observed that the CRSPIM consumes a large amount of power, about 1200W during the acceleration time under no load. The power input however reduces at steady state. For loads of 5.1Nm, 2Nm and 1Nm, the input power is 950 W, 670 W and 565 W respectively. In the efficiency-optimized modified SPIM, the power consumed at steady state for the same loads is 935 W, 368 W and 183 W respectively. This is a significant improvement over the power input to the CRSPIM, especially at light loads. The improvement in power consumption in the modified SPIM over that of the CRSPIM is 1.6%, 45.1% and 67.6% when driving loads of

5.1Nm, 2Nm and 1Nm respectively. The reduction in input power to the machine implies a significant amount of energy savings over the period of machine utilization, especially when a large number of such machines are considered. At no-load, the power input to the efficiency-optimized modified SPIM is as low as 80W. In order to understand the reason for the reduction



in power consumed in the modified SPIM under the efficiency-optimizing vector-controlled method, it is important to examine the input voltage across the stator windings and the winding currents of the machine. The voltages across the stator windings of the modified SPIM under the efficiency-optimizing vector-controlled scheme are shown in Figures 4.65.

Figure 4.65: Stator Voltages of the vector-controlled Modified SPIM 2 with the Efficiency-Optimizing Function

It can be seen in Figure 4.65 that the efficiency-optimizing function is initiated at 1.5s. It is also seen that the magnitude of the stator voltages reduces with load on the machine as an inherent energy saving measure of the proposed vector control strategy. The reduction in voltage is a direct

result of the significant reduction in flux to its optimal levels for each load. The stator voltages across the CRSPIM with time, on the other hand, are depicted in Figure 4.66.

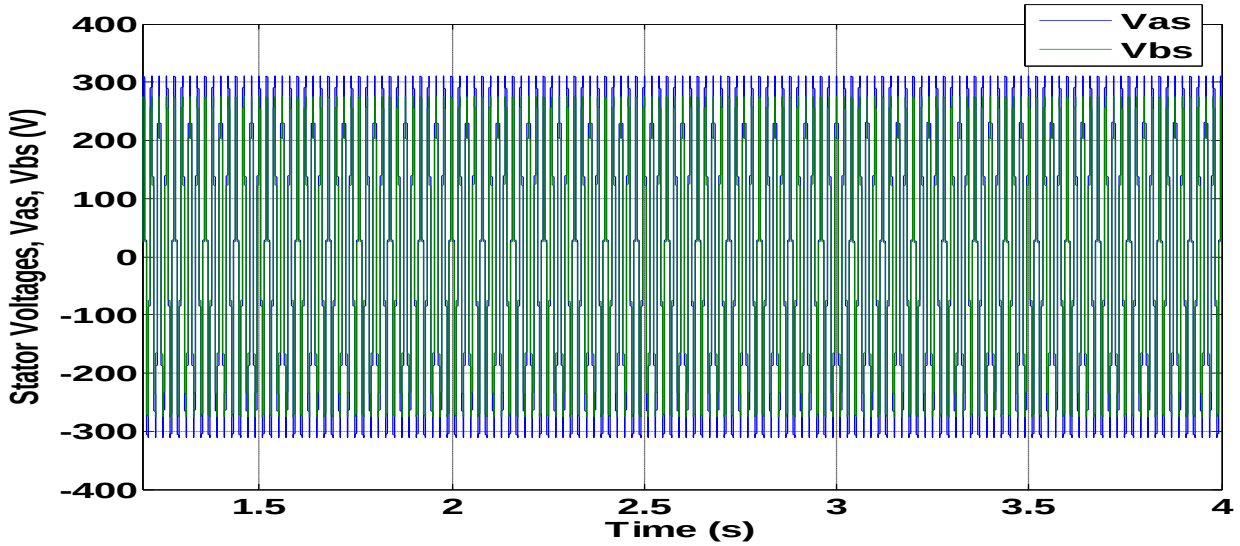


Figure 4.66: Stator Voltages with Time for the CRSPIM 2

Comparing the stator voltages of the modified SPIM to those of the CRSPIM, it is seen that stator voltages of the modified SPIM are lower in magnitude for all loads applied on the machine. Whereas the magnitude of the stator voltages in the modified SPIM is equal for both stator windings and the value dropping from a peak of 311V before the initiation of the efficiency-optimizing function to peak values of 280V, 180V and 130V for the 5.1Nm, 2Nm and 1Nm loads respectively, the magnitude of stator voltages in the CRSPIM is unequal for the main and auxiliary windings, that is, 311V and 280V respectively. Moreover, these values remain the same regardless of changes in the load applied on the machine and are therefore higher than the values of the magnitudes of voltages across the efficiency-optimizing vector-controlled modified SPIM. The main winding voltage is also the supply voltage to the CRSPIM. The stator winding currents in modified SPIM and the CRSPIM follow patterns that are similar to the voltages across the windings of the respective machines. Figure 4.67 shows the stator winding currents of the efficiency-optimizing vector-controlled Modified SPIM with time. It is seen that the stator

currents have equal magnitude and this magnitude reduces with load on the machine as part of the energy saving measure of the proposed vector control strategy.

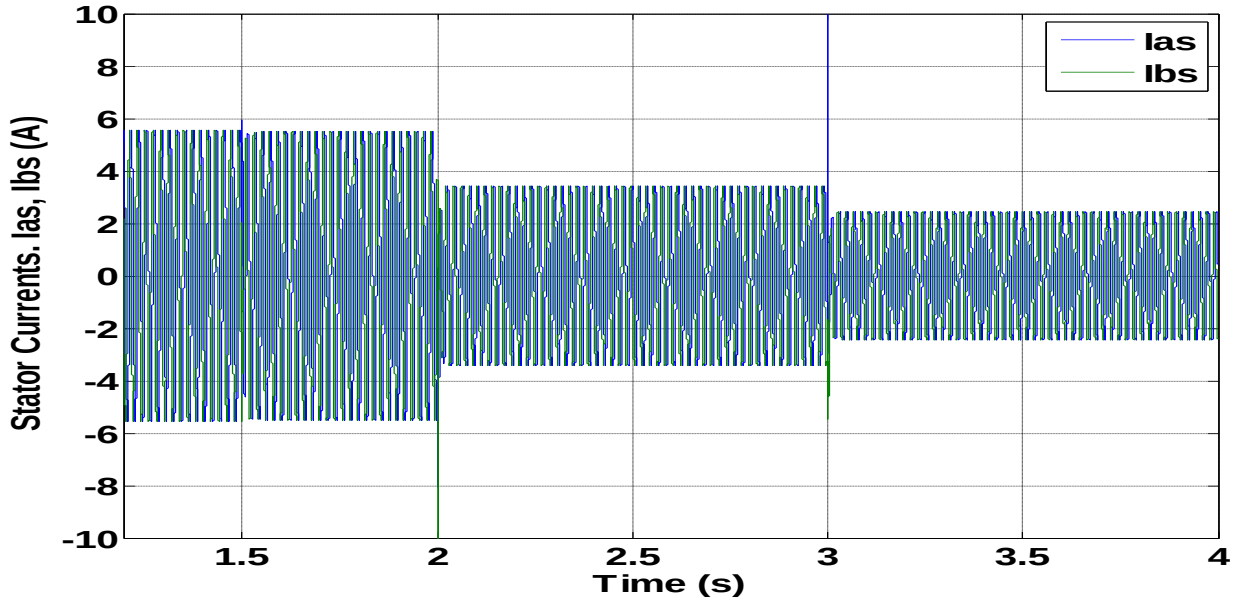


Figure 4.67: Stator Currents of the Vector-Controlled Modified SPIM 2 with the Efficiency-Optimizing Function

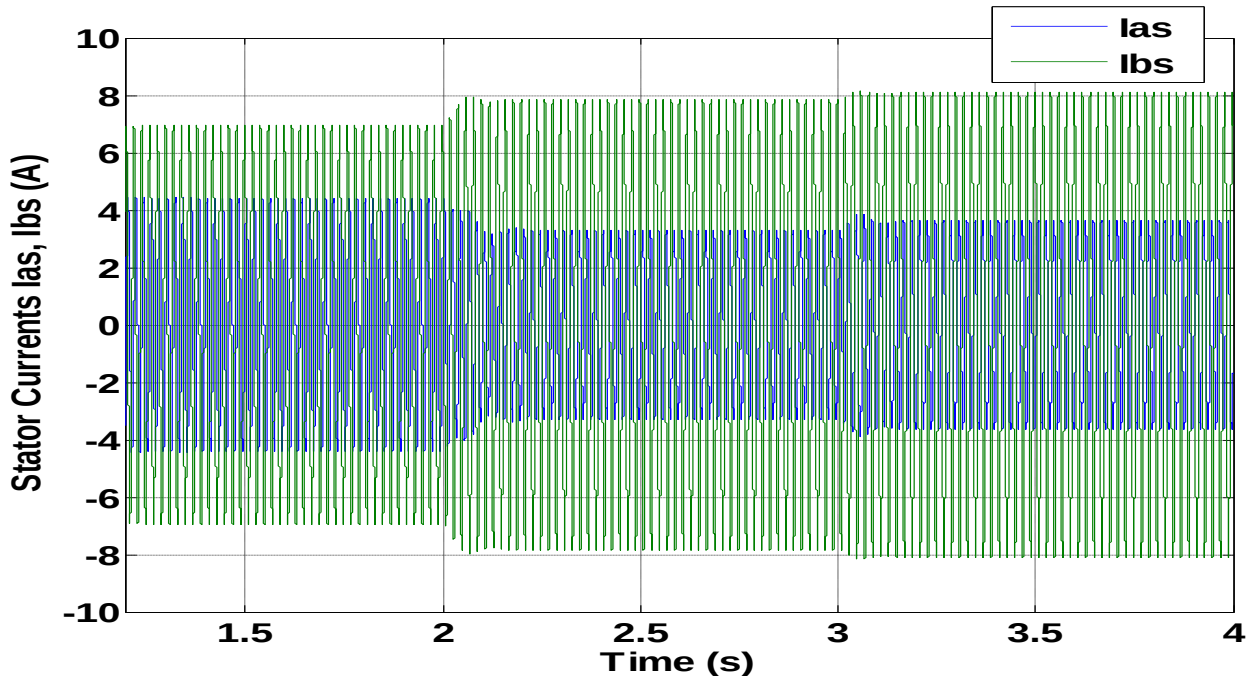


Figure 4.68: Stator Currents of the CRSPIM 2 with Time

The stator currents with time for the CRSPIM are shown in Figure 4.68. It is seen that the magnitudes of stator currents in the main and auxiliary windings of the CRSPIM are unequal for the main and auxiliary windings. The magnitudes of the currents are also seen to be higher than the magnitudes of currents in the efficiency-optimizing vector-controlled modified SPIM.

4.8 MODIFIED SPIM WINDING LAYOUT DESIGN RESULTS

The modified SPIM winding layout was designed using the design procedure of section 3.12. The results obtained are summarized in Table 4.1 for double layer, integral slot winding architecture.

Table 4.1: Winding Layout Design Parameters

Parameters	**Values**
Rated voltage	220V
Frequency	50Hz
Number of phases	2
Phase A winding resistance	4Ω
Phase B winding resistance	4Ω
Phase A winding leakage Inductance	0.0203mH
Phase B winding leakage Inductance	0.0203mH
Number of poles	4
Number of slots	32
Number of slots per pole per phase	4
Number of coils per group	4
Number of coils/phase	16 coils
Number of slots/phase	16 slots
Number of groups per phase	4
Slot pitch	22.5^o
Starting slot for Phase A	slot 1
Starting slot for Phase B	slot 5

Pole pitch	8 *slots*
Coil pitch	¾
Coil span	6 slots
Phase Spread	90^o

The outcome winding table for the 2- phase, 4 – pole, 32 slots modified SPIM is provided in Table 4.2.

Table 4.2: Winding Layout Table for the Modified SPIM 2

A+	**A-**	**B+**	**B-**
1	7	5	11
2	8	6	12
3	9	7	13
4	10	8	14
A-	**A+**	**B-**	**B+**
9	15	13	19
10	16	14	20
11	17	15	21
12	18	16	22
A+	**A-**	**B+**	**B-**
17	23	21	27
18	24	22	28
19	25	23	29
20	26	24	30
A-	**A+**	**B-**	**B+**
25	31	29	35(3)

26	32	30	36(4)
27	33(1)	31	37(5)
28	34(2)	32	38(6)

A clock diagram showing the arrangement of coil sides in the two layer winding is given in Figure 4.69.

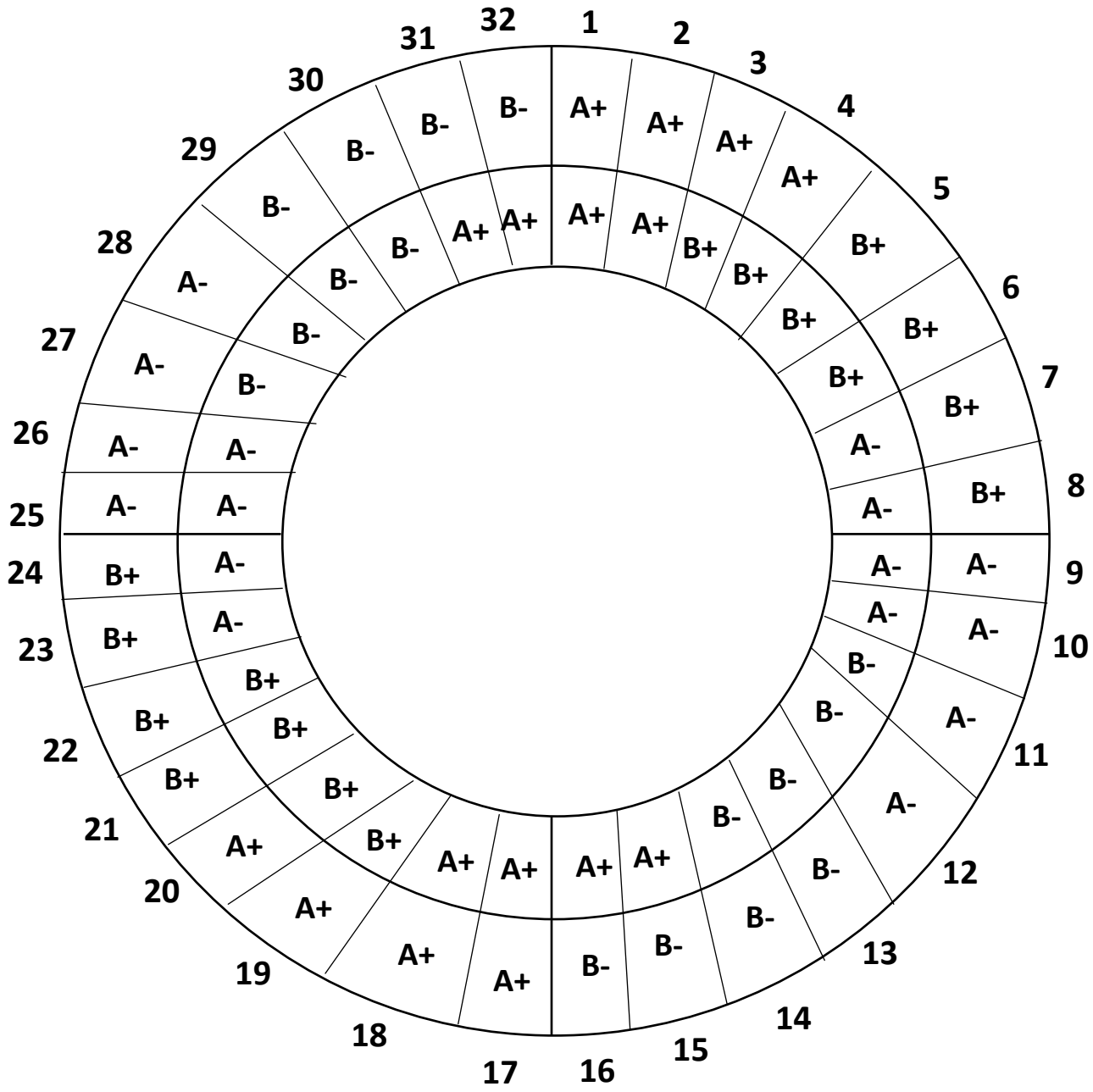


Figure 4.69: Winding Clock Diagram

It can be seen from the winding table and clock diagram, that a phase spread of 90^0 has slots 1, 2, 3 and 4 containing coil sides pertaining to phase A. Upper coil sides in these slots have their return coil-sides in the bottom of slots 7, 8, 9 and 10. The phase belt 7, 8, 9 and 10 is therefore labelled as A- and phase belt 1, 2, 3 and 4 is labelled as A+ on the table. The same can be said of

other phase belts of Phase A under other pole sections. Phase B starts from slot 5 and the first phase belt occupies slots 5, 6, 7 and 8. This phase belt is labelled as B+ in the table. The lower return coil-sides of this phase belt are contained in slots 11, 12, 13 and 14. The later phase belt is designated as B- on Table 4.2. From the clock diagram of Figure 4.69, it can be seen that all the 32 slots contain coil sides arranged at the top and bottom of each slot. It can also be observed that some slots contain coil sides pertaining to the same phase while some slots contain coil sides that pertain to different phases. The interconnection between the coils of each phase is shown in Figure 4.70. Phase A winding is printed in red while Phase B winding is printed in blue.

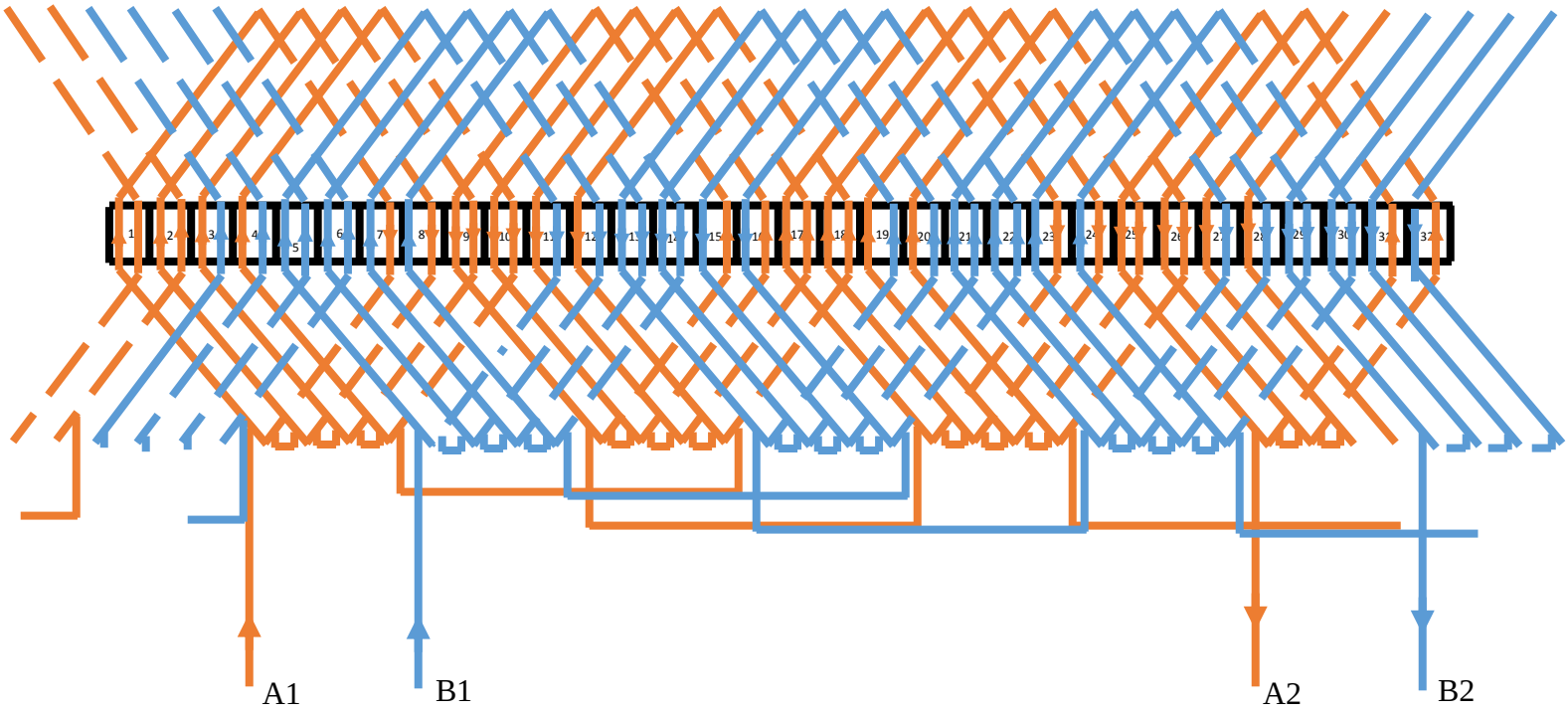


Figure 4.70: Two Phase, Double layer, Fractional Pitch Integral Slot Winding Layout

4.8.1 Coil Connections

The winding diagram of Figure 4.70was developed from Table 4.1 and the clock diagram. It can be observed that left hand terminal of the first coil group in slots 1-7, 2-8, 3-9 and 4-10 forms the Start terminal A1. For a series connection between the coil groups, the right hand terminal of this

coil group is then connected to the right hand terminal of the coil group in slots 9-15, 10-16, 11-17 and 12-18. The left hand terminal of this coil group is then connected to the left hand terminal of coil group 17-23, 18-24, 19-25 and 20-26 while the right hand terminal of this coil group is connected to the right hand terminal of coil group 25-31, 26-32, 27-1 and 28-2. The left hand terminal of this last coil group now forms the finish terminal of Phase A winding. The interconnection of the various coil groups of phase B follows the same procedure as highlighted for Phase *A* thereby yielding start and finish terminals B1 and B2 respectively.

It is seen from the winding diagram and Table 4.1 that each phase has four coil groups and each coil group consists of four coils forming a phase belt. For Phase A, coil group I forms phase belt A, coil group II forms phase belt –A, coil group III forms phase belt A and coil group IV forms phase belt –A. Similarly, for Phase B, coil groups I and III make phase belt B and coil groups II and IV form phase belt –B.

4.8.2 Establishing the Direction of Current in Coil Sides

If current direction is assumed for the first coil, then the current direction is fixed for the other coils. Therefore a clockwise direction is assumed for coil 1-7 as seen in the winding diagram of Figure 4.70. As a result, the direction of current in the other coils is as shown in the diagram. The winding layout of the existing CRSPIM is provided in Figure 2.33. Table 4.3 gives the differences that can be identified when this winding layout is compared with the winding layout developed for the modified SPIM.

Table 4.3: Differences between the Modified SPIM Winding Layout and the Layout of the Existing SPIM

S/N	Two Phase, Double Layer, Fractional Pitch Integral Slot Winding	Concentric Winding of the existing Machine

a)	Each coil group consists of four coils.	Each coil group consists of three coils.
b)	All slots have two coil sides in them.	Some slots have two coil sides, one each for the main and auxiliary winding while other slots have only one coil side
c)	Number of coils is always equal to the number of slots.	Number of coils is less than the number of slots.
d)	Size of coils of the windings is the same for the two phases	Size of coils of the windings is not the same for the main and auxiliary windings
e)	Coils are distributed with coil-sides spread one coil pitch away.	Coils are concentric.

While points (a), (c) and (e) suggest that the two phase distributed stator winding may be more expensive than the single phase concentric stator winding, points (b) and (d) suggest that the two phase distributed winding has a better utilization of stator slots and it is an easier design to process than that of the single phase concentric stator winding.

The similarities between the two winding layouts are identified as follows;

a) The axis of one phase winding is displaced 90^0 electrical degrees from the axis of the other phase winding.

b) Coil group connections are the same.

CHAPTER FIVE

CONCLUSION AND SUGGESTIONS FOR FURTHER WORK

5.1 SUMMARY

This research is a contribution towards addressing the problem of torque pulsations and low efficiency in the CRSPIM when operating under non-rated conditions, a situation that leads to wastage of electric power and undesirable noise and vibration in the machine. In efforts to address these problems, this research started by developing generalized d-q model for the CRSPIM. This model was validated by utilizing it to evaluate the performances of an existing CRSPIM. It was then used to explore the effects of changes in spatial angular displacement ∂ between the stator windings on torque production and efficiency in the CRSPIM because it was initially thought that non-quadrature angular displacement was potentially capable of providing increased motor performances with respect to torque production and efficiency. Research findings, however, clearly show that the standard motor design with quadrature angular displacement exhibits better performances particularly when balanced voltages are supplied to the stator windings. As a result, a motor performance improvement strategy using a pulse width modulated inverter and a PID controller was developed and implemented in MATLAB/Simulink environment. Simulation results showsome reduction in torque pulsations when the motor runs in steady state. Simulation results also show an increase in starting torque when the performances of the single phase inductionmotor are compared between the developed scheme and the line-operated scheme. The method was observed to be limited however because it could not eliminate torque pulsations in steady state. It was observed that although the supply voltages to the motor are balanced, the currents flowing in the stator windings are not balanced owing to the asymmetry in the stator windings. This limitation led to the proposition of a pragmatic design

modification to the parameters of the auxiliary winding of the existing machine. In addition to this design modification, the research also proposed a vector-controlled drive with an efficiency-optimizing function for the modified single phase induction machine. The proposed control scheme was developed by modifying the model of the existing CRSPIM and utilizing a sinusoidal pulse width modulated two-phase, two-leg inverter structure. In this scheme, the stator currents are made orthogonal, equal and independent by a coordinate transformation known as Park's transformation. The stator voltages calculated by the control system and delivered by the inverter are also orthogonal and equal. This method eliminates torque pulsations in steady state. For efficiency improvement, the proposed system regulates the torque and flux in the machine while keeping speed fixed at rated value, to ensure that the applied load torque keeps the flux in the machine at optimal levels. Consequently, the efficiency in the machine was observed to increase significantly above its level in the existing CRSPIM at non-rated conditions. At rated conditions, the efficiency was seen to increase only slightly. Power consumption in the motor was observed to decrease accordingly. The proposed scheme was implemented in the MATLAB/Simulink environment. For completeness, a balanced two phase winding layout design was developed for the existing SPIM based on the assumption of 4 poles and 32 slots architecture commonly utilized to house existing 50Hz, 220V CRSPIMs.

5.2 CONCLUSION

In this research, the performances of two CRSPIMs were evaluated using the generalized model developed for CRSPIMs with stator windings displaced at an arbitrary angle ∂ apart. The results of evaluation of the 110V, 60Hz CRSPIM served to verify the correctness of the generalized model. The steady state performances were particularly used to serve as bench mark for evaluating motor performances when the spatial angular displacement between the main and

auxiliary windings is changed from $90^0$to 60^0. The results of evaluation of the 220V, 50Hz CRSPIM served as bench mark for evaluating the effectiveness of the methods applied to improve the torque production and efficiency in this motor. Performances of the motor with non-quadrature angular displacements between $0^0$and 180^0were compared to motor performances with standard angular displacement of 90^0. A range of displacement angles that provides some improvement in torque and efficiency performances over that of the standard capacitor – run motor was identified as $50^0 – 80^0$.In this range, the spatial displacement angle of 60^0 is the only implementable angular displacement. The improvements observed with a displacement angle of $60^0$are only marginal and hence do not have any economic significance because the low speed region in which marginal improvement was observed is an unstable region for the existing designs of the machine and the machine is forbidden to operate in this region. At rated conditions where the machine is designed to operate and other non-rated conditions but within the stable operating region, the torque and efficiency performances of the 60^0 stator winding configuration are the same as those of the standard machine. The magnitude of torque pulsations at rated conditions was, in fact, lower in the case of the standard motor. With application of balanced winding currents, investigations have shown that changing the spatial angular displacement from 90^0 to 60^0 offers no advantage to machine performance but instead diminishes the performances for which we seek improvements. The optimum design angle of $90^0$was therefore retained going forward.

A SPWM control scheme employing a PID controller and a single phase inverter was developed to drive the auxiliary winding of two single phase induction machines.The auxiliary winding voltage was controlled with respect to the main winding voltage in order to supply balanced

currents to the main and auxiliary windings. Simulation resultsfor this method showed that although the voltages supplied to the stator windings are balanced, the currents in the stator windings are not balanced. The asymmetry or unbalance in the main and auxiliary winding parameters was identified to be the cause of unbalanced currents. In view of this, a second method utilizing a pulse width modulatedtwo-phase, two leg inverter topology and a vector control strategy was proposed and developed. In this scheme, both the stator voltages and currents are balanced. As a result, significant improvement in the electromagnetic torque production in the motors was observed by simulation.

An efficiency optimizing scheme was formulated and integrated to the vector control scheme in order to regulate the motor flux such that minimum losses occur for anyload torqueapplied on the motor. This method was observed to increase motor efficiency and to enable the motor operate in an energy-efficient manner.

Simulation results showedthat the method of using a pulse width modulated inverter and a PID controller provides a 75% and 400% increase in starting torque for the 110V, 60Hz CRSPIM and 220V, 50Hz CRSPIMrespectively. Results also showed that there is 71% and 15% reduction in the peak to peak value of torque pulsations inthe 110V, 60Hz CRSPIM and 220V, 50Hz CRSPIM respectively. These results are based on the comparison between the performances of the motors when driven by the developed scheme and the performances of the motors when driven conventionally by fixed voltage sources and with series-connected capacitors in their auxiliary winding circuits.Simulation results for the proposed efficiency-optimizing vector-controlled modified SPIM strategyhave demonstrated that motor torque pulsations are

eliminatedat steady state in comparison to the existing line-operated CRSPIM. The application of balanced voltage and current to the single phase inducton machine effectively eliminates the capacitors and any centrifugal switch from the motor circuit.Simulation results have also demonstrated that the drive control strategy helps to increase motor efficiency over that of the line-operated CRSPIM significantly at non-rated loads. Specifically, the proposed scheme yielded motor efficiency of 80.8% forall loads applied whereas the line-operated CRSPIM gives an efficiency of 79.3%, 47% and 28% for a rated load of 5.1Nm and non-rated loads of 2Nm and 1Nmrespectively. Consequently, the proposed drive scheme gives improvements of 1.5%, 33.8% and 52.8% respectively for the 5.1Nm, 2Nm and 1Nm loads over that of the line-operated CRSPIM.The corresponding improvement in power consumption is a decrease of 1.6%, 45.1% and 67.6% for torque loads of 5.1Nm, 2Nm and 1Nm respectively.These results unveil the capability of the proposed scheme toachieve significant energy savings at non-rated loads.

In view of the simulation results of the proposed efficiency-optimizing vector-controlled modified SPIM strategy, a new winding layout was developed for the existing CRSPIM. The parameters of the main winding of the existing CRSPIM were replicated conceptually for a second winding on the stator. A double layer, fractional pitch integral slot winding typically applied to poly phase windings was adapted for the existing motor. The spatial angular displacement of $90^0$and the coil group connections of the existing winding design was retained in the design. This type of winding layout is likely to be more expensive than the layout of the existing machine but itpromises better utilization of stator slots and an easier design process than that of the existing machine.

5.3 LIMITATIONS

a). The proposed drive scheme suffers from an inability to produce fast current responses as evidenced by the current overshoot during the time of initiation of the efficiency optimizing function and changes in the load torque.The current overshoot problem occurs because the PI controllers responsible for regulating the d-q axis currents cannot produce fast current responses during transient periods.

b). The effectiveness of the vector control drive scheme depends on accurate calculation of flux angle. Unfortunately, the flux angle depends on motor parameters. If motor parameters change due to temperature changes for instance then the computation of the flux orientation will be inaccurate and the scheme will fail as a result.

5.4 SIGNIFICANT CONTRIBUTIONS

A brief summary of the major contributions in this research are outlined as follows;

a) Development and evaluation of a generalized mathematical model for capacitor-run single phase induction machines.

b) Development and evaluation of an inverter drive strategy in which the run capacitor and centrifugal switch of the CRSPIMare eliminated thereby leading to increase in machine reliability and eliminationof torque pulsationsin steady state.

c) Development and evaluation of an efficiency-optimizing function for a vector-controlled modified SPIM drive in which motor efficiency is significantly increased by 33.8% and 52.8% for light loads of 2Nm and 1Nm respectively over that of the existing line-operated CRSPIM. In comparison to the efficiency optimizing control proposed in (Zahedi and Vaez-Zadeh, 2009) in which the same motor data was applied, the efficiency optimizing function gives an efficiency gain of 8.3% under 2Nm load and 14.8% under 1Nm.

d) Reduction of flux level in the existing CRSPIM by 21%, 55% and 68% for rated load, 2Nm and 1Nm loads respectively thereby leading to significant savings in energy consumed in the motor.

5.5 SUGGESTIONS FOR FURTHER WORK

a). It is recommended to use a time-optimal current controller which delivers faster current responsesin place of the PI controllers in order to overcome the problem of current overshoot during transient periods in the drive system.

b). The use of on-line parameter adaptive techniques is suggested to counter the effects of changes in motor parameters in order to ensure proper drive operation at all times.

c). It is suggested to explore the proposed scheme furtherbyvarying supply voltage frequency and thereby controlling speed and torque of the motor over a wide range while regulating motor flux at the same time. It is hoped thatby so doing, the energy-efficiency of the motorcan be increased.

d). It is also recommended that efforts be made to mount a test bed in order to verify the accuracy of the results obtained in this work experimentally. In view of this, an existing CRSPIM may be obtained and rewoundin the light of the modifications proposed in this report and drive performances evaluated via experiments. It is hoped that such efforts will lead to increased confidence in the viability of the performance improvement methods proposed in this research.

e). Finally, it is suggested to do a performance/cost analysis of the proposed drive scheme against the existing line-operated scheme for good decision making as to the use of such a scheme.

REFERENCES

Aganah, K., Karugaba, S. and Ojo, O. (2012). "Space vector and carrier-based PWM modulation schemes for maximum utilization of voltage sources of a nine-switch converter." *IEEE Energy Conversion Congress and Exposition (ECCE)*: 2521-2528.

Ang, K. H., Chong, G. and Li, Y. (2005). "PID control system analysis, design, and technology." *IEEE transactions on control systems technology*13(4): 559-576.

Asghari, S. and Fallah, E. (2012). "A new approach for efficiency optimizing of single-phase induction motors." *Power Electronics and Drive Systems Technology (PEDSTC)*: 500-505.

Azzolin, R., Bernardes, T., Vieira, R., Gastaldini, C. and Gründling, H. (2012). "Decoupling and sensorless vector control scheme for single-phase induction motor drives." *Annual Conference on IEEE Industrial Electronics Society (IECON)*: 1713-1719.

Ba-Thunya, A. S., Khopkar, R., Wei, K. and Toliyat, H. A. (2001). "Single phase induction motor drives-a literature survey." *IEEE International Electric Machines and Drives Conference (IEMDC)*: 911-916.

Baek, H., Oh, K., Sung, K., Park, S., Lim, Y., Cha, I. and Park, H. (1996). "Starting characteristics by auxiliary winding sequence control for a single-phase induction motor." *22nd IEEE International Conference on Industrial Electronics, Control, and Instrumentation (IECON)*2: 1222-1227.

Benbouzid, M., Beguenane, R. and Capolino, G. (1996). "Single-phase capacitor motor efficiency improvement by means of voltage control." *8th Mediterranean Electrotechnical Conference (MELECON'96)*.,1: 302-305.

Bhimbra, P. S. (1980). *Generalized Theory of Electrical Machines*. New Delhi, India, Khanna Publishers.

Bimbhra, P. (2004). *Electrical Machinery: Theory, Performance and Applications*. Delhi, India, Khanna.

Blaabjerg, F., Lungeanu, F., Skaug, K. and Tonnes, M. (2004). "Two-phase induction motor drives." *IEEE Industry Applications Magazine*10(4): 24-32.

Boldea, I. and Nasar, S. A. (2002). *The induction machine handbook*. Washinton D. C, CRC press.

Campos, R., Oliveira, J., Marques, L., Nied, A. and Seleme, S. I. (2007). "SVPWM-DTC strategy for single-phase induction motor control." *IEEE International Electric Machines & Drives Conference*: 1120-1125.

Caruso, M., Cecconi, V., Di Tommaso, A. and Rocha, R. (2012). "Sensorless variable speed single-phase induction motor drive system." *IEEE International Conference on Industrial Technology (ICIT)*: 731-736.

Chapman, S. J. (1999). *Electric Machinery Fundamentals. New York*, McGraw-Hill Companies.

Chapman, S. J. (2012). *Electric machinery fundamentals*, Tata McGraw-Hill Education.

Chomat, M. and Lipo, T. A. (2003). "Adjustable-speed single-phase IM drive with reduced number of switches." *IEEE Transactions on Industry Applications*39(3): 819-825.

Collins, E., Puttgen, H. and Sayle, W. (1988). "Single-phase induction motor adjustable speed drive: direct phase angle control of the auxiliary winding supply." *IEEE Industry Applications Society Annual Meeting*: 246-252.

Control system toolbox user's guide (2013a). U.S.A.

Crowley, I. F., Leung, H. F. and Bitar, S. J. (2011). "PWM Techniques: A Pure Sine Wave Inverter." *Worcester Polytechnic Institute Major Qualifying Project*.

Dong, G. (2005). Sensorless and Efficiency Optimized Induction Machine Control with Associated Converter PWM Modulation Schemes. *Electrical and Computer Engineering*, Tennessee Technological University, U.S.A.

Electrical machines, single phase motors (2015), Retrieved September 10, 2015 from http://www.studyelectrical.com/2015

Fating, V., Jadhav, S., Ugale, R. and Chaudhari, B. (2008). "Direct torque control of symmetrical and asymmetrical single phase induction motor." *Joint International Conference on Power System Technology and IEEE Power India Conference (POWERCON)*: 1-4.

Feraga, C. and Bouldjedri, A. (2012). "Indirect rotor field oriented control strategy for single phase induction motor drives." *Przeglad elektrotechniczny (electricalreview)***88**: 222-225.

Franklin, G. F., Powell, J. D., Emami-Naeini, A. and Powell, J. D. (2006). *Feedback control of dynamic systems*, Addison-Wesley Reading.

Fuchs, E. F., Huang, H., Vandenput, A., Hull, J., Zak, Z., J, A. and Erlicki, M. (1987). Optimization of Induction Motor Efficiency, Volume. 2: Single-Phase Induction Motors. Final Report.. U.S.A, Electric Power Research Institute.

Gholami, S. and Seifi, A. R. (2012). "Mathematical analysis on pulse width modulated switching functions of matrix converter." *Trends in Applied Sciences Research***7**(9): 706 - 723.

Hekmati, P., Yazdanpanah, R., Monfared, J. M. and Mirsalim, M. (2014). "Adjustable capacitor for the single-phase IM performance improvement." *Power Electronics, Drive Systems and Technologies Conference (PEDSTC)*: 7-12.

Hingorani, N. G. and Gyugyi, L. (2000). *Understanding FACTS: concepts and technology of flexible AC transmission systems*. New Jersey, Wiley-IEEE press.

Holmes, D. and Kotsopoulos, A. (1993). "Variable speed control of single and two phase induction motors using a three phase voltage source inverter." *Industry Applications Society Annual Conference*: 613-620.

Holmes, D. G. and Lipo, T. A. (2003). *Pulse width modulation for power converters: principles and practice*. Hoboken, Ney Jersey, John Wiley & Sons.

Hosseini, S.-M. (2016). "Performance improvement of capacitor-run single-phase induction motors by non-orthogonal armature windings." *International Symposium on Power Electronics, Electrical Drives, Automation and Motion (SPEEDAM)*: 1336-1341.

Huang, H., Fuchs, E. and White, J. (1988). "Optimal placement of the run capacitor in single-phase induction motor designs." *IEEE transactions on energy conversion* 3(3): 647-652.

Jain, A. (2004). *Power electronics and its applications*. India, Penram International Publishing Pvt. Ltd.

Jang, D.-H. (2007). "PWM methods for two-phase inverters." *IEEE Industry Applications Magazine*13(2): 50-61.

Jang, D.-H. (2013). "Problems incurred in a vector-controlled single-phase induction motor, and a proposal for a vector-controlled two-phase induction motor as a replacement." *IEEE Transactions on Power Electronics*28(1): 526-536.

Jang, D.-H. and Yoon, D.-Y. (1999). "Space vector PWM technique for two-phase inverter-fed single-phase induction motors." *Industry Applications Conference*1: 47-53.

Jannati, M., Asgari, S. H., Idris, N. R. N. and Aziz, M. J. A. (2014). "Speed sensorless direct rotor field-oriented control of single-phase induction motor using extended kalman filter." *International Journal of Power Electronics and Drive Systems*4(4): 430-438.

Kaźmierkowski, M. P. and Krishnan, R. (2002). *Control in power electronics: selected problems*.
Amsterdam, Bolton, Academic press.

Kim, C.-J., Choi, C.-Y., Lee, D.-E., Choi, G.-S. and Baek, S.-H. (2003). "Torque characteristics of single phase induction motor for phase control method." *Sixth International Conference on Electrical Machines and Systems*2: 510-513.

Krause, P. C., Wasynczuk, O. and Sudhoff, S. D. (2002). *Analysis of Electric Machinery and Drive*
. U.S.A.

Krause, P. C., Wasynczuk, O., Sudhoff, S. D. and Pekarek, S. (2013). *Analysis of electric machinery and drive systems*. U.S.A, John Wiley & Sons.

Krischan, K., Dannerer, G., Koenig, O. and Seebacher, R. R. (2008). "Low cost speed control for single phase induction motors-comparing different approaches with regard to efficiency." *International Symposium on Power Electronics, Electrical Drives, Automation and Motion, (SPEEDAM)*: 101-106.

Krishnan, R. (2001). *Electric motor drives-modeling, analysis and control*. New Jersey, Prentice Hall.

Kumsuwan, Y., Srirattanawichaikul, W., Premrudeepreechacharn, S. and Toliyat, H. (2010). "A four-LEG voltage source inverter fed asymmetrical two-phase induction motor drives." *5th IET International Conference on Power Electronics, Machines and Drives*,: 2469-2476.

Latt, A. Z. and Win, N. N. (2009). "Variable speed drive of single phase induction motor using frequency control method." *International Conference on Education Technology and Computer*: 30-34.

Lee, K., Kim, H., Lee, D., Chun, T. and Nho, E. (2001). "High performance drive of single-phase
induction motor." *IEEE International Symposium on Industrial Electronics (ISIE)*2: 983-988.

Ling, Z., Zhou, L., Li, H., Zhu, W., Guo, S. and Wang, J. (2014). "The Use of Electrical Steels in Single-Phase Induction Machines and the Modified Iron Loss Test Method." *IEEE Transactions on Magnetics*50(11): 1-4.

Liu, T.-H.and Wang, P-C, (1994). "Implementation of a single phase induction motor control on a DSP based system." *Power Electronics Specialists Conference*511: 514-521

Liu, T.-H. (1995). "A maximum torque control with a controlled capacitor for a single-phase

induction motor." *IEEE Transactions on Industrial Electronics* 42(1): 17-24.

Liwschitz-Garik, M. (1950). *Winding Alternating Current Machinery, A Book for Winders, Repair men and Designers of Electric Machines*. New York, Van Nostrand Company Inc.

Mademlis, C., Kioskeridis, I. and Theodoulidis, T. (2005). "Optimization of single-phase induction Motors-part I: maximum energy efficiency control." *IEEE transactions on energy conversion*20(1): 187-195.

Marouchos, C. C. (2006). *TheSwitching Function: Analysis of Power Electronic Circuits*. London, United Kingdom, the Institution of Engineering and Technology.

Mera, R. and Câmpeanu, R. (2012). "Optimal performance of capacitor-run single phase induction motor." *13th International Conference on Optimization of Electrical and Electronic Equipment (OPTIM)*: 718-723.

Mihret, M., Ojo, O. and Mefford, W. (2011). "Analysis and Implementation of Full Bridge Single Phase Solar-Power Inverter on PIC18F1320 Micro-Controller." *International Conference on Innovations in Engineering and Technology*.

Miller, T. J. (1985). "Single-phase permanent-magnet motor analysis." *IEEE Transactions on Applications*(3): 651-658.

Miranda, U. d. A., Rolim, L. and Aredes, M. (2005). "A DQ synchronous reference frame current control for single-phase converters." *IEEE 36th Power Electronics Specialists Conference*: 1377-1381.

Mittle, V. and Mittal, A. (1996). *Design of electrical machines*. Delhi, Standard Publishers Distributors.

Mohan, N. (2009). *Power electronics: a first course*. U.S.A, MNPERE.

Mohan, N. (2014). *Advanced electric drives: analysis, control, and modeling using /Simulink*. Hoboken, New Jersey, John wiley & sons.

Morrill, W. J. (1929). "The revolving field theory of the capacitor motor." *Transactions of the Institute of Electrical Engineers*48(2): 614-629.

Muljadi, E., Zhao, Y., Liu, T. H. and Lipo, T. A. (1993). "Adjustable AC capacitor for a single-phase induction motor." *IEEE Transactions on Industry Applications*29(3): 479-485.

Naxin, C., Chenghui, Z. and Min, Z. (2004). "Optimal efficiency control of field-oriented induction motor drive and rotor resistance adaptive identifying." *The 4th International Power Electronics and Motion Control Conference*,1: 414-419.

Nied, A., Oliveira, J. d., Stival, L. H. R. C. and Polli, H. B. (2013). "Improving washing machine performance using single-phase induction motor field-oriented control." 3*9th Annual Conference of the IEEE Industrial Electronics Society*: 2917-2922.

Omozusi, O. I. (1998). Dynamics and control of a battery inverter single-phase induction generator system: a thesis presented to the faculty of the Graduate School, Tennessee Technological University. USA.

Ong, C.-M. (1998). *Dynamic simulation of electric machinery: using MATLAB/SIMULINK*, Prentice Hall PTR Upper Saddle River, NJ.

Park, C.-S. (2001). "A study on the efficiency improvement and suppression of rising temperature of the 1-phase condenser motor." *Proceedings of the Fifth International Conference onElectrical Machines and Systems, (ICEMS).* 1: 64-66.

Patel, J. A. and Raval, H. H. (2015). "Design of Sinusoidal Pulse Width Modulation Inverter." *International Journal For Technological Research In Engineering***2**(8): 1446-1452.

Pawar, S. H. and Kulkarni, A. S. (2015) "Design and analysis of sinusoidal pwm inverter fed fuel pumpMotor for high horse-power locomotive in MATLAB." *Global journal of engineering science and researches***2**(2): 23-29.

Pei, Y., Liu, X., Wang, X. and Tian, M. (2016). "The starting performance research on the novel single-phase induction motor." *IEEE 11th Conference on Industrial Electronics and Applications (ICIEA)*: 2219-2222.

Rashid, M. H. (2004). *Power Electronics, Circuits, Devices and applications*, Pearson Education, Prentice Hall, Upper Saddle River, NJ.

Rokrok, E. and Golshan, M. H. (2009). "Comprehensive control scheme for an inverter-based distributed generation unit." *Iranian Journal of Science and Technology*33(B6): 477-490.

Rosenberg, R. (1970). *Electric motor repair: A practical handbook on the winding, repair and troubleshooting of A.C. and D.C motors and Controllers*. Japan, Rinehart and Winston Holt-Sanders.

Roshan, A. (2007). A dq rotating frame controller for single phase full-bridge inverters used in small distributed generation systems, MSc thesis presented to Faculty of the Virginia Polytechnic Institute and State University. U.S.A.

Rubio, G. J., Sánchez-Torres, J. D., Cañedo, J. M. and Loukianov, A. G. (2013). "Integral high order sliding mode control of single-phase induction motor." *10th International Conference on Electrical Engineering, Computing Science and Automatic Control (CCE)*: 25-30.

Saidur, R., Mekhilef, S., Ali, M., Safari, A. and Mohammed, H. (2012). "Applications of variable speed drive (VSD) in electrical motors energy savings." *Renewable and Sustainable Energy Reviews*16(1): 543-550.

Salem, F. A. and Rashed, A. A. (2013). "PID Controllers and Algorithms: Selection and Design Techniques Applied in Mechatronics Systems Design-Part II." *International Journal of Engineering Sciences*2(5): 191-203.

Sawhney, A. and Chakrabarti, A. (1996). *A Course in Electrical Machine Design*. Delhi, Dhanpat Rai & Sons.

Séguier, G. and Labrique, F. (1993). *Power Electronics Converter. DC-AC Conversion,* Springer-Verlag, Berlín.

Sharma, A. K., Sharma, A. K. and Vijay, N. (2014). "Unipolar and Bipolar SPWM Voltage Modulation Type inverter for improved switching frequencies." *International journal of engineering sciences & research technology*3(8): 106-110.

Sobhani, S., Yaghobi, H. and Samakoosh, M. (2013a). "Optimize efficiency and torque in the single-phase induction motor by adjusting the design parameters." *12th International Conference on Environment and Electrical Engineering (EEEIC)*: 237-241.

Sobhani, S., Talebian, M. E. and Nejad, H. V. (2013b). "Elimination the centrifugal switch in single-phase induction motor (SPIM) to increase torque and efficiency." *3rd International Conference on Electric Power and Energy Conversion Systems (EPECS)*,: 1-7.

Spirov, D. S. (2016). "Adaptive magnetizing current observer of single-phase collector motor drive." *XXV International Scientific Conference Electronics (ET)*: 1-4.

Sun, J. (2012). Pulse-width modulation. *Dynamics and Control of Switched Electronic Systems,* Springer**:** 25-61.

Torque-slip characteristics (2011), Retrieved November 12, 2015 from http://yourelectrichome.blogspot.com.ng

Trickey, P. H. (1932). "Design of capacitor motors for balanced operation." *Transactions of the American Institute of Electrical Engineers*51(4): 780-785.

Vaez-Zadeh, S. and Langari, H. (2000). "High average-low pulsating torque operation of single phase induction motors." *Industry Applications Conference*21(3): 1513-1518.

Vaez-Zadeh, S. and Reicy, S. (2005). "Sensorless vector control of single-phase induction motor drives." *International Conference on Electrical Machines and Systems*3: 1838-1842.

Vas, P. (1992). *Electrical machines and drives: a space-vector theory approach*. New York, Clarendon Press, Oxford.

Veinott, C. G. (1970). *Fractional and Subfractional Horsepower Electric Motors*. New York, U.S.A, McGraw-Hill Book Company.

Wang, L., Chai, S., Yoo, D., Gan, L. and Ng, K. (2015). *PID and Predictive Control of Electrical and Power Converters Using MATLAB/Simulink*. Singapore, John Wiley & Sons.

Yazdani, A. and Iravani, R. (2010). *Voltage-sourced converters in power systems*. Hoboken, New Jersey, John Wiley & Sons.

Zahedi, B. and Vaez-Zadeh, S. (2007). "Analysis of electrical loss in single phase induction motors." *IEEE International Electric Machines & Drives Conference***2**: 1621-1625.

Zahedi, B. and Vaez-Zadeh, S. (2009). "Efficiency optimization control of single-phase induction motor drives." *IEEE Transactions on Power Electronics*24(4): 1062-1070.

Appendix A: Parameters of CRSPIM 1 and CRSPIM 2

Table A.1: Parameters of the CRSPIM 1 (Ong, 1998; Krause *et al.*, 2002; Jannati *et al.*, 2014)

Parameters	**Values**
Turn's ratio	1.18
Main winding resistance	2.02 Ω
Auxiliary winding resistance	7.14Ω
Main winding leakage inductance	0.0074H
Aux. winding leakage inductance	0.0085H
Mutual Inductance	0.1772H
Rotor resistance	4.12Ω
Rotor leakage inductance	0.056H
Run capacitive Impedance	$9 - j172$ Ω
Start capacitive Impedance	$3 - j14.5$Ω
Moment of Inertia	0.0146 kgm^2
Rated voltage	110V
Rated power	¼ hp
Rated speed	1728rpm
Rated Torque	1Nm
Rated frequency	60Hz

Table A.2: Parameters of the CRSPIM 2(Zahedi and Vaez-Zadeh, 2007; Zahedi and Vaez-Zadeh,
2009)

Parameters	**Values**
Turn's ratio	1.1293
Main winding resistance	4 Ω
Auxiliary winding resistance	6.5Ω
Main winding leakage inductance	0.0203H
Aux. winding leakage inductance	0.0210H
Mutual Inductance	0.1954H
Rotor resistance	3.61Ω
Rotor leakage inductance	0.0304H
Run capacitance	40μF
Core loss resistance	910Ω
Moment of Inertia	0.01424kgm^2
Rated voltage	220V
Rated power	1hp
Rated speed	1395rpm
Rated Torque	5.1Nm
Rated frequency	50Hz

AppendixB: Derivation of Expressions for Winding Currents

The dynamic model of the capacitor-run single phase induction machine is given in the equations (3.84(a)-(j)). Equations (3.84(f)-(i)) may be written as given in equations (B.1) – (B.4)

$$\lambda_{qs} = L_{las} i_{qs} + \lambda_{mqc} \quad \text{(B.1)}$$

$$\lambda'_{qr} = L'_{lr} i'_{qr} + \lambda_{mqc} \quad \text{(B.2)}$$

$$\lambda'_{ds} = L'_{lbs} i'_{ds} + \lambda_{mdc} \quad \text{(B.3)}$$

$$\lambda'_{dr} = L'_{lr} i'_{dr} + \lambda_{mdr} \quad \text{(B.4)}$$

Equations for currents may be obtained from equations (B.1) – (B.4) as follows;

$$i_{qs} = \frac{\lambda_{qs} - \lambda_{mqc}}{L_{las}} \quad \text{(B.5)}$$

$$i'_{qr} = \frac{\lambda'_{qr} - \lambda_{mqc}}{L'_{lr}} \quad \text{(B.6)}$$

$$i'_{ds} = \frac{\lambda'_{ds} - \lambda_{mdc}}{L'_{lbs}} \quad \text{(B.7)}$$

$$i'_{dr} = \frac{\lambda'_{dr} - \lambda_{mdr}}{L'_{lr}} \quad \text{(B.8)}$$

Where λ_{mqc}, λ_{mdc} and λ_{mdr} are dummy variables and may be evaluated as follows in equations (B.9) – (B.11)

$$\lambda_{mdc} = \left[\frac{\lambda'_{ds}}{L'_{lbs}}\left(1 - \frac{L_{MR}\sin^2\partial}{L'_{lr}} - \cos^2\partial L_{AR} L_{MS}\right) + \frac{\lambda'_{dr}\sin\partial}{L'_{lr}}\left(1 - \frac{L_{MR}}{L'_{lr}}\right) - \frac{\lambda_{qs}\cos\partial}{L_{las}}(1 - L_{AR}L_{MS}) - \frac{\lambda'_{qr}\cos\partial}{L'_{lr}}(1 - L_{AR}L_{MS})\right]\left[L_{MB} - \frac{L_{MR}\sin^2\partial}{L'_{lbs}L'_{lr}} - \frac{L_{AR}L_{MS}\cos^2\partial}{L'_{lbs}}\right] \quad \text{(B.9)}$$

$$\lambda_{mdr} = \left[\frac{\lambda'_{ds}\sin\partial}{L'_{lbs}} - \frac{\lambda_{mdc}\sin\partial}{L'_{lbs}} + \frac{\lambda'_{dr}}{L'_{lr}}\right] L_{MR} \quad \text{(B.10)}$$

$$\lambda_{mqc} = \left[\frac{\lambda_{qs}}{L_{las}} + \frac{\lambda'_{qr}}{L'_{lr}} - \frac{\lambda'_{ds}\cos\partial}{L'_{lbs}} + \frac{\lambda_{mdc}\cos\partial}{L'_{lbs}}\right] L_{MS} \quad \text{(B.11)}$$

Where

$$L_{MB} = \left[\frac{1}{L_{mas}} + \frac{1}{L'_{lbs}}\right] \tag{B.12}$$

$$L_{MR} = \left[\frac{1}{L_{mas}} + \frac{1}{L'_{lr}}\right]^{-1} \tag{B.13}$$

$$L_{AR} = \left[\frac{1}{L_{las}} + \frac{1}{L'_{lr}}\right] \tag{B.14}$$

$$L_{MS} = \left[\frac{1}{L_{mas}} + \frac{1}{L_{las}} + \frac{1}{L'_{lr}}\right]^{-1} \tag{B.15}$$

For the steady state model, the equation that solves for winding currents is given a

$$\begin{bmatrix} \bar{i}_{qs} \\ \bar{i}'_{ds} \\ \bar{i}'_{qr} \\ \bar{i}'_{dr} \end{bmatrix} = \begin{bmatrix} r_{as} + j\frac{\omega_e}{\omega_b}X_{as} & -j\frac{\omega_e}{\omega_b}X_{mas}\cos\partial & j\frac{\omega_e}{\omega_b}X_{mas} & 0 \\ -j\frac{\omega_e}{\omega_b}X_{mas}\cos\partial & (r'_{bs} + j(\frac{\omega_e}{\omega_b}X'_{bs} - \frac{\omega_b}{\omega_e}X_c) & -j\frac{\omega_e}{\omega_b}X_{mas}\cos\partial & j\frac{\omega_e}{\omega_b}X_{mas}\sin\partial \\ j\frac{\omega_e}{\omega_b}X_{mas} & -(j\frac{\omega_e}{\omega_b}X_{mas}\cos\partial + \frac{\omega_r}{\omega_b}X_{mas}\sin\partial) & r'_r + j\frac{\omega_e}{\omega_b}X'_r & -\frac{\omega_r}{\omega_b}X'_r \\ \frac{\omega_r}{\omega_b}X_{mas} & j\frac{\omega_e}{\omega_b}X_{mas}\sin\partial - \frac{\omega_r}{\omega_b}X_{mas}\cos\partial & \frac{\omega_r}{\omega_b}X'_r & r'_r + j\frac{\omega_e}{\omega_b}X'_r \end{bmatrix}^{-1} \begin{bmatrix} \bar{V}_{qs} \\ \bar{V}'_{ds} \\ 0 \\ 0 \end{bmatrix} \tag{B.16}$$

Appendix C: Program Listings

```
%This program solves the generalized dynamic model of the CRSPIM with del set
%to 90 degrees
function
[pVpc,plambda_qs,plambda_pds,plambda_pqr,plambda_pdr,pwr,Te,Vqs,Vds,Vbs,Iqs,i
as,Ids,ibs,is,Vc,puwr,mechwr,mechrad] = ...
    SPIM(Vas,lambda_qs,lambda_pds,lambda_pqr,lambda_pdr,wr,TL, Vpc)
% This block supports the Embedded MATLAB subset.
% See the help menu for details.
del=pi/2;
f=60;
wb=2*pi*f;
Nabs = 1/1.18;
Nbas = 1.18;
Lmas = 0.1772;
Lplr = 0.0056;
Llas = 0.0074;
Llbs = 0.0085;
Lplbs = (Nabs^2)*Llbs;
ras = 2.02;
rbs = 7.14;
rpbs = (Nabs^2)*rbs;
rpr = 4.12;
J =0.0146;
P = 4;
zstart=3-14.5*1i;
zrun=9-172*1i;
zp=(zstart*zrun)/(zstart+zrun);
cutoffspeed=0.75;
puwr=wr/wb;
mechwr=(120*wr)/(2*pi*P);
mechrad=2*pi*mechwr/60;
if puwr<cutoffspeed
    cstart=1/(2*pi*f*-imag(zp));
    Cp = cstart*(Nbas^2);
rcstart=real(zp)*(Nabs^2);

%=========================================================================
===
%supply voltages
Vqs = Vas;
Vps = Nabs*Vas;
Vpqr = 0;
Vpdr = 0;

%=========================================================================
===
%My Identities

LMB=((1/Lmas) + (1/Lplbs));
LMR=(1/((1/Lmas) + (1/Lplr)));
LAR=(1/Llas) + (1/Lplr);
LMS=1/(1/Lmas + 1/Llas + 1/Lplr);
Lmdc=1/(LMB-((sin(del)^2*LMR)/(Lplbs*Lplr))-((cos(del)^2*LAR*LMS)/Lplbs));
```

```
lambda_mdc=Lmdc*((lambda_pds/Lplbs)*(1-((LMR*sin(del)^2)/Lplr)-
(cos(del)^2*LAR*LMS))+((lambda_pdr*sin(del))/Lplr)*(1-(LMR/Lplr))-
((lambda_qs*cos(del))/Llas)*(1-LAR*LMS)-((lambda_pqr*cos(del))/Lplr)*(1-
(LAR*LMS)));
lambda_mdr=LMR*(((lambda_pds*sin(del))/Lplbs)-
((lambda_mdc*sin(del))/Lplbs)+lambda_pdr/Lplr);
lambda_mqc=LMS*((lambda_qs/Llas)+(lambda_pqr/Lplr)-
((lambda_pds*cos(del))/Lplbs)+((lambda_mdc*cos(del))/Lplbs));

%=========================================================================
%solution of differential equations

plambda_qs = (Vqs + (ras/Llas)*(lambda_mqc - lambda_qs));
Iqs = (1/Llas)*(lambda_qs - lambda_mqc);
ias=Iqs;
plambda_pqr = (Vpqr + wr*lambda_pdr + (rpr/Lplr)*(lambda_mqc - lambda_pqr));
Ipqr = (1/Lplr)*(lambda_pqr - lambda_mqc);
plambda_pdr = (Vpdr - wr*lambda_pqr + (rpr/Lplr)*(lambda_mdr - lambda_pdr));
pVpc = -(1/Cp)*(1/Lplbs)*(lambda_pds - lambda_mdc);
Vc=Nbas*Vpc;
Vpds=Vps+Vpc;
Vds=Nbas*Vpds;
Vbs=-Vds;
plambda_pds = (Vpds -  (rcstart+rpbs)*((lambda_pds - lambda_mdc)/Lplbs));
Ipds = (1/Lplbs)*(lambda_pds - lambda_mdc);
Ids=Nabs*Ipds;
ibs=-Ids;
Ipdr = (1/Lplr)*(lambda_pdr - lambda_mdr);
Te = (P/2)*Lmas*(Ipdr*Iqs - Ipqr*Ipds*sin(del)-Ipds*Ipdr*cos(del));
pwr=(P/(2*J))*(Te+TL);
else
    crun=1/(2*pi*f*-imag(zrun));
    Cp = crun*(Nbas^2);
rcstart=real(zrun)*(Nabs^2);
Vqs = Vas;
Vps = Nabs*Vas;
Vpqr = 0;
Vpdr = 0;

LMB=(1/Lmas) + (1/Lplbs);
LMR=1/((1/Lmas) + (1/Lplr));
LAR=(1/Llas) + (1/Lplr);
LMS=1/(1/Lmas + 1/Llas + 1/Lplr);
Lmdc=1/(LMB-((sin(del)^2*LMR)/(Lplbs*Lplr))-((cos(del)^2*LAR*LMS)/Lplbs));
lambda_mdc=Lmdc*((lambda_pds/Lplbs)*(1-((LMR*sin(del)^2)/Lplr)-
(cos(del)^2*LAR*LMS))+((lambda_pdr*sin(del))/Lplr)*(1-(LMR/Lplr))-
((lambda_qs*cos(del))/Llas)*(1-LAR*LMS))-((lambda_pqr*cos(del))/Lplr)*(1-
(LAR*LMS)));
lambda_mdr=LMR*(((lambda_pds*sin(del))/Lplbs)-
((lambda_mdc*sin(del))/Lplbs)+lambda_pdr/Lplr);
lambda_mqc=LMS*((lambda_qs/Llas)+(lambda_pqr/Lplr)-
((lambda_pds*cos(del))/Lplbs)+((lambda_mdc*cos(del))/Lplbs));

plambda_qs = (Vqs + (ras/Llas)*(lambda_mqc - lambda_qs));
Iqs = (1/Llas)*(lambda_qs - lambda_mqc);
ias=Iqs;
```

```
Ipqr = (1/Lplr)*(lambda_pqr - lambda_mqc);

plambda_pqr = (Vpqr + wr*lambda_pdr + (rpr/Lplr)*(lambda_mqc - lambda_pqr));
plambda_pdr = (Vpdr - wr*lambda_pqr + (rpr/Lplr)*(lambda_mdr - lambda_pdr));
pVpc = -(1/Cp)*(1/Lplbs)*(lambda_pds - lambda_mdc);
Vc=Nbas*Vpc;
Vpds=Vps+Vpc;
Vds=Nbas*Vpds;
Vbs=-Vds;

plambda_pds = (Vpds -  (rcstart+rpbs)*((lambda_pds - lambda_mdc)/Lplbs));
Ipds = (1/Lplbs)*(lambda_pds - lambda_mdc);
Ids=Nabs*Ipds;
ibs=-Ids;
Ipdr = (1/Lplr)*(lambda_pdr - lambda_mdr);
Te = (P/2)*Lmas*(Ipdr*Iqs - Ipqr*Ipds*sin(del)-Ipds*Ipdr*cos(del));
pwr=(P/(2*J))*(Te+TL);
end


%Script to calculate and plot graphs of steady state performances...
%for the case of del equal to 90degs for the CRSPIM
clc;
clear all;
format bank;
f = 60;
P = 4;
we=pi*f;
wb=we;
del=pi/2;
s=1:-0.02:0;
Nas = 1/1.18;
rqs = 2.02;
xlqs = 2.79;
xlds = 3.22;
rds = 7.14;
rpds = (Nas^2)*rds;
xplds = (Nas^2)*xlds;
xplr = 2.12;
rpr = 4.12;
xmq = 66.8;
xqs = xlqs + xmq;
xpds = xplds+xmq;
xpr = xplr+xmq;
zrun=9-172*1i;
zprun = (Nas^2)*zrun;
rpc=real(zprun);
xpc=imag(zprun);
vqs = 110;
vqs_bar = vqs + j*0;
vpds_bar = (Nas)*vqs_bar;
imatrix = zeros(4,51);
vmatrix = [vqs_bar; vpds_bar; 0; 0;];

for k = 1,
for n = 1:51,
```

```
    wr(n) = we*(1-s(n));
A = [(rqs+j*((we/wb)*xqs)), -j*((we/wb)*xmq*cos(del(k))), j*((we/wb)*xmq),...
    0;-j*((we/wb)*xmq*cos(del(k))), ((rpds-j*(we/wb)*xpds)),...
    -j*((we/wb)*xmq*cos(del(k))),j*((we/wb)*xmq*sin(del(k)));...
    j*((we/wb)*xmq),-
((wr(n)/wb)*xmq*sin(del(k))+j*(we/wb)*xmq*cos(del(k))),...
    (rpr+j*((we/wb)*xpr)),(-
wr(n)/wb)*xpr;(wr(n)/wb)*xmq,(j*(we/wb)*xmq*sin(del(k))-
(wr(n)/wb)*xmq*cos(del(k))),...
    (wr(n)/wb)*xpr,(rpr+j*((we/wb)*xpr))];
imatrix(:,n)=A\vmatrix;

%Calculate for Average Torque
conjIqs_bar=conj(imatrix(1,n));
product_Idr_conjIqs_bar=imatrix(4,n)*conjIqs_bar;
conjIqr_bar=conj(imatrix(3,n));
product_Ids_conjIqr_bar=sin(del(k))*imatrix(2,n)*conjIqr_bar;
conjIdr_bar=conj(imatrix(4,n));
product_Ids_conjIdr_bar=cos(del(k))*imatrix(2,n)*conjIdr_bar;
minus_of_product_currents=product_Idr_conjIqs_bar-product_Ids_conjIqr_bar-
product_Ids_conjIdr_bar;
average_torque(k,n)= (P/4)*(xmq/wb)*real(minus_of_product_currents);

%Calculate for Pulsating Torque
product_Iqs_Idr_bar=imatrix(1,n)*imatrix(4,n);
product_Ids_Iqr_bar=sin(del(k))*imatrix(2,n)*imatrix(3,n);
product_Ids_Idr_bar=cos(del(k))*imatrix(2,n)*imatrix(4,n);
minus_of_product_pulsatingcurrents=product_Iqs_Idr_bar-product_Ids_Iqr_bar-
product_Ids_Idr_bar;
mag_pulsating_torque(k,n)=(P/4)*(xmq/wb)*abs(minus_of_product_pulsatingcurren
ts);

%Calculate for Stator current Magnitude and phase angle between Iqs and Ids
magIqs(k,n)=abs(imatrix(1,n));
magIpds(k,n)=abs(imatrix(2,n));
stator_current_magnitude(n)=abs(sqrt(imatrix(1,n).^2+imatrix(2,n).^2));
angIqs(k,n)=angle(imatrix(1,n))*180/pi;
angIpds(k,n)=angle(imatrix(2,n))*180/pi;
 stator_current_magnitude(k,n)=abs(sqrt(imatrix(1,n).^2+imatrix(2,n).^2));

% %Calculate for Apparent Power
apparent_power(k,n)=[vmatrix(1) matrix(2)]*conj([imatrix(1,n);imatrix(2,n)]);

end

%Calculate for Power Input

P_in(k,:)=real(apparent_power(k,:));

%Calculate for efficiency

P_out(k,:)=average_torque(k,:).*wr;
efficiency(k,:) = (100*P_out(k,:))./P_in(k,:);

%Calculate for phase difference
```

```
Theta(k,:)=angIpds(k,:)-angIqs(k,:);

end

figure (1)
plot(wr,average_torque,wr, mag_pulsating_torque), xlabel('speed (rad/s)'),
ylabel('Tavg, Tpuls (Nm)')

figure (2)
plot(wr,efficiency), xlabel('speed (rad/s)'), ylabel('efficiency (%)')
grid on
figure (3)
plot(wr,angIqs(1,:),wr,angIpds(1,:)),xlabel('speed (rad/s'), ylabel('angle
Iqs, Ipds (degs)')
legend('Phase Angle of Main Winding Current','Phase Angle of Auxiliary
Winding Current')


%Script to calculate and plot graphs of steady state performances...
%for the case of del equal to values between 0degs and 180degs for the
capacitor-run SPIM
clc;
clear all;
format bank;
f = 60;
P = 4;
we =pi*f;
wb=we;
del=0:pi/18:pi;
s=1:-0.02:0;
Nqd = 1/1.18;
rqs = 2.02;
xlqs = 2.79;
xlds = 3.22;
rds = 7.14;
rpds = (Nqd^2)*rds;
xplds = (Nqd^2)*xlds;
xplr = 2.12;
rpr = 4.12;
xmq = 66.8;
xqs = xlqs + xmq;
xpds = xplds+xmq;
xpr = xplr+xmq;
zrun=9-172*1i;
zprun = (Nqd^2)*zrun;
rpc=real(zprun);
xpc=imag(zprun);
vqsm = 110;
vqs_bar = vqsm + j*0;
vpds_bar = Nqd*vqs_bar;
imatrix = zeros(4,51);
vmatrix = [vqs_bar; vpds_bar; 0; 0;];

%Influence of angle del on Average Torque
for k = 1:19,
for n = 1:51,
```

```
    wr(n) = we*(1-s(n));
A = [(rqs+j*((we/wb)*xqs)), -j*((we/wb)*xmq*cos(del(k))), j*((we/wb)*xmq),...
    0;-j*((we/wb)*xmq*cos(del(k))),
((rpds+rpc)+j*((we/wb)*xpds+(wb/we)*xpc)),...
    -j*((we/wb)*xmq*cos(del(k))),j*((we/wb)*xmq*sin(del(k)));...
    j*((we/wb)*xmq),-
((wr(n)/wb)*xmq*sin(del(k))+j*(we/wb)*xmq*cos(del(k))),...
    (rpr+j*((we/wb)*xpr)),(-
wr(n)/wb)*xpr;(wr(n)/wb)*xmq,(j*(we/wb)*xmq*sin(del(k))-
(wr(n)/wb)*xmq*cos(del(k))),...
    (wr(n)/wb)*xpr,(rpr+j*((we/wb)*xpr))];
imatrix(:,n)=A\vmatrix;

%Calculate for Average Torque

conjIqs_bar=conj(imatrix(1,n));
product_Idr_conjIqs_bar=imatrix(4,n)*conjIqs_bar;
conjIqr_bar=conj(imatrix(3,n));
product_Ids_conjIqr_bar=sin(del(k))*imatrix(2,n)*conjIqr_bar;
conjIdr_bar=conj(imatrix(4,n));
product_Ids_conjIdr_bar=cos(del(k))*imatrix(2,n)*conjIdr_bar;
minus_of_product_currents=product_Idr_conjIqs_bar-product_Ids_conjIqr_bar-
product_Ids_conjIdr_bar;
average_torque(k,n)= (P/4)*(xmq/wb)*real(minus_of_product_currents);

%Calculate for Pulsating Torque

product_Iqs_Idr_bar=imatrix(1,n)*imatrix(4,n);
product_Ids_Iqr_bar=sin(del(k))*imatrix(2,n)*imatrix(3,n);
product_Ids_Idr_bar=cos(del(k))*imatrix(2,n)*imatrix(4,n);
minus_of_product_pulsatingcurrents=product_Iqs_Idr_bar-product_Ids_Iqr_bar-
product_Ids_Idr_bar;
mag_pulsating_torque(k,n)=(P/4)*(xmq/wb)*abs(minus_of_product_pulsatingcurren
ts);

%Calculate for Apparent Power
apparent_power(k,n)=[vmatrix(1)
vmatrix(2)]*conj([imatrix(1,n);imatrix(2,n)]);

end

%Calculate for Power Input

P_in(k,:)=real(apparent_power(k,:));

%Calculate for efficiency

P_out(k,:)=average_torque(k,:).*wr;
efficiency(k,:) = (100*P_out(k,:))./P_in(k,:);


end

figure (1)
```

```
plot(wr,average_torque(1,:),wr,average_torque(2,:),...

wr,average_torque(3,:),wr,average_torque(4,:),wr,average_torque(5,:),wr,avera
ge_torque(6,:),...
   wr,average_torque(7,:),wr,average_torque(8,:),wr,average_torque(9,:),...

wr,average_torque(10,:),wr,average_torque(11,:),wr,average_torque(12,:),wr,av
erage_torque(13,:),wr,average_torque(14,:),...

wr,average_torque(15,:),wr,average_torque(16,:),wr,average_torque(17,:),wr,av
erage_torque(18,:),wr,average_torque(19,:))

legend('del= 0 deg','del= 10 deg','del= 20 deg','del= 30 deg','del= 40
deg','del= 50 deg','del= 60 deg',...
'del= 70 deg','del= 80 deg','del= 90 deg','del= 100 deg','del= 110 deg','del=
120 deg','del= 130 deg','del= 140 deg','del= 150 deg'...
    ,'del= 160 deg','del= 170 deg','del= 180 deg')

figure (2)
plot(wr,mag_pulsating_torque(1,:),wr,mag_pulsating_torque(2,:),wr,mag_pulsati
ng_torque(3,:),wr,mag_pulsating_torque(4,:),wr,mag_pulsating_torque(5,:),wr,m
ag_pulsating_torque(6,:),wr,mag_pulsating_torque(7,:),wr,mag_pulsating_torque
(8,:),...

wr,mag_pulsating_torque(9,:),wr,mag_pulsating_torque(10,:),wr,mag_pulsating_t
orque(11,:),wr,mag_pulsating_torque(12,:),wr,mag_pulsating_torque(13,:),wr,ma
g_pulsating_torque(14,:),...

wr,mag_pulsating_torque(15,:),wr,mag_pulsating_torque(16,:),wr,mag_pulsating_
torque(17,:),wr,mag_pulsating_torque(18,:),wr,mag_pulsating_torque(19,:))
legend('del= 0 deg','del= 10 deg','del= 20 deg','del= 30 deg','del= 40
deg','del= 50 deg','del= 60 deg',...
'del= 70 deg','del= 80 deg','del= 90 deg','del= 100 deg','del= 110 deg','del=
120 deg','del= 130 deg','del= 140 deg','del= 150 deg'...
    ,'del= 160 deg','del= 170 deg','del= 180 deg')


figure (3)

plot(wr,efficiency(1,:),wr,efficiency(2,:),wr,efficiency(3,:),wr,efficiency(4
,:),wr,efficiency(5,:),...

wr,efficiency(6,:),wr,efficiency(7,:),wr,efficiency(8,:),wr,efficiency(9,:),w
r,efficiency(10,:),wr,efficiency(11,:),wr,efficiency(12,:),...

wr,efficiency(13,:),wr,efficiency(14,:),wr,efficiency(15,:),wr,efficiency(16,
:),wr,efficiency(17,:),wr,efficiency(18,:),wr,efficiency(19,:))

legend('del= 0 deg','del= 10 deg','del= 20 deg','del= 30 deg','del= 40
deg','del= 50 deg','del= 60 deg',...
'del= 70 deg','del= 80 deg','del= 90 deg','del= 100 deg','del= 110 deg','del=
120 deg','del= 130 deg','del= 140 deg','del= 150 deg'...
    ,'del= 160 deg','del= 170 deg','del= 180 deg')
```

```
%Script to calculate and plot graphs of steady state performances...

%.. for the cases of del equal to 60degs and 90degs for the CRSPIM
clc;
clear all;
format bank;
f = 60;
P = 4;
we =pi*f;
wb=we;
del=[pi/2,pi/3];
s=1:-0.02:0;
Nas = 1/1.18;
rqs = 2.02;
xlqs = 2.79;
xlds = 3.22;
rds = 7.14;
rpds = (Nas^2)*rds;
xplds = (Nas^2)*xlds;
xplr = 2.12;
rpr = 4.12;
xmq = 66.8;
xqs = xlqs + xmq;
xpds = xplds+xmq;
xpr = xplr+xmq;
zrun=9-172*1i;
zprun = (Nas^2)*zrun;
rpc=real(zprun);
xpc=imag(zprun);
vqs = 110;
vqs_bar = vqs + j*0;
vpds_bar = (Nas)*vqs_bar;
imatrix = zeros(4,51);
vmatrix = [vqs_bar; vpds_bar; 0; 0;];

for k = 1:2,
for n = 1:51,
    wr(n) = we*(1-s(n));
A = [(rqs+j*((we/wb)*xqs)), -j*((we/wb)*xmq*cos(del(k))), j*((we/wb)*xmq),...
    0;-j*((we/wb)*xmq*cos(del(k))), ((rpds-j*(we/wb)*xpds)),...
    -j*((we/wb)*xmq*cos(del(k))),j*((we/wb)*xmq*sin(del(k)));...
    j*((we/wb)*xmq),-
((wr(n)/wb)*xmq*sin(del(k))+j*(we/wb)*xmq*cos(del(k))),...
    (rpr+j*((we/wb)*xpr)),(-
wr(n)/wb)*xpr;(wr(n)/wb)*xmq,(j*(we/wb)*xmq*sin(del(k))-
(wr(n)/wb)*xmq*cos(del(k))),...
    (wr(n)/wb)*xpr,(rpr+j*((we/wb)*xpr))];
imatrix(:,n)=A\vmatrix;

%Calculate for Average Torque

conjIqs_bar=conj(imatrix(1,n));
product_Idr_conjIqs_bar=imatrix(4,n)*conjIqs_bar;
conjIqr_bar=conj(imatrix(3,n));
product_Ids_conjIqr_bar=sin(del(k))*imatrix(2,n)*conjIqr_bar;
conjIdr_bar=conj(imatrix(4,n));
```

```
product_Ids_conjIdr_bar=cos(del(k))*imatrix(2,n)*conjIdr_bar;
minus_of_product_currents=product_Idr_conjIqs_bar-product_Ids_conjIqr_bar-
product_Ids_conjIdr_bar;
average_torque(k,n)= (P/4)*(xmq/wb)*real(minus_of_product_currents);

%Calculate for Pulsating Torque

product_Iqs_Idr_bar=imatrix(1,n)*imatrix(4,n);
product_Ids_Iqr_bar=sin(del(k))*imatrix(2,n)*imatrix(3,n);
product_Ids_Idr_bar=cos(del(k))*imatrix(2,n)*imatrix(4,n);
minus_of_product_pulsatingcurrents=product_Iqs_Idr_bar-product_Ids_Iqr_bar-
product_Ids_Idr_bar;
mag_pulsating_torque(k,n)=(P/4)*(xmq/wb)*abs(minus_of_product_pulsatingcurren
ts);

% %Calculate for Apparent Power
apparent_power(k,n)=[vmatrix(1)
vmatrix(2)]*conj([imatrix(1,n);imatrix(2,n)]);

end

%Calculate for Power Input

P_in(k,:)=real(apparent_power(k,:));

%Calculate for efficiency

P_out(k,:)=average_torque(k,:).*wr;
efficiency(k,:) = (100*P_out(k,:))./P_in(k,:);

end


figure (1)
plot(wr,efficiency), xlabel('speed (rad/s)'), ylabel('efficiency (%)')
grid on
legend('90 deg','60 deg','BEST')
figure (2)
plot(wr,average_torque)
xlabel('speed (rad/s)')
ylabel('Average Torque (Nm)')
legend('90 deg','60 deg','BEST')

figure (3)
plot(wr,mag_pulsating_torque)
xlabel('speed (rad/s)')
ylabel('Magnitude of Pulsating Torque (Nm)')
legend('90 deg','60 deg','BEST')
```

```
%This program calculates the torque of the generalized SPIM model for 90 degs
and 60 degs cases when balanced conditions are imposed on the winding
currents

% The parameters of the machine
clc
clear all;
format bank;
f = 60;
P = 4;
we =pi*f;
wb=we;
del=[pi/3, pi/2];
Nab = 1/1.18;
a=1.18;
rqs = 2.02;
xlqs = 2.79;
xlds = 3.22;
rds = 7.14;
rpds = (Nab^2)*rds;
xplds = (Nab^2)*xlds;
xplr = 2.12;
rpr = 4.12;
xmq = 66.8;
xqs = xlqs + xmq;
xpds = xplds+xmq;
xpr = xplr+xmq;
%=====================================================
zrun=9-172*1i;
zprun = (Nab^2)*zrun;
rpc=real(zprun);
xpc=imag(zprun);
%=====================================================
vm = 110;
n=51;
tetae=linspace(0,2*pi,n);
vas=vm*sin(tetae);
%vbs=vas;
vqs_bar=vm;
vpds_bar = 0;
vqr=0;
vdr=0;
x=1:-0.02:0;
N=length(x);

for k=1:2,
for j = 1:n,
    s=x(j);
    wr(j) = we*(1-s);

A=[((rqs+i*(we/wb*xqs))-i*(we/wb*xmq*cos(del(k)))*exp(i*(pi-del(k)))/a)
i*(we/wb*xmq)                    0                                0;

  (-i*(we/wb*xmq*cos(del(k)))+((rpds)+i*(we/wb*xpds))*exp(i*(pi-del(k)))/a)
-i*(we/wb*xmq*cos(del(k)))      i*(we/wb*xmq*sin(del(k)))                    -
1;
```

```
  (i*we/wb*xmq-
((wr(j)/wb)*xmq*sin(del(k))+i*we/wb*xmq*cos(del(k)))*exp(i*(pi-del(k)))/a)
(rpr+i*we/wb*xpr)               -wr(j)/wb*xpr                  0;

  (wr(j)/wb*xmq+(i*we/wb*xmq*sin(del(k))-
(wr(j)/wb)*xmq*cos(del(k)))*exp(i*(pi-del(k)))/a)          (wr(j)/wb)*xpr
(rpr+i*(we/wb*xpr))           0];

 imatrix(:,j)=inv(A)*[vqs_bar;vpds_bar;vqr;vdr];
 iqs=imatrix(1,j);
 is(j)=iqs;
 idsp=iqs*exp(i*(pi-del(k)))/a;
 ids(j)=idsp;
 iqrp=imatrix(2,j);
 idrp=imatrix(3,j);
  vd(k,j)=imatrix(4,j);
  mag_vc=abs(vd);
 ang_vc=angle(vd)*180/pi;
ang_lead(j)=angle(idsp)*180/pi-angle(iqs)*180/pi;

%Calculate for Average Torque
  conjIqs_bar=conj(iqs);
  product_Idrp_conjIqs_bar=idrp*conjIqs_bar;
  conjIqrp_bar=conj(iqrp);
  product_Idsp_conjIqrp_bar=sin(del(k))*idsp*conjIqrp_bar;
  conjIdrp_bar=conj(idrp);
  product_Idsp_conjIdrp_bar=cos(del(k))*idsp*conjIdrp_bar;
  minus_of_product_currents=product_Idrp_conjIqs_bar-
product_Idsp_conjIqrp_bar-product_Idsp_conjIdrp_bar;
  average_torque(k,j) = (P/4)*(xmq/wb)*real(minus_of_product_currents);

%Calculate for Pulsating Torque

 product_Iqs_Idrp_bar=iqs*idrp;
 product_Idsp_Iqrp_bar=sin(del(k))*idsp*iqrp;
 product_Idsp_Idrp_bar=cos(del(k))*idsp*idrp;
 minus_of_product_pulsatingcurrents=product_Iqs_Idrp_bar-
product_Idsp_Iqrp_bar-product_Idsp_Idrp_bar;

mag_pulsating_torque(k,j)=(P/4)*(xmq/wb)*abs(minus_of_product_pulsatingcurren
ts);


end
end
figure(1)
plot(wr, mag_vc)
legend('60 degs', '90 degs')
grid on
figure(2)
plot(wr, average_torque)
legend('60 degs', '90 degs')
grid on
figure(3)
```

```
plot(wr, mag_pulsating_torque)
legend('60 degs', '90 degs')
grid on
figure(4)
plot(wr, ang_lead)
grid on


%This program calculates the dynamic performance of the Modified SPIM 1 under
%the scheme of Figure 3.9
function
[plambda_qs,plambda_ds,plambda_qr,plambda_dr,pwr,Te,Iqs,Ids,ia,ib,wm] = ...
    SPIM(Vqs,Vds,lambda_qs,lambda_ds,lambda_qr,lambda_dr,wr,TL)
% This block supports the Embedded MATLAB subset.
% See the help menu for details.
Nqd = 1/1.18;
Ndq=1.18;
rqs = 2.02;
rds = 7.14;
rpr = 4.12;
Lmas = 0.1772;
Lplr = 0.0056;
Llqs = 0.0074;
Llds = 0.0085;
rpds = (Nqd^2)*rds;
Lplds = (Nqd^2)*Llds;

J =0.0146;
P = 4;
Vqr = 0;
Vdr = 0;
LMq = 1/(1/Lmas + 1/Llqs + 1/Lplr);
LMd = 1/(1/Lmas + 1/Lplds + 1/Lplr);
lambda_mq = LMq*((lambda_qs/Llqs)+(lambda_qr/Lplr));
lambda_md = LMd*((lambda_ds/Lplds)+(lambda_dr/Lplr));
plambda_qs = (Vqs + (rqs/Llqs)*(lambda_mq - lambda_qs));
plambda_ds = (Vds + (rpds/Lplds)*(lambda_md - lambda_ds));
plambda_qr = (Vqr + Nqd*wr*lambda_dr + (rpr/Lplr)*(lambda_mq - lambda_qr));
plambda_dr = (Vdr - Ndq*wr*lambda_qr + (rpr/Lplr)*(lambda_md - lambda_dr));
Iqs = (1/Llqs)*(lambda_qs - lambda_mq);
Ids = (1/Lplds)*(lambda_ds - lambda_md);
Iqr = (1/Lplr)*(lambda_qr - lambda_mq);
Idr = (1/Lplr)*(lambda_dr - lambda_md);
ia=Iqs;
ib=-Ids;
Te = (P/2)*Lmas*(Idr*Iqs - Ids*Iqr);
pwr=(P/(2*J))*(Te-TL);
wm=(120*wr)/(2*pi*P);
```

```
%This program calculates the dynamic performance of the Modified SPIM 2 under
%the scheme of Figure 3.9

function
[plambda_qs,plambda_ds,plambda_qr,plambda_dr,pwr,Te,Iqs,Ids,ia,ib,wm] = ...
    SPIM(Vqs,Vds,lambda_qs,lambda_ds,lambda_qr,lambda_dr,wr,TL)
% This block supports the Embedded MATLAB subset.
% See the help menu for details.
Nqd = 1/1.1293;
Ndq=1.1293;
Lmas = 0.1954;
Lplr = 0.0304;
Llqs = 0.0203;
Llds = 0.0210;
rqs = 4;
rds = 6.5;
rpr = 3.61;
rpds = (Nqd^2)*rds;
Lplds = (Nqd^2)*Llds;
J =0.01424;
P = 4;
Vqr = 0;
Vdr = 0;
LMq = 1/(1/Lmas + 1/Llqs + 1/Lplr);
LMd = 1/(1/Lmas + 1/Lplds + 1/Lplr);
lambda_mq = LMq*((lambda_qs/Llqs)+(lambda_qr/Lplr));
lambda_md = LMd*((lambda_ds/Lplds)+(lambda_dr/Lplr));
plambda_qs = (Vqs + (rqs/Llqs)*(lambda_mq - lambda_qs));
plambda_ds = (Vds + (rpds/Lplds)*(lambda_md - lambda_ds));
plambda_qr = (Vqr + Nqd*wr*lambda_dr + (rpr/Lplr)*(lambda_mq - lambda_qr));
plambda_dr = (Vdr - Ndq*wr*lambda_qr + (rpr/Lplr)*(lambda_md - lambda_dr));
Iqs = (1/Llqs)*(lambda_qs - lambda_mq);
Ids = (1/Lplds)*(lambda_ds - lambda_md);
Iqr = (1/Lplr)*(lambda_qr - lambda_mq);
Idr = (1/Lplr)*(lambda_dr - lambda_md);
ia=Iqs;
ib=-Ids;
Te = (P/2)*Lmas*(Idr*Iqs - Ids*Iqr);
pwr=(P/(2*J))*(Te-TL);
wm=(120*wr)/(2*pi*P);


%This program calculates the dynamic performance of the Modified SPIM 1 under
%the scheme of Figure 3.23

function
[plambda_qs,plambda_ds,plambda_qr,plambda_dr,pwr,Te,Vqs,Vds,Iqs,Ids,Iqr,Idr,w
m] = ...
    SPIM(Vas,Vbs,lambda_qs,lambda_ds,lambda_qr,lambda_dr,wr,TL)
% This block supports the Embedded MATLAB subset.
% See the help menu for details.
Ndq=1;
Nqd=1;
Lmas = 0.1772;
Lplr = 0.0056;
Llqs = 0.0074;
Llds = Llqs;
```

```
rqs = 2.02;
rds = rqs;
rpr = 4.12;
J =0.0146;
P = 4;
Vqs = Vas;
Vds = Vbs;
Vqr = 0;
Vdr = 0;
lambda_mq=((lambda_qs/Llqs)+(lambda_qr/Lplr))/((1/Lmas)+(1/Llqs)+(1/Lplr));
lambda_md=((lambda_ds/Llds)+(lambda_dr/Lplr))/((1/Lmas)+(1/Llds)+(1/Lplr));
Iqs = (1/Llqs)*(lambda_qs-lambda_mq);
Ids = (1/Llds)*(lambda_ds-lambda_md);
Iqr = (1/Lplr)*(lambda_qr-lambda_mq);
Idr = (1/Lplr)*(lambda_dr-lambda_md);
plambda_qs=Vqs-(rqs*Iqs);
plambda_ds=Vds-(rds*Ids);
plambda_qr=Vqr-(rpr*Iqr)+wr*Nqd*lambda_dr;
plambda_dr=Vdr-(rpr*Idr)-wr*Ndq*lambda_qr;
Te = (P/2)*Lmas*(Idr*Iqs - Ids*Iqr);
pwr=(P/(2*J))*(Te-TL);
wm=(120*wr)/(2*pi*P);


%This program calculates the dynamic performance of the Modified SPIM 2 under
%the scheme of Figure 3.23
function
[plambda_qs,plambda_ds,plambda_qr,plambda_dr,pwr,Te,Vqs,Vds,Iqs,Ids,Iqr,Idr,w
m] = ...
    SPIM(Vas,Vbs,lambda_qs,lambda_ds,lambda_qr,lambda_dr,wr,TL)
% This block supports the Embedded MATLAB subset.
% See the help menu for details.

Ndq=1;
Nqd=1;
Lmas = 0.1954;
Lplr = 0.0304;
Llqs = 0.0203;
Llds = Llqs;
rqs = 4;
rds = rqs;
rpr = 3.61;
J =0.01424;
P = 4;
Vqs = Vas;
Vds = Vbs;
Vqr = 0;
Vdr = 0;
lambda_mq=((lambda_qs/Llqs)+(lambda_qr/Lplr))/((1/Lmas)+(1/Llqs)+(1/Lplr));
lambda_md=((lambda_ds/Llds)+(lambda_dr/Lplr))/((1/Lmas)+(1/Llds)+(1/Lplr));
Iqs = (1/Llqs)*(lambda_qs-lambda_mq);
Ids = (1/Llds)*(lambda_ds-lambda_md);
Iqr = (1/Llpr)*(lambda_qr-lambda_mq);
Idr = (1/Lplr)*(lambda_dr-lambda_md);
plambda_qs=Vqs-(rqs*Iqs);
plambda_ds=Vds-(rds*Ids);
plambda_qr=Vqr-(rpr*Iqr)+wr*Nqd*lambda_dr;
```

```
plambda_dr=Vdr-(rpr*Idr)-wr*Ndq*lambda_qr;
Te = (P/2)*Lmas*(Idr*Iqs - Ids*Iqr);
pwr=(P/(2*J))*(Te-TL);
wm=(120*wr)/(2*pi*P);


%This program calculates the electric power loss and efficiency vs flux for
%rated, 2 and 1Nm Load Torques applies to Modified SPIM 2
clc
clear all;
Rs=4;
Rr=3.61;
we=157.1;
wr=151.5;
Te=[1,2,5.1];
p=4;
Lm=0.1954;
Llr = 0.0304;
Lr=Lm+Llr;
Lls = 0.0203;
Ls=Lm+Lls;
Lx=Ls-(Lm^2/Lr);
rpr=3.61;
rc=910;
k=1+Rs/rc;
r=Rs+(k*Lm^2*rpr/Lr^2);
kt=(p/2)*(Lm/Lr);
cons1=Rs+Lm^2*Rr/Lr^2+(r^2+k^2*we^2*Lx^2)/(rc*k)+2*Rs^2/(rc*k);
cons2=(Rr+wr^2*Lr^2)*k*Lm^2/(rc*Lr^4)-Rr/Lr^2+2*(k*Lx*Lr*we*wr-Rr*r)/(rc*Lr);
flux=0:0.02:1;
fluxS=flux.^2;
for m=1:3;

for n=1:51;

PL(m,n)=((Lm^2*Te(m)^2+flux(n)^4*kt^2)/(Lm^2*kt^2*flux(n)^2))*cons1+flux(n)^2
*cons2+((2*Lm*Te(m))/(kt*rc*Lr))*(wr*Lr*r+we*(Rs+k*Rr*Lx));
eff(m,n)=(Te(m)*wr)*100/(Te(m)*wr+PL(m,n));
end
end
figure (1)
plot(flux,PL), xlabel('flux (Wb)'), ylabel('Electrical Power loss (W)')
legend('Te = 1Nm','Te = 2Nm','Te = 5.1Nm')
figure (2)
plot(flux,eff), xlabel('flux (Wb)'), ylabel('efficiency (%)')
legend('Te = 1Nm','Te = 2Nm','Te = 5.1Nm')


%This program calculates the value of the initial rotor flux to drive the
%Modified SPIM 2 for the Vector-controlled efficiency-optimizing scheme
clc
clear all

% parameters of machine for the Modified SPIM control

Rs=4;
```

```
Rr=3.61;
Jeq=0.01424;
p=4;
P=4;
Lmas=0.1954;
Llr =0.0304;
Lr=Lmas+Llr;
Lls =0.0203;
Ls=Lmas+Lls;
Lx=Ls-Lmas^2/Lr;
rc=910;
k=1+Rs/rc;
r=Rs+(k*Lmas^2*Rr/Lr^2);
kt=(p/2)*(Lmas/Lr);
a=1+Rs/(k*rc);
x=Rs*(a^2+Rs/(k^2*rc));


% Steady State Operating Condition
f=50;
Vm= sqrt(2)*220;
Ns=1500; Nm=1447;
s=(Ns-Nm)/Ns;
We=2*pi*f;
Wm=(1-s)*We;
Vs_0 = Vm;
ThetaVs_0 = angle(Vs_0);
Theta_0 = 0;
Vds_0 =  Vm*sin(ThetaVs_0 - Theta_0);
Vqs_0 =  Vm*cos(ThetaVs_0 - Theta_0);

% Calculations of winding currents
A = [Rs        k*We*Ls       0         k*We*Lmas;...
     -k*We*Ls    Rs            -k*We*Lmas    0;...
     0         s*We*Lmas     Rr        s*We*Lr;...
     -s*We*Lmas    0             -s*We*Lr  Rr];
Ainv = inv(A);
Vqd_0=[Vqs_0; Vds_0; 0; 0];
Iqd_0=Ainv*Vqd_0;
Iqs_0=Iqd_0(1)
Ids_0=Iqd_0(2)
Iqr_0=Iqd_0(3)
Idr_0=Iqd_0(4)

% mechanical Rotor speed in rad/s
Wmech_0=(2/p)*Wm;

% Inductance matrix
M = [Ls 0  Lmas 0 ;...
     0  Ls 0  Lmas;...
     Lmas 0  Lr 0 ;...
     0  Lmas 0  Lr];

% qd winding Flux Linkages
lambda_qd_0 = M * [Iqs_0; Ids_0; Iqr_0; Idr_0];
lambda_qs_0 = lambda_qd_0(1)
```

```
lambda_ds_0 = lambda_qd_0(2)
lambda_qr_0 = lambda_qd_0(3)
lambda_dr_0 = lambda_qd_0(4)
[thetar, lambda_r_qd_0]=cart2pol(lambda_qr_0, lambda_dr_0)
[thetas, lambda_s_qd_0]=cart2pol(lambda_qs_0, lambda_ds_0)

% d-axis is aligned with the rotor flux :
lambda _dr_0=lambda _r_qd_0       %lambda_qr_0 equals zero
```